Max-Planck-Institut für Polymerforschung

Max Planck Institute for Polymer Research

Dynamics of Polymer in Confined Environment

Dissertation

zur Erlangung des Grades

„Doktor der Naturwissenschaften“

im Promotionsfach Chemie

am Fachbereich Chemie, Pharmazie und Geowissenschaften

der Johannes Gutenberg-Universität Mainz

Young-Gon Kim

geboren in Buan, Süd Korea

Mainz, 2020

The thesis was carried out from November 2016 until July 2020 within the Department of Physical Chemistry of Polymers of [redacted] in the group of [redacted] at the Max Planck Institute for Polymer Research, Mainz.

Dekan: [redacted]
Prodekan: [redacted]

Gutacher 1: [redacted]
Gutacher 2: [redacted]
Date of oral examination:

Declaration

I hereby declare that I wrote the dissertation submitted without any unauthorized external assistance and used only sources acknowledged in the work. All textual passages which are appropriated verbatim or paraphrased from published and unpublished texts as well as all information obtained from oral sources are duly indicated and listed in accordance with bibliographical rules. In carrying out this research, I complied with the rules of standard scientific practice as formulated in the statutes of the Johannes Gutenberg University Mainz to ensure standard scientific practice.

Mainz, 2020 .....

(Young-Gon Kim)

Abstract

Surface modification of nanoparticles by grafting polymer brushes is an efficient approach to finely control the surface properties of nanoparticles and their behavior in suspensions. The conformation of the grafted polymer chains is influenced by the architecture of the polymer canopy defined by the grafting density or the length of the polymer chains. The constrained conformation of polymer brushes on a curved substrate influences the thermal and mechanical properties of the polymer chains and affects the colloidal behavior of polymer-functionalized nanoparticles. However, to grasp why these changes are observed, an in-depth understanding of the dynamics of end-tethered polymer chains is required. Furthermore, the influence of the substrate stiffness has mainly been overlooked, and the impact of the dynamics of the core when using soft and deformable polymer nanoparticles needs to be better analyzed. The primary goal of this dissertation is to study and understand the behavior of suspension of surface-functionalized soft polymer nanoparticles functionalized with polymer chains and to correlate local properties like chain dynamics and macroscopic behavior like the viscoelastic properties of the colloidal suspensions.

In order to understand how structural factors affected the properties and behavior of the colloids, a flexible and versatile preparation method was developed to produce a variety of polymer nanoparticles functionalized with end-grafted polymer chains. First core poly(styrene) nanoparticles were prepared *via* miniemulsion polymerization, the softness of the core can be tuned by controlling the degree of cross-linking of the polystyrene by the addition of various amounts of divinylbenzene. Those polystyrene nanoparticles were then functionalized with a thin layer of inimer containing layer. By controlling the composition of the inimer layer, it was possible to control the grafting density of the end-grafted polymer chains. Finally, surface-initiated atom transfer radical polymerization was used to grow poly(methyl acrylate) chains from the inimer layer with a well-controlled degree of polymerization. This yields a library of nanoparticles with a defined size, softness, grafting density, and degree of polymerization.

Then the effect of the architecture of the poly(methyl acrylate) canopy on the viscoelastic behavior of nanoparticle suspensions was studied using different selective solvent (**Section 5.1**). The results showed that the softness of the core influences the properties of the colloidal gels, softer core yielding more

deformable materials, and showed that the softness of the core was as important as the architecture of the canopy on the final properties of the colloidal material. To further understand how the properties of the nanoparticles influenced the behavior of the suspension, the local subsegmental motion of polymer chain was studied using NMR spectroscopy (**Section 5.2, 5.3, and 5.4**). The results revealed an interplay between the dynamics of the soft core and the dynamics of the grafted polymer canopy and the effect of the architecture of the nanoparticles on the dynamics of such confined polymer systems. The influence of the different parameters affecting the rheological properties of the nanoparticles suspension on the dynamics of the polymer systems was investigated: the degree of polymerization of grafted chains (**Section 5.2, and 5.4**), grafting density (**Section 5.1 and 5.4**), the rigidity/swelling of the core (**Section 5.2, and 5.3**), and solvent quality (**Section 5.3**).

This doctoral dissertation presents a comprehensive overview of the parameters influencing the dynamics of the local chain in polymer nanoparticles functionalized with a canopy of end-tethered polymer chains. One of the key insights provided is the clear interplay between the dynamics of the core and the dynamics of the canopy.

Zusammenfassung

Die Oberflächenmodifizierung von Nanopartikeln mithilfe von Polymerbürsten ist ein effizienter Ansatz zur Steuerung der Oberflächeneigenschaften von Nanopartikeln und ihres Verhaltens in Suspensionen. Die Konformation der angebrachten Polymerketten wird durch die Architektur der Polymerbedeckung beeinflusst, wie beispielsweise der Pfropfdichte oder der Länge der Polymerketten. Die eingeschränkte Konformation von Polymerbürsten auf einem gekrümmten Substrat beeinflusst die thermischen und mechanischen Eigenschaften der Polymerketten und das kolloidale Verhalten von polymerfunktionalisierten Nanopartikeln. Um zu verstehen, warum diese Änderungen beobachtet werden, ist jedoch ein gründliches Verständnis der Dynamik endgebundener Polymerketten erforderlich. Darüber hinaus wurde der Einfluss der Substratsteifigkeit bisher überwiegend übersehen, und der Einfluss der Dynamik des Kerns bei Verwendung von weichen und verformbaren Polymer-Nanopartikeln muss besser analysiert werden. Das Hauptziel dieser Dissertation ist es, das Suspensionsverhalten von oberflächenfunktionalisierten weichen Polymernanopartikeln, die mit Polymerketten funktionalisiert sind, zu untersuchen und zu verstehen, sowie lokale Eigenschaften wie Kettendynamik und makroskopisches Verhalten wie die viskoelastischen Eigenschaften der kolloidalen Suspensionen zu korrelieren.

Um zu verstehen, wie strukturelle Faktoren die Eigenschaften und das Verhalten der Kolloide beeinflussen, wurde ein flexibles und vielseitiges Herstellungsverfahren entwickelt, um eine Vielzahl von Polymernanopartikeln herzustellen, die mit endgepfropften Polymerketten funktionalisiert sind. Erste Kernpolystyrol-Nanopartikel wurden durch Miniemulsionspolymerisation hergestellt. Die Weichheit des Kerns kann durch Steuern des Vernetzungsgrades des Polystyrols durch Zugabe verschiedener Mengen Divinylbenzol eingestellt werden. Diese Polystyrolanopartikel wurden dann mit einer dünnen Schicht, die ein Inimer enthielten, funktionalisiert. Durch Steuern der Zusammensetzung der Inimerschicht war es möglich, die Pfropfdichte der endpfropften Polymerketten zu steuern. Schließlich wurde eine oberflächeninitiierte radikalische Atomtransferpolymerisation verwendet, um Polymethylacrylat-Ketten aus der Inimerschicht mit einem gut kontrollierten Polymerisationsgrad zu züchten. Dies ergibt eine Bibliothek von Nanopartikeln mit einer definierten Größe, Weichheit, Pfropfdichte und einem definierten Polymerisationsgrad. Anschließend wurde der Einfluss der Architektur des Poly(methylacrylat)-Dachs

auf das viskoelastische Verhalten von Nanopartikelsuspensionen unter Verwendung verschiedener selektiver Lösungsmittel untersucht (**Abschnitt 5.1**). Die Ergebnisse zeigten, dass die Weichheit des Kerns die Eigenschaften der kolloidalen Gele beeinflusst, wobei ein weicherer Kern mehr verformbare Materialien ergibt, und dass die Weichheit des Kerns für die endgültigen Eigenschaften des kolloidalen Materials ebenso wichtig war wie die Architektur der Schale. Um besser zu verstehen, wie das Verhalten der Suspension durch die Eigenschaften der Nanopartikel beeinflusst wurde, wurde die lokale subsegmentale Bewegung der Polymerkette mittels NMR-Spektroskopie untersucht (**Abschnitt 5.2, 5.3 und 5.4**). Die Ergebnisse zeigten ein Zusammenspiel zwischen der Dynamik des weichen Kerns und der Dynamik der gepfropften Polymerkorona. Der Einfluss der verschiedenen Parameter, die die rheologischen Eigenschaften der Nanopartikelsuspension beeinflussen, auf die Dynamik der Polymersysteme wurde untersucht: der Polymerisationsgrad der gepfropften Kette (**Abschnitt 5.2 und 5.4**), die Pfropfdichte (**Abschnitt 5.1 und 5.4**), die Steifigkeit / Quellung des Kerns (**Abschnitt 5.2 und 5.3**) und die Lösungsmittelqualität (**Abschnitt 5.3**).

Diese Dissertation bietet einen umfassenden Überblick über die Parameter, welche die Dynamik der lokalen Kette in Polymer-Nanopartikeln beeinflussen. Eine der wichtigsten Erkenntnisse ist das klare Zusammenspiel zwischen der Dynamik des Kerns und der Dynamik der Polymerschale .

Table of Contents

1. Motivation

In the past three decades, nanoparticles have been extensively studied and have become an integral part of technological advances in chemistry and physics.[1-3] Nanoparticles have shown superior chemical and mechanical properties due to their size – they are defined as particles with a size between 1×10^{-9} and 1×10^{-7}m – [4] and to their dramatically increased surface area in comparison to bulk materials.[5] In particular, polymer nanoparticles have unique advantages such as a wide range of source materials, tunability in surface functionalities and architectures, or even, controllable swelling in a stimuli-responsive manner. [6-9] Owing to such attractive properties, nanoparticles are employed in a number of applications such as functional coatings, inks, adhesives, nutrition, cosmetics, biomedical, and pharmaceutical applications.[10-15]

The control of the interface between nanoparticles and the suspension media around them is an indispensable step when dealing with nanoparticles due to the high surface energy of nanoparticles.[16] The grafting of polymer chains – refer to as polymer brushes when they stretch out from the surface – can efficiently control the stability of nanoparticles in a suspension.[17] The tethering of polymer chains changes the surface properties of the nanoparticles but preserved the intrinsic properties of the core.[18] The behavior of densely grafted polymer chains on flat substrates was described by De Gennes,[19] but their behavior when grafted to polymer nanoparticles is not yet fully understood. Nevertheless, over the past 20 years, polymer brushes have been successfully used to tailor the properties of nanoparticles used in a variety of applications such as scratch-resistant coatings, precursors of nanoporous polymers and drug delivery.[20-24] In addition, the development of surface-initiated controlled radical polymerization enabled us to finely tune the conformation of grafted chains.[25, 26] The conformation of tethered chains grafted to nanoparticles dispersed in a solvent varies significantly from random coil to stretched brush regime according to the grafting density and solvent condition. At low grafting density, the conformation of grafted chains is not dissimilar to that of untethered chains. However, with increasing grafting density, the grafted chains are confined by neighboring chains and adopt a stretched conformation. Of course, the conformation of grafted chains is also closely related to the chain length and the size of the core.[19]

Although the conformation of systems composed of grafted polymer chains has been studied, there is an evident lack of understanding of the relaxation dynamics of the grafted chains, [27] especially when the polymer chains are grafted to soft polymer nanoparticles. The tethering of polymer chains to the surface of a nanoparticle can influence the timescale of chain relaxation.[28] The changes in the relaxation of the polymer chains caused by grafting, eventually result in new mechanical properties for the polymer-functionalized systems, such as variation of the loss and storage modulus, glass transition temperature, and stress relaxation of the final material.[29, 30] For example, the relaxation dynamics of polyisoprene-grafted-nanoparticles has been studied by using broadband dielectric spectroscopy,[31] a reduced segmental dynamics was observed with low molecular weight chains at low grafting density and was due to the increase in the entanglements of the grafted chains with the polymer chains of the matrix. For the same polymer system, rheological studies found a relationship between moduli and grafting densities.[31] At higher grafting density, the stretched chains were limiting the entanglements and the interpenetration between brush layers, resulting in low elastic moduli. Neutron spin-echo was used to access a wide range of relaxation time at different time scales.[32] The dynamics of the system showed that longer relaxation times were observed in the stretched brush regime (high grafting density) in comparison to the random coil regime and caused by the confinement by neighboring chains experienced at higher grafting density. Depending on the measurement method, relaxation times can be observed at the different time scale and length scale, [33] and very similar system have shown drastically different behavior because the different studies looked at the same material at different time scale and length scale.

So far, most of the studies of the chain dynamics have been limited to polymer chains grafted to inorganic hard cores nanoparticles.[27, 34] The increasing number of applications involving soft nanoparticle functionalized with end-grafted polymer chains is the driving force to study more in-depth the dynamics of polymer-polymer soft core-canopy nanoparticles systems. The results observed for such systems are expected to be different from that of systems based on nanoparticles that have hard and rigid cores due to the mobile nature of the grafting points between core and the canopy in the softer systems.

Herein, the main objective was to get a comprehensive understanding of the consequences of the grafting of polymer chains on soft and deformable polymer nanoparticles. The related composition, architecture and resulting properties, (a) a library of nanoparticles made of poly(methyl acrylate) chains grafted to cross-linked polystyrene cores was prepared, and the properties and behavior of the resulting nanoparticles

suspensions were characterized using (b) NMR relaxation to understand the local dynamics and (c) rheology to study the macroscopic behavior of the suspensions.

The present dissertation consists of six chapters. Chapter 1 describes the motivation of the present study. Chapter 2 introduces the key information about polymer nanoparticles and polymer brushes to understand the need for the study of local dynamics. Chapter 3 gives an introduction to the characterization tools used to study the polymer-functionalized polymer nanoparticles, including NMR relaxometry, rheology, and dynamic light scattering. Chapter 4 describes the experimental details. Chapter 5 presents the key results obtained in the study of the dynamics of polymer-polymer soft core-canopy system. First, the macroscopic properties of the suspension were studied by rheology in different systems. Then the dynamics of polymer-polymer soft core-canopy in a suspension was studied by NMR spin relaxation.

2. State-of-the-art

2.1 Polymer nanoparticles

Polymer nanoparticles are ultrafine particles with a size in the range of 1 to 500 nanometers in diameter. The interest for polymer nanoparticles is due to their unique combination of small size, high surface area, softness, and the ability to carry materials. Depending on the synthetic strategies, they can be fabricated into various shapes such as a sphere, core-shells, bottles, and so on. The advances in the control of their size and shape, preparation method, surface modification have made them an ideal platform in a wide range of applications.

2.1.1 Preparation of nanoparticles by polymerization in dispersed media.

Polymerization, including free radical polymerization (one of the polymerization methods the most favored by the industrial sector), can be performed in different types of media. Bulk polymerization is the easiest way to synthesize polymers. Even if the monomers are liquid, the synthesized polymers are usually solids and can be easily separated from the monomers. Most free radical polymerizations are highly exothermic reactions, and bulk reactions can get out of control due to poor heat exchange. Additionally, an increase in the viscosity of the monomer/polymer mixture during the course of the polymerization hinders the diffusion of the reagents and the heat during the reaction. Polymerization in dispersed media (emulsion) is an ideal method to solve these issues. In general, polymerization in dispersed media requires a monomer immiscible in the solvent chosen as the continuous phase and usually requires the addition of surfactants as stabilizers. When a hydrophobic monomer is dispersed in water, the system is called oil-in-water (O/W) type emulsion. In the case where a hydrophilic monomer and a hydrophobic continuous phase are used, the system is called a water-in-oil (W/O) type emulsion.

2.1.1.1 Emulsion polymerization

Emulsion polymerization is one of the most widely used methods in the industry to produce polymer nanoparticles.[35-37] The main components of a conventional O/W emulsion polymerization are hydrophobic monomer, water, amphiphilic surfactant, and hydrophilic initiator. During the polymerization reaction, there are three physical regions in the reaction medium: the continuous water phase, monomer reservoirs, and growing polymer particle. The emulsion polymerization process is schematically described in Figure 2.1.1.

The amphiphilic surfactants are dissolved in the continuous water phase at a concentration above critical micelle concentration (CMC). They immediately adsorb on the large monomer drops forming the monomer reservoirs, and the excess of surfactant forms micelles in the continuous phase. For a successful emulsion polymerization, the monomers must be hydrophobic, and most of the monomers are in the monomer reservoirs, and a minor fraction of the monomers are inside the micelles, and only a few monomer molecules are present in the continuous phase, diffusing between the reservoirs and the micelles.

The free-radical polymerization is initiated by initiators from the continuous phase using temperature, light, or other stimuli to create radicals. After the formation of a radical in the water phase, the radical reacts with monomer molecules that are present in the continuous phase. Oligomeric radicals become insoluble. The growing oligomers are then captured by micelles where the subsequent polymerization will occur. As soon as the monomers are consumed in the continuous phase, monomers from the reservoir will diffuse in the continuous phase to keep a constant monomer concentration Those monomer molecules, diffusing from the reservoir into the continuous phase, will also be able to enter the micelles. In the course of the reaction, new monomers will diffuse from the reservoir through the continuous phase into the growing particle to feed the polymerization. The emulsion polymerization technique can produce particles with sizes ranging from 20 to 500 nm.

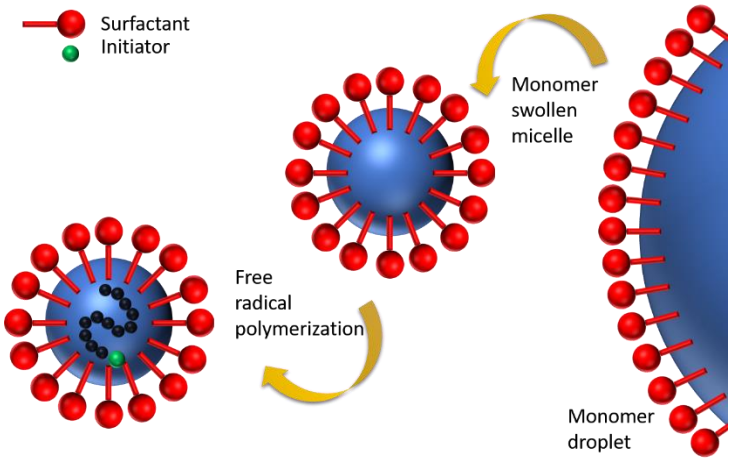

Figure 2.1.1 Schematic representation of emulsion polymerization.

2.1.1.2 Microemulsion polymerization

Microemulsion polymerization has also been used to prepare polymer nanoparticles of hydrophobic monomers in water-based media.[38-40] A microemulsion is a spontaneously formed, macroscopically homogeneous and thermodynamically stable mixture of oil, water, and surfactant (Figure 2.1.2). In comparison to emulsion polymerization, microemulsion polymerization uses a much larger concentration of surfactant. Typically, a bicontinuous network of the two phases is formed by the addition of a large quantity of the surfactant in the oil/water system. Then, a perturbation, like the change of temperature, is used to disturb the bicontinuous network to obtain very homogenous nanodroplets. Different surfactants can be used such as natural surfactant (lecithin), non-ionic surfactants (polysorbates - Tween 20) and ionic surfactants (sodium dodecyl sulfate, cetyltrimethyl ammonium bromide, and cetyltrimethyl ammonium chloride). Still, they all share the properties of displaying lyotropic behavior at high concentration in the final continuous phase. Short- and medium-chain alcohols (ethanol or 1-butanol) or alcoholic derivatives (propylene glycol) are often used as co-surfactants. In oil-in-water microemulsion polymerization, hydrophobic monomers are used, and initiators are dissolved in the continuous phase. Microemulsion polymerization can form particles size in the range of 10 to 100 nm. Despite the fact that this is a powerful technique to prepare nanoparticles, the use of a large amount of surfactant is a severe drawback and limits its use in general applications.

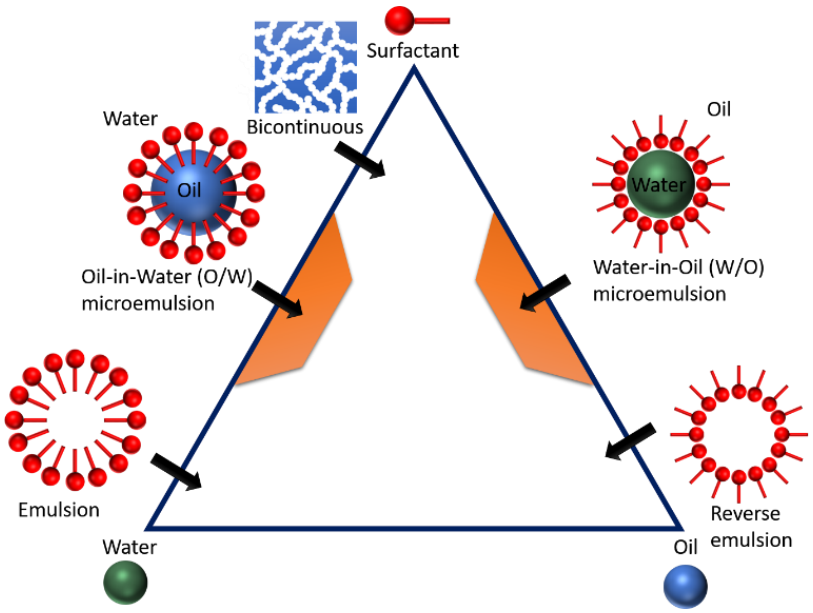

Figure 2.1.2 Phase diagram for the formation of a microemulsion.

2.1.1.3 Miniemulsion polymerization

The miniemulsion enables the preparation of nanoparticles with small size (30~500 nm) and narrow size distribution.[41-43] In a simple system, a miniemulsion is composed of kinetically stable droplets of a dispersed phase in suspension in a continuous phase. The stable droplets are produced by high shear forces such as ultrasound or microfluidizer (Figure 2.1.3). In order to maintain the miniemulsion system stable for an extended period, several factors have to be controlled. The presence of a surfactant is required to hinder the coalescence of the droplets caused by Brownian motion, creaming, or settling. However, in miniemulsion, the concentration of free surfactant molecules in the continuous has to be below the CMC. Most of the surfactant molecules are adsorbed at the surface of droplet or dissolved as single molecules, but without the formation of empty micelles in the continuous phase. The addition of highly oil-soluble costabilizer inside the droplets is necessary to limit Ostwald ripening.

One of the unique features of a miniemulsion system that there is no net mass transport between the droplets. The polymerization occurs inside the preformed droplet and each droplet can be considered as independent nanoreactors. The particle size and composition are defined by the initial amount of monomers and other chemical species present in the droplets before the polymerization.

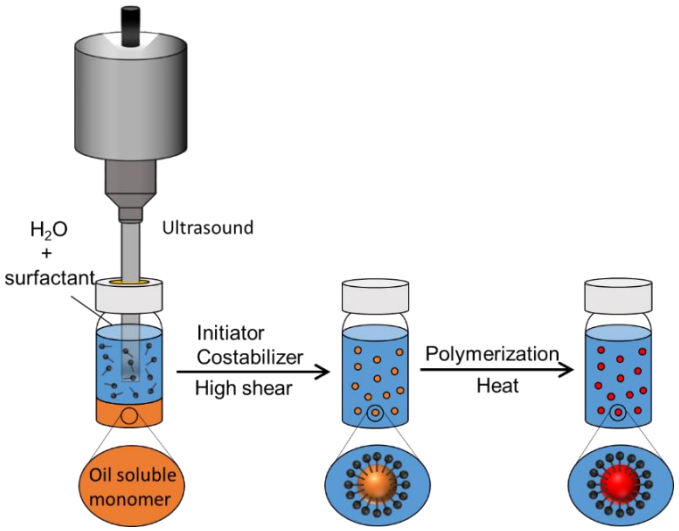

Figure 2.1.3 Schematic illustration of a miniemulsion polymerization.

2.1.1.4 Stability of miniemulsion

Because miniemulsions are thermodynamically metastable, different stabilization processes are needed to assure their long term stability by avoiding coalescence and Ostwald ripening. Coalescence occurs through the collision and merging of droplets to reduce the surface area of the droplets and the interfacial energy of the system (Figure 2.1.4a). Ostwald ripening occurred by diffusion of molecules from a smaller droplet to a bigger one (Figure 2.1.4b). The use of surfactants and co-stabilizers can successfully suppress the coalescence and Ostwald ripening.

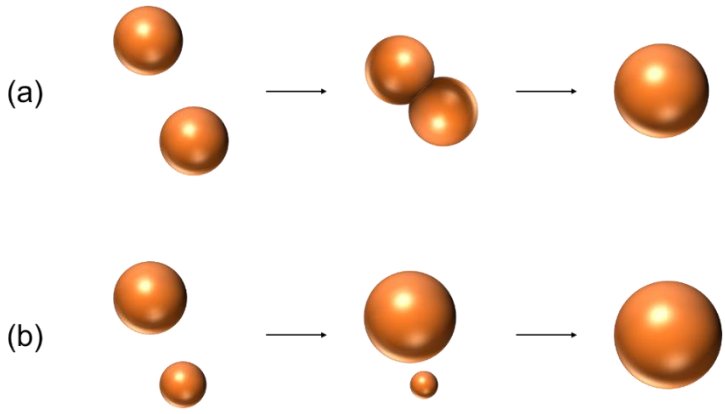

Figure 2.1.4 Schematic illustration of destabilization mechanism of the miniemulsion (a) coalescence of droplets and (b) Ostwald ripening in miniemulsion.

2.1.1.4.1 Surfactants

The formation of a miniemulsion is inevitably accompanied by the formation of an interface between the immiscible phases. The addition of surfactants can reduce the surface tension between the two media to favor the formation and stability of the nanodroplets.[44] In most cases, the surfactant is an amphiphilic molecule consisting of a hydrophilic polar head and a hydrophobic aliphatic tail.[45] Surfactants can be categorized into two main categories, either *ionic surfactants* and *non-ionic surfactants*, depending on the types of hydrophilic moieties in the surfactant molecules.[46]

Ionic surfactants have an ionic group for their hydrophilic head, which is responsible for the electrostatic stabilization of the miniemulsion droplets resulting from the presence of Columbic repulsion forces. The ionic surfactants class is divided into two sub-categories, *anionic*- and *cationic-surfactants*. When the hydrophilic head consists of an anion like sulfate and phosphate, they are classified as *anionic surfactants*, such as sodium dodecyl sulfate (SDS). On the other hand, if the cation is used instead of anion like trimethylammonium of cetyltrimethylammonium bromide (CTAB), they are known as *cationic surfactants*.

Unlike ionic surfactants, *non-ionic surfactants*, are molecules, often copolymers, having no ionic groups, but they instead carry hydrophilic and hydrophobic segments. For example, poly(ethylene oxide)-*b*-poly(butylene/ethylene), can provide a steric stabilization with its hydrophilic block (PEO) and its hydrophobic block (PB/E). When droplets, stabilized with non-ionic surfactants, approach each other, the local concentration of the polymer chains providing the steric stabilization increases in the overlapping area. This causes an osmotic pressure and results in the uptake of continuous phase into the overlapping area. Hence, the droplets push each other away.

When the surfactants are dissolved in a mixture of water and oil, they are likely to self-assemble at the interface to minimize the contact between the immiscible medium. The critical micellar concentration (CMC) is an important parameter defining the phase of the mixture. At low concentration, below the CMC, the surfactant molecules can be molecularly dissolved in the continuous phase, or they are preferentially located at the air/solvent interface, or the solvent/solvent interface. As the concentration increase, the number of molecules at the interface (and inside the continuous phase) increases and consequently, the surface tension readily decreases. As the concentration of surfactant increases, the surface tension steadily decreases until it reaches the minimum at the CMC. At the CMC, the interface is

populated by the maximal number of surfactant molecules and additional surfactant molecules are forced to the continuous phase where they start to self-assemble into micelles. When the continuous phase is water, the hydrophilic heads are exposed to the exterior of the micelle, while the hydrophobic tails hide inside the micelle, and inversely when the continuous phase is oil. The micelles are formed spontaneously and their formation is entropically favored. [45-47]

A suitable surfactant has to be chosen to stabilize the emulsions against the coalescence. The emulsion can either be water-in-oil (W/O) or oil-in-water (O/W), and depending on the composition, the choice of surfactant needs to be tuned by having more hydrophilic or hydrophobic character.[48] The HLB (hydrophilic-lipophilic balance) parameter, which was proposed by Griffin provides a guide for the selection of suitable surfactant:[49]

$$HLB = \frac{20 \cdot M_h}{M} \qquad (2.1.1)$$

where M_h is the molar mass of the hydrophilic head and M is the molar mass of the entire molecule. The HLB ranges between 0 and 20. If the HLB value of a surfactant is between 3 and 8, the surfactant is suitable for W/O system, while O/W emulsifier is between 8 and 18.

The choice of ionic surfactant can also be estimated by using an incremental method, which was proposed by Davis:[50]

$$HLB = 7 + \sum m \cdot H - \sum n \cdot L \qquad (2.1.2)$$

where H and L are experimentally defined numbers with respect to the hydrophilic and lipophilic parts, and m and n are the numbers of hydrophilic and lipophilic groups in the surfactant. For instance, HLB=40 is given for the SDS consisting of SO_4^- head and –(CH2)–12 tail (H=38.7, L=0.47) and substantial polar contribution is to be expected.

2.1.1.4.2 Ostwald ripening

The molecules in small droplets can diffuse into the bigger droplets through the continuous phase. This can lead to an increase in average size of the droplets due to the disappearance of small droplets, a

phenomenon known as *Ostwald ripening*.[51, 52] This arises from the difference in Laplace pressure (P_L), caused by the pressure difference between the inner- and the outer- part of a curved surface, between droplets of different sizes:

$$\Delta P_L = P_{inner} - P_{outer} = \frac{2 \cdot \gamma}{r} \qquad (2.1.3)$$

where γ and r are the interfacial tension and radius of the droplet, respectively. The Laplace pressure is proportional to the interfacial tension between two immiscible phases and inversely proportional to the droplet size. Hence, the molecular diffusion is driven by the higher Laplace pressure in smaller droplets. If all droplets in an emulsion system are the same in size, there is no difference in Laplace pressure between the droplets. Therefore, there would be no net molecular mass transfer among the droplets (caused by Laplace pressure).

It is particularly important to control the Ostwald ripening in the emulsion to obtain uniform and stable droplets. The co-stabilizer (also called osmotic pressure agent) is dissolved in the dispersed phase and creates an osmotic pressure inside the droplets. The osmotic pressure is used to effectively counteract the effect of the Laplace pressure.[53] The addition of the osmotic pressure agent enhances the stability of the miniemulsion.[54, 55] For example, let us consider a model system composed of styrene, water, and hexadecane as a co-stabilizer. After the emulsification, the styrene droplets are dispersed in the continuous phase, and the styrene molecules will diffuse through the continuous phase from smaller droplets to the bigger due to the larger Laplace pressure in the smaller droplets. Since hexadecane is much less soluble in water in comparison to styrene, it will not significantly diffuse through the water phase, at least not on the same timescale as the styrene molecules. Thus, as styrene molecules are diffusing out of the droplet, the local concentration of hexadecane inside the droplet increases and the osmotic pressure in the droplet increases. To minimize the difference of osmotic pressure between the droplets, the concentration of hexadecane should be the same in each droplet. Since the hexadecane molecules are trapped in the droplets, the transport of styrene molecules is required to equilibrate the osmotic pressure between the different droplets. Increasing the droplet size, i.e. having new styrene molecules diffusing in the droplet, would result in a decrease in osmotic pressure. The changes in osmotic pressure and Laplace pressure counterbalance each other and the system reaches a steady-state where the net molecular diffusion of styrene is largely limited.[56, 57] However, since the Laplace pressure is usually (at least in direct

miniemulsions) higher than the osmotic pressure inside the droplet. Directly after the miniemulsion, the overall pressure difference in the system is not zero, but equal in all droplets. Hence, the droplets remain in a metastable state. The collision between the droplets results in a thermodynamic equilibrium of the miniemulsion system, and Laplace pressure and osmotic pressure become equal.

2.1.2 Polymer nanoparticles with complex architectures

Polymer nanoparticles are designed and prepared with various architectures for different applications. The shape, the structure, and the surface functionalization influence the final properties and behavior of the polymer nanoparticles. One interesting method to gain some control over these properties is to design non-homogenous nanoparticles composed of two or more polymers (Figure 2.1.5).

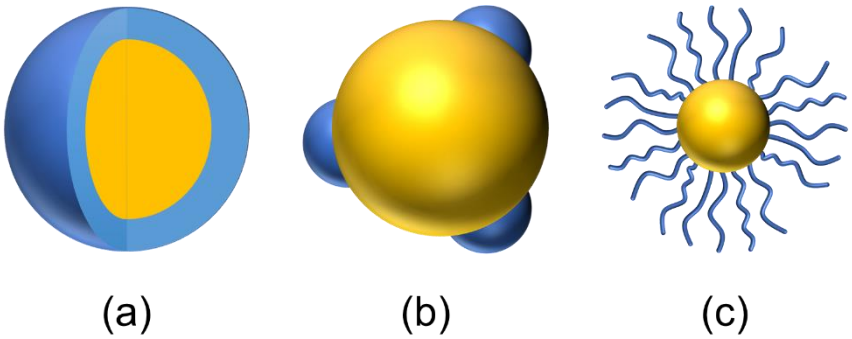

Figure 2.1.5 Multicomponent polymer nanoparticles with (a) core-shell, (b) multidomain, and (c) hairy architecture.

2.1.2.1 Core-shell nanoparticles

Core-shell nanoparticles are composite nanoparticles with a well-defined structure consisting of at least two different materials, one forms a core and another covers the core producing a shell.[58] Core-shell NPs can be fabricated when one of the components interacts more favorably with the continuous phase. For example, in a mixture of polymers, if one of the components has a lower interfacial tension with the solvents in comparison to other components, it will form a shell encapsulating the other components.[59]

A variety of core-shell NPs has been reported with the different combinations of polymers and solvents. When a mixture of amine-functionalized polystyrene and polyisoprene (PI) is added into a solvent mixture of THF and water, PI forms a core and PS-NH_2 covers the core making a shell.[60] In the case of inorganic cores not interacting favorably with the solvent, the inorganic cores tend to be encapsulated by the polymer shell to minimize the interfacial energy.[61] Hence, it is important to choose the suitable components and solvent condition to design the core-shell nanoparticles.

2.1.2.2 Multi-domain nanoparticles

Multi-domain nanoparticles are nanomaterials where the main component includes domains or islands of one or multiple other components, in the particle itself or on the surface, caused by site-specific functionalization or by the constrained phase separation of two or more components.[62] When nanomaterials are composed of two parts with different compositions or properties, they are called *Janus nanoparticles*. The multi-domain nanoparticles can be prepared by various methods such as hierarchical self-assembly of block copolymer, seeded emulsion polymerization, phase separation of two mixtures, direct grafting of hetero-component from the surface, and so on.[63-65] This kind of multi-domain nanoparticles provides different chemical or physical properties in one object. For instance, multidomain nanoparticles can aggregate into hierarchical complex superstructures in a selected solvent or heating condition.[66-68] In addition, the mobile chains in multidomain nanoparticles are able to respond to different external stimuli.[69] Particularly, it is useful to design a suitable nanovehicle for controlled motion.[70]

2.1.2.3 Hairy nanoparticles

The direct immobilization of polymer chains onto the surface of a NP *via* covalent bond provides a new type of multicomponent NP architecture, called hairy NPs. Interestingly, hairy NPs combine the unique features of both NP cores and tethered polymer chains.[71] The surface properties and behavior of hairy NPs are largely influenced by the chain conformation of the polymer chains grafted on the NP surfaces. There are few parameters affecting the chain conformation, such as grafting density (σ), chain length and particle size, shape and solvent condition. The methods for the preparation of hairy NPs can be divided into three categories: “grafting from”, “grafting to”, and one-pot synthesis.[72] When brushes with high grafting density are desired, the direct grafting-from method is preferred.

2.1.3 Behavior of nanoparticles in suspension

2.1.3.1 Interaction between nanoparticles

There are several important interactions to consider that occurs between nanoparticles in a colloidal suspension such as Van der Waals force, hydrophilic and hydrophobic interactions, hydrogen bonding. Van der Waals forces are very important interactions at short distances to determine the behavior of nanoparticles. It is a distance dependent attraction of intermolecular forces between molecules, atoms, or particles. The attractive VdW forces are the result of the induced dipoles in particles due to the random fluctuation of electron density. Van der Waals interactions are very strong at short distances, but decrease rapidly when the distance between the objects increases. Thus, particles aggregating because of the VdW attractive force are difficult to redisperse in suspension without the use of high energy. However, at longer distances, Van der Waals forces are not very effective and do not significantly influence the stability of colloids.[73]

Hydrogen bonding is responsible for the interaction of nanoparticles in a suspension. This is particularly important to tailor the properties of nanoparticles used in the presence of biomolecules. It has been used to trigger the reversible assembly of nanoparticles in suspension.[74-76]

2.1.3.2 Stabilization of nanoparticles

Electrostatic stabilization is often obtained by repulsive coulombic forces caused by the interaction of charged surfaces.[77] In particular, when a colloidal system is stabilized using ionic surfactants or stabilizers, the Deryaguin-Landau-Verwey-Overbeek (DLVO) theory can be used to analyze the stability of the system.[77, 78] The DLVO theory combines van der Waals attractive force and electrostatic repulsion created by the interactions between the electric double layer of the NPs caused by the presence of counterions at the surface induced by the presence of surface charges. The DLVO theory can be used to predict if a suspension will be aggregated or dispersed:

$$G_T = G_R + G_A \tag{2.1.4}$$

where G_T is the total potential energy of interaction between two particles at a certain distance, G_R is the potential energy of repulsion and G_A the potential energy of attraction.

The interaction between the particles varies as a function of the distance between two particles (Figure 2.1.6). The primary minimum (I) results from van der Waals attraction at close range and represents the coagulation. The electrostatic repulsion generates the primary maximum at a longer distance (II). The energy barrier determines the stability of colloids. Hence, when the energy barrier is high enough, the colloidal system is stable and there is no irreversible coagulation caused by the high van der Waals force at a short distance. The secondary minimum (III) is observed a longer distance than II, and it is where weak reversible aggregation of particles can take place.[77, 79]

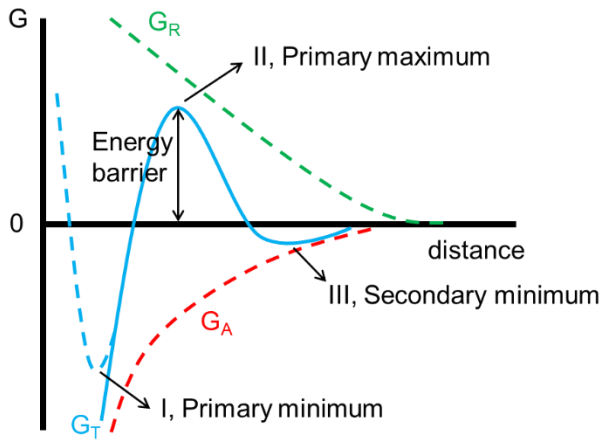

Figure 2.1.6 Illustration of the potential energy of interaction between two particles as a function of distance.

The colloidal stability can also be achieved by steric stabilization by adsorbing non-ionic surfactant at the surface of particles.[78] The block-copolymer type surfactants possessing hydrophilic and hydrophobic chain adsorb at the surface of particles. The block exposed to the continuous phase provides the steric hindrance to the particles to avoid the attractive forces. When the entire surface of the particle is covered by surfactants, the steric stabilization is very effective in comparison to particles that are only partially covered by surfactants.[77, 78]

2.1.3.3 Flow behavior of colloidal suspensions

The behavior of NPs in suspension is important for the use and the processing of colloidal dispersion. For example, some colloidal suspensions have shown shear thickening behavior, characterized by a sudden increase in viscosity at a high shear rate, and their rheological behavior was investigated to resolve

problems occurring during processing steps such as coating and mixing.[80, 81] The understanding of the behavior of the NPs in suspension has now led to the development of colloids taking advantage of this unique behavior, for example, smart fluids used in protective systems to prevent damages by absorbing shocks created by direct impacts.[82]

Shear-thinning behavior, characterized by a decrease of viscosity at high shear rates, occurs in colloidal suspension when the NPs or NPs assemblies are deformable under the application of a shear force (Figure 2.1.7).[83, 84] The soft NPs experience the spatial rearrangement deviating from the equilibrium arrangement. When the applied shear rate is removed, the deformed arrangement of the NPs in suspension is restored to the equilibrium conformation due to the Brownian motion.

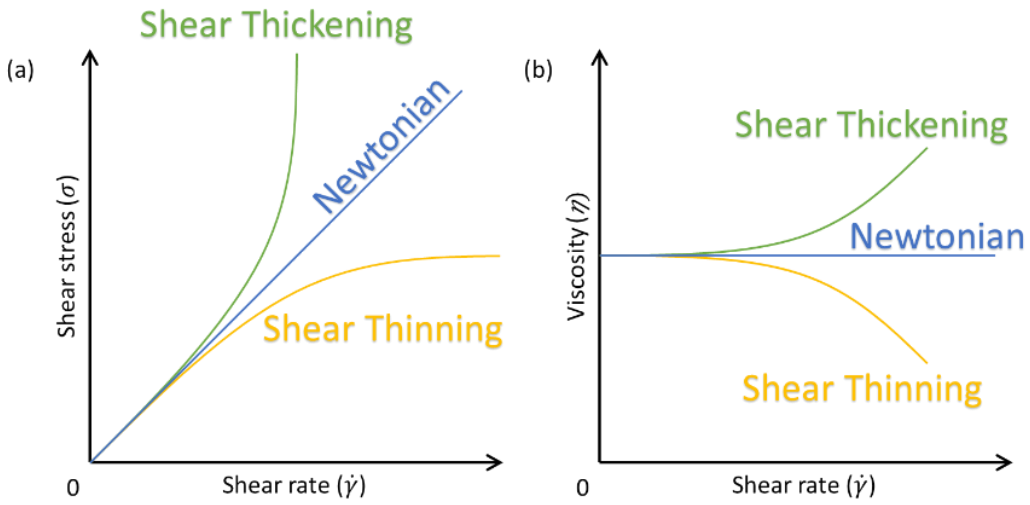

Figure 2.1.7 (a) Shear stress and (b) viscosity of shear thickening, shear thinning, and Newtonian fluids influenced by variable imposed shear rate.

Shear thickening behavior, observed in the shock-absorbing fluid, is a non-Newtonian behavior and it can be observed in colloidal suspensions where solid particles (SiO_2, $CaCO_3$, CNT) are dispersed in pure liquids (water, ethylene glycol, poly(ethylene glycol)).[85, 86] Since pure liquids behave like Newtonian fluids, the shear-thickening behavior is attributed to the presence of NPs in suspension. At a low shear rate, the NPs are randomly distributed in the pure liquid. Once the shear rate increases, NPs start to align through pseudo-layer structures and exhibit shear-thinning behavior characterized by a decrease in viscosity. When the shear rate further increases beyond a critical shear rate, the aligned structures of NPs

are broken down, and the NPs form clusters by hydroclustering, and the suspension shows a shear thickening behavior characterized by a dramatic increase in viscosity (Figure 2.1.8).[87, 88]

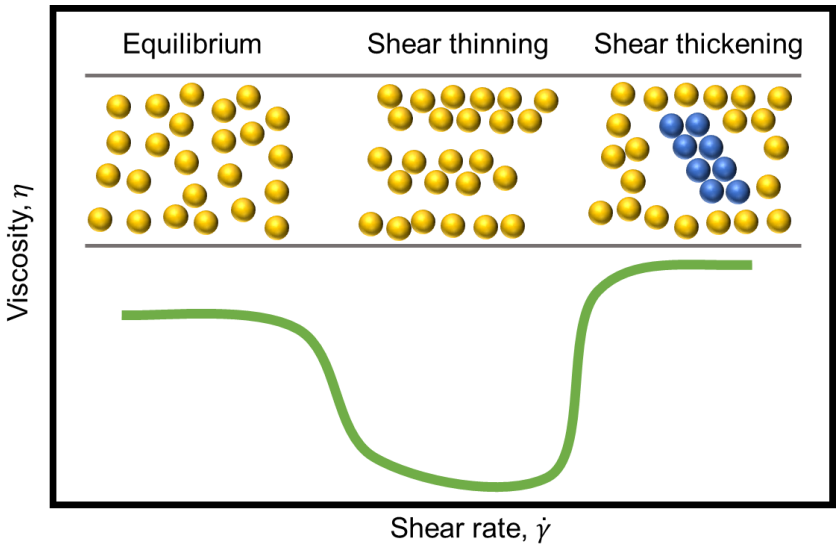

Figure 2.1.8 Schematic description of equilibrium, shear thinning and shear thickening behavior of suspensions.

2.2 Functionalization of nanoparticles with end-tethered polymer chains

Polymer chains grafted to a surface have been extensively chosen to tailor the chemical and physical properties of surfaces in the field of surface and interface engineering, such as stimuli-responsive surfaces, antibiofouling surfaces, colloidal stabilization, wetting and lubrication.[17, 89-94] Once the polymer brushes are tethered to the surface, the properties are changed compared to both the unmodified surface and the untethered polymer chains. There are two main reasons that polymer brushes have unique properties. One is the immobilization of chain end and the other is the brush regimes due to the close proximity of tethered chains to the neighboring ones. When individual polymer chains are immobilized by one chain end to a surface, at a relatively high surface coverage, they are called *polymer brushes*. [95]

2.2.1 Behavior of end-tethered polymers

2.2.1.1 Alexander-de Gennes model

Alexander and de Gennes (AdG) established the basic theory describing the behavior of end-tethered polymer chains. In the AdG scaling model, the thickness of the grafted polymer layer (h) at the equilibrium is obtained by a balance of the free energy associated with the stretching of the polymer "blobs" and the energy involved in the excluded volume interactions.[19] However, the AdG theory has some limitations when it comes to discussing the details of the polymer structure, such as the chain conformations. In the AdG theory, the density profile is modeled by a step-like density profile.

In a good solvent, the chains stretch away from the surface to avoid unfavorable segment-segment interaction, the polymer chains lose conformational entropy due to the reduction in the possible number of conformations, and the interaction between polymer segments and solvent molecules are favored. At

the swelling equilibrium, the height (h) of the grafted polymer layer is described as a function of the number and diameter of the polymer blobs.

$$h = Na(\sigma a^2)^{1/3} \quad (2.2.1)$$

where N and a are the number of monomers and the size of the monomer units, σ is grafting density.

2.2.1.2 Daoud-Cotton model

Daoud and Cotton extended the AdG model by studying polymer grafted to curved substrates.[96] The major difference in comparison to the AdG model is the size of the blobs increases with increasing distance from the surface, all blobs at the same distance from the surface have the same size. The Daoud-Cotton model describes the decay of the density of monomers (ϕ) from the center by a scaling law. There are f arms (polymer chains) linked at the center of the star shape. The arms are considered to each have N statistical units with length l.

There are three different regions with different chain conformation of the end-grafted polymers (Figure 2.2.1). In the swollen region ($r > r_1$), the random coil domain the distance from the center is large. The arms inside the blob behave like a single chain. Hence, the arms are supposed to be swollen in a good solvent. In this region, excluded volume effects are present in the blob. The diameter of the blob ($\xi(r)$) is described as a function of the distance (r) from the center:

$$\xi(r) \sim rf^{-1/2} \quad (2.2.2)$$

The local monomer concentration in this region is also defined:

$$\varphi(r) \sim \left(\frac{r}{l}\right)^{-4/3} v^{-1/3} f^{2/3} \quad (2.2.3)$$

where v is the monomer excluded volume parameter.

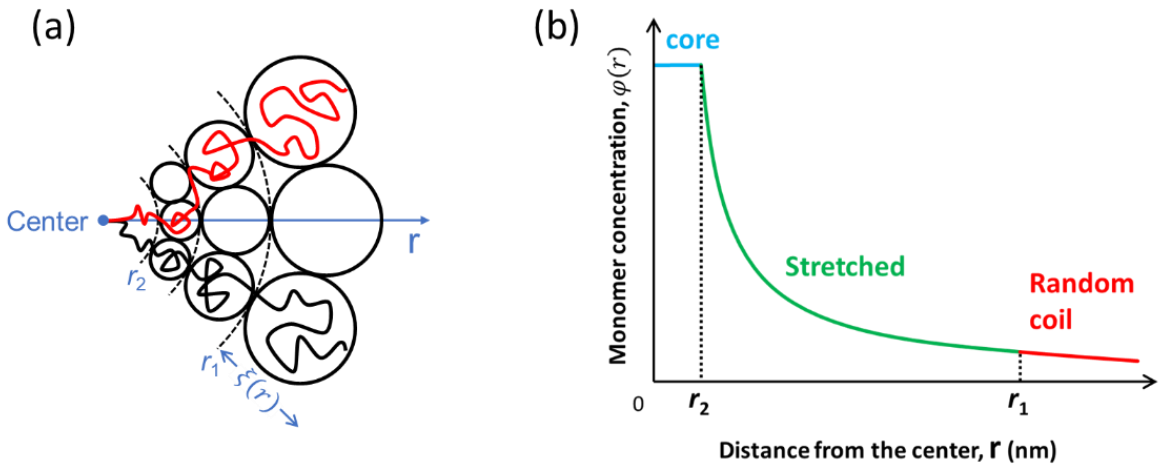

Figure 2.2.1 (a) Representative illustration of stretched polymer chains from star-shape polymers. (b) The monomer concentration profile from the core of the star-shape polymer.

In the unswollen region (r_2 < r < r_1), the distance from the center is small and the swelling parameter becomes unity. Thus, the concentration of monomer is sufficiently high to ignore the excluded volume. The crossover distance from random coil to stretched (r_1) is obtained between swollen and unswollen regime of the blobs (see also Figure 2.2.1):

$$r_1 \sim f^{1/2} v^{-1} l \tag{2.2.4}$$

If the distance from the blob to the center is smaller than r_1, the blobs are not swollen any longer. In this situation, blob size and local monomer density are defined:

$$\xi(r) \sim r f^{-1/2} \tag{2.2.5}$$

$$\varphi(r) \sim \left(\frac{r}{l}\right)^{-1} f^{1/2} \tag{2.2.6}$$

In the core region ($r_2 > r$), the monomer concentration is unity and no blobs are found in this region:

$$r_2 \sim f^{1/2} l \tag{2.2.7}$$

From the above results, the radius of a star shape polymer (R) can be evaluated:

$$R \sim \left[Nf + \frac{1}{10}\frac{f^{3/2}}{v^2} + \frac{1}{6}f^{3/2}\right]^{3/5} v^{1/5} f^{-2/5} l \qquad (2.2.8)$$

Depending on the chain regime, the radius of star shape polymer has a different relationship in a good solvent (Table 2.2.1). In the case of nanoparticles functionalized with polymer chains, the core region is redefined as the combination of the NPs core itself.

Table 2.2.1 Relationship between radius, number of arms and monomers and excluded volume in the different regime

	Regime	**Radius, *R***
Random coil	$N > f^{1/2}v^{-2}$	$N^{3/5}v^{1/5}f^{1/5}l$
Swollen Polymer chain	$f^{1/2}v^{-2} > N > f^{1/2}$	$N^{1/2}f^{1/4}l$
Unswollen polymer chains	$f^{1/2} > N$	$(Nf)^{1/3}l$

2.2.1.3 Grafting density

The end-tethered polymer chains on flat substrates show three different regimes depending on the grafting density: mushroom, constrained polymer chains, and stretched polymer chains, also called polymer brushes (Figure 2.2.2). For the mushroom conformation, the distance between neighboring chains is large enough ($D > 2R_g$), and the thickness of mushroom layer is $h{\sim}2R_g$. In this regime, the conformation of the polymer chain is a random coil not dissimilar to a free chain. As the grafting density increases, the distance between neighboring chains becomes short ($D < 2R_g$), and to avoid overlapping, chains stretches away showing stretched conformation. The thickness of the polymer brush layer scaled as functions of degree of polymerization and grafting density ($h{\sim}N\sigma^x, \frac{1}{3} \leq x < 1$). When the polymer chains are grafted to a flat substrate, the polymer brush regime does not change with the increase of thickness of the brush layer.

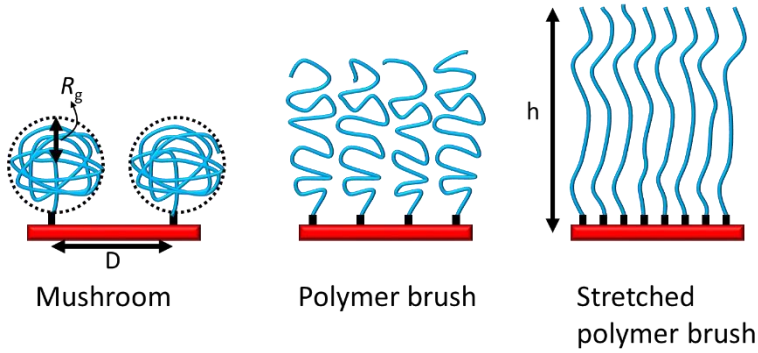

Figure 2.2.2 Graphical description of polymer brushes on a flat substrate.

Unlike planar substrate, as chain length increases, polymer brushes on the curved-substrate show a transition of brush regimes from unswollen to swollen (Figure 2.2.3).

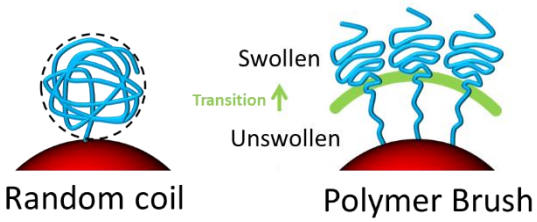

Figure 2.2.3 Illustration of polymer brushes on a curved substrate.

In the random coil regime, the bushes are sparsely grafted on the substrate, and the distance between the chains is far enough. Thus, there is no overlapping of chains. The thickness of the brush layer (h) can be scaled as a function of the degree of polymerization (N) and grafting density (σ):[97, 98]

$$h \propto N^{0.6} \approx R_g \tag{2.2.9}$$

where R_g is the radius of gyration of the grafted chain.

In swollen polymer brush regime, as the grafting density increases, it reaches to the threshold grafting density. In this region, chains start to overlap. The thickness scaled as:

$$h \propto N^{0.6}\sigma^{0.2}{R_c}^{0.4} \tag{2.2.10}$$

where R_c is the radius of core.

In the unswollen polymer brush regime, the polymer chains are densely grafted and placed at a close distance on the substrate. In a good solvent, the repulsive interaction occurs between neighboring brushes. Therefore, the brushes adopt a stretched conformation to compensate for the entropy loss:

$$h \propto N^{x}\sigma^{0.5x}(0.6 < x \leq 1) \quad (2.2.11)$$

2.2.2 Dynamics of polymer brushes

A polymer chain consists of small repeating monomeric subsegments bonded together to form a long chain. A subsegment composed of between 6~12 monomers represents a Kuhn segment. This is the basic scale to define the size of a chain segment. The Kuhn segment of a given polymer is derived from the end-to-end distance of a chain under the θ-condition of Flory.

The *Rouse-Bueche model* describes a polymer chain composed of a series of segments or beads connected by springs (Figure 2.2.4a).[99, 100] The beads can be viewed as the mass connected by springs following Hooke's law with a restoring force (spring) constant (f). When the segments are immersed in a solvent, they shift through other polymer chains and segments. This viscous medium causes a drag force to the system and slows down the motion. Since the Rouse model only considers friction factor (ρ), to explain intermolecular interactions, this model is limited to unentangled polymer systems such as polymer melt, low concentration of polymer solution, or low molecular weight below entanglement:

$$f = \rho(\frac{dx}{dt}) \quad (2.2.12)$$

$$D \sim N^{-1} \quad (2.2.13)$$

$$T \sim NR^{-1} \quad (2.2.14)$$

where $\frac{dx}{dt}$ is the displacement of a bead over time, D is the diffusion coefficient, T is the relaxation time, and N and R are the number of beads and size of the chain, respectively.

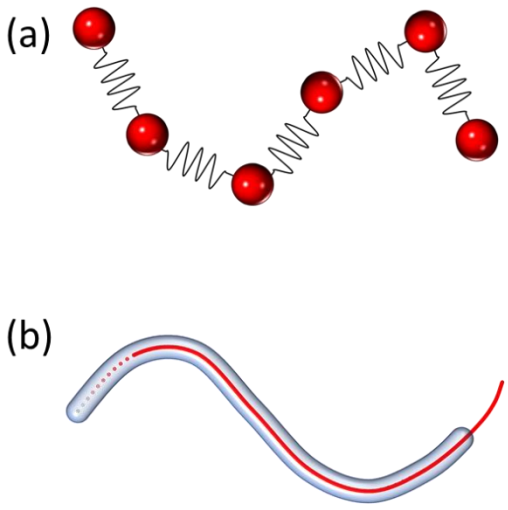

Figure 2.2.4 Illustrations of (a) Rouse's bead and spring model and (b) de Gennes' reptation model for a polymer chain.

Later, *Zimm* introduced the concepts of Brownian motion and hydrodynamic interactions. The friction factor was then replaced by the macroscopic viscosity of the medium. In consequence, the diffusion coefficient and relaxation times of polymer solution can be described by:

$$D \sim R^{-1} \tag{2.2.15}$$

$$T \sim R^{3} \tag{2.2.16}$$

De Gennes established a model for the long-range motion of polymer chains (Figure 2.2.4b).[101] The *reptation theory* which involves polymer chains trapped inside a tube-like structure. The chain moves through the tube-like structure with a snake-like motion, the reptation. The tube is made up of the entanglements of the surrounding polymer chains. Using scaling concepts, de Gennes found a relationship between self-diffusion coefficient *D* of a chain with a molecular weight *M* trapped in an entangled polymer system to scaled as: [102]

$$D \propto M^{-2} \tag{2.2.17}$$

De Gennes and Doi Edwards developed the tube reptation model predicting five different regimes for the chain motion (Figure 2.2.5).[101, 103] These motions are observed at distinct ranges of correlation time

and distance; and the different regimes of movement can be probed using different characterization methods.

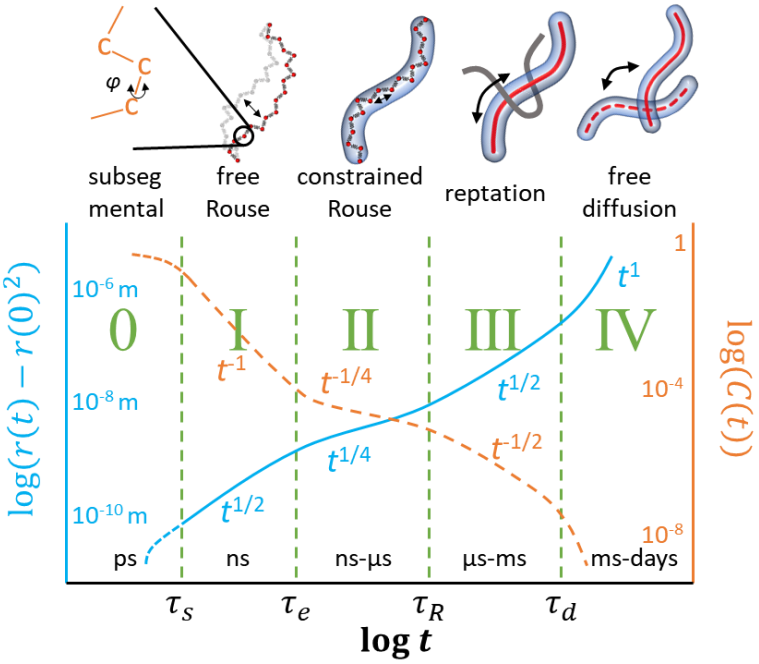

Figure 2.2.5 Tube-reptation regimes of linear polymers and mean-square displacements.[104]

The dynamics of polymer brushes is distinct from free polymer chains. For example, even if the grafted chain length is longer than the entanglement molecular weight, no entanglement can be found. The dynamics of end-tethered polymer chains vary depending on the grafting density, length of the chain and size of the core.[103] The relaxation time of free polymer chain in a good solvent condition follows standard Rouse and Zimm model as provided in eq. 2.2.14 and 2.2.16.[105] However, when the chains are fixed to the substrate, the polymer brushes can interact with the substrate or with the neighboring chains differently than free chains. Thus, the relaxation times of grafted polymer chains cannot be predicted, in a straight forward manner, using the standard models due to the intrinsic physical constraints in grafted polymer systems.[106, 107]

Experimentally, the dynamics of polymer brushes has been shown to be different from that of free polymer chains. Because one end of the chain is anchored to the substrate and the brush adopts stretched conformation under the influence of the steric hindrance created by neighboring chains, this completely hinders the free diffusion of the chains itself, but also affects the segmental and subsegmental motions of

the chains. For example, only the local subsegmental chain motions have been observed for polymer chains in the unswollen polymer brush regime as measured using NMR spin relaxation, neutron back scattering, or dielectric spectroscopy.[33] However, for chains in the swollen polymer brush regime, when the length of polymer brushes was sufficiently long, the chains adopt a more relaxed conformation and long-range movements, similar to constrain Rouse motion, have been observed.

2.2.3 Synthesis of brushes

2.2.3.1 Grafting strategy

There are two main strategies to synthesize polymer brushes: grafting-to and grafting-from. In the "grafting-to" approach, pre-polymerized polymer chains having functional groups at the end of the chain are attached to a surface. The pre-synthesized polymer chains are often prepared by living or controlled polymerization techniques by adding the functional groups at the beginning or at the end of the reaction. The advantages of this approach are the simplicity of synthesis and well-controlled polymer chain length. The main limitation of this approach is the difficulty in obtaining high grafting densities due to steric interactions between grafted chains and incoming species.

In the "grafting-from" approach, polymer brushes are grown *in situ*. The first step in the preparation brushes using this approach is to immobilize an initiator to the substrate. Then, the polymer chains are grown, monomer by monomer, from those tethering points using controlled polymerization methods such as reversible addition−fragmentation chain-transfer polymerization, nirtoxide mediated polymerization and atom transfer radical polymerization. The important advantage of the "grafting-from" approach is the ease in obtaining high grafting density. It is possible to precisely control the grafting density by controlling the number of initiators on the surface. However, the associated drawback is that the dispersity of chain length increased when the grafting density is very large due to the steric hindrance during the polymerization.

2.2.3.2 Surface initiated-atom transfer radical polymerization

Atom transfer radical polymerization (ATRP) has imposed itself as one of the most used methods to perform controlled polymerization due to its versatility in terms of initiators, monomer choices, and the relatively mild reaction conditions required.[108] Most ATRP systems are based on the use of a complex between a transition metal and an initiator having a carbon-halogen bond. The control of ATRP reaction

highly depends on the reversible redox activation of a dormant alkyl halide terminated polymer chain end by a halogen transfer to the transition metal complex, commonly a copper complex. The cleavage of the carbon-halogen linkage produces a free and active carbon-centered radical species at the initiating site. The activation is based on an electron transfer from the transition metal-ligand complex to the halogen atom. This process results in the oxidation of the transition metal-ligand complex. Afterward, a fast reversible reaction occurs involving the reduction of the catalyst to change the growing radical chain end back to the halogen-ended dormant species. Various parameters influence the kinetics of ATRP and can be used to tune the reaction condition, such as ligand to transition metal ratio, $Metal^{II}$ to $Metal^{I}$ ratio, ligand, counterion, solvent, or initiator:

$$R_p = k_p K_{ATRP} \frac{[RX][Mt^n Ligand]}{[Mt^{n+1} Ligand - X]}[M] \qquad (2.2.18)$$

Surface initiated-ATRP (SI-ATRP) was first reported in 1997 when poly(acrylamide) brushes were successfully grafted from benzylchloride-derivatized silica particles.[25, 109] To perform SI-ATRP, the initiator used for traditional ATRP must be immobilized on a surface (Figure 2.2.6). The same transition metal complexes are used as in conventional ATRP to graft polymer brushes in a controlled manner from the functionalized substrates. The number of initiators on the surface directly controls the grafting density of brushes. However, the kinetics of SI-ATRP is different from the kinetic of conventional ATRP.[110] When a high concentration of catalysts is used in the polymerization, a high concentration of radicals can be produced. Thus, rapid initial growth is found with the early termination. However, low catalyst concentration yields limited chain growth. If the solution is strongly agitated, this can also lead to early termination. This might be due to the increased mobility of chain ends, leading to an increased possibility of termination via combination or disproportionation.

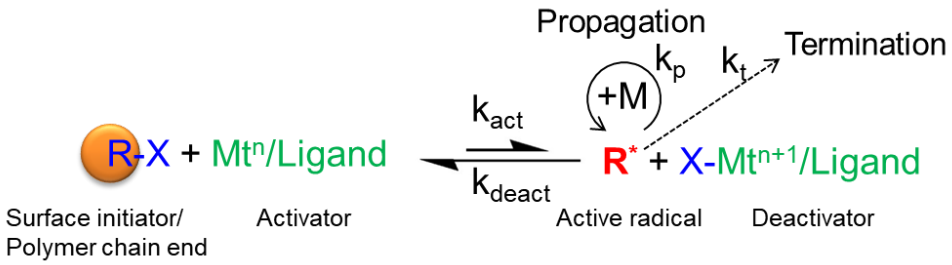

Figure 2.2.6 Schematic description of SI-ATRP.

2.2.4 Application

Nanoparticles modified with surface-immobilized polymer chains have been used in a variety of applications due to the functionalities that the brushes can provide. For example, polymer-functionalized nanoparticles are being used in nanocomposites, drug delivery and lubricants. In such applications, the influence of the nanoparticles can be enhanced by the presence of a layer of end-tethered chains.

2.2.4.1 Nanocomposite

A nanocomposite is composed of NPs used as a reinforcing agent dispersed in a polymer matrix. Nanocomposites show a unique feature that they have the functionality of NPs as well as the processability of a polymer matrix. As NPs are incorporated in the polymer matrix, nanocomposite can provide good mechanical, electrical, optical or magnetic properties to the polymer matrix and these enhanced properties can be easily tuned by varying the concentration of NPs or molecular weight of polymer matrix. Depending on the composition, nanocomposites can be classified into several subcategories, for example, inorganic/polymer nanocomposite,[111] inorganic/organic hybrid nanocomposite,[112] polymer/polymer nanocomposite,[113] and bionanocomposite.[114] Owing to the improvements in mechanical, thermal, electrical (and so on) properties, nanocomposites are finding more and more industrial applications and are, as well, a topic of fundamental studies. Such nanocomposites have been used in an array of applications such as drug delivery system,[115] anti-corrosion coatings,[116] UV protective agents,[117] lubricants,[118] scratch-free paint,[119] flame retardant,[120] abrasion resist agents,[121] high-performance fibers and films.[122, 123]

The state of dispersion of nanoparticles in a polymer matrix is one of the key factors to achieve reinforced properties of nanocomposites. [124-126] Controlling the surface properties of the nanoparticles is crucial in the development of nanocomposites for industrial materials. An efficient manner to produce nanocomposite consists of dispersing nanoparticles functionalized with grafted polymer chains in a polymer matrix. The presence of strong interaction, such as interpenetration and entanglement, between the grafted chains and the polymer matrix leads to a significant enhancement in the mechanical properties of the composite. For instance, polystyrene grafted silver nanoparticles were dispersed in a polystyrene matrix and showed excellent miscibility with effective antibacterial activity.[127] When dealing with polymer brush grafted nanoparticles, it is possible to fabricate the nanocomposites composed solely of hairy nanoparticles. It is called one-component-

nanocomposites.[128-130] The big advantage of this approach is that a high loading amount of nanoparticles in the nanocomposite can be achieved. This high NPs loading is closely related to the thermomechanical properties of nanocomposite. For example, polystyrene reinforced by polystyrene-grafted silica nanoparticles showed significant reinforcement in the elastic modulus of the resulting composite. [131]

2.2.4.2 Drug delivery

In some cases, the therapeutic effect of a drug can be improved and its side effects reduced when the active molecule is encapsulated in a nanocarrier. The use of nanocarriers for drug delivery can improve the local concentration of drug by protecting the drug from rapid degradation, delivering the drug safely to the destination, and releasing the drug at the targeted tissue.[132] By designing the right polymer nanocarrier systems for drug delivery it is possible to improve the efficacy of drugs while reducing their side-effect. Nanocarriers also have additional advantages in terms of solubility, bioavailability, surface area, and versatility of use.

A nanocarrier-based drug delivery system consists of at least two components, the pharmaceutically active ingredient and the carrier material. However, there is an accumulation of experimental evidence that the surface functionalization of the nanocarrier is an important factor in controlling the fate of the nanocarrier both in vitro and in vivo. In order to achieve high efficiency of drug delivery using nanoparticles, it is essential for the carriers to have high biocompatibility, colloidal stability in the physiological environment and during blood circulation. Those properties can be influenced by attaching polymer chains to the surface of the nanocarriers. [133-137]

2.2.4.3 Lubricant

Polymer-grafted nanoparticles can be utilized as a lubricant. The low friction of surfaces functionalized with end-tethered polymer chains has been observed for surface-functionalized with chains having a low degree of polymerization.[138] This is consistent with the expectation that stretched chain conformations absorb solvent molecules and repel other bigger external molecules and other components. Thus, a high grafting density and a low degree of polymerization of the grafted chains are required to achieve high lubrication efficiency.[139] For example, poly(3-sulfopropyl methacrylate potassium salt) (PSPMK) brushes were grafted from the surface of PNIPAM particle, and the negatively charged PSPMK brushes played the role of a bio-mimicking lubricant.[140] Recently, poly(alkyl methacrylate)-grafted

nanoparticles were used as an additive in poly(α-olefin) lubricating oil.[141] The polymer brush-based additive was stable in the base oil at a temperature of 100 °C over 55 days. The friction between surfaces covered with this lubricating oil was considerably decreased.

3. Characterization methods

3.1 NMR relaxometry

Nuclear magnetic resonance (NMR) spectroscopy is a powerful tool for the study of polymer materials. In addition to the identification of the chemical composition, NMR spectroscopy can be used to address questions like structure and dynamics using a variety of acquisition techniques and pulse sequences. For example, NMR spectroscopy can be used to measure the relaxation times of the excited nucleus and thus provides detailed information on the molecular motions of polymers in the nanosecond to picosecond time scale.

3.1.1 Relaxation in NMR

The resonance of the nuclear spins in a magnetic field occurs due to the interaction of the magnetic moment of nuclei with an external magnetic field, B_0. When a nucleus with a non-zero spin is placed in a magnetic field, the energy difference between different orientations of the spin becomes non-null (the Zeeman effect), $\triangle E$, increases when the strength of applied magnetic field increases:[142]

$$\Delta E = \gamma \hbar B_0 \qquad (3.1.1)$$

where $\hbar$ is the reduced Planck constant $h/2\pi$ and γ is the gyromagnetic ratio. For a proton, of spin ± ½, two orientations of the spin are possible, and at thermal equilibrium, the population ratio of between the two energy levels of the spins of a proton in an external magnetic field is governed by the Boltzmann distribution;[143]

$$\frac{n_\beta}{n_\alpha} = e^{-\Delta E/k_B T} \tag{3.1.2}$$

where k_B is the Boltzmann's constant and T is the temperature, and n_α and n_β are the populations of lower (m=+1/2) and upper (m=-1/2) energy levels. The spin transition ($\alpha \rightarrow \beta$) can be induced by the application of a radio-frequency pulse to the system corresponding to the Larmor frequency, ω_0, of the nuclei:

$$\omega_0 = \gamma B_0 \tag{3.1.3}$$

When the RF pulse is removed, the excited spins return to the equilibrium population. This process is called NMR relaxation. As the population of spins returns the equilibrium magnetization in the z-axis, the energy released is dissipated in the surrounding environment, also called the lattice. Such changes in the spin populations can be described by first-order exponential equation and be characterized by a time constant T_1:

$$\Delta n(\tau) = \Delta n_{eq}[1 - \exp\left(-\frac{\tau}{T_1}\right)] \tag{3.1.4}$$

where $\triangle n_{eq}$ is the equilibrium population difference and τ is the delay time.

Transverse or spin-spin relaxation (T_2) is another relaxation mechanism, T_2 is the measure of the decay of the magnetization in the perpendicular plane (transverse) to the external magnetic field B_0 after the RF pulse. The decay of the transverse magnetization results from the loss of phase coherence in the spin system due to the local magnetic field fluctuations during the measurement. The spins are mobile depending on their surroundings, and these spins experience marginally different local magnetic field strengths in the system. Thus, each spin precesses at a slightly different frequency deviating from the average Larmor frequency. The dephasing of transverse magnetization is also affected by the imperfection of the external magnetic field as well as the energy exchange between spins. There is no transfer of the spin-spin potential energy into the surrounding. T_2 relaxation takes place faster than T_1. In general, the decrease of magnetization in transverse plane M_{xy} is described by an exponential function with a time constant T_2.

3.1.2 Measurement of NMR relaxation

The inversion recovery pulse sequence is widely used to measure T_1 relaxation. The pulse sequence is described in Figure 3.1.1.[143] Before any perturbation, the net magnetization is aligned along the +z-axis due to the field of the magnet B_0. At the beginning of the inversion recovery sequence, a $180°_x$ pulse is applied to rotate the net nuclear magnetization to the –*z*-axis. During the delay time τ, the spins undergo fragmentary spin-lattice relaxation. The net magnetization returns toward its equilibrium state to the +*z*-axis. After a delay time τ, a $90°_x$ pulse is applied to rotate the longitudinal nuclear magnetization to the $x-y$ plane. The spins rotated to the x-y plane have a precession motion around the *z*-axis. A free induction decay is recorded for different delay time τ. The observed signal intensity $M_z(\tau)$ is described by an exponential decay:

$$\frac{M_z(\tau)}{M_z(0)} = 1 - 2\exp\left(-\frac{\tau}{T_1}\right) \tag{3.1.5}$$

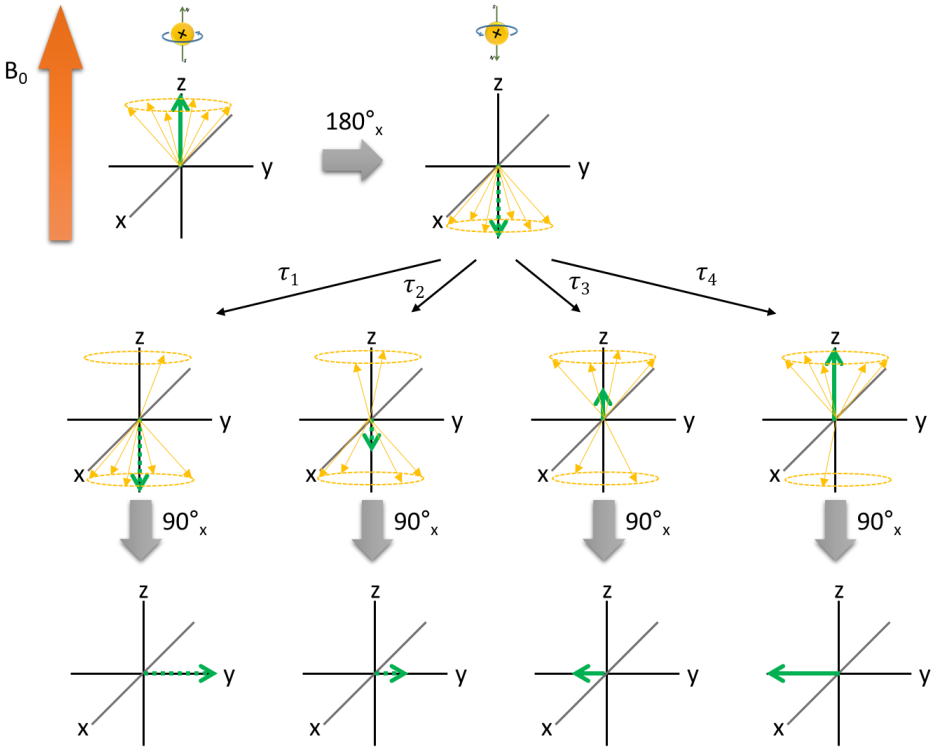

Figure 3.1.1 (a) The inverse recovery sequence and (b) the illustration of recovery of M_z.

T_2 can be numerically explained that the time required to lose 63% of the phase of the magnetization in the transverse (x-y) plane after the perturbation by a $90°_x$ pulse.[143] The dephasing is mainly caused by

the spin-spin interactions without energy exchange with the surroundings due to the local variation of the magnetic field. However, the inhomogeneities in the magnetic fields promote the dephasing, resulting in shorter decay times. In order to avoid the effects of the inhomogeneity of the magnet and the consequence of molecule diffusing during the measurement, the Carr-Purcell-Meiboom-Gill (CPMG) pulse sequence ($90°_x - (\tau - 180°_y - \tau)_n$-acquisition) was developed in 1950, based on the classic spin-echo pulse-sequence (Figure 3.1.2). The magnetization is aligned along the x-axis by the first $90°_x$ pulse. During the following period τ, the x-y magnetization dephases and, then, the magnetization is flipped by a $180°_y$ pulse. The magnetization refocuses along the x-axis to yield the echo after a time τ. Due to the relaxation, an incomplete refocusing of the initial magnetization is observed. The value of T_2 is obtained from the reduction of the signal after a different number of echo cycles. After repeating multiple $180°_y$ pulse separated by a time 2τ – corresponding to multiple echo cycles – the reduction of magnetization after the spin-echo can be fitted to:

$$M_{xy}(\tau) = M_{xy}(0)\exp\left(-\frac{\tau}{T_2}\right) \qquad (3.1.6)$$

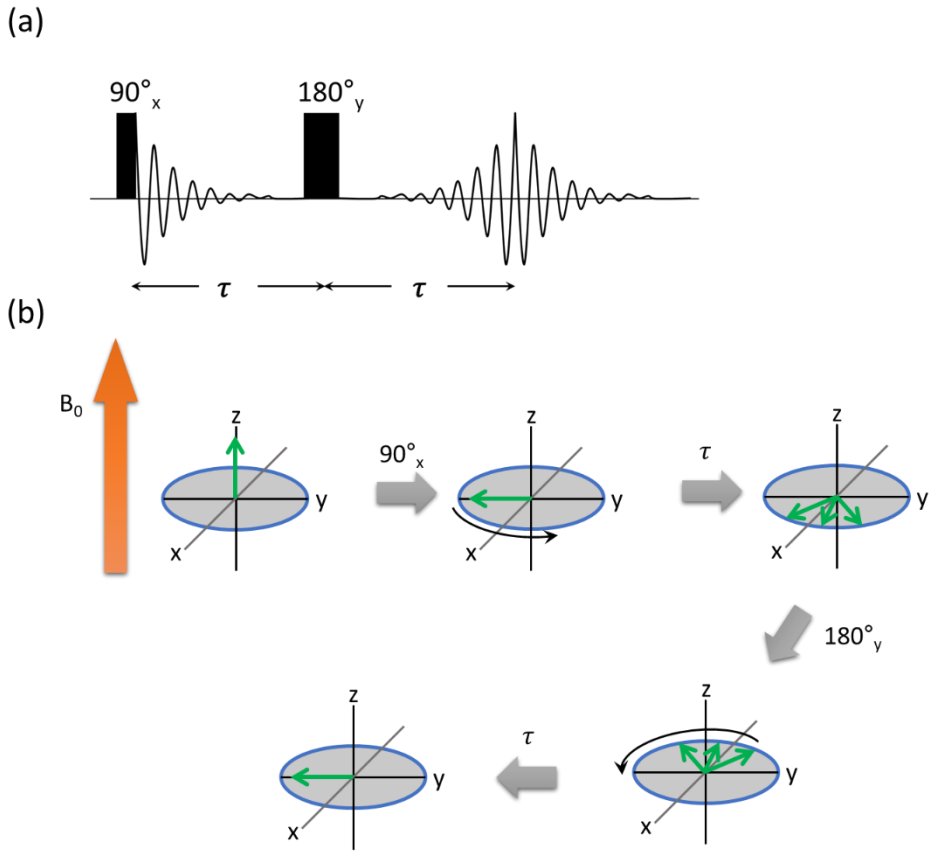

Figure 3.1.2 (a) The CPMG sequence and (b) the description of dephasing of transverse magnetization.

3.1.3 NMR relaxation for the molecular dynamics

T_1 and T_2 relaxation processes involve transitions between excited and ground state energy levels. The transitions are stimulated by fluctuating magnetic fields at the transition frequencies. Thus, the relaxation times can be determined by measuring the relaxation of the relevant nuclei. Fluctuations of the local magnetic fields in nuclei part of polymer chains are ascribed to the movements of nuclei relative to adjacent spins or lattices, or relative to the overall external magnetic fields. Therefore, relaxation processes are highly sensitive to molecular motion. And the time scale of the motion accessible by measuring T_1 and T_2 relaxation is in the range of picoseconds to nanoseconds.

The magnetic field dependence of spin-lattice, spin-spin relaxation time, T_1 and T_2 can be described by using semi-classical, Bloembergen, Purcell and Pound (BPP) model.[144] According to the BPP model, the relaxation times are closely related to the rotational correlation time (τ_c). This parameter, τ_c, is the time needed for the nucleus to rotate one radian:

$$\frac{1}{T_1} = K \cdot [J(\omega_0) + 4J(2\omega_0)] \tag{3.1.7}$$

$$\frac{1}{T_2} = \frac{K}{2} \cdot [3J(0) + 5J(\omega_0) + 2J(2\omega_0)] \tag{3.1.8}$$

$$J(\omega) = \frac{\tau_c}{1 + \omega^2 {\tau_c}^2} \tag{3.1.9}$$

$$K = \frac{3}{160} \cdot \frac{{\mu_0}^2}{\pi^2} \cdot \frac{\gamma^4 \hbar^2}{r^6} \tag{3.1.10}$$

where $J(\omega)$ is the spectral density equation for the exponential correlation function, K is the second moment of the two spin system defined by the strength of the dipole-dipole interaction, μ_0 is the permittivity of free space, $\hbar$ is the reduced Planck constant, r is the effective ^{1}H-^{1}H distance, and γ is the proton magnetogyric ratio.

Using the BPP model, the relaxation time measured by NMR can be related to the local motions of the molecules (Figure 3.1.3). The T_2 relaxation time always increases with the increase of molecular motion (reduction of the correlation time). However, T_1 relaxation time describes a parabola having a minimum

that is a function of both the correlation time and the magnetic field. The effect of this dependency is particularly visible for slow local dynamics as observed in large and hindered molecules, like polymer chains.[145] For large molecules, the T_1 relaxation time decreases when the molecular motion becomes faster. Furthermore, T_1 relaxation time is highly influenced by the magnetic field in this slow region. When the magnetic field increases, T_1 relaxation time increases. Additionally, temperature affects both the T_1 and T_2 relaxation times.[146] The increase in temperature causes the acceleration of the molecular motions resulting in the shorter correlation time. Thus, in the slow molecular region, the T_1 relaxation time decreases, whereas T_2 relaxation time increases.

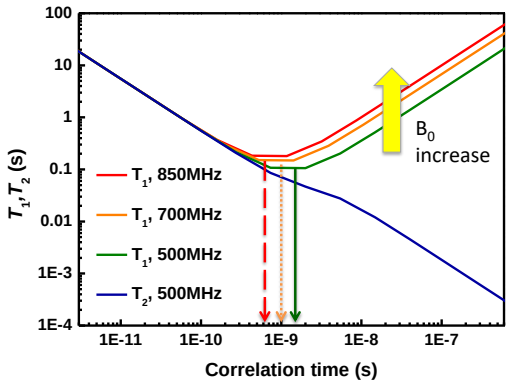

Figure 3.1.3 Dependence of the relaxation times as a function of the correlation time for the spin of ^{1}H according to the BPP model.

3.2 Rheology

Rheology is the study of deformation and flow of materials. It measures the response of a material to an applied stress on a macroscopic level. The aim of rheology is to establish the relationship between deformations and stresses, in order to understand the behavior of a material subjected to the deformation. Rheology measurement is used to analyze the characteristics of rubbers, plastics, paints, and so on, to optimize their processing conditions.[147-149]

In a purely viscous medium, a steady laminar flow can be described by a simple model (Figure 3.2.1). If a medium is placed between two plates when the top plate, having an area of *A*, moves in a certain direction with a force $\vec{F}$ the medium is deformed. The stress tensor ε is a ratio of the applied force $\vec{F}$ and the area *A*. It is conventional to separate the stress tensor into two components based on the direction of applied forces. On the one hand, stresses applied perpendicularly to the area A will result in elongation or compression of the medium. On the other hand, stresses applied parallel to the plane of area A cause shearing defined by the shear stress of σ.

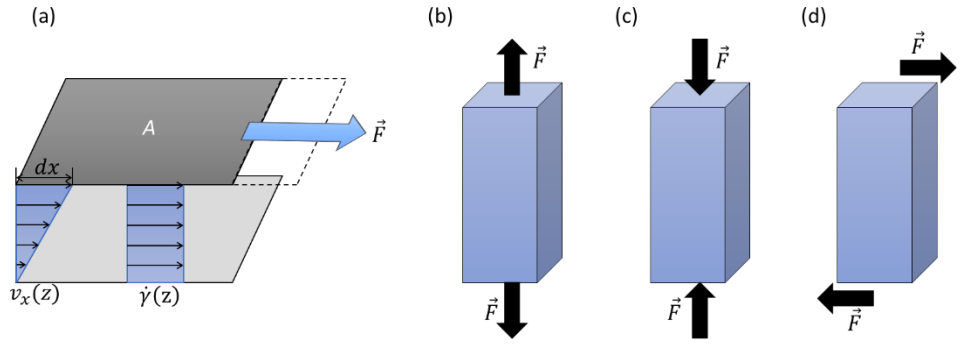

Figure 3.2.1 (a) velocity distribution v_x(z) and shear rate $\dot{\gamma}$(z) in the plate-plate model. Variation in the applied direction of the force $\vec{F}$ resulting in the elongation (b), compression (c), or shear (d) of the medium.

When a medium is confined between two parallel plates separated by a gap (z), and that a force is applied on one of the plates in the direction parallel to the plane of the plate, it will result in a constant shearing, and a velocity gradient v_x(z) for the displacement of pseudo-layers of the medium will be created between

the plates The magnitude of this velocity gradient defines the shear rate or shear velocity $\dot{\gamma}$ and can be related to the viscosity of the medium:[150]

$$\dot{\gamma}(\mathrm{z}) = \dot{\gamma} = \frac{1}{dt}\frac{dx(z)}{dz} = \frac{dv_x}{dz} \tag{3.2.1}$$

There are three types of deformation behavior for materials: viscosity, elasticity, and viscoelasticity.

In the deformation of purely viscous, the deformation is completely irreversible. The viscous behavior of a fluid can be described by the *Newtonian equation*:

$$\frac{F}{A} = \sigma = \eta \cdot \dot{\gamma} \tag{3.2.2}$$

In Newtonian fluids, there is a linear relationship between shear stress (σ) and shear rate ($\dot{\gamma}$) of fluid, if the viscosity (η) is independent of the shear rate. Non-Newtonian fluids have a viscosity that is dependent on the shear rate of the deformation applied.

The second ideal case involves purely elastic deformation, an ideal elastic material experiences a deformation when a force is applied, and the deformation is completely reversible. This behavior can be described by *Hooke's law*:

$$\sigma = G \cdot \gamma \tag{3.2.3}$$

where *G* denotes shear modulus and γ is shear strain or shear deformation. The shear stress is proportional to the shear strain with a slope *G*.

Viscoelastic flow and deformation can be found in most of the polymer materials having both viscous and elastic properties. By combining Newton's and Hooke's law, the viscoelasticity can be explained by two fundamental models. Viscoelastic deformation in solid involves delayed deformation and slow recovery. Different models have been developed to explain such behavior and are described in Figure 3.2.2. The Maxwell model explains the viscoelastic flow of material by connecting a dashpot (viscous module) with a spring (elastic module) in series. In the Kelvin-Voigt model, a dashpot and a spring are linked in a parallel manner and each module is deformed to the same extent at the same time. On the other hand,

viscoelastic flow is observed as viscous flow over a long period with an elastic deformation observed over a short time period.

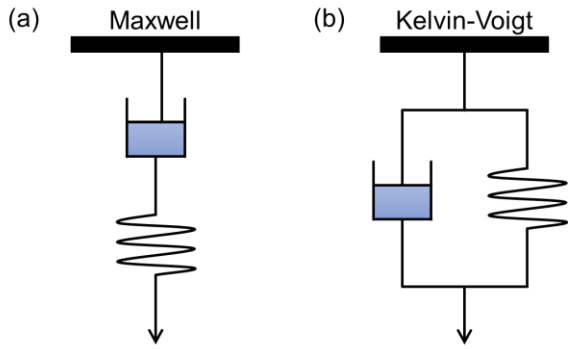

Figure 3.2.2 (a) Maxwell and (b) Kelvin-Voigt models for viscoelastic materials.

There are two important methods to measure the flow behavior using a rheometer. In the continuous shear experiments, a shear rate $\dot{\gamma}$ is applied in a certain range. Then, a shear stress σ and viscosity η are measured under the steady-state conditions.

When an oscillatory shear is applied, the dynamic behavior of the fluid is measured. The direction of the applied shear is changed; this causes a variation in the strain and shear rate. The variation of the deformation follows a sine wave with the angular frequency $\omega = 2\pi f$. The deformation strain γ is given by the amplitude of strain γ_0 with the sinusoidal movement:

$$\gamma = \gamma_0 \sin(\omega t) \tag{3.2.4}$$

where ωt is the frequency of the strain applied. Since the applied shear strain is accompanied by a sinusoidal deformation, the stress response to applied strain also follows the same function, but with a phase shift:

$$\sigma = \sigma_0 \sin(\omega t + \delta) \tag{3.2.5}$$

The derivative of the strain function gives the shear rate of the system:

$$\dot{\gamma} = \omega \gamma_0 \cos(\omega t) \tag{3.2.6}$$

The shear stress is divided into two components, $\sin(\omega t)$ in phase and $\cos(\omega t)$ 90° out of phase:

$$\sigma = \sigma'(t) + \sigma''(t) = \sigma'_0 \sin(\omega t) + \sigma''_0 \cos(\omega t) \quad (3.2.7)$$

The shear storage modulus $G'(\omega)$ and the shear loss modulus $G''(\omega)$ are obtained from sinusoidal varying shear strain and stress:[150]

$$G^* = \frac{\sigma^*}{\gamma^*} = G' + iG'' \quad (3.2.8)$$

$$G'(\omega) = \frac{\sigma'_0}{\gamma_0} = \frac{\sigma_0}{\gamma_0}\cos(\delta) \quad (3.2.9)$$

$$G''(\omega) = \frac{\sigma''_0}{\gamma_0} = \frac{\sigma_0}{\gamma_0}\sin(\delta) \quad (3.2.10)$$

The component G' is representative of the elastic behavior of the medium being deformed and the component G'' reflects the viscous behavior of the medium. Typically, an oscillatory shear experiment probes the response of the material on the time scale of 1/ω.[151] It distinguishes the frequency responses of viscoelastic solids (or gel) from that of viscoelastic liquids. In the viscoelastic gel, G' is bigger than G'' while a viscoelastic liquid shows larger G'' than G'. Sometimes, polymer systems show a transition from viscoelastic gel to the viscoelastic liquid by exhibiting the crossover as the frequency of the deformation applied is changed.

3.3 Dynamic light scattering

Dynamic light scattering (DLS) is a useful characterization method for determining the size and polydispersity of nanoparticles in suspensions. DLS measures the displacement of the NPs caused by the Brownian motion of the suspended nanoparticles in highly diluted solutions. An incident laser beam is focused on the center of suspension. While the beam is passing through the suspension, the light is scattered by the colloids present in the path of the incident light. A detector measures the fluctuation of the intensity of the scattered light as a function of time. Since the smaller particle diffuses faster than the bigger ones, the fluctuations in the intensity of the scattered light can be used to calculate the diffusion coefficient of the suspended nanoparticles. The intensity of the scattered light is treated with an autocorrelation function. When the suspension is monodispersed, it is described by an exponential decay:[152]

$$g(t) = e^{(-Dq^2t)} \tag{3.3.1}$$

where q is the scattering vector, t is the time, and D denotes the diffusion coefficient. The obtained diffusion coefficient can be converted to the hydrodynamic radius (R_h) of the colloids through the Stokes-Einstein equation:

$$D = \frac{k_B T}{6\pi\eta R_h} \tag{3.3.2}$$

where k_B is the Boltzmann constant, T is the absolute temperature, and η represents the viscosity of solvent:

4. Preparation of materials and characterization methods

4.1 Preparation of the nanoparticles

4.1.1 Chemicals

Styrene, methylacrylate and divinylbenzene were purified on a column of basic aluminum oxide. Methacryloyl chloride was purified by distillation under reduced pressure. 2,2'-azobis(2-methylbutyronitrile) was recrystallized in MeOH. All other chemical reagents, 2-hydroxyethyl disulfide, 2-bromoisobutyrylbromide, trimethylamine. Cu(II) chloride, ascorbic acid, polydimethylsiloxane (5 cSt), *N,N,N′,N″,N″*-pentamethyldiethylenetriamine, sodium dodecyl sulfate, cetyltrimethylammonium chloride, hexadecane, DL-dithiothreitol, 1,8-diazabicyclo[5.4.0]indec-7-ene, hydrochloric acid, ammonium chloride, sodium hydrogen carbonate, sodium chloride, ethyl acetate, dichloromethane, *N,N'*-dimethylformamide, anisole, tetrahydrofuran, hexane, diethylether, and methanol, were used as received.

4.1.2 Synthesis of the ATRP inimer

2-((2-(3-Methyl-2-oxobut-3-en-1yl)xy)ethyl)disulfanyl)ethyl 2-bromo-2-methylpropanoate (MA-SS-Br)

MA-SS-Br was synthesized via 2-step esterification (Figure 4.1.1).[153] 600 mL of DCM was added to a round bottom flask with 1000 mL volume and cooled to 0 °C. Under stirring, 23.8 g of (2-hydroxyethyl) disulfide (1.1 eq) and 67.8 mL of trimethylamine (2.6 eq) was added. Then, 21.6 mL of 2-bromoisobutyryl bromide (1.0 eq) was slowly added to the reaction mixture using a syringe pump (15 mL/h). The reaction

mixture was left stirring overnight at room temperature and was then filtered using filter paper. The organic phase was then washed by extraction with sequentially 1 M HCl (3 X 400 mL), sat. $NaHCO_3$ (3 X 600 mL) and sat. NaCl (3 X 600 mL). The organic phase was then dried with $MgSO_4$ and evaporated at 40 °C under 500 mbar. The resulting oil was purified by silica filled column chromatography (hexane:EtOAc = 6:4, R_f = 0.56). The purified solution was evaporated at 40 °C under 200 mbar and further dried at 50 °C under 1 mbar for 24 hours. ^{1}H-NMR spectroscopy (300 MHz, $CDCl_3$): chemical shift (δ/ppm) of 4.46 (t, 2H), 3.91 (t, 2H), 2.99 (t, 2H), 2.90 (t, 2H), 1.96 (s, 6H) (Figure 4.1.1(i)). The resulting 2-((2-hydroxyethyl)disulfanyl)ethyl-2-bromo-2-methylpropanoate (HO-SS-Br, 16g, 1.0 eq) and 144 mL of DCM were added to a round bottom flask with 500 mL volume, 15 ml of trimethylamine (2.5 eq) was added to the solution which was then cooled to 0 °C using ice water bath. Then, 14.26 mL of freshly distilled methacryloyl chloride (3.0 eq) was added dropwise to the reaction mixture and the reaction was left stirring overnight at room temperature. The precipitate was filtered off using filter paper and the solution was washed by extraction with 1 M HCl (3 X 360 mL) and sat.$NaHCO_3$ (3 X 430 mL). After drying the organic phase with $MgSO_4$, the solvent was evaporated at 40 °C under 500 mbar and the product was purified with a silica column chromatography (hexane:EtOAc = 6:4, R_f = 0.2). After evaporation of the solvents, in order to eliminate the remaining impurities, the mixture was purified with a second silica filled column chromatography (hexane:diethyl ether = 9:1, R_f = 0.46) resulting in the pure MA-SS-Br. ^{1}H-NMR spectroscopy (300 MHz, $CDCl_3$): δ/ppm of 6.07 (m, 1H), 5.53 (m, 1H), 4.36 (m, 4H), 2.91 (m, 4H), 1.87 (m, 9H) (Figure 4.1.1(ii)).

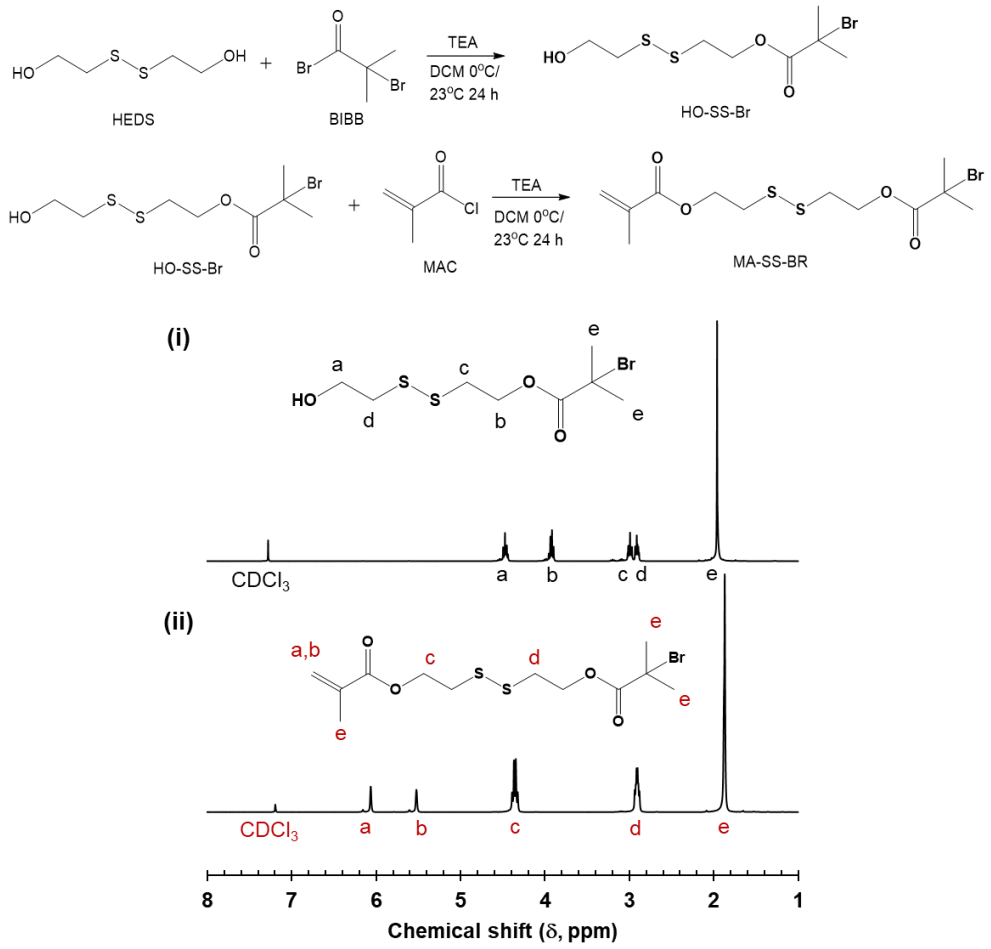

Figure 4.1.1 Synthesis and characterization of the ATRP inimer containing a disulfide bond (MA-SS-Br). ^{1}H-NMR spectra of (i) 2-((2-hydroxyethyl)disulfanyl)ethyl-2-bromo-2-methylpropanoate and (ii) 2-((2-(3-methyl-2-oxobut-3-en-1yl)xy)ethyl)disulfanyl)ethyl 2-bromo-2-methylpropanoate.

4.1.3 Synthesis of a PS nanoparticle core

Typically, 6.5 mL of styrene (St, 1 eq.), 82 µL of divinylbenzene (DVB, 0.01 eq.) and 0.65 mL of hexadecane (HD, 0.04 eq.) were added to a beaker and were mixed with 0.0552 g of a 2,2′-azobis(2-methylbutyronitrile) initiator (V-59, 0.005 eq.). After 10 minutes, 48 mL of sodium dodecyl sulfate (SDS) aqueous solution (10 mM) was added and the mixture was pre-emulsified for 15 min by magnetic stirring at 600 rpm. The biphasic mixture was sonicated for 2 min at 0 °C (20 kHz, 70% A, 10 s on/2 s off) to obtain a miniemulsion before being transferred to a 50 mL round bottom flask and heated to 80 °C. After

2.5 h of polymerization, 4 mL of SDS aqueous solution (250 mM) was added and the system was purged by bubbling Ar for 10 min. Then, to create a thin layer of an inimer (MA-SS-Br, Figure 4.1.1) containing polymer network at the surface of the NP, a mixture of 89–98 mol% of St (1.33 mL), 1 mol% DVB (16.6 μL), 1–10 mol% of MA-SS-Br (0.0326–0.326 mL) and V-59 (0.0115 g) was subsequently added dropwise with a syringe pump at a rate of 1 mL h^{-1}. The reaction mixture was left stirring overnight at 80 °C before being filtered using filter paper. The PS NPs in the aqueous suspension were then precipitated in 200 mL of MeOH and air-dried. To completely eliminate HD and SDS from the PS NPs, the NPs were dispersed in 40 mL of THF and precipitated in 500 mL of MeOH three times. Finally, the NPs were air-dried. Alternatively, PS NPs were also prepared by tuning the amount DVB added during the synthesis from 0.5 mol% to 10 mol%.

4.1.4 Synthesis of the end-tethered canopy of PMA on the surface of the PS core

In a typical reaction, 0.4 mL of methyl acrylate, 0.1 mL of a solution containing Cu(II)Br_2 (2000 ppm) and PMDETA (Cu(II) : ligand = 1 : 10 molar ratio) in DMF were added into a vial containing a suspension of 50 mg PS-SS-Br NPs dispersed in 4 mL of anisole. PDMS (0.1 mL) was added to the suspension. The mixture was stirred and purged with argon for 30 min. Then, a 0.5 mL solution of ascorbic acid (1600 ppm) in DMF was added. This resulting suspension was degassed with argon for another 10 min, and the vial was then placed into an oil bath at 60 °C and allowed to react. Once the appropriate monomer conversion was reached, the reaction mixture was diluted with THF, precipitated in MeOH and dried overnight under vacuum. The reaction was repeated with various amounts of the monomer, Cu(II)/ligand and bromoisobutyrate grafted moieties.

To characterize the end-tethered PMA, the chains were cleaved from the PS@PMA NPs. The disulfide bonds between the PS core and the PMA chains were cleaved by reduction with dithiothreitol. A suspension of PS@PMA NPs was prepared by mixing 0.1 g of PS@PMA NPs with 10 mL of DCM for 24 h. Then, DL-dithiothreitol (DTT, 10 mg) and two drops of 1,8-diazabicyclo[5.4.0]undec-7-ene (*ca.* 20 mg) were added to the NP suspension and stirred for 24 h. After evaporation of the solvent, the dried and cleaved polymer/particle mixture was mixed in 10 mL of THF with an additional 5 mg of DTT and stirred overnight. The suspension was then filtered through a syringe filter (PTFE, Ø = 0.2 μm). The solutions

were centrifuged at 29 068 *g* for 20 min to eliminate the residual PS core and the molecular weight of PMA in solution was measured by SEC in THF.

4.2 Characterization methods

4.2.1 Composition of the core and canopy nanoparticles

FTIR spectra of PMA, PS NPs, PS@PMA NPs and binary mixtures of PS NPs and PMA were recorded (Figure 4.2.1). The peak at 696 cm^{-1} originating from aromatic C-H bending was used to quantify the presence of PS and the peak at 1736 cm^{-1} due to the C=O stretching was used for PMA. The area ratio observed for the PS@PMA was used to quantify the amount of PMA in each sample in comparison to a set of binary mixtures of PS NPs and free PMA.

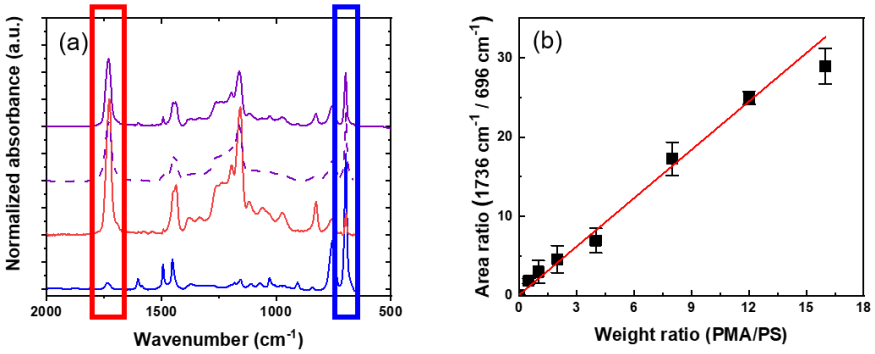

Figure 4.2.1 FTIR analysis of the PS@PMA NPs. (a) FTIR spectra of PS NPs (——), free PMA_{40k} (——), $PS_m@PMA_{20k}$ (——) and a binary mixture composed of 50 wt% of PS NPs and 50 wt% of PMA_{40k} (- - -). (b) Calibration curve used for the analysis of the PMA/PS fraction by FTIR.

4.2.2 Volume occupied by the nanoparticles in suspension

When the volume of a solvated particle measured by DLS was used to calculate the volume occupied by the NPs in suspensions, the volume fraction obtained (ϕ_{cal}) was largely overestimated due to the possible compression and interdigitation of the polymer as the concentration of the suspension increased.

$$\phi_{cal} = \frac{V_{Swollen\ NP,\ \ DLS}}{V_{suspension}} \qquad (4.2.1)$$

Figure 4.2.2 also displays that mixing known volume of dry NPs with known volumes of anisole led to no significant variation of the final volume (less than 1 vol%) suggesting that in concentrated suspension, the volume occupied by a NP was much smaller than the volume occupied by the same NP in the diluted suspensions measured by DLS. Models have been developed to estimate the effective volume fraction of hard particles in suspension, like the Krieger-Dougherty model:[154]

$$\eta_r = \left(1 - \frac{\phi_{KD}}{\phi_{max}}\right)^{-\phi_{max}[\eta]} \qquad (4.2.2)$$

where η_r is the relative zero-shear viscosity of the suspension and $[\eta]$ is its intrinsic viscosity, ϕ_{KD} and ϕ_{max} are respectively the effective volume fraction and the maximal volume fraction. However, this model also tends to inaccurately describe the volume fraction of suspensions of soft and deformable particles (Figure 4.2.2).

Sample	PS_h	PS_hPMA_{50k}	PS_mPMA_{50k}	PS_lPMA_{50k}	PS_lPMA_{50k}
M_{NP} (g)	0.252	0.251	0.252	0.253	0.505
M_A (g)	4.738	4.726	4.738	4.762	4.5
C_{NP} (wt%)	5.05	5.04	5.05	5.05	10.09
V_{NP} (dry) (cm^3)	0.24	0.21	0.21	0.22	0.45
V_A (mL)	4.762	4.75	4.762	4.786	4.523
# of NPs	2.52e14	2.55e13	6.77e13	2.25e14	4.49e14
R_h (nm)	104	296	168	161	161
V_{NP} (swolen) (cm^3)	1.21	2.8	1.34	3.9	7.8
V_{Total} (cm^3)	5	5	5	5	5.05
φ	0.24	0.56	0.27	0.79	1.5
φ_{KD}	0.48	0.63	0.57	0.6	0.64

Figure 4.2.2 Swelling of nanoparticles in concentrated solutions.

4.2.3 Rheological behavior of suspensions

Suspensions of PS and PS@PMA NPs and a solution of free PMA (M_n of 40 K) were prepared in anisole at a concentration ranging from 0.1 to 15 wt%. The rheological properties of the suspensions were measured with a Bohlin Gemini 200 rotational rheometer at 25 °C equipped with a cone and plate geometry of 40 mm diameter and 4° cone angle. The gap was set at 150 µm. Continuous shear experiments were performed by varying the shear rate between 0.1 and 1000 s^{-1}. The dynamic behavior of the suspensions was studied using oscillatory shear experiments; for frequency-sweep experiments, the strain applied to the system was fixed to 10% and the frequency varied from 0.1 to 100 rad s^{-1} and in strain-sweep experiments, the frequency was fixed to 10 rad s^{-1} and the strain varied from 0.1 to 1000%.

4.2.4 Size and size distribution of nanoparticles

The radius of the NPs was determined by dynamic light scattering (DLS) measured with a Malvern Instruments Zetasizer Nano S90 at a fixed angle of 90° (λ=633 nm, 15 runs, run duration of 10 seconds). The NPs were dispersed either in a good solvent (DCM, anisole, DCM/acetone or DCM/cyclohexane) or in an aqueous solution of cetyltrimethylammonium chloride (0.2 wt%). All the measurements were carried out at 25 °C with a concentration of 0.05 mg/mL.

4.2.5 Grafting density of nanoparticles

To determine the number of initiating sites at the surface of the NP, the sulfur content in the NPs was analyzed. The NPs were dispersed in water and stabilized with cetyltrimethyl ammonium chloride (CTAC). A PS-SS-Br NP suspension in DCM was added dropwise to 10 mL of an aqueous solution containing 5.0 mg of CTAC and sonicated at 0 °C (20 kHz, 70% A, 10 s on/2 s off). Then, DCM was evaporated under a mild vacuum (200 mbar, 40 °C). The sulfur content in the resulting aqueous suspension of PS NPs was measured by inductively coupled plasma atomic emission spectrometry (ICP-AES) with an ACTIVA M spectrometer (Horiba Jobin Yvon) equipped with a Meinhardt-type nebulizer and a cyclone chamber, and processed with ACTIVAnalyst 5.4. ICP-AES was operated at 1250 W forward plasma power with 12 L min^{-1} of Ar flow and 15 rpm of peristaltic pump flow. The argon emission line at 404.442 nm was chosen for the reference line. The measurements were conducted using three different

standard concentrations and 5 s of integration time. A dynamic underground correction was used for the baseline correction. The measurement was repeated three times with the same sample.

4.2.6 Spin-lattice relaxation (T_1)

The PS-PMA core-corona hairy NPs were dispersed in CD_2Cl_2 at a concentration of 16.7 mg·mL^{-1}. The relaxation experiments were performed on a series of NMR AVANCE spectrometers (Bruker) working at nominal frequencies of 500.13 MHz, 700.02 MHz and 850.27 MHz. The spin-lattice relaxation time constants (T_1) were measured using a standard inversion-recovery pulse sequence (180–τ–90–acquire). The recovery time (τ) was varied from 20 ms to 10 s and the temperature was set at 278 K, 288 K, 298 K and 308 K. The protons in the aromatic ring of PS (7.1 to 6.6 ppm) and in the methoxy group (3.7 ppm) were chosen for the analysis. The area of the NMR peak at each recovery time was fitted with a monoexponential decay (Eq. 4.2.3) to calculate the relaxation time T_1 (Figure 4.2.3).

$$\frac{I(\tau)}{I(0)} = A \times (1 - 2 \times \exp(\frac{-\tau}{T_1})) \qquad (4.2.3)$$

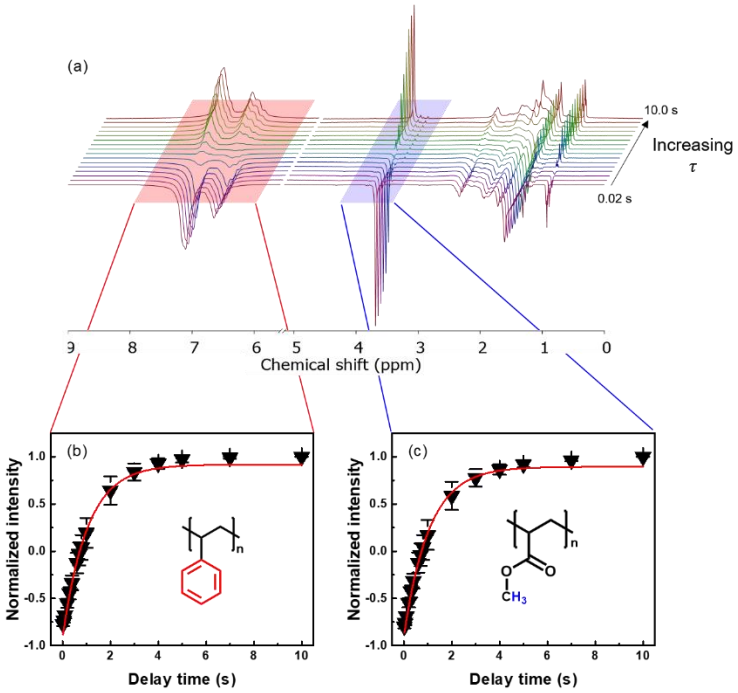

Figure 4.2.3 (a) Inversion-recovery NMR experiment of PS-PMA NPs at a Larmor frequency of 500.13 MHz at 298 K. ^{1}H magnetization recovery for (b) aromatic protons of PS and (c) methoxy protons of PMA in PS-PMA NPs fitted with Eq. 4.2.3.

The correlation time (τ_c) was determined from the relaxation time T_1 measured at different magnetic fields with the Bloembergen-Purcell-Pound model: (Eq. 4.2.4)

$$T_1^{-1} = K\left[\frac{\tau_c}{1+\omega_0{}^2\tau_c{}^2} + \frac{4\tau_c}{1+4\omega_0{}^2\tau_c{}^2}\right] \quad (4.2.4)$$

where ω_0 is Larmor frequency of the spin system, and K is the temperature-independent dipolar coupling constant given by:

$$K \propto \left(\frac{3\mu_0{}^2}{160\pi^2}\right)\left(\frac{\hbar{}^2\gamma^4}{r^6}\right) \quad (4.2.5)$$

where μ_0 is the permittivity of free space, γ is proton magnetogyric ratio, $\hbar$ is the reduced Planck constant, and r is the effective ^{1}H-^{1}H distance.

4.2.7 Spin-spin relaxation (T_2)

The PS NPs, PS-PMA NPs and PMA free chain were dispersed in deuterated solvent mixtures at a concentration of 16.7 mg mL^{-1}. The relaxation experiments were performed on NMR AVANCE spectrometers (Bruker) working at a nominal frequency of 300.13 MHz. The spin-spin relaxation time constants (T_2) were measured using the Carr-Purcell-Meiboom-Gill (CPMG) pulse sequence using 16 spin-echo times (τ). The τ was varied from 4 ms to 8.3 s and the temperature was set at 298 K. The protons in the aromatic ring of PS (7.1 to 6.6 ppm) and in the methoxy group (3.7 ppm) were chosen for the analysis. The area of the NMR peak at each spin-echo time (M) was fitted with a stretched exponential function (Eq. 4.2.6) to calculate the apparent relaxation constant $T_{2,\,App}$ (Figure 4.2.4). The average relaxation $T_{2,\,Ave}$ was obtained from the Eq. 4.2.7:[155]

$$M(\tau) = A_0 \times \exp\left(-\left(\frac{\tau}{T_{2,App}}\right)^{\beta}\right) \quad (4.2.6)$$

$$T_{2,Ave} = \frac{T_{2,App}}{\beta} \times \Gamma\left(\frac{1}{\beta}\right) \quad (4.2.7)$$

where β is stretched exponent, Γ is gamma function.

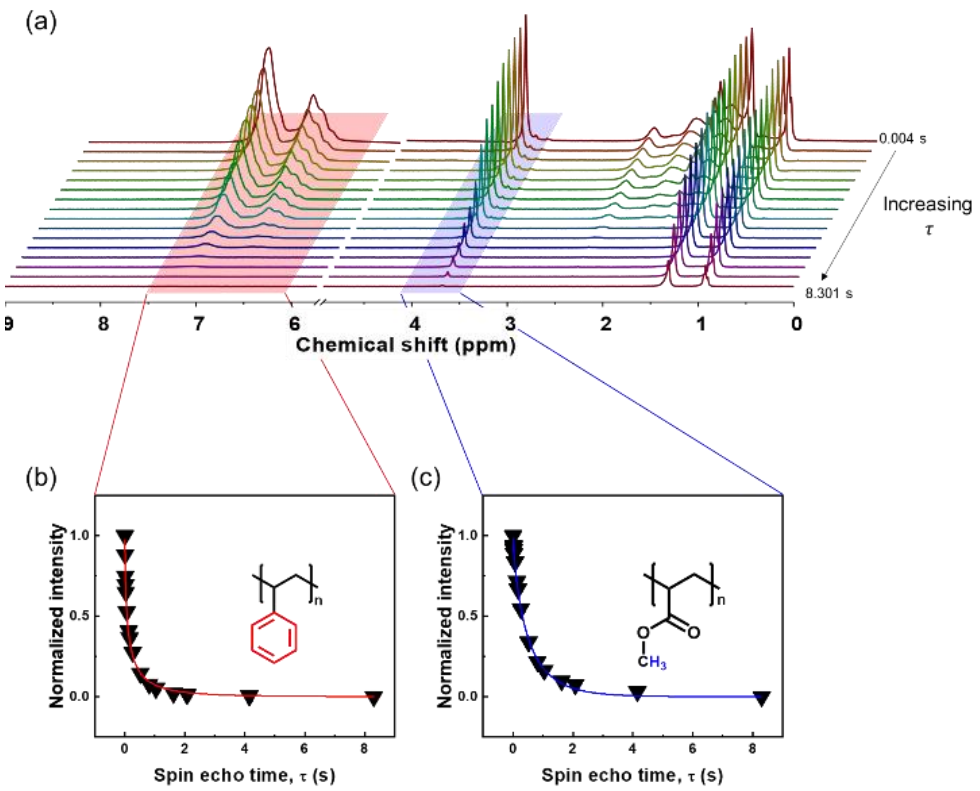

Figure 4.2.4 Measurement of the T_2 relaxation time in a sample of PS-PMA NPs. (a) ^{1}H NMR spectra of PS-PMA NPs obtained with Carr-Purcell-Meiboom-Gill pulse sequence at a Larmor frequency of 300.13 MHz at 298 K. Decay of the signal intensity during the spin-echo extracted from the spectra for (b) aromatic protons of PS and (c) methoxy protons of PMA in the PS-PMA NPs fitted with Eq. 4.2.6.

4.2.8 Calculation of Flory-Huggins polymer-solvent interaction parameters

The Flory-Huggins polymer-solvent interaction parameters (χ_{12}) were calculated using the Hansen solubility parameters (Eq. 4.2.8):[156]

$$\chi_{12} = \alpha \frac{v_1}{RT}\left(\left(\delta_{1,d} - \delta_{2,d}\right)^2 + 0.25\left(\delta_{1,p} - \delta_{2,p}\right)^2 + 0.25\left(\delta_{1,hb} - \delta_{2,hb}\right)^2\right) \qquad (4.2.8)$$

where, α is a constant, v_1 is molar volume of solvent, R is universal gas constant, T is absolute temperature, $\delta_{1,d}$ is the Hansen dispersion parameter for the solvent, $\delta_{2,d}$ is the Hansen dispersion parameter for the polymer, $\delta_{1,p}$ is the Hansen polarity parameter for the solvent, $\delta_{2,p}$ is the Hansen polarity parameter for the polymer, $\delta_{1,hb}$ is the Hansen hydrogen bonding parameter for the solvent, $\delta_{2,hb}$ is the Hansen hydrogen bonding parameter for the polymer.

4.2.9 Measurement of glass transition temperature

Differential scanning calorimetry (DSC) was carried out to measure the glass transition of PS-PMA NPs by using DSC, 204F1 / ASC Phönix, Netzsch in a temperature range between –80 °C and +200 °C with a heating and cooling rate of 10 °C min^{-1}.

5. Results and discussion

End-tethered polymer chains, or polymer brushes, are used extensively to modify the properties of nanoparticles (NPs) such as their stability, solvent compatibility, dispersibility, and assembly. However, there are currently no guidelines to design the ideal canopy of end-tethered polymer chains, especially when the polymer chains are grafted onto soft and deformable NPs. Understanding the behavior of the polymer canopy and its effect on the NP behavior would improve the design of future NP-based systems. A comprehensive library of polymer-functionalized soft polymer NPs with a variable degree of core softness and length of grafted polymer chains was designed, and their behavior studied by rheology and NMR relaxometry.

Controlling the thickness of the grafted polymer layer and the surface coverage is one of the most important parameters to be considered when designing polymer-functionalized NPs because these parameters determine the conformation of the grafted chains.[19, 27, 97, 157-160] As the grafting density increases, polymer chains start to overlap and hence stretch because of steric repulsion. In a densely crowded regime, as described by the Alexander–de Gennes model, polymer chains are highly stretched and only local polymer movement confined within a polymer blob unit can be observed. [19] When such a polymer layer is immobilized on a spherical surface, the size of the blobs expands as the distance with the substrate increases. [96] Consequently, the influence of the neighboring chains on the stretching and extension of the chains decreases with respect to the distance from the curved substrate or with the degree of polymerization (N) of the grafted chains. This radial dependency results in a transition between brush regimes from stretched chains to coiled polymer chains. [96]

The behavior of the functionalized NPs is not only influenced by the architecture of the polymer canopy, but also by the solvent quality. The chain dynamics and the conformation of end-grafted chains are also affected by the polymer-solvent interaction,[161, 162] and changes in the solvent quality have been used to control the properties of polymer-functionalized NPs.[163, 164] When end-tethered polymer chains are in a good solvent (Flory-Huggins interaction parameter, $\chi_{12}<0.5$), both enthalpic attraction between chain segments and solvent molecules and entropic repulsion between chain segments occur in the polymer

canopy,[165] and results in an extended chain conformation of the end-grafted polymer chains. Consequently, the swelling of the polymer canopy on the NPs in the suspension provides colloidal stability through steric repulsions. However, when the quality of the solvent decreases, the conformation of the end-grafted polymer chains can undergo a transition from a stretched regime to a more collapsed regime and can be accompanied by the formation of non-uniform polymer canopy,[166, 167] or lead to the self-assembly of polymer chain grafted NPs into various mesostructures.[168, 169]

The swelling behavior of core NPs in the suspension can also affect the behavior of the polymer chain grafted soft NPs. The degree of swelling can be controlled by varying the cross-linking density of soft NP cores. Highly cross-linked NPs show less swelling and this is related to the relatively rigid particle property. Soft NPs can be deformed in response to external stimuli such as solvent quality, pH, and temperature. Solvent quality efficiently controls the swelling of core NPs as well as the polymer canopy. In a good solvent, the core of the NPs is swollen, resulting in an increase in the surface area and a decrease of effective grafting density of the end-tethered polymer chains. Hence, the transition of chain conformation can be found from the stretched regime to the random coil regime. When the solvent quality for the core NP decreases, the NP deswells resulting in the decrease of particle size and increase of effective grafting density. Consequently, the grafted chain can be more stretched.

The behavior of colloidal dispersions can be measured by rheology. This the viscoelastic behavior of the nanoparticle suspension not only depends on the volume fraction occupied by the colloids and the colloid–colloid interaction,[170] but is also affected by the reorganization and reorientation of the particles in suspension and their effects on the local flow patterns,[88, 171] and the formation (or destruction) of colloidal mesostructures.[172, 173] Furthermore, when dealing with soft and deformable colloids in suspension, both the shape and the volume occupied by the particles can change under the application of shear, leading to strong flow-dependent behavior.[174-176] The softness of the NPs affects the mechanical properties of the resulting gels and glasses and the concentration needed to observe a liquid to gel transition.[177, 178] Soft and deformable particles are expected to form stronger gels than hard spheres.[179]

Studies of the relaxation dynamics of grafted chains, both experimentally and by simulation, have demonstrated that the presence of a substrate significantly affects the subsegmental dynamics of the tethered polymer chains and can impact the mechanical properties of the resulting materials. [31, 32, 131,

180] The presence of the substrate usually creates a confinement effect influencing the relaxation of the tethered polymer chains, and this effect decreases with an increase in *N*. [181-183]

Since a variety of parameters can potentially influence and control the behavior of the polymer-functionalized soft NPs, a robust model system is required to understand the fate of the NPs. Here, an approach combining the use of rheology to measure the macroscopic properties of the NPs suspensions and NMR relaxometry to investigate the dynamics of such systems was developed to elucidate the effect of architecture and environment on the behavior of polystyrene NPs functionalized with poly(methyl acrylate) end-tethered chains. A library of soft and swollen cross-linked polystyrene (PS) nanoparticles functionalized with a canopy of end-tethered poly(methyl acrylate) (PMA) chains was designed. Using surface-initiated atom transfer radical polymerization (SI-ATRP) the length of the polymer chains was precisely controlled, and the grafting density was tuned during the synthesis of the PS core. The softness of the core was controlled either by the cross-linking degree of the PS or the choice of solvent. The impact of the swelling and rigidity of the core (**Section 5.1, 5.2 and 5.3**), degree of polymerization of the grafted chains (**Section 5.1, 5.2, and 5.4**), grafting density (**Section 5.1 and 5.4**), and solvent quality (**Section 5.1 and 5.3**) on the macroscopic and local behavior of the NPs were investigated.

5.1 Polymer-functionalized polymer nanoparticles and their behavior in suspensions[1]

In this section, soft polymer nanoparticles functionalized with end-tethered polymer chains influencing their solvent compatibility and stability were studied. Controlling and understanding the behavior of such functionalized latex suspensions are critical for their comprehensive applications. To investigate the effect of the nanoparticle architecture on their rheological behavior, a library of polystyrene nanoparticles functionalized with a canopy of end-tethered poly(methyl acrylate) chains with different degrees of polymerization and grafting densities were prepared. When the end-tethered polymer chains were long enough, the suspensions of polymer-functionalized nanoparticles underwent a liquid to gel transition when the concentration of the nanoparticles was increased. The architecture of the polymer canopy was the determining factor for the mechanical properties of the resulting gels; nanoparticles with moderate grafting density where the polymer chains adopt a relaxed polymer brush conformation led to the formation of the strongest and most robust gels. In comparison with suspensions prepared with polymer functionalized nanoparticles, particles with a soft and swollen core formed gels with higher yield stress at a lower solid content.

5.1.1 Motivation

Nanoparticles (NPs) with a grafted layer of polymers have become ubiquitous building blocks for applications from the biomedical field to the production of sustainable energy.[17, 72, 184-188] In these systems, end-tethered polymer chains are often used to modify the properties of NPs, such as stability, solvent compatibility, dispersibility, and assembly. Polymer chains tethered to latex nanoparticles

[1] This section is based on the article:

[redacted] Polymer-functionalized polymer nanoparticles and their behaviour in suspensions. *Polymer Chemistry* **2020**, *11*, 2119-2128, DOI: 10.1039/C9PY01558B. Reproduced permission from open access license from Creative Commons Attribution 3.0 Unported License.

Author contribution: [redacted] designed and performed the experiments. [redacted] analyzed the data. [redacted] discussed the results and wrote the manuscript.

represent a particular challenge since both the canopy of end-tethered chains and the core of the nanoparticles are soft and deformable. Thus, designing an ideal polymer layer to optimize the behavior of the NPs for a specific application is non-trivial and new design principles are needed to rationally engineer such polymer canopies. Polymer NPs functionalized with a canopy made of end-tethered polymer chains combine the complex rheological behavior of polymer chains and polymer colloids. Furthermore, to facilitate the processing of such materials, it is essential to understand how the architecture of such particles influences their behavior in flow.

Polymer solutions can be complex non-Newtonian viscoelastic fluids, especially in the semi-dilute and concentrated regime, when the concentration of the polymer in solution is above the critical overlap concentration. The behavior of the polymer chains in solution depends on not only the concentration but also the architecture, topology, and flexibility of the chains.[186, 187] Branched polymers, such as star-, H-, or comb-shaped macromolecules, exhibit larger shear viscosities than their linear analogs.[188, 189] The viscosity of solutions of branched polymers increases as the number of branches increases, while the effect of the branch length becomes more marginal as the number of arms increases.[190] One of the key features of branched systems is the restricted arm interpenetration and arm entanglement as the branching degree increases.[191] In comparison with solutions of linear polymer chains, the overlap concentration of solutions of dendrimers or of solutions of polymers having a branched architecture occurs at higher concentrations because of the limited effective chain entanglement.[192]

The behavior of nanoparticles in suspension could be tuned by the functionalization of the surface of the nanoparticles with a canopy of end-tethered polymer chains.[72, 167, 193] The behavior of such nanoparticles dispersed in a polymer matrix has been shown to depend on the composition of the canopy as determined by the degree of polymerization (N) and grafting density (σ) of the chains since these parameters influence both the particle/particle interaction and the particle/environment interaction.[194, 195] The influence of N and σ on the stability of polymer functionalized nanoparticles dispersed in a solvent or in a solid matrix has been widely studied for nanoparticles with a rigid core. In such systems, the dynamics of the nanoparticle suspensions and the particle/particle interactions in suspension were mostly governed by the architecture of the polymer canopy[196] *via* the excluded volume interactions and chain configuration entropy,[197, 198] and fluctuations of the polymer canopy influenced the fragility of the particle assemblies.[199] Furthermore, for similar polymer canopies, the degree of swelling of the

polymer canopy changes the chain conformation in the canopy and the resulting behavior of the suspensions.[200]

However, when the core particle is soft and deformable, the influence of the architecture of the canopy (N and σ) has not been addressed, and significant differences could be expected. On the one hand, gel nanoparticles display a more polymer-like behavior when they are highly swollen because of their compressibility and facilitated interpenetration. On the other hand, the swelling of the polymer canopy could promote the canopy interpenetration or the solvation shell surrounding the NPs can create new slipping planes and act as a lubricating agent for the nanoparticle suspensions.

Here, to understand the relationship between the rheological and mechanical properties of the suspension and the structure of soft-core/soft-corona polymer nanoparticles dispersed in a good solvent, the rheological properties of suspensions of these PS@PMA NPs in different solvents were investigated. This gave insights into how the architecture of the canopy of end-tethered polymer chains and how the combination of a swollen gel core with the swollen polymer canopy affect the NP suspension and the behavior of colloidal glasses formed at high NPs concentration.

5.1.2 Results and discussion

A library of core–corona nanoparticles with a core of polystyrene grafted with a canopy of poly(methyl acrylate) chains (PS_{σ}@PMA_{N}) with different chain lengths (N) and grafting densities (σ) was prepared (Table 5.1.1). The synthesis of the particles proceeded *via* a three-step process (Figure 5.1.1). First, miniemulsion polymerization[201] was used to prepare PS nuclei used to form core–shell NPs through a starve-fed emulsion polymerization process[202] to create a thin layer of a copolymer of styrene and the inimer at the surface of the PS NP. The grafting density was tuned by controlling the concentration of the inimer in the outer layer of the PS core. Finally, each inimer was used to initiate the polymerization of methyl acrylate by surface-initiated atom transfer radical polymerization (SI-ATRP).[203] In the dry state, at room temperature, the resulting NPs were composed of a rigid glassy core surrounded by a soft rubbery corona (Figure 5.1.1c). PS and PMA were selected because they are strongly immiscible ($\chi_{PS/PMA} = 0.03 \cdot N = 169 \cdot \chi_{PS/PMMA}$) [204, 205] as observed experimentally with binary mixtures of PS and PMA and PS/PMA block copolymers readily phase segregating.[204, 206] Thus, the choice of PS and PMA prevented any specific interaction between the PS core and the PMA canopy potentially influencing the behavior of the resulting NPs suspensions.

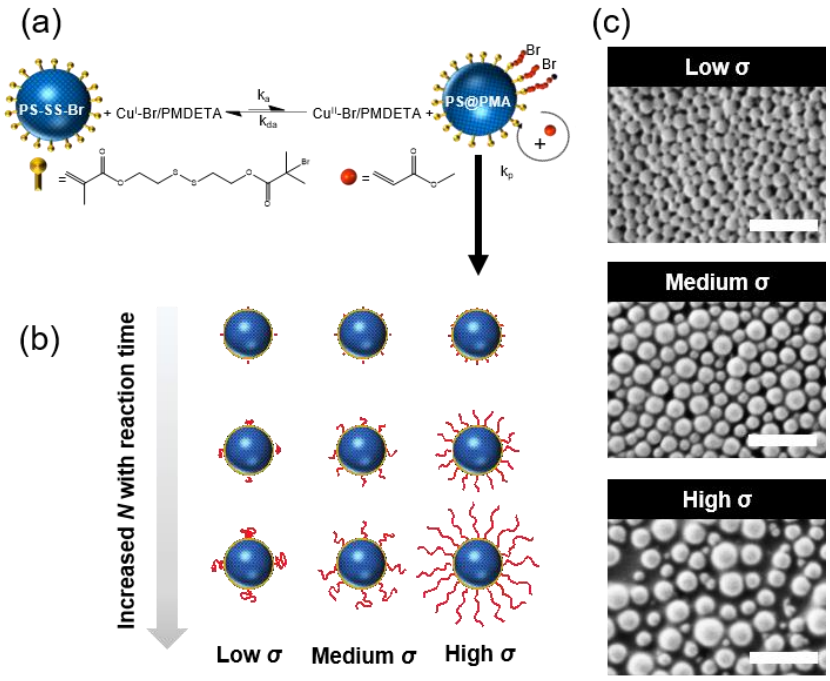

Figure 5.1.1 Preparation of a library of PS@PMA nanoparticles. (a) Synthetic scheme; (b) NPs with different grafting densities (σ) and chain lengths (N); and (c) SEM of the resulting $PS_x@PMA_{20k}$ NPs. Scale bars are 500 nm.

Furthermore, using SI-ATRP to grow PMA from the PS surface allowed to precisely tune the length of the grafted chains, since the polymerization of the methyl acrylate was controlled as demonstrated by the linear increase of monomer conversions with the polymerization time (Figure 5.1.2). The experimental molecular weights of the PMA brushes determined by SEC ($M_{n,SEC}$) were in good agreement with the expected values based on the monomer conversion measured by NMR spectroscopy and the number of initiating sites measured by ICP (Table 5.1.2). The chemical composition in PS and PMA within the NPs could be controlled by the architecture of the PMA canopy. The chemical composition of the NPs was quantified by FTIR spectroscopy using a series of binary mixtures of pure PS NPs and linear PMA in known weight ratios as a calibration (Figure 4.2.1). The contents of PMA in each sample scaled as expected with the different σ and N (Figure 5.1.3a). The combined analysis of the NPs by ICP, GPC, NMR and FTIR spectroscopy showed that the length and grafting density of the PMA chains in the PS@PMA NPs were precisely controlled. This allowed to tune the architecture of the PMA canopy.

Table 5.1.1 Library of PS@PMA nanoparticles.

Sample	Reaction Time (h)	M_n PMA (10^3 g/mol)	N	Effective grafting density σ (nm^{-2})		
				H_2O	DMSO	Anisole
PS_h@PMA_{3k}	0.5	3.1	36	2.5	2.5	0.82
PS_h@PMA_{6k}	1	6.0	70			
PS_h@PMA_{10k}	2	10.0	128			
PS_h@PMA_{15k}	2.5	15.0	171			
PS_h@PMA_{20k}	3	19.0	220			
PS_h@PMA_{30k}	1	35.0	406			
PS_h@PMA_{40k}	3	42.0	493			
PS_h@PMA_{50k}	6	54.0	623			
PS_m@PMA_{3k}	0.5	2.6	31	0.80	0.80	0.22
PS_m@PMA_{6k}	0.5	6.9	79			
PS_m@PMA_{20k}	3	20.0	228			
PS_m@PMA_{30k}	2	30.0	349			
PS_m@PMA_{40k}	3	42.0	493			
PS_m@PMA_{50k}	4.5	51.0	593			
PS_l@PMA_{3k}	0.5	3.8	44	0.17	0.13	0.04
PS_l@PMA_{6k}	1	8.5	99			
PS_l@PMA_{20k}	2	23.0	267			
PS_l@PMA_{30k}	1.5	32.0	377			
PS_l@PMA_{40k}	2	41.0	474			
PS_l@PMA_{50k}	2.5	52.0	610			

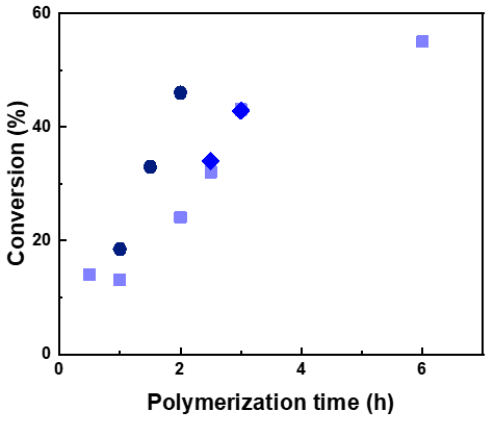

Figure 5.1.2 Monomer conversion as a function of polymerization time for the synthesis of PS@PMA using the ratio of I/MA/Cu of 1/533/0.1; (■) PS_h@PMA (2.5 chains/nm^2), (◆) PS_m@PMA (0.80 chains/nm^2) and (●) PS_l@PMA (0.17 chains/nm^2).

Table 5.1.2. Library of PS@PMA nanoparticles.

Sample	Initiator/MA/Cu(II)/ PDMETA/ASAC	Time (h)	*N*	$M_{n\ NMR}$ (kDa)	SEC		Particle size (nm)		
					M_n (kDa)	Đ	Water	DMSO	Anisole
PS with high grafting density (PS_h, σ = 2.5±0.3 chains/nm^2)							120	120	210
PS_h@PMA_{3k}	1/266/0.1/1.0/0.5	0.5	36	3.1	4.2	1.7	120	--	220
PS_h@PMA_{6k}	1/533/0.1/1.0/0.5	1	70	6.0	6.6	1.9	160	--	320
PS_h@PMA_{10k}	1/533/0.1/1.0/0.5	2	128	10.0	12	2.1	140	200	300
PS_h@PMA_{15k}	1/533/0.1/1.0/0.5	2.5	171	15.0	18	2.0	120	230	340
PS_h@PMA_{20k}	1/533/0.1/1.0/0.5	3	220	19.0	21	2.1	140	--	340
PS_h@PMA_{30k}	1/1066/0.1/1.0/0.5	1	406	35.0	27	2.4	140	250	390
PS_h@PMA_{40k}	1/1066/0.1/1.0/0.5	3	493	42.0	40	2.5	140	250	440
PS_h@PMA_{50k}	1/1066/0.1/1.0/0.5	6	623	54.0	44	2.0	150	320	600
PS with medium grafting density (PS_m, σ = 0.80±0.03 chains/nm^2)							110	110	210
PS_m@PMA_{3k}	1/133/0.1/1.0/0.5	0.5	31	2.6	4.2	1.9	110	--	250
PS_m@PMA_{6k}	1/266/0.1/1.0/0.5	0.5	79	6.9	8.9	2.6	100	--	260
PS_m@PMA_{20k}	1/533/0.1/1.0/0.5	3	228	20.0	20	2.2	110	200	290
PS_m@PMA_{30k}	1/1066/0.1/1.0/0.5	2	349	30.0	27	2.1	120	240	330
PS_m@PMA_{40k}	1/1066/0.1/1.0/0.5	3	493	42.0	29	2.1	120	250	320
PS_m@PMA_{50k}	1/1066/0.1/1.0/0.5	4.5	593	51.0	35	2.4	130	260	340
PS with low grafting density (PS_l, σ = 0.17±0.02 chains/nm^2)							100	115	210
PS_l@PMA_{3k}	1/266/0.1/1.0/0.5	0.5	44	3.8	4.2	1.8	95	--	290
PS_l@PMA_{6k}	1/533/0.1/1.0/0.5	1	99	8.5	8.0	2.1	97	--	290
PS_l@PMA_{20k}	1/533/0.1/1.0/0.5	2	267	23.0	19	2.3	95	170	300
PS_l@PMA_{30k}	1/1066/0.1/1.0/0.5	1.5	377	32.0	15	2.2	103	180	300
PS_l@PMA_{40k}	1/1066/0.1/1.0/0.5	2	474	41.0	18	2.7	107	200	300
PS_l@PMA_{50k}	1/1066/0.1/1.0/0.5	2.5	610	52.0	34	2.2	97	180	320

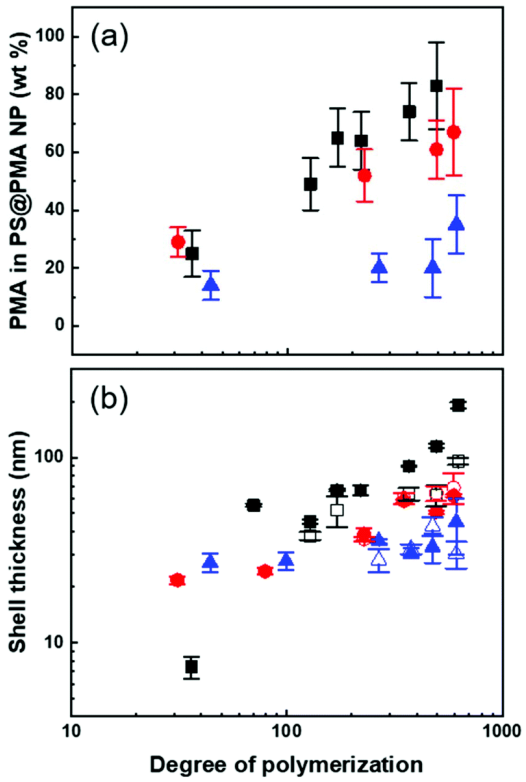

Figure 5.1.3 Effect of the architecture of the PMA canopy on (a) the mass fraction of PMA in the NPs measured by FT-IR, and (b) the shell thickness of the PMA layer for NPs in dilute suspensions in anisole (solid symbol) and in DMSO (open symbol) measured by DLS for PS@PMA NPs with increasing grafting density (▲) PS$_l$@PMA (0.17 chains per nm^2), (●) PS$_m$@PMA (0.80 chains per nm^2) and (■) PS$_h$@PMA (2.5 chains per nm^2).

The PS@PMA NPs with their well-defined composition were used to investigate the effect of the NP architecture on the behavior of their resulting suspensions. The thickness of the canopy of PMA was dependent on the solvent quality and decreased when the solvent quality became poorer.[207] In water, a poor solvent for both PS and PMA (Table 5.1.3), both PS and PMA were shrunken, and the variation in the diameter with the increase in the *N* of PMA was limited (Table 5.1.2). The difference in the swelling of the PS core in the various solvents used resulted in a variation of the effective grafting density observed for a given NPs (Table 5.1.1). In anisole, a good solvent for both PS and PMA, and in DMSO, a poor solvent for PS but a good solvent for PMA (Table 5.1.3), the PS@PMA NPs swelled and a variation of the thickness of the canopy with its architecture was observed. When pure PS NPs were dispersed in

anisole, they experienced swelling of *ca.* 100%, whereas when the same NPs were dispersed in DMSO they only experienced swelling of less than 15% (Table 5.1.2). PS@PMA NPs were dispersed in the same solvents and the difference in the size of the swollen PS@PMA NPs was compared to the size of the pure PS NPs in the same solvent to calculate the thickness of the PMA canopy. At low grafting density, only a marginal increase in diameter was observed because the canopy of PMA was collapsed on the surface and occupied a limited volume (Figure 5.1.3 and Table 5.1.2). At higher σ, an increase in the diameter of the NP was observed in water due to the crowding of neighboring polymer chains forcing PMA to adopt a stretched conformation.

Table 5.1.3 Flory-Huggins interaction parameters.

Solvent	Solvent quality (χ)×	
	PS	PMA
Anisole	0.18	0.25
DMSO	1.40	0.30
Water	3.13	2.33

× Calculated from the Hansen solubility parameters[208]

The thickness of the layer of tethered polymer chains on a substrate varies with *N*, the repulsion between the monomers, the solvent type, σ and blob size.[209, 210] When the substrate is the curved surface of a NP, the behavior of the end-tethered chains is more complex than that on a flat substrate due to the curvature dependence of the conformation of the polymer chain since the local polymer concentration decreases with an increase in the distance from the surface of the NPs.[96, 207] Here, the solvated radius of the NPs was used to calculate the thickness of the PMA corona (Figure 5.1.3b). The correlation between the thickness of the brush layer (*T*) and *N* in various solvents scales with:

$$T \propto k(N)^{\alpha} \qquad (5.1.1)$$

where α is the stretching parameter of the polymer chain, with $\alpha = 0$ for a canopy where the chains are completely collapsed on the surface and $\alpha = 1$ for canopies where the chains are completely stretched; the value of the scaling exponent α is a function of the grafting density and the solvent quality.[160] According to the extended Daoud–Cotton model and modelization and self-consistent field

theory, in good solvents, under semi-diluted grafting conditions, the thickness of the polymer canopy scales with $\sim N^{3/5}$ while at high grafting density the thickness of the brush layer should scale linearly with N.[27]

The results of the fit of Eq. 5.1.1 to the thickness of the PMA canopy (Table 5.1.4) show that in anisole and in DMSO, α increased as σ increased due to the steric constraints of tethered polymer chains. At a high grafting density, the variation in the thickness of the PMA canopy suggested that due to a high local polymer concentration and high solvent quality, the brushes adopted a stretched conformation. For NPs with moderate grafting density, the brushes were extended, but not fully stretched, indicative of the semi-dilute brush regime.[129] For samples with low σ, the polymer brushes adopted a more collapsed conformation. When the NPs were dispersed in water, no clear trend in the variation of the thickness of the PMA canopy with N and σ could be observed. The effects of N and σ on the thickness of the PMA canopy in good solvent suggest that, in anisole, the tethered chains were forced to adopt a stretched conformation on the surface of NPs with high and medium σ due to the steric hindrance, while at lower σ the tethered chain adopted a more relaxed conformation.

Table 5.1.4 The stretching parameter (α) calculated from the fitting of the variation of shell thickness and N (Eq. 5.1.1).

Solvent	Stretching parameter (α)		
	$PS_h@PMA_x$	$PS_m@PMA_x$	$PS_l@PMA_x$
Anisole	0.8 ± 0.3	0.6 ± 0.3	0.3 ± 0.2
DMSO	0.7 ± 0.3	0.7 ± 0.3	0.3 ± 0.3
Water	0.1 ± 0.4	0.2 ± 0.5	--

The behavior of the suspension of PS@PMA NPs, naked PS NPs and a binary mixture of PS NPs and free PMA_{40k} in anisole was investigated under a continuous shear. The solution of free PMA_{40k} chains and the solution containing a binary mixture of PS NPs and PMA_{40k} chains both displayed mostly Newtonian behaviors (Figure 5.1.4a) because of the limited interaction and entanglements in these systems. In contrast, suspensions of PS NPs and PS@PMA NPs exhibited a shear-thinning behavior attributed to the presence of highly swollen PS or PS@PMA in anisole leading to the formation of either jammed suspensions or interdigitated networks. [175, 211]

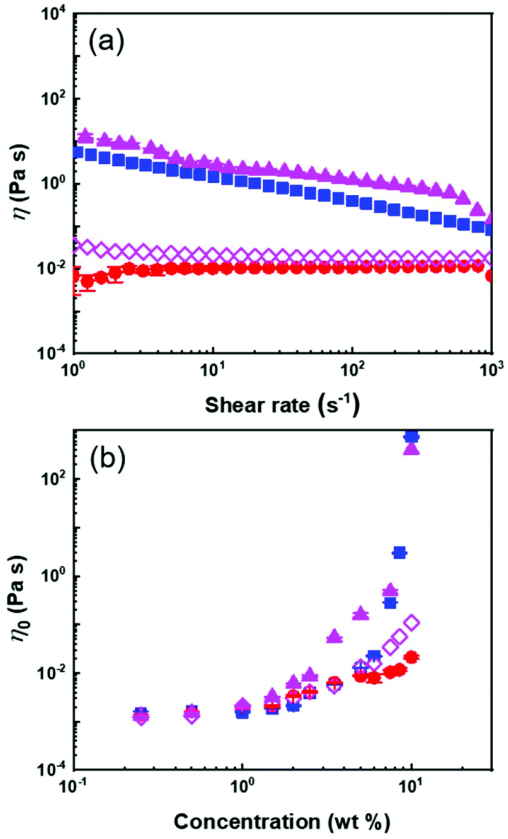

Figure 5.1.4 (a) Dynamic viscosity of 10 wt% suspensions and (b) the effect of the NP concentration of the zero-shear viscosity of suspensions of (■) PS NPs, (▲)PS_h@PMA_{40k} NPs, (●) free PMA_{40k} and (◇) a binary mixture of PS NPs and free PMA_{40k} in anisole.

The influence of the concentration on the viscosity of the NP suspensions was measured between 0 and 10 wt% in anisole. In continuous shear experiments, the viscosity of the PS@PMA suspension was affected by the number of NPs in the suspension and the architecture of the PMA canopy. The suspensions of PS@PMA displayed two regimes of distinct shear-dependent behavior (Figure 5.1.5); at a low concentration, the suspension behaved as a simple Newtonian liquid over the entire range of the shear rate studied, while at a higher concentration (*ca.* 5 wt% for PS_h@PMA_{40k}) the suspensions behaved like shear-thinning fluids.

The zero-shear viscosity (η_0) obtained for the suspensions prepared with the different NPs systematically increased with an increase in the concentration of NPs in the suspension (Figure 5.1.4b). The viscosity of the suspensions at a given concentration increases with an increase in N. However, the effect of σ was not as straightforward (Figure 5.1.6); for 10 wt% suspensions of NPs with relatively long brushes (N *ca.* 500),

the viscosities of high and medium grafting density samples were similar but larger than those of samples with the lowest grafting density. The influence of the architecture of the PMA canopy was especially evident when comparing suspensions containing the same number concentration of NPs (or the same number concentration of PS core) (Figure 5.1.7); for the same number of NPs in the suspensions, η_0 increased with σ, while the influence of the architecture was less critical when comparing suspensions containing the same amounts of methyl acrylate (Figure 5.1.7).

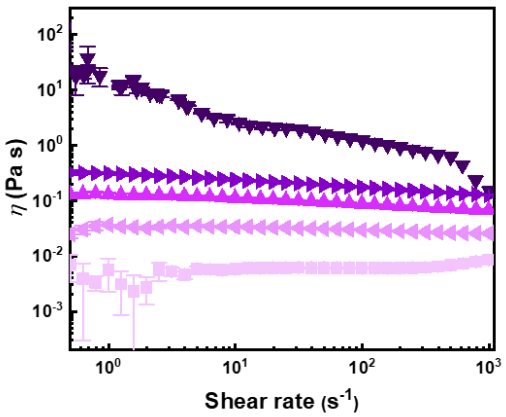

Figure 5.1.5 Influence of NPs concentration on the dynamic viscosity of suspensions of $PS_h@PMA_{40k}$ in anisole at different concentration; (■) 2.5 wt% (ϕ_{cal} = 0.014), (◀) 3.5 wt% (ϕ_{cal} = 0.20), (▲) 5 wt% (ϕ_{cal} = 0.29), (▶) 7.5 wt% (ϕ_{cal} = 0.43) and (▼) 10 wt% (ϕ_{cal} = 0.57).

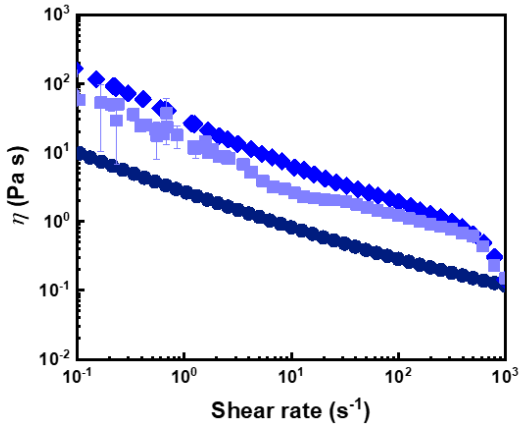

Figure 5.1.6 Continuous shear experiments of 10 wt% suspensions of $PS_x@PMA_{40k}$ NP. (■) $PS_h@PMA_{40k}$, (◆) $PS_m@PMA_{40k}$ and (●) $PS_l@PMA_{40k}$.

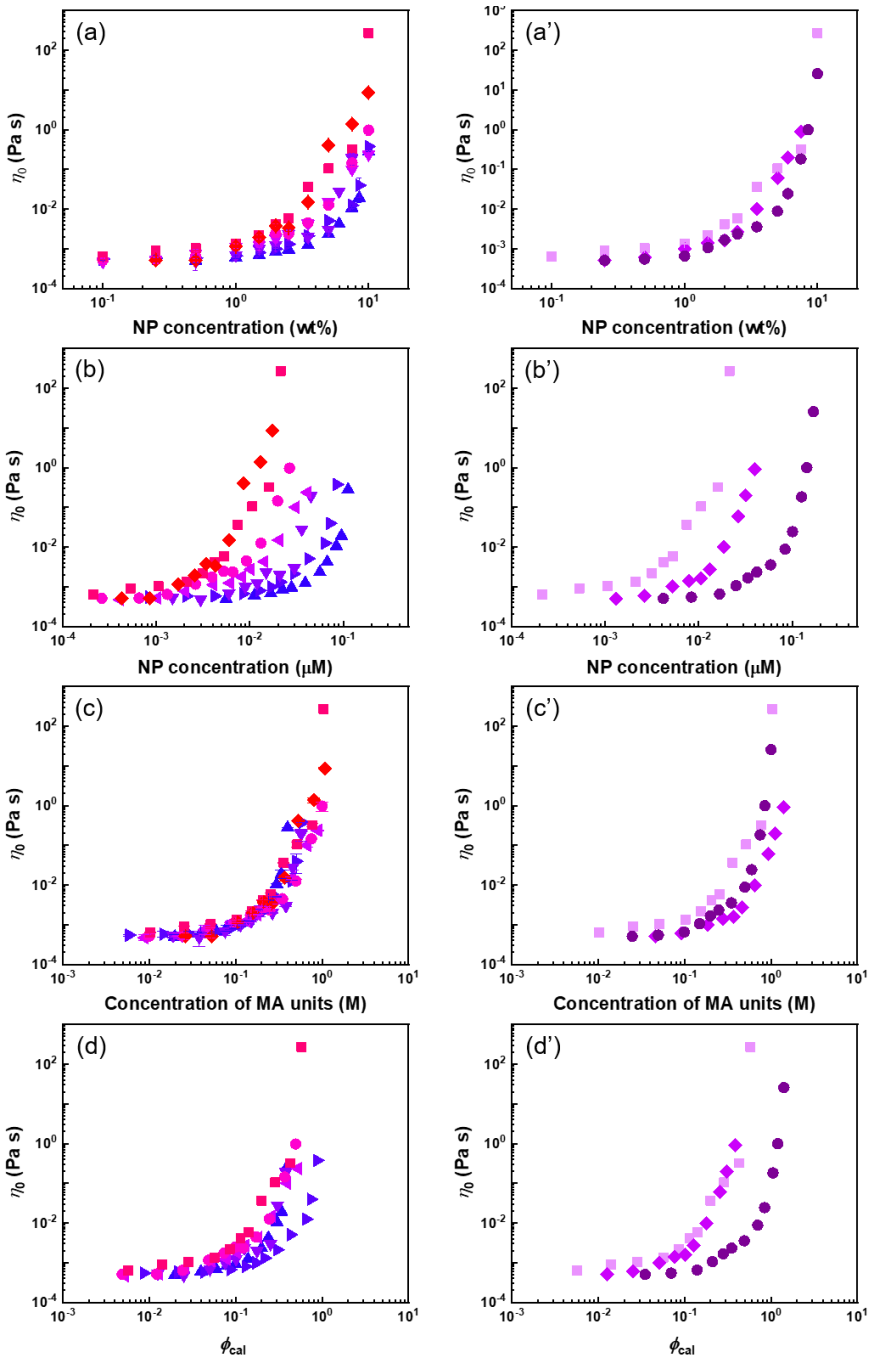

Figure 5.1.7 Zero-shear viscosities of PS@PMA NPs suspensions at different concentrations in anisole given in weight fraction of NPs (a), in molar concentration of NPs in suspension (b), in molar concentration of methyl acrylate units in the suspension (c) or in the calculate volume fraction (Eq. 4.2.1) occupied by the NPs (d). For (a,b,c,d) (▲) $PS_h@PMA_{3k}$, (▶) $PS_h@PMA_{6k}$, (▼) $PS_h@PMA_{10k}$, (◀) $PS_h@PMA_{20k}$, (●) $PS_h@PMA_{30k}$, (■) $PS_h@PMA_{40k}$ and (◆) $PS_h@PMA_{50k}$ and for (a', b', c') (■) $PS_h@PMA_{40k}$, (◆) $PS_m@PMA_{40k}$ and (●) $PS_l@PMA_{40k}$.

The transition between the dilute and semi-diluted regimes (C') was defined as the inflection point in the variation of η_0 with NP concentration (Figure 5.1.4b).[198] The C' of the PS suspension, caused by space jamming, was *ca.* 6 wt% and the C' of PS@PMA NPs decreased with the increase in the N and σ of the PMA chains (Figure 5.1.8). In comparison with PS NPs, PS@PMA NPs could, in addition to space jamming, also undergo interpenetration of the PMA canopy and entanglement of the PMA chains can occur for the chains with larger N, leading to an increase in viscosity. However, the addition of free PMA chains decreased the viscosity of the suspension (Figure 5.1.4).

Figure 5.1.8 shows that the concentration of NPs in the suspension required to observe the transition between the dilute and semi-dilute regimes decreased with increasing N and increasing σ. The interpenetration of the PMA canopy led to an earlier onset of the transition between the viscoelastic regimes. The rheological behavior of the suspensions, at any given N and σ, was mainly influenced by the methyl acrylate content in the suspension (Figure 5.1.9), and the observed C' decreased linearly with the number of methyl acrylate units decorating the PS core. The relation between C' and the NP architecture was further evidenced when the concentration of C' was calculated in terms of the number of NPs in the suspension ([NP]′ in Figure 5.1.9). In this case, as both N and σ increased, a decrease in [NP]′ was observed. However, the total amount of the polymer on the NP was the key factor influencing [NP]′, and similar effects on [NP]′ were observed for NPs with a few long PMA chains or multiple short PMA chains, an increase in either N or σ promoting the NP–NP interactions and reducing the number of NPs needed to achieve the same effect of the flow behavior of the suspensions.

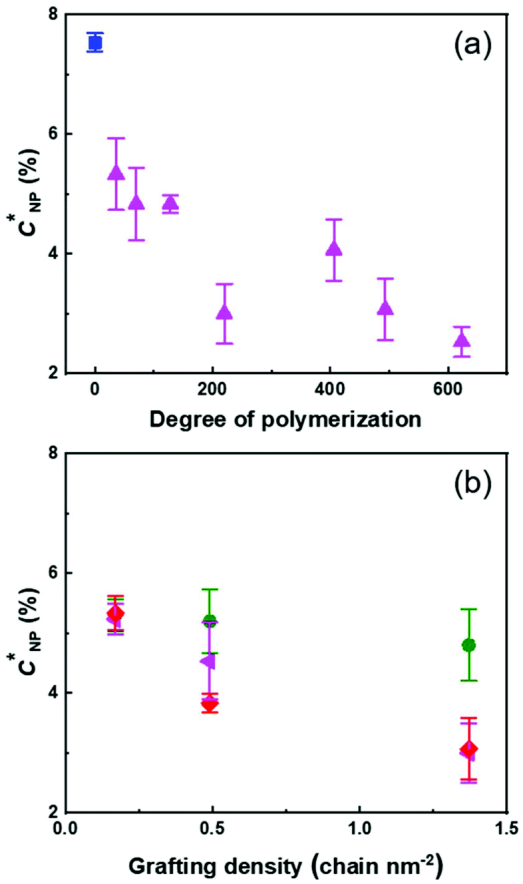

Figure 5.1.8 Effect of the architecture of the PMA canopy on the NP concentration at the transition between the dilute and semi-dilute regimes for a suspension of PS@PMA in anisole. (a) Effect of the PMA chain length for (▲) PS_h@PMA_x and (■) PS NPs, and (b) the effect of grafting density for (●) PS_x@PMA_{6k}, (◀) PS_x@PMA_{20k} and (◆) PS_x@PMA_{40k}.

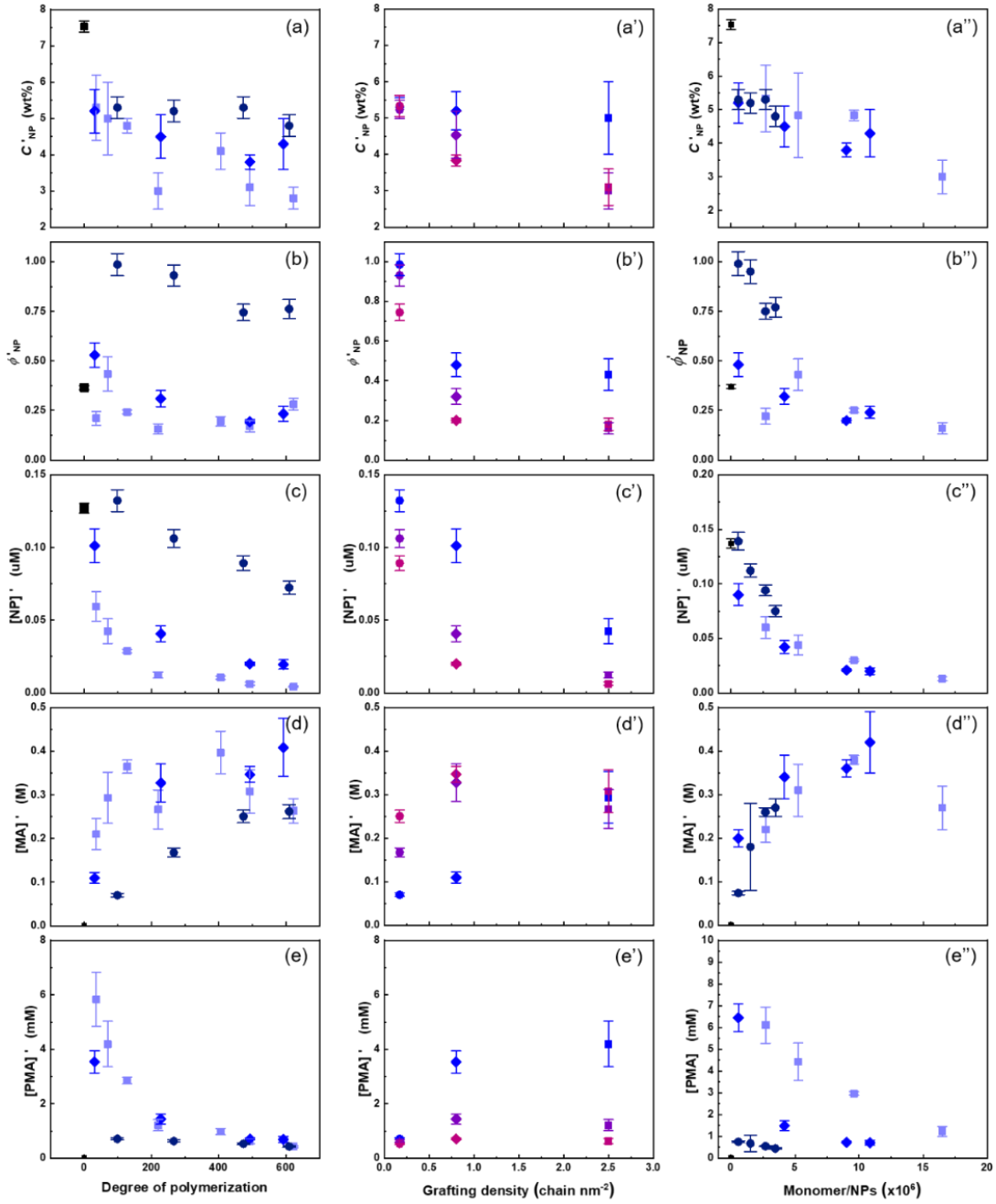

Figure 5.1.9 Variation of *C*' in anisole with the architecture of the PMA canopy. With *C*' expressed in (a) weight fraction of NPs in suspension, (b) volume fraction (Eq. 4.2.1) of NPs in suspension, (c) molar concentration of NPs, (d) molar concentration of methyl acrylate units in suspension and (d) molar concentration of poly(methyl acrylate) chains in suspension. For (■) PS NPs, (■) PS_h@PMA, (◆) PS_m@PMA and (●) PS_l@PMA and (●) PS_x@PMA_{6k}, (●) PS_x@PMA_{20k} and (●) PS_x@PMA_{40k}.

When the concentration of PS@PMA increased above *C′*, a transition between a liquid-like state and a gel-like state was observed for some NP architectures (Figure 5.1.10). Concentrated suspensions of PS NPs formed gels at a concentration greater than *ca.* 8 wt%, while suspensions of PS@PMA NPs with long chains (N > 200 units) formed gels at concentrations ranging from 2 to 15 wt%. However, suspensions of PS@PMA NPs with short chains (N < 175 units) did not form gels even at concentrations as high as 20 wt%. Similarly, binary mixtures of PS NPs and free PMA chains did not form gel-like suspensions even at high concentrations.

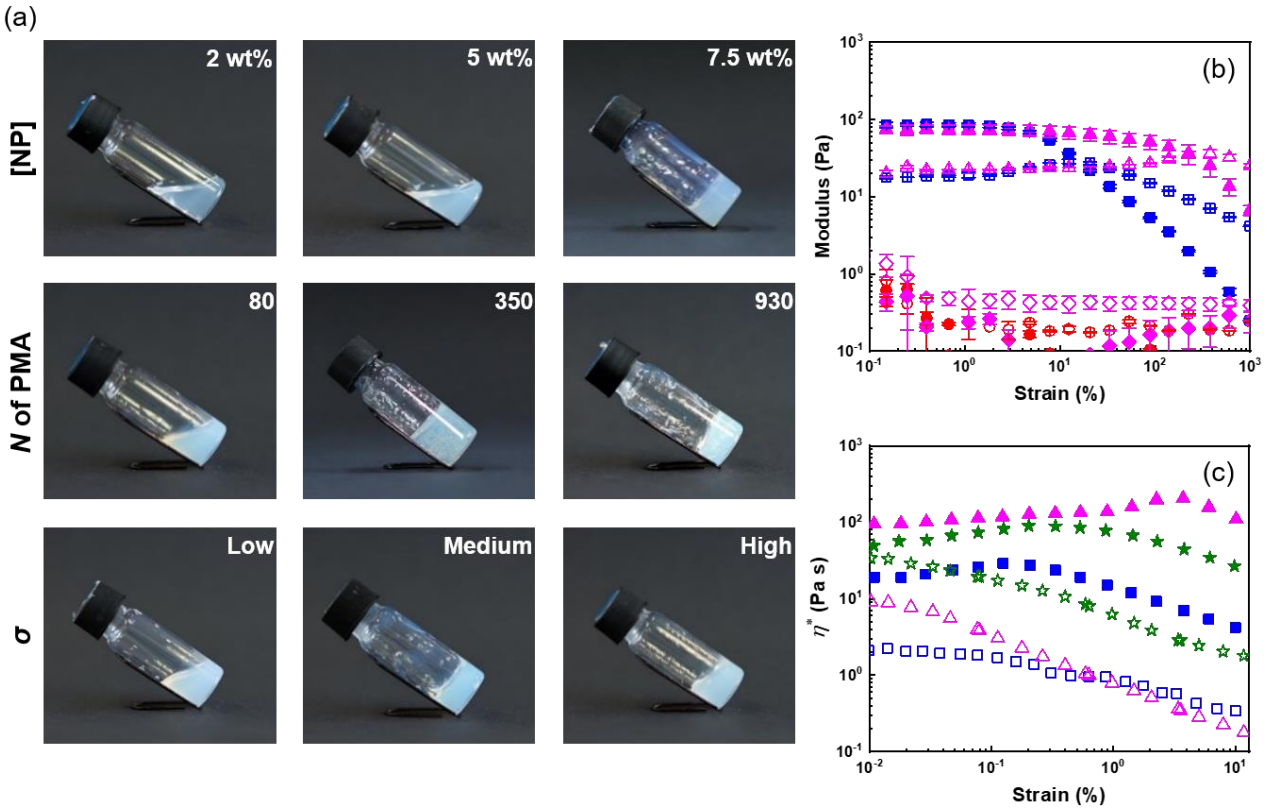

Figure 5.1.10 Formation of colloidal gels in concentrated suspensions of PS@PMA NPs. (a) influence of the NP concentration (PS_m@PMA_{20k}) and architecture of the PMA canopy (PS_m@PMA_x and PS_x@PMA_{20k}). (b) Elastic (solid symbol) and viscous (open symbol) moduli of 10 wt% suspensions of (■) PS NPs, (▲)PS_h@PMA_{40k} NPs, (●) free PMA_{40k} and (◆) a binary mixture of PS NPs and free PMA_{40k}. (c) Complex viscosity of 10 wt% suspensions of (■) PS NPs, (▲)PS_h@PMA_{40k} NPs, and (★)PS_m@PMA_{40k} NPs in anisole (filled symbol) and DMSO (open symbol).

Figure 5.1.10b shows that at 10 wt% in anisole, solutions of free PMA and binary mixtures of PS NPs and free PMA displayed viscous behavior while concentrated suspensions of pure PS NPs and of grafted PS@PMA behaved as viscoelastic solids ($G' > G''$). Furthermore, gels formed with pure PS NPs displayed a lower yield strain than the gels made of PS@PMA NPs. While PS@PMA NPs formed viscoelastic solids, the binary mixture of PS NPs and free PMA, with the same chemical composition, did not. The formation of colloidal gels by the PS NP suspensions could only be ascribed to core–core interactions and colloidal jamming. The addition of free PMA chains to the PS NPs suspension prevented the formation of such networks leading to a transition between a viscoelastic solid and a viscous liquid. Similarly, the grafting of short PMA chains also prevented efficient PS–PS interactions required to form a colloidal gel. However, when the PMA chains grafted to the PS core were much longer than the critical entanglement length ($N_{e,PMA} = 125$)[212] of PMA, the interpenetration, and potential entanglement, of the PMA canopies led to the formation of a network of PS@PMA NPs, where the PS core in the PS@PMA NPs acted as junction points. In addition to anisole, which is a good solvent for both the PS core and the PMA canopy, suspensions of PS@PMA were also prepared in DMSO, a selective solvent for PMA. When the same NPs were dispersed in DMSO and in anisole at the same concentration (Figure 5.1.10c and Figure 5.1.11), the suspensions in anisole systematically displayed more solid-like behavior and a larger complex viscosity than the suspensions in DMSO. Even when taking into account the volumes occupied by the NPs in different solvents (Figure 5.1.12), only weak gels were formed in DMSO, although the polymer canopies were similarly swollen in both solvents (Figure 5.1.3 and Table 5.1.4). The swelling of the core in anisole in comparison with that in DMSO was the only variable parameter and the easier gelation in anisole must be ascribed to the interplay between the PS core and the PMA canopy.

Both the modulus and the yield strain of the PS@PMA NP suspensions were affected by the architecture of the PMA canopy. Figure 5.1.13 shows that, at a fixed σ, as N of the canopy increased, the modulus of a 10 wt% suspension increased and the behavior of the suspension transitioned from liquid-like to gel-like. This transition was observed at a concentration much lower than what was observed with hard NPs functionalized with polymer chains. This was even more directly observed by comparing the mechanical properties of PS@PMA NPs in suspensions in anisole and in DMSO. The suspensions in anisole contained soft core NPs surrounded by a soft canopy and suspensions in DMSO were composed of a hard core functionalized with the same polymer canopy (Figure 5.1.12). The suspensions in anisole of PS@PMA NPs functionalized with short PMA chains ($N < 150$ units) did not form gels in the concentration range studied. The stiffness of the suspension, defined as $G^* (G' + iG'')$ in the low strain regime, increased as a

function of N (Figure 5.1.14 and Figure 5.1.11). However, when the chain length was kept constant and σ increased (Figure 5.1.13b) the properties of the colloidal gels prepared with the NPs varied in a more complex manner. For suspensions of PS_x@PMA_{20k} NPs (short brushes of N *ca.* 225 units) at 10 wt% in anisole only PS_m@PMA_{20k} and PS_l@PMA_{20k} displayed a gel-like behavior, the suspension of NPs with the highest grafting density, PS_h@PMA_{20k}, remained a viscous liquid. The colloidal gel of PS_m@PMA_{20k} NPs was the stiffest (higher G^*) and strongest (higher yield strain). However, for PS_x@PMA_{40k} NPs having longer PMA chains (N *ca.* 500 units) the formation of colloidal gels was observed for the three different σ (Figure 5.1.12) and the gels prepared with the PS_l@PMA_{40k} NPs were both the weakest and the most fragile, those prepared with PS_h@PMA_{40k} NPs showed the highest yield strain, and those prepared with PS_m@PMA_{40k} NPs were the strongest. These results show that high σ can prevent the efficient interdigitation of the PMA canopy and the resulting effective NP–NP interactions due to the large local PMA concentration in the canopies with high σ. Increasing the length of the polymer brush alleviated this effect likely because the effective local concentration of the polymer decreased as the distance between the surface of the PS core and the surface of the PMA canopy increased. In DMSO, the formation of colloidal gels was only observed for highly concentrated suspensions of PS_m@PMA and PS_h@PMA with long PMA chains.

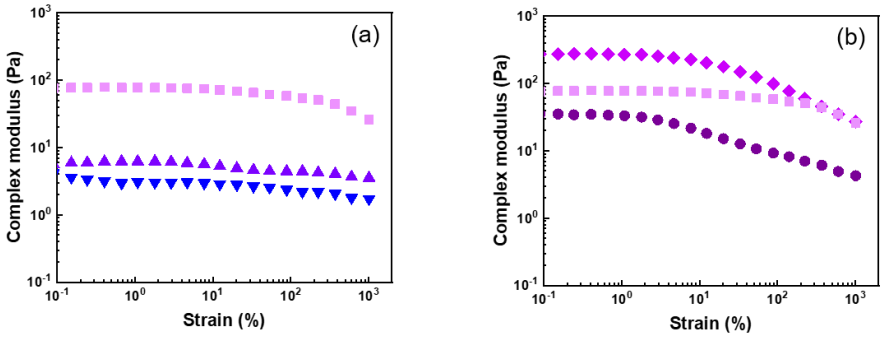

Figure 5.1.11 Complex modulus (G*) as a function of strain for PS@PMA suspensions at 10 wt% in anisole. (a) (▼) PS_h@PMA_{20k}, (▲) PS_h@PMA_{30k} and (■) PS_h@PMA_{40k} and (b) (●) PS_l@PMA_{40k}, (◆) PS_m@PMA_{40k} and (■) PS_h@PMA_{40k}.

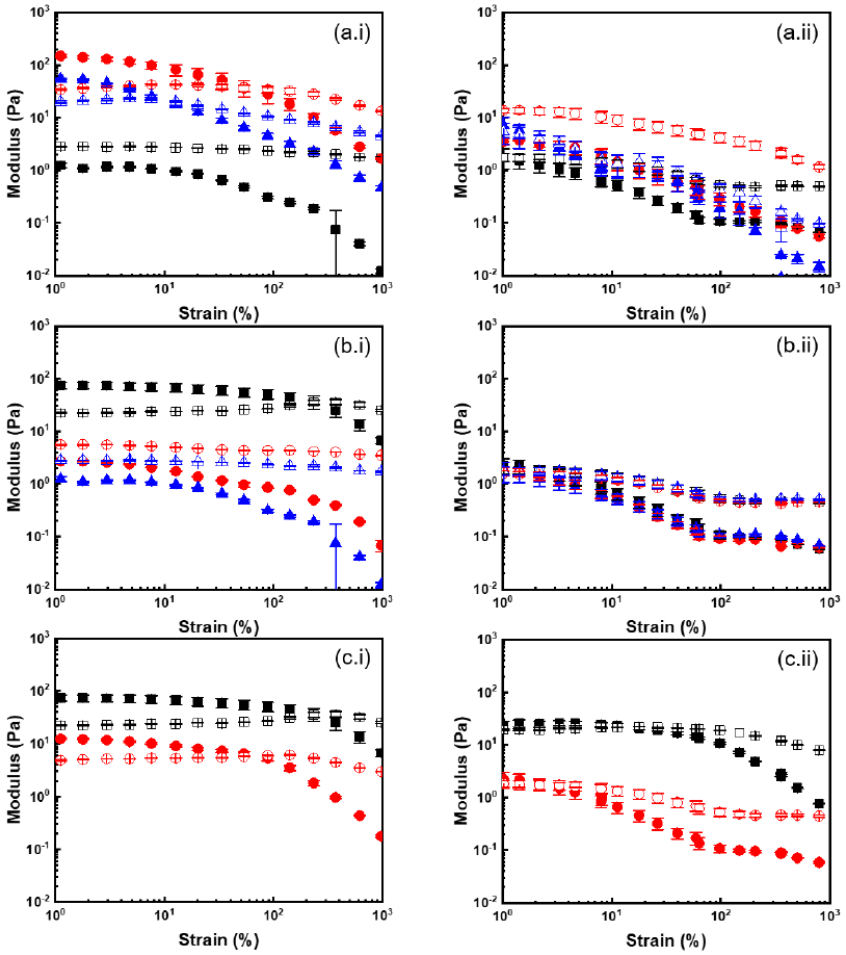

Figure 5.1.12 Elastic (close) and viscous (open) modulus of PS@PMA suspension in (i) anisole and (ii) DMSO. (a) Effect of the grafting density on 10 wt% suspension of (■) PS_h@PMA_{20k}, (●) PS_m@PMA_{20k} and (▲) PS_l@PMA_{20k}. (b) Effect of the brush length on 10 wt% suspension of (■) PS_h@PMA_{40k}, (●) PS_h@PMA_{30k} and (▲) PS_h@PMA_{20k}. (c) Effect of nanoparticle concentration in suspension of PS_h@PMA_{40k} in anisole at (■) 10 wt% (ϕ_{cal} = 0.62) and (●) 4.5 wt% (ϕ_{cal} = 0.27) and in DMSO at (■) 19 wt% (ϕ_{cal} = 0.50) and (●) 10 wt% (ϕ_{cal} = 0.25).

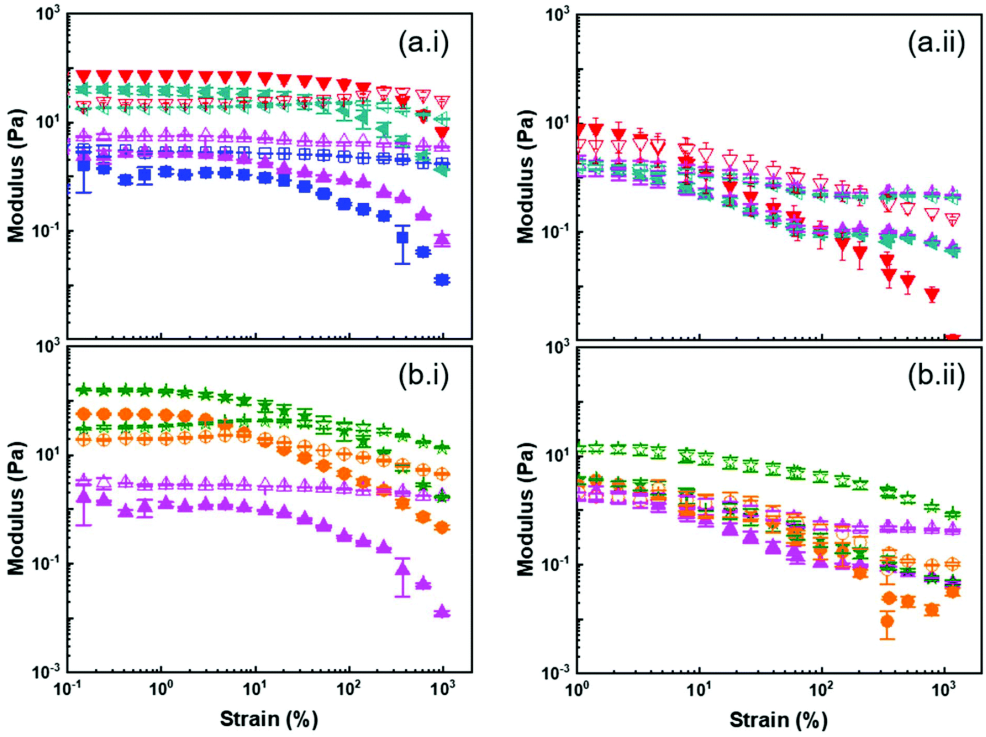

Figure 5.1.13 Visco-elastic behaviour (G' (solid symbol) and G'' (open symbol)) of 10 wt% suspensions of PS_x@PMA_N in anisole (i) and DMSO (ii). (a) Effect of the PMA brush length for (■)PS_h@PMA_{10k} NPs, (▲) PS_h@PMA_{20k}, (◀) PS_h@PMA_{30k}, and (▼) PS_h@PMA_{40k}. (b) Effect of grafting density for (●) PS_h@PMA_{20k}, (★) PS_m@PMA_{20k} and (▲) PS_l@PMA_{20k}.

Figure 5.1.14 shows that the gelation of PS@PMA NPs with longer PMA chains, for which interdigitation of the PMA canopy was favored, led to an increase in the cohesion of the network formed. Yet, increasing the grafting density over a certain point decreased the efficiency of the canopy interdigitation. However, when the gels were prepared with a constant number of NPs in concentration (Figure 5.1.15), an increase in both N and σ led to an increase in the modulus and yield strain of the colloidal gels. The mechanical properties of the colloidal gels suggested that both the number of PS cores acting as either a cross-linking point or a filler in the polymer network and the fraction of PMA in the samples and thus the canopy interdigitation were critical in determining the final behavior of the suspension.

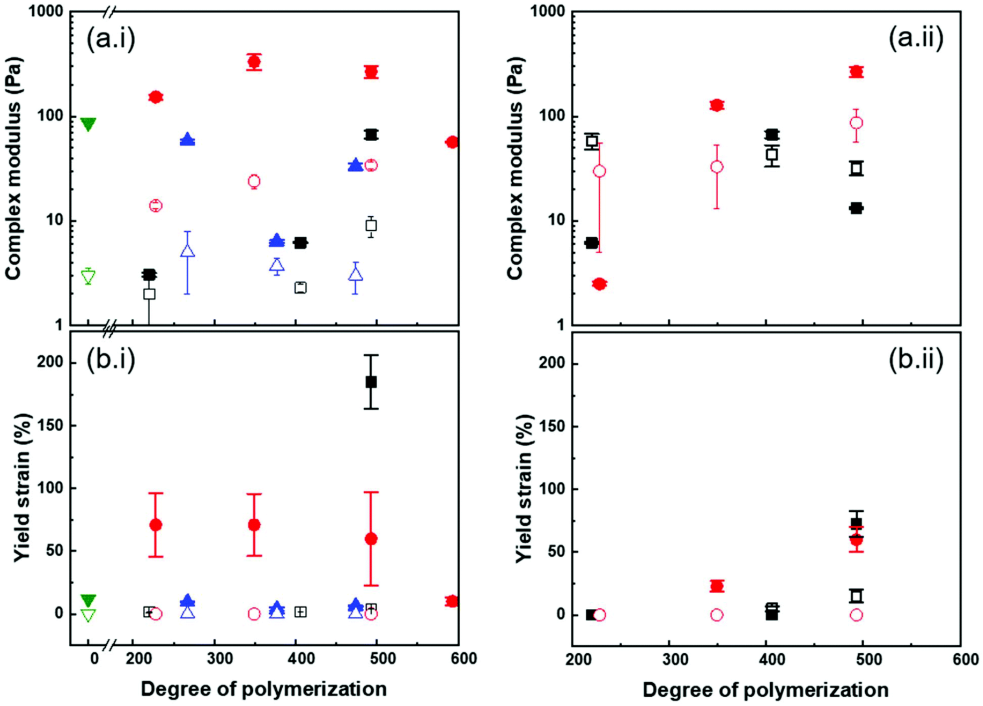

Figure 5.1.14 Effect of the architecture of the PMA canopy on the properties of the colloidal gels formed with (i) C = 10 wt% or (ii) ϕ_{cal} *ca.* 0.5 of (■) PS$_h$@PMA, (●) PS$_m$@PMA, (▲) PS$_l$@PMA and (▼) PS$_h$@PMA$_{40k}$ in suspensions in anisole (closed symbol) or DMSO (open symbol).

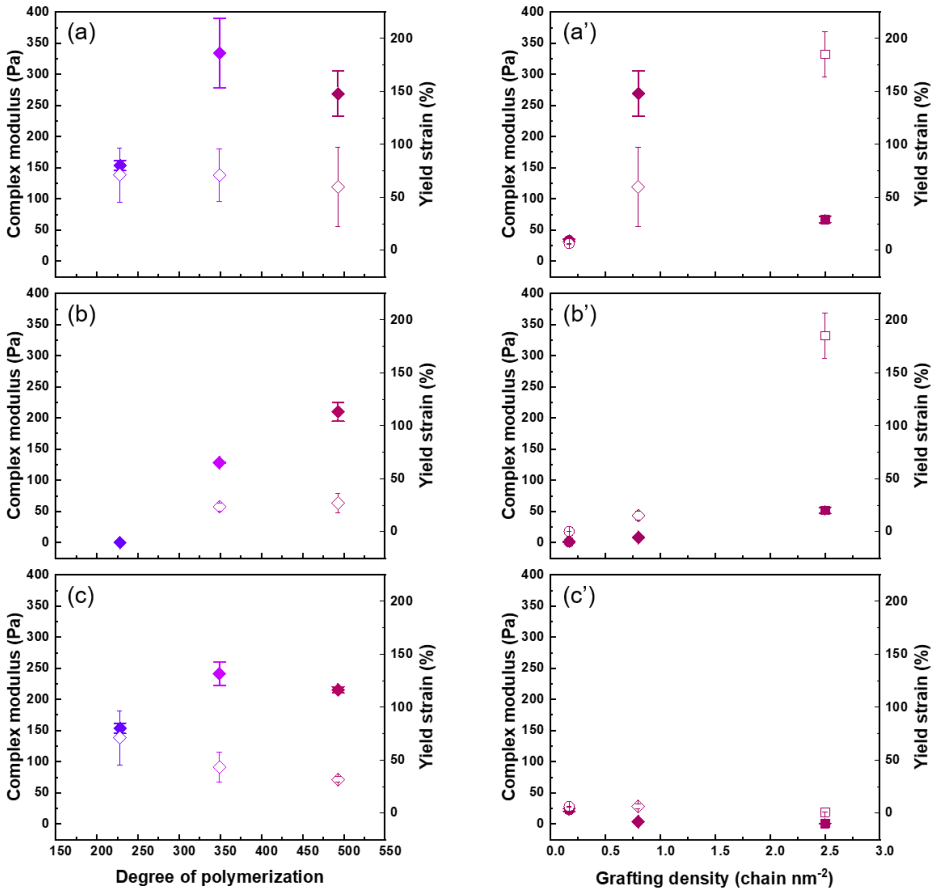

Figure 5.1.15 Effect of the architecture of the PMA canopy on the stiffness (closed symbol) and the strength (open symbol) of the colloidal gels formed with (◆) $PS_m@PMA_{20k}$, (◆) $PS_m@PMA_{30k}$ and (◆) $PS_m@PMA_{40k}$, (■) $PS_h@PMA_{40k}$ and (●) $PS_l@PMA_{40k}$. For suspension with constant weight fraction (a, a'), molar concentration of NPs (b, b') and constant concentration of methyl acrylate units (c, c').

At a constant mass fraction of NPs, suspensions of PS@PMA NPs in anisole were systemically stiffer and tougher than the suspensions of the same NPs in DMSO. While the canopies of the PS@PMA NPs were undergoing similar swelling in both solvents, it was not the case for the PS core. Taking into account the volume occupied by each NP in the different solvents, the concentration of NPs in suspension in DMSO needed to be higher than in anisole to reach the same volume fraction. Even when comparing suspensions with similar volume fractions of NPs, the suspensions in anisole behaved in a more solid-like manner and these suspensions were tougher, with significantly larger yield strain than the suspensions prepared in DMSO (Figure 5.1.14). The difference in yield strain cannot be ascribed to the difference in the canopy architecture. Even if the variation of the grafting density during the swelling of the PS core was taken into

account, the samples prepared PS_h@PMA dispersed in anisole should be directly comparable to the suspension of PS_m@PMA in DMSO. The respective effective grafting density was 0.80 chains per nm^2 for PS_m@PMA in DMSO and 0.82 chains per nm^2 for PS_h@PMA in anisole. Since the PMA canopies had similar structures in anisole and in DMSO, the conformation of the chain in the canopy was similar in both solvents; thus the ease of interpenetration between adjacent NPs should be similar in both solvent, since the main difference between the two systems was only the swelling of the PS core. The results suggest that having NPs with a soft core functionalized with a polymer canopy favors the formation of tough and strong gels even at low concentrations.

5.1.3 Conclusion

In summary, a library of PS@PMA core-canopy particles with different canopy architectures, *i.e.*, chain length (N) and grafting density (σ), was prepared and their behavior in suspensions was analyzed using rheology. The conformation of the end-tethered polymer chains transitioned from collapsed chains, to brushes, to stretched brushes and was influenced by the degree of polymerization, grafting density and solvent quality. Using selective solvents uniquely for the canopy or a common solvent for the core and the canopy, suspensions with different behaviors were obtained, those with a "hard core" and those with a "soft core".

Polymer-functionalized soft core NPs displayed similar trends as expected for more traditional hard core NPs. As expected, suspensions of soft PS NPs and soft PS@PMA NPs displayed a non-Newtonian behavior. The soft PS NPs formed jammed suspensions while for suspensions of soft PS@PMA NPs the interdigitation of the PMA canopy could be the main contributor to the shear thinning behavior. The viscosity of the suspension was governed by both the concentration of the NPs in the suspension and the architecture of the PMA canopy. The concentration at which the transition between the dilute and semi-dilute regimes occurred shifted to a lower concentration with increasing N and σ.

As the concentration increased, the PS@PMA suspensions transitioned from a viscous liquid to a gel in which the PS core was a junction point for the entangled grafted PMA chains. This transition was observed at lower concentrations for NPs dispersed in a solvent where both the core and the canopy were swollen. The key factor affecting the sol–gel transition of the PMA functionalized PS NPs was the number of MA

units decorating the PS core, but the properties of the resulting gels were largely influenced by the architecture of the PMA canopy and the swelling of the core. More effective interdigitation between the NPs occurred at high N and moderate σ due to the increased opportunity for canopy interpenetration. Gels were formed with either naked PS NPs or PS@PMA NPs with long PMA chains, where the interdigitation of the PMA canopy could be accompanied by chain entanglements, but not with $PS_x@PMA_N$ NPs with short polymer brushes ($N < 200$ methyl acrylate units) or binary mixtures of PS NPs and free PMA chains. It was found that the mechanical properties of the suspension, both moduli and yield strain, were affected by both the corona architecture and concentration of NPs in the suspension. The direct comparison of soft-PS@soft-PMA NP and hard-PS@soft-PMA NP suspensions revealed that the soft NPs formed gels at lower concentrations and that the gels at similar NP contents were stronger and tougher when the core of PS@PMA was softer in comparison with suspensions prepared with a hard core. These results provide information to tailor the behavior of the polymer latex by controlling the architecture of a layer of the grafted polymer to tune the rheological and mechanical properties of the latex suspensions.

5.2 Dynamics of soft and hairy polymer nanoparticles in a suspension by NMR relaxation[2]

The previous section explored the macroscopic behavior of suspension of polymer nanoparticles functionalized with end-tethered polymer chains. The results show that the macroscopic behavior was influenced by interparticle interactions such as chain entanglement and interdigitation. In this section, the local behavior of the grafted system was studied by NMR spectroscopy to understand more precisely how the NPs architecture influences the behavior of the system at the polymer subsegmental scale.

The design of surface-modified functional nanoparticles (NPs) is used to control the properties of the NPs and the NP/environment interactions. The efficient control of the final behavior of the NPs demands a comprehensive understanding of the resulting system. This is particularly challenging for systems with an architecture of the type polymer core–polymer canopy. In such systems, one of the key parameters influencing the behavior of the NPs is the local dynamics of the polymer canopy. However, because the grafting points of the canopy are experiencing their own local dynamics, predicting the final behavior of such systems is difficult. To get a deeper understanding of NPs made of a soft and swollen polymer core and a swollen polymer canopy, a library of hairy NPs made of a polystyrene (PS) core and a canopy of grafted poly(methyl acrylate) (PMA) chains was prepared. The softness of the PS core and the thickness of the PMA canopy were controlled, and the behavior and dynamics of the soft and hairy PS–PMA NPs in suspension were measured by ^{1}H NMR relaxation and dynamic light scattering. It was observed that the rigid PS core slowed down the subsegmental dynamics of the PMA chains, while thick PMA canopies

[2] This section is based on the article:

[redacted] Dynamics of Soft and Hairy Polymer Nanoparticles in a Suspension by NMR Relaxation. *Macromolecules* **2020,** *53*, 844-851. DOI:10.1021/acs.macromol.9b01813 Reproduced permission from copyright 2020 American Chemical Society.

Author contribution: [redacted] designed the experiments. [redacted] performed the experiments. [redacted] conducted relevant characterization [redacted] analyzed the data [redacted] discussed the results. [redacted] wrote the manuscript.

accelerated the relaxation of the PS core. The dynamics of the NPs in suspension was the result of the interplay between the PS core and the PMA canopy.

5.2.1 Motivation

Previous studies of the relaxation dynamics of grafted chains, both experimentally and by simulation, have demonstrated that the presence of a substrate significantly affects the subsegmental dynamics of the tethered polymer chains and can impact the mechanical properties of the resulting materials. [31, 32, 131, 180] However, there are significant discrepancies in the effect of different canopies architectures of the local chain dynamics. The presence of the substrate usually creates a confinement effect influencing the relaxation of the tethered polymer chains, and this effect decreases with increase in N. [181-183] For example, studies of the relaxation dynamics of a polymer chain grafted on inorganic NPs have shown that the relaxation rate of short tethered chains was increased by orders of magnitude in comparison to the untethered chains because of the conformational changes of the polymer chains, and as the chain length increased, the relaxation rate of the tethered chains converged to the relaxation rate observed for untethered chains of similar molecular weight. [31] Other studies have shown that the relaxation of grafted polymer chains was impeded in comparison to free polymer chains of the same molecular weight because of their immobilization on a substrate. [213]

Such differences arise from different methods used to analyze the polymer dynamics, which can probe different types of relaxation processes and give access to different physical characteristics. For example, a study, using neutron spin echo (NSE), has shown significantly faster chain dynamics for poly(methyl acrylate) (PMA) grafted to silica particles when the length of the chain was increased above the threshold for the transition from the concentrated brush region, close to the substrate, and the semidiluted brush region. [32] However, a recent study using neutron backscattering (BS) of a similar system of PMA chains grafted to silica NPs has shown that there is only a limited effect of N of the grafted chain on the local relaxation of the polymer. [214] These studies were not probing the same dynamics; NSE measures the global dynamics over a wide range of correlation time, [33] , whereas BS was used to probe the subsegmental dynamics. [215] Similarly, nuclear magnetic resonance (NMR) spectroscopy can be used

to probe local subsegmental relaxation of grafted polymer chains and gives access to faster subsegmental dynamics that involve motions, vibrations, and rotation of side groups. [216]

NMR spectroscopy is a versatile method to interpret the local dynamics of polymers[217] and has been used to study functionalized NPs in suspension. [218-220] NMR relaxation is an ideal method to study the behavior of swollen soft NPs functionalized with polymer chains because it allows for the simultaneous and independent characterization of the local behavior of the core particle and the canopy of end-tethered polymer chains. In NMR spectroscopy, the spin–lattice (T_1) and spin–spin (T_2) relaxation times can be correlated with the local molecular motions in the molecules. [221] In particular, unlike other methods used to probe polymer dynamics, such as dielectric spectroscopy, NMR relaxation provides information on the local dynamics of specific chemical groups in the macromolecular structure without the need for labeling. [216]

Most of the studies devoted to the relaxation of end-tethered polymer chains have focused on the polymer grafted to rigid solid substrates, such as silica or gold NPs, where the tethering points can be considered as fixed. The effect of having softer substrates with faster relaxation dynamics has been largely overlooked so far. [222-224] In such systems, in addition to the dynamics of the canopy of end-tethered polymer chains, the dynamics of the core also need to be taken into account. Then, the system becomes more complex, and the interpretation of the results is more challenging in comparison to polymer chains grafted on rigid inorganic cores.

Here, to address the complex dynamics in a system where both the canopy of the end-grafted polymer and the particle core undergo relaxation in a similar frequency range, the study of the local dynamics of hairy NPs with a polymer–polymer core–canopy architecture was studied by NMR spectroscopy. The core–canopy architecture was designed with a polystyrene (PS) core and a canopy of PMA (Figure 5.2.1). The cross-linking density of the core, and thus the softness of the core of the particle, was tuned by the addition of different amounts of divinylbenzene (DVB) during the synthesis of the PS nanonetwork. Then, SI-ATRP was used to grow the PMA chains from the initiators immobilized on the PS surface. The relaxation dynamics of the resulting PS–PMA hairy NPs in suspension was investigated by NMR relaxation at different temperatures and magnetic fields. The length of the PMA chains and the cross-linking density of PS cores were controlled to understand the relationship between the rigidity of core and the degree of polymerization of the polymer canopy and the local dynamics in NPs.

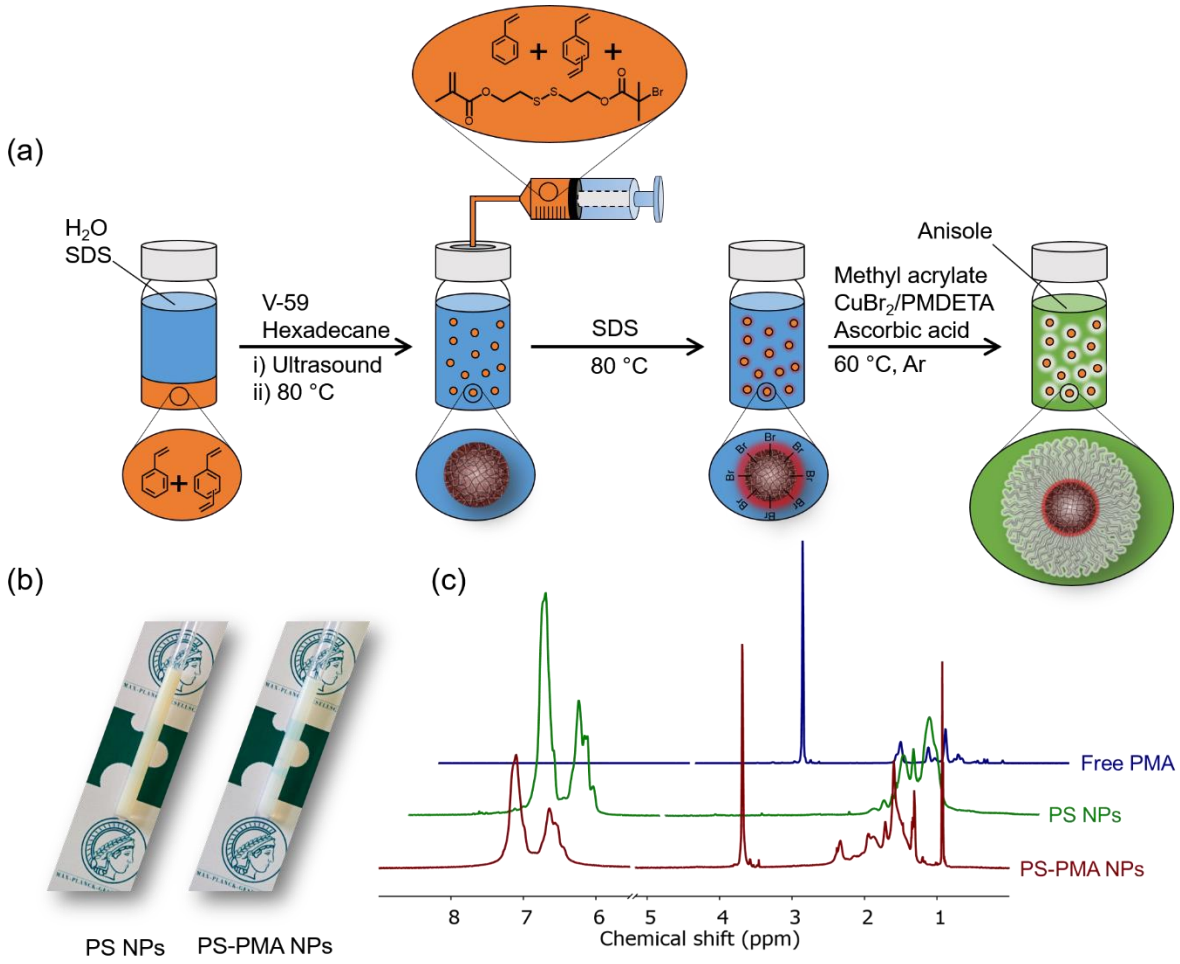

Figure 5.2.1 (a) Synthesis of PS NPs and PS–PMA NPs by a tandem approach based on miniemulsion polymerization and SI-ATRP. (b) Photographs of stable suspensions of PS NPs and PS–PMA NPs in DCM. (c) NMR spectra of free PMA chains, PS NPs, and PS–PMA NPs (CD_2Cl_2, 700.02 MHz, 298 K).

5.2.2 Results and discussion

The synthesis of a library of PS NPs functionalized with PMA chains was carried out in a multistep manner. First, PS–DVB NPs were prepared by miniemulsion polymerization using different amounts of DVB (from 0.5 to 10 mol % of cross-linkers). Afterward, a layer of cross-linked PS containing 5 mol % of the ATRP initiator was polymerized at the surface of the PS–DVB NPs in a starved–fed regime. The

resulting cross-linked PS NPs swelled in a good solvent, such as DCM, and their swelling varied between 370 and 1000% depending on the cross-linking density (Table 5.2.1) and provided NPs with different softness used as the "core" to graft a "canopy" of PMA. Then, using a "grafting from" approach, PMA chains were polymerized from the ATRP initiators immobilized at the surface of the PS NPs. The molecular weight of the resulting end-tethered polymer chains varied from 3.5 to 26.2 kg mol^{-1} (or 41 to 305 units). The density of the ATRP initiators on the surface of the PS–DVB NPs was ca. 0.8 chains nm^{-2} in water and after redispersion and swelling in DCM ca. 0.2 chains nm^{-2} (Table 5.2.1).

Table 5.2.1 Grafting density and size of PS NPs in H_2O and in DCM.

DVB in PS Core (mol%)	Grafting density in H_2O (chains nm^{-2})	Radius of NPs in H_2O (nm)	Radius of NPs in DCM (nm)
0.5	0.81±0.06	45	95
3	0.86±0.07	51	92
10	1.08±0.08	69	85

Dispersing the hairy PS–PMA NPs in a good solvent, such as DCM, resulted in a stable suspension because of the combined swelling of the core and the polymer canopy. The change of the solvated radii (R_h) of PS–PMA NPs with different degrees of cross-linking was studied in DCM, a good solvent for both PS and PMA (Figure 5.2.2). The particles systematically swelled in DCM in comparison to the particles dispersed in water (in the presence of surfactant) a non-solvent for both PS and PMA (Figure 5.2.3). The results show that in DCM the size distribution of the unfunctionalized NPs was systematically larger than for the NPs functionalized with short PMA chains, although the unfunctionalized PS NPs were used as the substrate to grow the PMA chains for the preparation of the PS–PMA samples. DCM is a better solvent for PMA than for PS, and the addition of PMA likely increased the colloidal stability of the NPs by preventing particle agglomeration more efficiently. Nevertheless, all the PS–PMA NPs cross-linked with different amounts of DVB showed a similar overall trend; as N of the grafted PMA chains increased, an increase in the size of the NP was observed and the relationship between the thickness of the grafted polymer layer (H) and N of the PMA chains scaled as $H \propto N^{0.75\sim0.72}$ (Figure 5.2.4). This scaling relationship was similar to what has been observed for chains grafted on spherical NPs adopting a stretched brush conformation ($H \propto N^{0.83}$ for poly(methyl methacrylate) in acetone and $H \approx N^{0.7}$ for PS in benzene).

[27, 97, 98, 225] These stretching factors suggest that in the PS–PMA NPs, the end-tethered PMA chains were in a stretched brush regime.

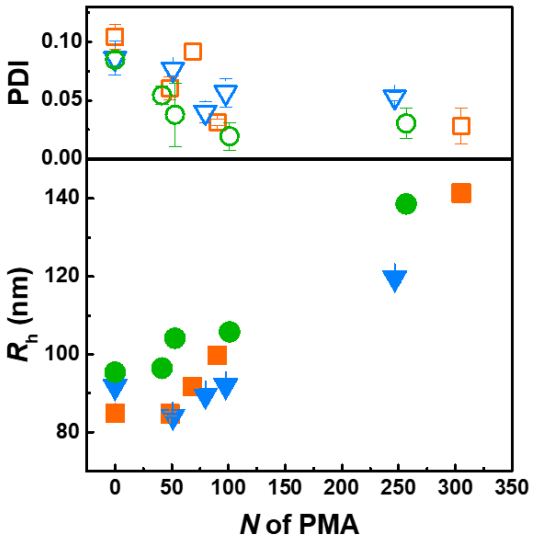

Figure 5.2.2 Size (R_h) and size distribution (PDI) of PS–PMA NPs functionalized with PMA chains with a degree polymerization (N) ranging from 0 to 305 units, measured by DLS in DCM. NPs with cross-linked PS cores prepared with 0.5 mol % of DVB (green circle), 3 mol % of DVB (blue triangle), and 10 mol % of DVB (orange square).

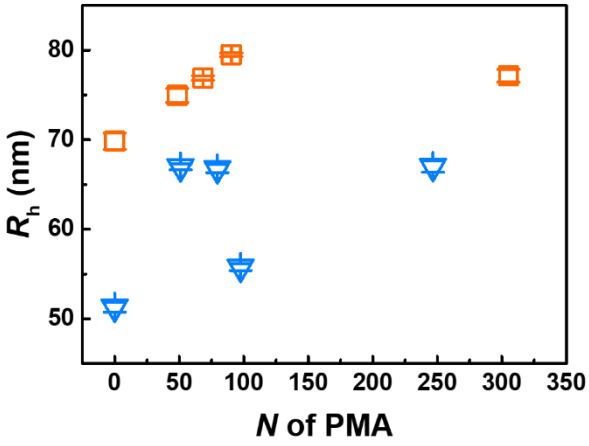

Figure 5.2.3 Hydrodynamic radius of PS-PMA NPs in water (in the presence of surfactant) measured by dynamic light scattering for NPs prepared with 3 mol% of DVB (blue triangle) and 10 mol% of DVB (orange square) as cross-linker.

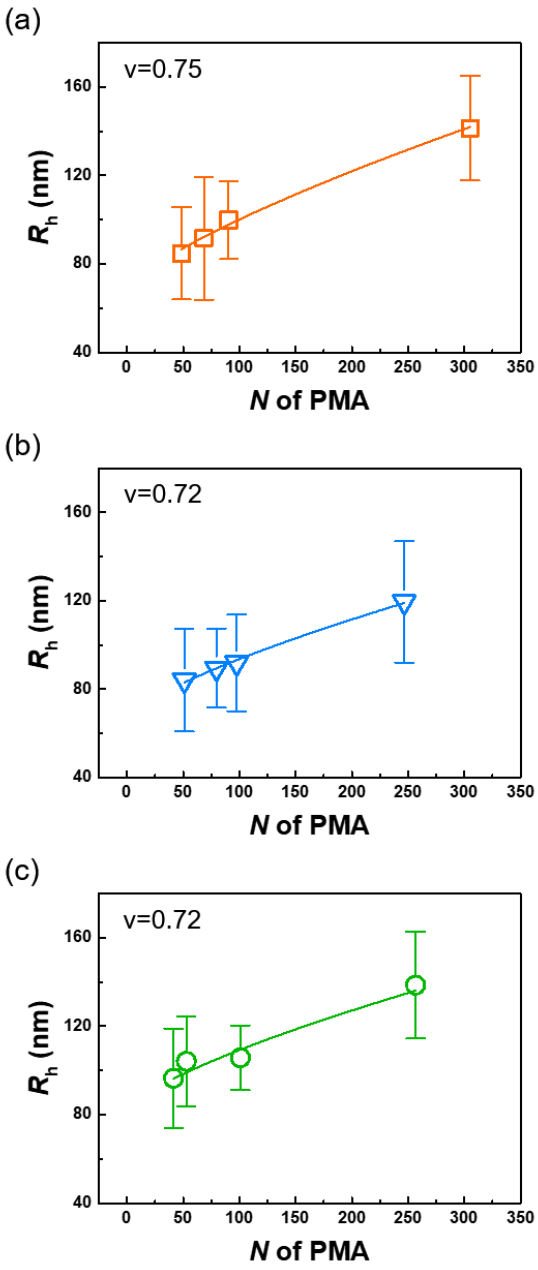

Figure 5.2.4 Radius of PS-PMA NPs with (a) 10 mol%, (b) 3 mol%, and (c) 0.5 mol% of DVB in DCM versus degree of polymerization (N) with the curve fit of $H \sim \mathrm{DP}^{\nu}+\mathrm{A}$.

NMR spectroscopy was used to individually study the average relaxation of the PS and PMA in different PS–PMA NPs. All the relaxation curves could be fitted to a monoexponential decay (Figure 4.2.3), indicating that the relaxation process of every type of proton could be described by one single relaxation mechanism or by a distribution of T_1 averaged by spin diffusion. T_1 is the measure of the rate of energy

transfer from an excited nucleus (the spin) to other molecules or nucleus in its immediate environment (the lattice) and is influenced by the local dynamics of the group bearing the spin under observation and the presence of other spins in the immediate environment as described by the Bloembergen–Purcell–Pound (BPP) model (Eq. 4.2.4 and 4.2.3). [144] The influence of swelling and cross-linking density on the relaxation of the NP core was studied by measuring the T_1 of naked PS NPs (Figure 5.2.5). The longest T_1 observed was 2.8 s for highly cross-linked PS NPs and decreased gradually with the decrease in the cross-linker concentration. The variation of T_1 with the correlation time of the local relaxation process describes a parabola with a frequency-dependent minimum, and for relatively slow local subsegmental motions, like those observed in the systems under study, one would expect T_1 to decrease as the subsegmental dynamics becomes faster. [144] The increase in T_1 observed with the increasing cross-linking density was in agreement with the expected trend for macromolecules and gels, [226] where, as the network becomes more cross-linked and rigid, the local subsegmental dynamics slows down leading to an increase in T_1.

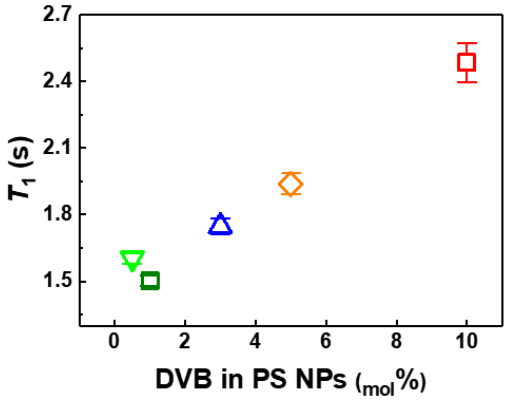

Figure 5.2.5 T_1 relaxation of PS aromatic ^{1}H in DCM-swollen naked PS NPs with different cross-linking density, NMR at a Larmor frequency of 700.02 MHz at 298 K.

Figure 5.2.6 shows that for any length of the PMA chains, the T_1 of the PS aromatic protons in the samples of PS–PMA–DVB10 was systematically longer than the T_1 of PS in PS–PMA with a lower degree of cross-linking in the PS core. This result was consistent with the decrease of T_1 observed for the naked PS NPs when the cross-linking density was decreased (Figure 5.2.5). Additionally, all NPs prepared using 3 and 10 mol % of cross-linker showed a decrease in T_1 when increasing N of the PMA chains. This result suggests that the grafting of PMA chains on the cross-linked PS core speeded up the local dynamics of

the PS and that longer PMA chains facilitate more efficiently the relaxation of the PS network. The effect of the end-tethered chains was the most prominent with the relatively rigid core and less effective in NPs with a softer core because of the initially faster subsegmental dynamics of the PS in the sparsely cross-linked core associated with the larger swelling of the softer NP core.

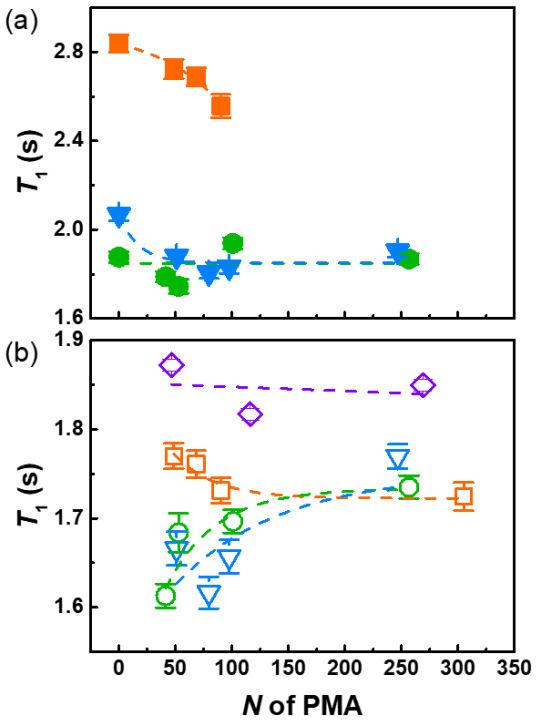

Figure 5.2.6 ^{1}H spin–lattice relaxation of the (a) aromatic ring of PS and (b) methoxy group of PMA in PS–PMA NPs with different degrees of polymerization of the PMA chains (*N*) grafted on PS cores with different cross-linking densities, measured at a Larmor frequency of 850.27 MHz at 298 K. NPs with cross-linked PS cores prepared with 0.5 mol % of DVB (green circle), 3 mol % of DVB (blue triangle), 10 mol % of DVB (orange square), and untethered PMA chains (violet diamond)

Figure 5.2.6b shows the relaxation of the protons in the methoxy group of PMA for free PMA chains and PMA chains tethered to a PS surface in PS–PMA NPs. In the range of *N* studied, the T_1 of the free PMA chains did not vary significantly and the T_1 values of the free chains were consistently longer than the T_1 values of the grafted chains. This decrease in T_1 upon grafting could be the consequence of an increase in the local subsegmental chain dynamics of the tethered PMA triggered by changes to the polymer chain conformation caused by grafting, in agreement with other studies, [214] or to an increase

in the efficiency of the spin–lattice interaction. The T_1 of the PMA chains grafted to the more rigid PS cores, cross-linked with 10 mol% of DVB, remained constant over the range of N analyzed. However, for chains grafted to the softer PS cores (PS–DVB0.5 and PS–DVB3), an increase in T_1 was observed when N increased. The T_1 relaxation time observed for three different systems all converged to a similar value, independent of the cross-linking density of the PS cores when long PMA chains were immobilized to the surface of the PS NPs. However, when short PMA chains were grafted to the PS NPs, the decrease in T_1 observed between the free PMA chains and the end-tethered chains was more pronounced for the chains grafted to the soft and deformable PS cores in comparison to chains grafted to PS–DVB10. The T_1 values measured by NMR spectroscopy are the average values over every methoxy group in the PMA chains, and the results suggest that the PMA units close to the surface of the PS core were experiencing a larger variation in T_1 relaxation times than the PMA units further removed from the grafting point. The T_1 values measured could be the average of the relaxation time of PMA units located close to the PS surface and others further removed from the substrate. However, the difference observed between the T_1 relaxation time of the PMA chains with similar N grafted to PS cores with different cross-linking degrees decreased as N increased. Thus, the results suggested that the substrate effect only had a short-range influence. The substrate effect on the T_1 values measured did not disappear for long PMA chains but was masked because of the increased number of methoxy groups not experiencing the effect of the substrate.

To better understand the local chain dynamics in both the core and the canopy of the PS–PMA NPs, the correlation between the T_1 relaxation time of PS and PS–PMA NPs was measured at different temperatures and Larmor frequencies. An increase in temperature should result in faster local subsegmental dynamics, and thus, shorter T_1. While most of the NPs analyzed displayed the expected decrease in T_1 with increasing temperature (Figure 5.2.7), it was not the case for the PS core of highly cross-linked NPs (Figure 5.2.8 and Figure 5.2.9). Both the unfunctionalized PS NPs and the PS–PMA NPs cross-linked with 10 mol % of DVB showed an increase in T_1 relaxation time with increasing temperature, suggesting the existence of a slower relaxation mechanism at high temperatures in these samples. This result could be attributed to changes in the swelling of the PS core. In the same temperature range, the size of the densely cross-linked PS NPs in DCM decreased with increasing temperature, while the size of sparsely cross-linked PS NPs increased (Figure 5.2.10). Similarly, the deswelling of highly cross-linked PS gels in toluene has been observed when increasing temperatures. [227] Thus, counterintuitively, in highly cross-linked NPs, although the local dynamics of the solvated free PS chains should be faster with

increasing temperature, an overall increase in T_1 relaxation time was observed and was related to the deswelling of the highly cross-linked PS NPs resulting in a more rigid polymer network.

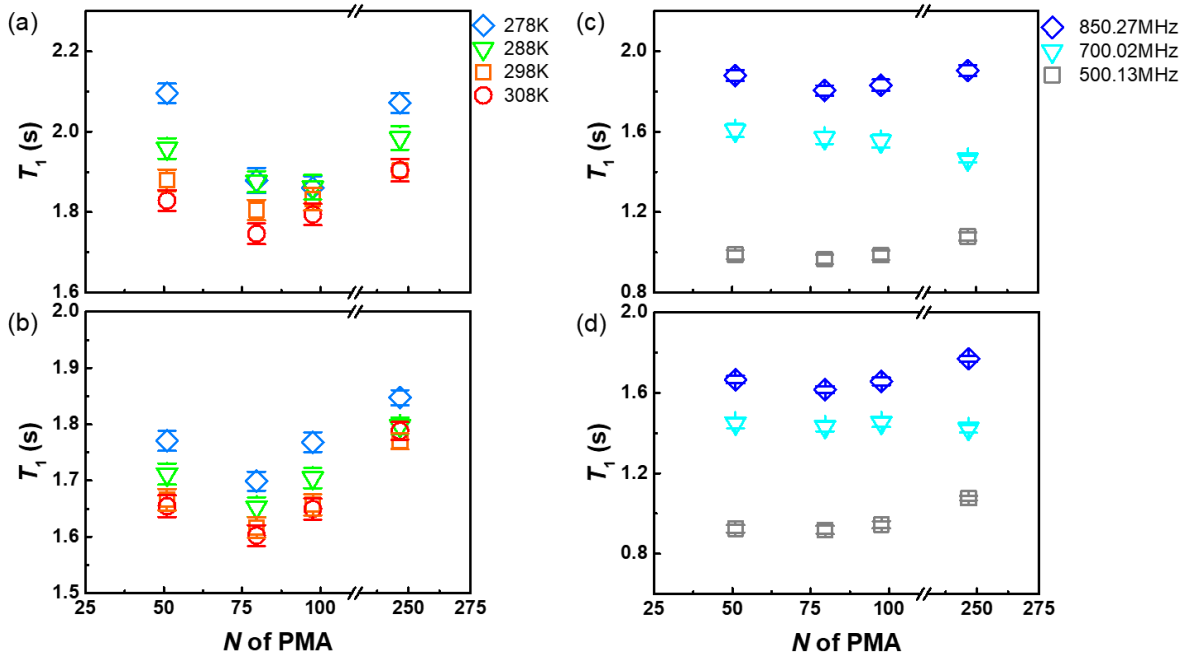

Figure 5.2.7 Temperature and magnetic field strength dependence of ^{1}H spin–lattice relaxation time of PS–PMA hairy NPs cross-linked with 3 mol% of DVB. (a,b) Influence of the temperature on the relaxation of the aromatic ring of the PS core (a) and of the methoxy group of PMA chains (b) at 278, 288, 298, and 308 K measured with a Larmor frequency of 850.27 MHz. (c,d) Influence of the magnetic field on the relaxation of the aromatic ring of the PS core (c) and of the methoxy groups of PMA chains (d) measured at 298 K with Larmor frequencies of 500.13, 700.02, and 850.27 MHz.

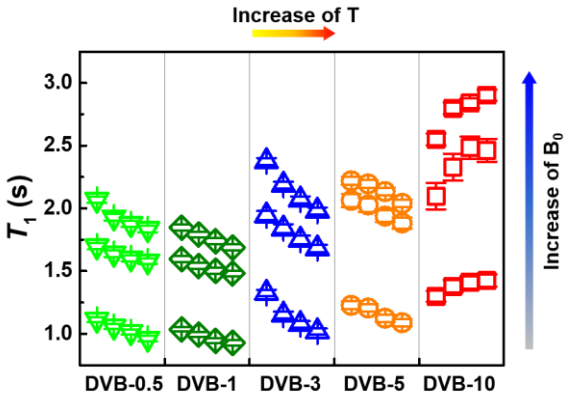

Figure 5.2.8 Temperature and magnetic field strength dependence of ^{1}H spin-lattice relaxation time of PS core NPs with different cross-linking density at Larmor frequencies of 500.13 MHz, 700.02 MHz and 850.27 MHz NMR at 278 K, 288 K, 298 K and 308 K

When using NMR relaxometry, molecular motions that are occurring at a rate similar to the resonance frequency of the nucleus under investigation are more effective in influencing the efficiency of the spin–lattice relaxation. In addition to the temperature and the resonance frequency of the nucleus, the observed T_1 is also a function of the distance between two interacting spins. The BPP model take those last two factors into account in describing the subsegmental motions and can be used to relate T_1 to the local chain dynamics in the PS–PMA NPs (Eq. 4.2.4 and 4.2.5) [144] and to evaluate the correlation time (τ_c) associated with the local subsegmental motions in the PS–PMA NPs.

For all NPs, an increase of T_1 was observed when the magnetic field was increased, indicative of a relatively slow local motion (Figure 5.2.9). When using different NMR magnets to vary the magnetic field, the relaxation time will change. This effect is attributed to the fact that minimum T_1 value is observed when the rotational correlation time of the relaxation under study is equal to the inverse of the Larmor frequency of the nucleus observed. [144] This variation in T_1 relaxation times at different magnetic fields was used to calculate the correlation time (τ_c) of the segmental motions of PS–PMA NPs (Figure 5.2.11) with the BPP model (Eq. 4.2.4). For the naked PS NPs, τ_c increased with an increase in the degree of cross-linking in agreement with the reduction of the subsegmental dynamics of the PS network as the cross-linking increased. The τ_c of PS in PS–PMA NPs decreased with increasing N of the PMA because the PMA chains were promoting the local relaxation of the PS core. The τ_c of PMA chains also showed a variation with the degree of cross-linking of the PS core and N of the PMA chains. The τ_c of the methoxy

group of the free PMA chains with an *N* of 36 units was 135 ps in DCM. The τ_c of all the grafted PMA was either equal or longer than that of the free chains. As the cross-linking of the PS core increased, the $\tau_{c,PMA}$ increased indicative of a reduction in the subsegmental dynamics of the grafted PMA chains. Furthermore, as *N* of the PMA chains increased, the average $\tau_{c,PMA}$ decreased because of the faster subsegmental dynamics of the PMA units located farther from the substrate, and as *N* increased, the effect of the substrate decreased, and consequently, $\tau_{c,PMA}$ for the grafted PMA chains converged to the $\tau_{c,PMA}$ measured for free PMA chains.

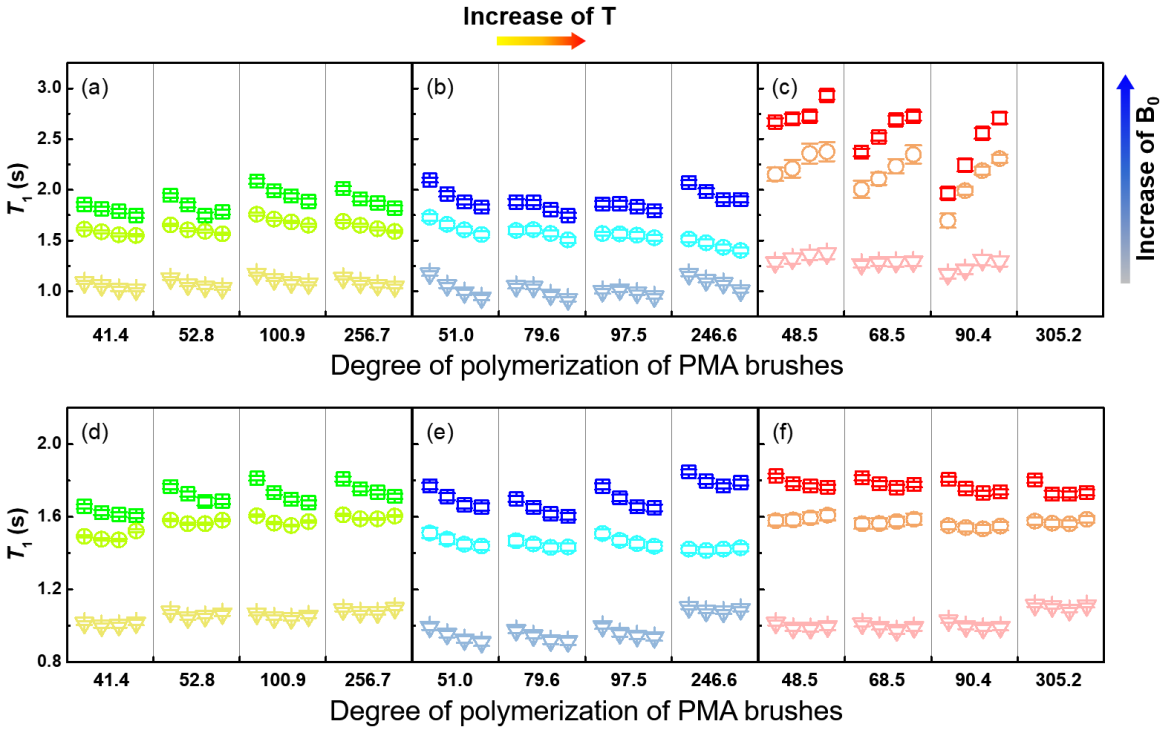

Figure 5.2.9 Temperature and magnetic field strength dependence of ^{1}H spin-lattice relaxation time of (a), (b), (c) PS core and (d), (e), (f) of PMA brushes with DVB0.5, DVB3, DVB10 hairy NPs at Larmor frequencies of 500.13 MHz, 700.02 MHz and 850.27 MHz NMR at 278 K, 288 K, 298 K and 308 K. The magnetic field strength increases from the bottom set of T_1 relaxation times to the above set. The temperature rises from the left (278 K) to the right (308 K) within one column.

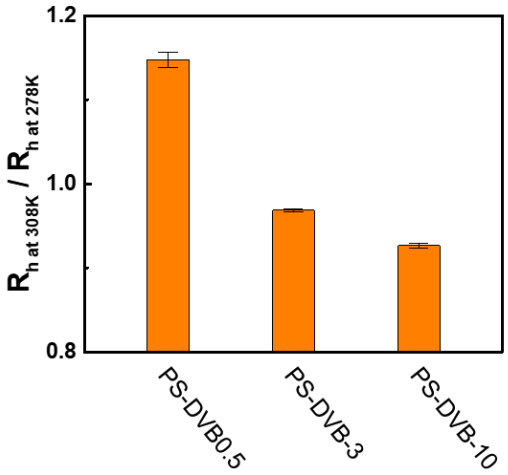

Figure 5.2.10 Normalized swelling of naked PS NPs in DCM at 308 K normalized by radii of NPs at 278 K.

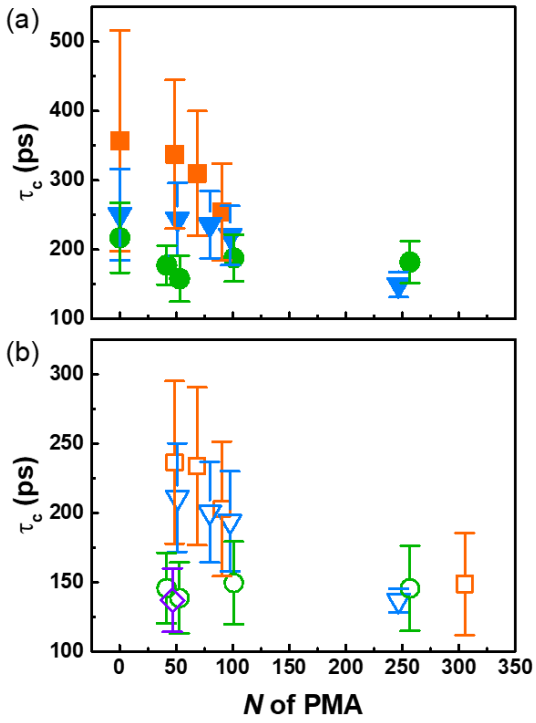

Figure 5.2.11 Correlation time of the ^{1}H spin–lattice relaxation in the (a) PS core and the (b) PMA chains in PS–PMA hairy NPs at 298 K. NPs with cross-linked PS cores prepared with 0.5 mol % of DVB (green circle), 3 mol % of DVB (blue triangle), 10 mol % of DVB (orange square), and untethered PMA chains (violet diamond).

The τ_c for both PS and PMA was faster with lower cross-linking and a longer PMA canopy, suggesting that covalently tethering PMA chains to the PS core accelerated the subsegmental dynamics of the PS core and that this effect increased with the increasing degree of polymerization of the PMA chains. Similarly, the presence of the substrate slowed down the subsegmental dynamics of the tethered chains, and this effect was more pronounced for more rigid substrates and decreased for longer chains. Figure 5.2.12 summarizes the interrelation between the composition of the core and the local dynamics of the canopy and between the composition of the canopy and the local dynamics of the core. On the one hand, the presence of PMA chains softened the PS core and facilitated the local relaxation. This effect increased as *N* increased, and was more pronounced when the rigidity of the substrate increased. On the other hand, grafting the PMA chains to the PS substrate impeded the local relaxation of the PMA in comparison to free PMA chains in solution; this effect was stronger when the PMA chains were grafted to a more rigid PS core, and more visible for short chains which can be relatively more strongly influenced by the substrate effect than long chains.

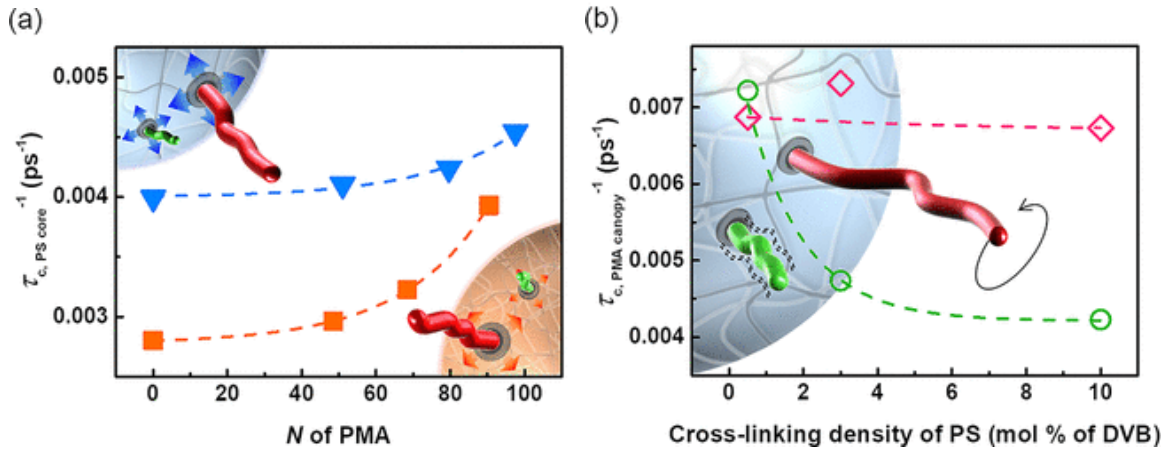

Figure 5.2.12 Effect of the interplay between the PS core and the PMA canopy on the local dynamics of PS–PMA NPs. (a) Effect of the length of the PMA canopy on the local dynamics of the PS core measured for the PS core cross-linked with 3 mol % of DVB (blue triangle) and 10 mol % of DVB (orange square). (b) Effect of the rigidity of the PS core on the local dynamics of the PMA canopy measured for PMA chains of *N* ca. 50 units (green circle) and *N* ca. 250 units (pink diamond).

To fully understand the relaxation mechanism in the PS–PMA NPs, the temperature influence on τ_c of the core and the canopy of PS–PMA NPs was measured between 278 and 308 K (Figure 5.2.13). An increase in temperature is associated with faster local subsegmental chain dynamics resulting in a decrease of τ_c. The dynamics of the free PMA chains and PMA chains grafted to sparsely cross-linked PS cores followed

the expected trend with the increase in temperature. However, $\tau_{c,PS}$ of highly cross-linked PS NPs increased at higher temperatures. When PMA chains were grafted to the NPs, the $\tau_{c,PS}$ of the highly cross-linked core in PS–PMA NPs showed an even more severe increase. In contrast, sparsely cross-linked PS NPs and the PS core in PS–PMA NPs only exhibited a slight increase in $\tau_{c,PS}$ as the temperature increased. This effect of temperature on the $\tau_{c,PS}$ observed for different cross-linking densities was in accordance with the negative thermal expansion observed for highly cross-linked PS NPs swollen in DCM (Figure 5.2.13); the deswelling of NPs at high temperatures led to a slower local relaxation dynamics. The subsegmental dynamics of PMA chains grafted on the highly cross-linked PS core followed a similar trend and $\tau_{c,PMA}$ increased at higher temperatures. Thus, the local dynamics of the PS core directly affected the local dynamics of the PMA canopy.

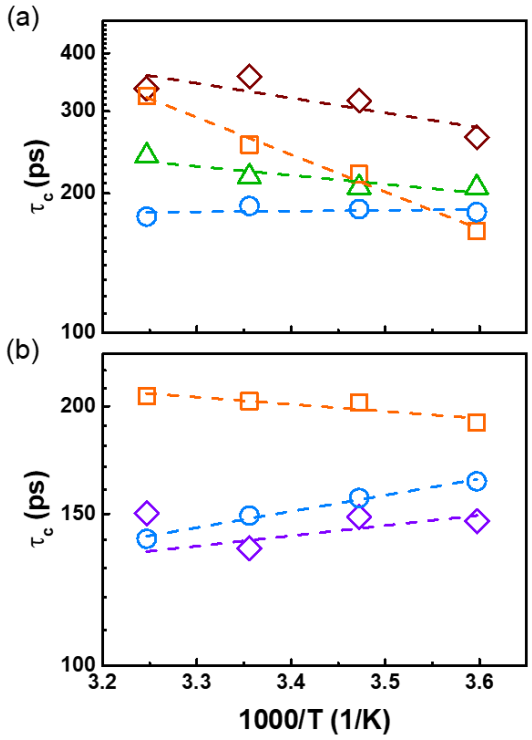

Figure 5.2.13 Effect of temperature on the correlation time (τ_c) for the ^{1}H spin–lattice relaxation. (a) Relaxation of the aromatic ^{1}H of PS for unfunctionalized PS NPs prepared with 10 mol % of DVB (brown diamond) and with 0.5 mol % of DVB (green triangle) and for the PS core of PS–PMA NPs cross-linked with 10 mol % of DVB (orange square) and 0.5 mol % of DVB (blue circle). (b) Relaxation of the methoxy ^{1}H of PMA for free PMA chains (N = 46) (violet diamond), PMA chains (N = 100) of PS–PMA NPs prepared with 10 mol % of DVB (orange square) and with 0.5 mol % of DVB (blue circle).

5.2.3 Conclusion

In summary, ^{1}H spin–lattice NMR relaxation was used to characterize the dynamics of soft and hairy PS–PMA NPs in suspension in DCM, a good solvent for both the PMA canopy and the PS core. The length of the PMA chains and the amount of the cross-linker in the PS cores were controlled by miniemulsion followed by SI-ATRP. The resulting NPs had a low size dispersity, formed stable suspensions in DCM, and the grafted polymer chains were in an extended brush conformation in all samples. DLS measurements showed that the swelling of the PS–PMA NPs was influenced both by the degree of cross-linking of the PS core and the length of the PMA canopy. NMR relaxation was used to analyze the subsegmental dynamics of the system. As observed by other techniques, grafting polymer chains slowed down the subsegmental relaxation dynamics of the grafted chain, but more interestingly, grafting polymer chains on soft and deformable NPs allowed us to address a new phenomenon, the relation between the local relaxation dynamics of the core and the local relaxation dynamics of the canopy. A clear interplay between the PMA canopy and the PS core was observed. More rigid PS cores slowed down the subsegmental relaxation dynamics of the PMA chains more efficiently than softer cores, whereas the presence of longer chains in the PMA canopy accelerated the local relaxation dynamics of the PS cores more efficiently than short chains. Canopies prepared with long PMA chains showed marginally faster subsegmental dynamics than the ones made with shorter chains because of the stronger influence of the substrate on short PMA chains. However, the local dynamics of the grafted chains, especially short ones, was strongly influenced by the local dynamics of the substrate. The relaxation dynamics of the PS cores was mainly determined by the degree of cross-linking, but the tethering of long PMA chains accelerated the constrained subsegmental motions in the cross-linked PS.

The results show the influence of the local dynamics of the substrates on the overall dynamics of the system. A clear relationship between the local dynamics of the core particles and the local dynamics of the end-tethered polymer chains was found. Grafting a canopy of polymer chains that are pulling and tugging on the tethering points on a soft and deformable NP influences the local dynamics of the soft core. Moreover, the local dynamics of the tethered chains is affected by the softness and the dynamics of the substrate.

5.3 Impact of the solvent quality on the local dynamics of soft and swollen polymer nanoparticles functionalized with polymer[3]

The architecture of polymer-functionalized polymer nanoparticles is important in determining the behavior of the nanoparticles in suspensions and their potential applications. Another important factor influencing the behavior of the NPs in suspension is the interaction between the solvent used as the continuous phase and the different components of the polymer-functionalized polymer nanoparticles.

To explore the relationship between the solvent quality and the dynamics of polymer-functionalized soft polymer NPs, we designed a system based on cross-linked polystyrene (PS) NPs grafted with a canopy of poly(methyl acrylate) (PMA). PS and PMA, two immiscible polymers, can be selectively solvated by using binary mixtures of solvents. NMR spectroscopy was used to address the effect of those selective solvents on the local mobility of the PS-PMA core-canopy NPs and revealed an interplay between the local mobility of the core and the local mobility of the canopy. A selective reduction of the solvent quality for the PMA canopy resulted in the expected reduction of the local mobility of the PMA chains, but also in the slower dynamics of the PS core. Similarly, a selective reduction of the solvent quality for the PS core resulted in a slower dynamics for both the PS core and the PMA canopy.

5.3.1 Motivation

The grafting of end-tethered polymer chains on a surface is an excellent strategy to control the properties of interfaces such as the surface of nanoparticles (NPs) in suspension.[95, 228] Nanoparticles functionalized with a canopy of end-tethered polymer chains have been used in a variety of applications,

[3] This section is based on the article:

[redacted] Impact of the Solvent Quality on the Local Dynamics of Soft and Swollen Polymer Nanoparticles Functionalized with Polymer. *Macromolecules* **2020**, *Accepted*

Author contribution [redacted] designed the experiments. and [redacted] performed the experiments. [redacted] analyzed the data and discussed the results. [redacted] wrote the manuscript.

such as drug delivery, adhesives, or coatings.[17, 229-231] Using a canopy of end-tethered polymer chains to tune the interactions between the nanoparticles and their environment is a strategy widely employed to control the dispersibility of nanoparticles both in suspension and in polymer matrixes for the formation of nanocomposites with specific properties.[195, 232] The properties of the resulting functionalized NPs are affected by the chemical composition of the polymer canopy, its architecture, and its interaction with the environment. The dynamics of the tethered chains is a piece of crucial information to understand the behavior of such systems. The chain dynamics in polymer-functionalized NPs have been studied for a variety of rigid nanoparticles core[27] such as gold,[233] silica,[32] or carbon black.[234] However, new polymer-grafted systems used in drug delivery or tissue engineering rely on softer NP cores like polymer micelles or swollen nanogels.[235, 236] When the polymer chains are tethered to such soft and deformable NP cores, tuning the properties of the polymer canopy to optimize the behavior of the functionalized nanoparticles represent a particular challenge since both the canopy of end-tethered chains and the core of the nanoparticles are soft, deformable, and strongly affected by the conditions of the surrounding environment such as the solvent quality.[237]

The behavior of polymer-grafted NPs is tunable through the control of the polymer chain conformation, which is influenced by the architecture of the polymer canopy defined by the grafting density and the chain length of the end-tethered polymer chains. For example, polystyrene-grafted silica nanoparticles in a polystyrene matrix displayed tunable aggregation states, forming short strings, sheets, or clusters, by controlling the molecular weight and grafting density of the end-grafted polystyrene chains.[195] This behavior was attributed to the conformation of the end-tethered chains and the architecture of the polymer-grafted nanoparticles. The conformational changes experienced by the end-tethered chains are related to the local concentration of monomer units. Chains tethered to a substrate at a high grafting density will experience a stronger steric hindrance from the neighboring chains leading to a larger reduction of conformational entropy than chains tethered at a lower grafting density. Similarly, when chains are tethered to a spherical substrate, like a nanoparticle, the local monomer concentration will decrease radially from the surface of the core nanoparticle to the interface between the surface of the polymer canopy and the surrounding environment, and the steric hindrance and the reduction of conformational entropy will decrease analogously. Consequently, the chains grafted to a NP experience distribution of confinement states.[96] The variation in the extent of confinement results in different interactions between the polymer-functionalized NPs themselves and between the polymer-functionalized NPs and their environment.[96, 238]

The study of the polymer chain dynamics and conformation is used to understand the effects of architecture and solvent quality on the behavior of functionalized NPs.[32, 162, 239, 240] Different techniques such as dielectric spectroscopy, neutron spin-echo, or neutron backscattering spectroscopy[31, 33, 241, 242] are probing different time scale and thus different aspects of the polymer dynamics.[243] High-field NMR relaxometry compares advantageously to other techniques. It can be used to investigate fast relaxation processes associated with the motions, vibrations, and rotation of side groups and it probes the subsegmental and Rouse dynamics of the polymer chains.[218, 243-249] NMR spectroscopy provides results in keeping with other techniques like dielectric spectroscopy or quasielastic neutron scattering[216] with the added bonus of allowing for the analysis of the local dynamics of specific chemical groups without the need for labeling. Both NMR spectroscopy and more specifically NMR relaxometry have become more popular to characterize polymer functionalized nanoparticles both in the solid-state and in suspension.[250-253]

When dealing with swollen polymer NPs, the influence of the solvent quality for the core NPs on the behavior of the suspension is also critical. Soft NPs are deformable in comparison to the inorganic hard NPs and can respond to external stimuli such as temperature, pH, and solvent quality. Under good solvency conditions, the polymer NPs are swollen with solvent and are soft and deformable, but when the solvent quality decreases, deswelling is observed and results in a variation in the rheological behavior, optical properties, interfacial behavior, aggregation, self-assembly of the NPs in suspension.[254-258] For example, when the quality of the solvent of aqueous suspensions of poly-N-isopropylacrylamide (PNIPAM) soft microgels is decreased either by increasing the temperature or by the addition of a cononsolvent, the volume occupied by the particles in suspension decrease leading to the obtention of collapsed microgel, a reduced segmental chain dynamics, and a diminution in the viscosity of the suspension.[259, 260]

In the case of polymer NPs functionalized with end-tethered polymer chains, the role of solvent quality is complex, but understanding the role of solvent quality on the dynamics, conformation, colloidal stability and properties is crucial in the design of new functional and responsive nanomaterials used for example in drug release application.[261] The contribution of the solvent quality on the swelling and dynamics of both the core and the end-tethered layers needs to be studied in more detail. The interplay between the dynamics of the shell and of the core NP needs to be better understood.[262, 263] Here, to understand the effect of solvent quality on the dynamics of swollen polymer NPs functionalized with a canopy of polymer

chains, we functionalized cross-linked polystyrene (PS) NPs with a canopy of poly(methyl acrylate) (PMA) (Table 5.3.1). PS and PMA are two immiscible polymers that can be selectively solvated using binary mixtures of solvent (Figure 5.3.1).

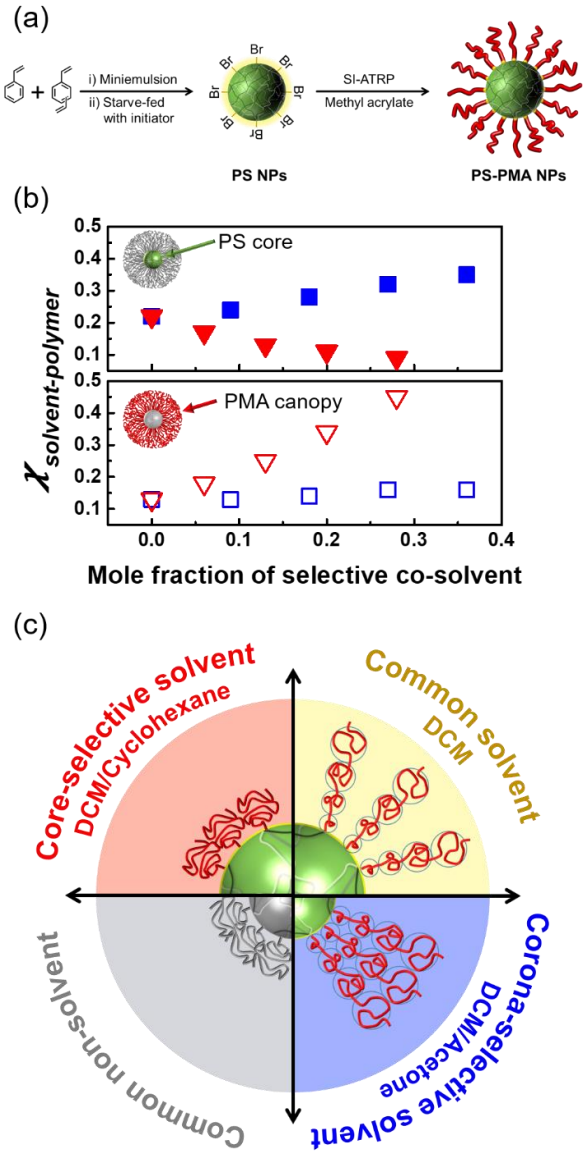

Figure 5.3.1. (a) Synthesis of PS-PMA NPs. (b) Polymer-Solvent Flory-Huggins interaction parameter ($\chi_{\text{polymer-solvent}}$) for PS (upper panel, closed symbol) and PMA (lower panel, open symbol) with solvent mixtures of DCM and co-solvents, cyclohexane (red) and acetone (blue). The $\chi_{\text{polymer-solvent}}$ was calculated from the Hansen solubility parameters of the polymers and solvents (Table 5.3.2 and Table 5.3.3) using eq 4.2.8. (c) The expected effect of the relative solvent quality on the swelling of the PS-PMA NPs.

Table 5.3.1. Library of PMA and PS-PMA NPs analyzed

Sample	Initiator/MA/Cu(II)/ PMDETA	Reaction time (h)	N^a	$M_{n,\,NMR}{}^b$ (kg mol^{-1})	$M_{n,\,GPC}$ (kg mol^{-1})	$D_{s,\,DCM}$ (nm)	PDI
PS	--	--	0	--	--	179 ± 2	0.04 ± 0.02
PS-PMA$_{4k}$	1/249/0.1/1	1.5	50	4.3	--	192 ± 2	0.02 ± 0.01
PS-PMA$_{22k}$	1/702/0.1/1	1	257	22.1	--	248 ± 2	0.06 ± 0.02
PS-PMA$_{28k}$	1/766/0.1/1	1	320	27.5	21.3	307 ± 2	0.05 ± 0.02
PS-PMA$_{42k}$	1/991/0.1/1	1	487	42.0	33.1	379 ± 2	0.04 ± 0.02
PS-PMA$_{52k}$	1/1404/0.1/1	1	600	51.7	47.2	407 ± 4	0.05 ± 0.02
Free PMA$_{4k}$	1/148/0.1/1	1	43	3.7	4.0	--	--
Free PMA$_{22k}$	1/702/0.1/1	1	264	22.7	22.6	--	--
Free PMA$_{116k}$	1/1685/0.1/1	6	1312	113	116		

a: degree of polymerization

b: $\frac{[MA]_{t=1}}{[MA]_{t=0}} \times molar\ ratio\ of\ MA\ to\ Initiator$

Table 5.3.2. Molar volume and Hansen solubility parameter of polymers and solvents. [156, 264]

Polymer or solvent composition	Molar volume / (cm^3 mol^{-1})	δ_d (MPa)$^{1/2}$	δ_p (MPa)$^{1/2}$	δ_{hb} (MPa)$^{1/2}$
PS	-	18.5	4.5	2.9
PMA	-	18.6	10.5	7.5
$x_{DCM\ 1.00}$	63.9	17	7.3	7.1
$x_{Acetone\ 1.00}$	74.1	15.5	10.4	7.0
$x_{Cyclohexane\ 1.00}$	108.0	16.8	0	0.2
$x_{Acetone\ 0.09}+x_{DCM\ 0.91}$	64.8	16.9	7.6	7.1
$x_{Acetone\ 0.18}+x_{DCM\ 0.82}$	65.7	16.7	7.9	7.1
$x_{Acetone\ 0.27}+x_{DCM\ 0.73}$	66.6	16.5	8.2	7.1
$x_{Acetone\ 0.36}+x_{DCM\ 0.64}$	67.6	16.4	8.5	7.1
$x_{Cyclohexane\ 0.06}+x_{DCM\ 0.94}$	66.6	17.0	6.6	6.4
$x_{Cyclohexane\ 0.13}+x_{DCM\ 0.87}$	69.5	17.0	5.8	5.7
$x_{Cyclohexane\ 0.20}+x_{DCM\ 0.80}$	72.8	16.9	5.1	5.0
$x_{Cyclohexane\ 0.28}+x_{DCM\ 0.72}$	76.3	16.9	4.4	4.3

Table 5.3.3. Flory-Huggins interaction parameters of the solvent mixtures

	Flory-Huggins interaction parameter, χ_{12}	
Solvent composition	PS	PMA
$x_{\text{DCM 1.00}}$	0.22	0.13
$x_{\text{Acetone 1.00}}$	0.65	0.29
$x_{\text{Cyclohexane 1.00}}$	0.43	1.92
$x_{\text{Acetone 0.09}}+x_{\text{DCM 0.91}}$	0.24	0.13
$x_{\text{Acetone 0.18}}+x_{\text{DCM 0.82}}$	0.28	0.14
$x_{\text{Acetone 0.27}}+x_{\text{DCM 0.73}}$	0.32	0.16
$x_{\text{Acetone 0.36}}+x_{\text{DCM 0.64}}$	0.35	0.16
$x_{\text{Cyclohexane 0.06}}+x_{\text{DCM 0.94}}$	0.17	0.18
$x_{\text{Cyclohexane 0.13}}+x_{\text{DCM 0.87}}$	0.13	0.25
$x_{\text{Cyclohexane 0.20}}+x_{\text{DCM 0.80}}$	0.11	0.34
$x_{\text{Cyclohexane 0.28}}+x_{\text{DCM 0.72}}$	0.09	0.45

5.3.2 Results and discussion

PMA grafted PS soft NPs were prepared *via* miniemulsion polymerization, followed by surface-initiated atom transfer radical polymerization.[41, 203, 265] In the present study, PS NPs were sparsely cross-linked (0.5 mol% of divinylbenzene), and functionalized with PMA chains of increasing lengths, and the five different molecular weight varied from 4 kDa to 52 kDa. The grafting density of the PMA chains was 0.20±0.02 chains nm^{-2} when the NPs were dispersed in dichloromethane (DCM). The increase in the size of PS-PMA NPs was observed in DLS and TEM measurements (Figure 5.3.2). The NPs were dispersed in solvent mixtures of DCM with either cyclohexane or acetone to selectively control the solvent quality. The local dynamics of the PS core and of the PMA canopy were addressed independently using the spin-spin relaxation time obtained by NMR spectroscopy.

NMR relaxometry is especially ideal for interpreting the dynamics of soft NPs with a surface functionalization of end-tethered polymer chains because the measurements can resolve the relaxation of specific chemical entities such as the polymer chains anchored on the surface, or the cross-linked polymer network in the core NPs.[221, 263, 266] The spin-spin relaxation characterized by the relaxation time T_2

is the result of the interactions between the rotating spins in the system without energy exchange,[267] and it is used to study the effect of temperature, molecular weight, cross-linking density or entanglement on the molecular mobility. The T_2 is an ideal marker of the local dynamics in the swollen PS-PMA NPs and to study the segmental motions of their polymer chains in the picosecond timescale. The T_2 time is related to the spectral density function ($J(\omega_0)$ at the Larmor frequency ω_0) of the spin system, as $1/T_2 \propto 3J(0) + 5J(\omega_0) + 2J(2\omega_0)$.[144] In the simplest system, for an isotropic rotation, the spectral density function can be used to calculate the correlation time associated with the rotation since $J(\omega_0) = \tau_r/(1-\omega_0^2\tau_r^2)$. Similarly, the correlation time of more complex relaxation mechanisms can be extracted from the NMR data.[268] In every case an increase in T_2 is associated with an increase in the local mobility of the segment under study and probes relaxation mechanisms occurring on a time scale similar to the Larmor frequency of the magnet,[243] 300 MHz in the present study. To characterize the dynamics of PS core and PMA corona, the T_2 of the aromatic ring from the polystyrene core and of the methoxy group of the poly(methyl acrylate) canopy were measured using the Carr-Purcell-Meiboom-Gill pulse sequence (Figure 4.2.4).[269, 270] A stretched exponential function (eq. 4.2.6) was used to describe the NMR decay in order to take into account the distribution of confinement states experienced by the polymer chains. The T_2 values reported for the PS core and of the PMA canopy are the average T_2 for a given polymer component calculated using eq. 4.2.7. The relaxation of PS NPs, PS-PMA NPs, and free PMA chains was investigated in mixtures of DCM and cyclohexane and mixtures of DCM and acetone. To understand the effect of the solvent, the NPs were first dispersed in DCM, a good solvent for both PMA and PS, then the addition of a selective non-solvent, cyclohexane or acetone, was used to tune the solvent quality (Table 5.3.4).

Table 5.3.4. Flory-Huggins interaction parameter ($\chi_{\text{polymer-solvent}}$) for the different polymer-solvent pairs used. The $\chi_{\text{polymer-solvent}}$ was calculated from the Hansen solubility parameters of the polymers and solvents (Table 5.3.2 and 5.3.3) using eq 4.2.8.

Polymer	$\chi_{\text{polymer-solvent}}$		
	DCM	Acetone	Cyclohexane
PS	0.22	0.65	0.43
PMA	0.13	0.29	1.92

The quality of the solvent remained below χ =0.5 for both the PS core and the PMA canopy to ensure that the suspensions remained stable during the experiments (Figure 5.3.1b). The swelling of the NPs was characterized by their diameter obtained by dynamic light scattering (DLS) in the different solvent mixtures (Figure 5.3.3) and normalized to the diameter of the same NPs measure in pure DCM. The solvodynamic diameter (D_s) of pure PS NPs increased when the mole fraction of cyclohexane increased in the solvent mixture (Figure 5.3.2a) and decreased with the addition of acetone. The swelling observed is in agreement with the Flory-Huggins interaction parameter ($\chi_{\text{polymer-solvent}}$) of PS in those solvent mixtures (Table 5.3.3). For free PMA chains, the radius of gyration of the chain (R_g) moderately increased with the addition of acetone and decreased with the addition of cyclohexane (Figure 5.3.4). The mixed system composed of a PS core functionalized with a canopy of end-tethered PMA chains displayed a more intricate behavior (Figure 5.3.3b) due to the simultaneous swelling and deswelling of the different polymer components. PS-PMA$_{4k}$ displayed a similar swelling behavior as the PS NPs (Figure 5.3.5). However, as the length of the PMA chains in the PS-PMA NPs increased, the swelling behavior of the PS-PMA particles became sharply distinct from the swelling of pure PS NPs (Figure 5.3.5). The effect of the solvent quality on the swelling of the PS-PMA NPs must take into account the simultaneous swelling of the PS core and deswelling of the PMA canopy upon the addition of cyclohexane or the swelling of the PMA canopy accompanied by the deswelling of the PS core upon the addition of acetone.

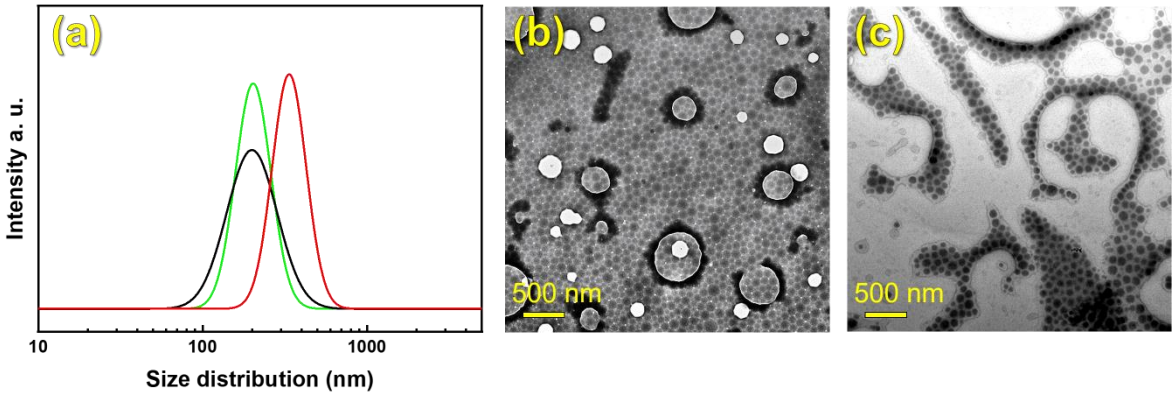

Figure 5.3.2. (a) Solvodynamic size distribution of PS NPs (black line), PS-PMA$_{4k}$ NPs (green line) and PS-PMA$_{28k}$ NPs (red line) in DCM measured by DLS and transmission electron microscopy image of (b)PS NPs and (c)PS-PMA$_{28k}$ NPs .

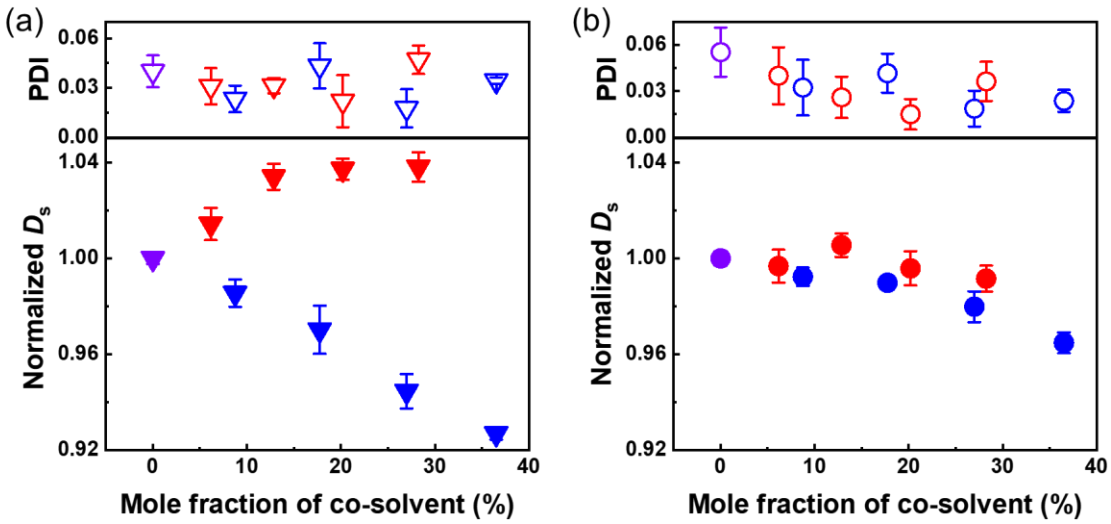

Figure 5.3.3. Normalized solvodynamic diameter and size distribution (PDI) of (a) PS NPs (▼triangle), and (b) PS-PMA$_{22k}$ (●circle), measured by light scattering at 298k in solvent mixtures of DCM (violet) with cyclohexane (red), and with acetone (blue). D_s were normalized by D_s measured in DCM.

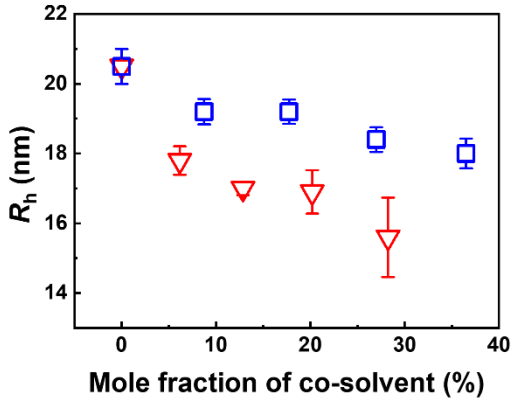

Figure 5.3.4. Hydrodynamic radii of free PMA$_{116k}$ measured by static light scattering in solvent mixtures at 298k. Normalized by D_s in DCM. For solvent mixtures of DCM with cyclohexane (red triangle), and with acetone (blue square).

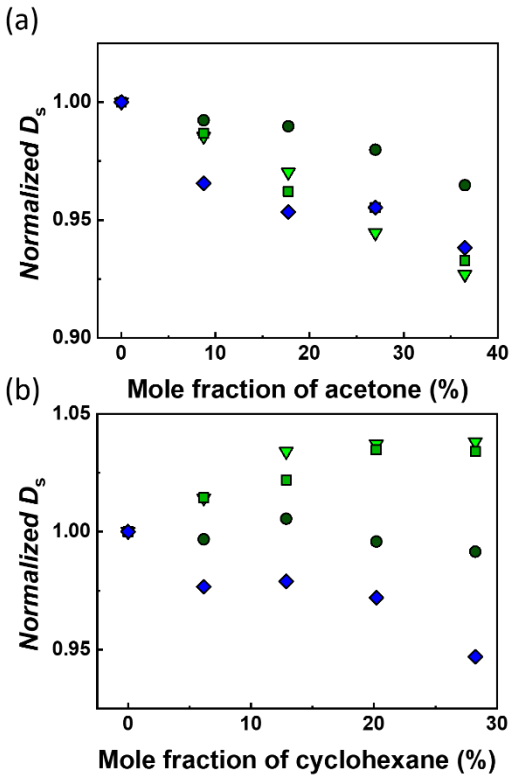

Figure 5.3.5. Normalized solvodynamic diameter of PS of PS NPs (light green triangle), PS-PMA$_{4k}$ (green square), PS-PMA$_{22k}$ (dark green circle), PS-PMA$_{28k}$ (blue diamond) in the solvent mixture of (a)DCM/acetone and (b)DCM/cyclohexane measured by light scattering in solvent mixtures at 298k.

As the solvent quality changed and the PS core swelled and deswelled, so did the effective grafting density of the chains. Because of the initial size of the NPs and the limited swelling of the PS core, the effective grafting density only moderately changed, ranging from 0.19 chains·nm^{-2} in DCM/cyclohexane to 0.24 chains·nm^{-2} in DCM/acetone (Table 5.3.5). Similarly, the swelling and collapse of the PMA canopy could also affect the conformation and dynamics of the system. However, when measuring the variation in the thickness of the polymer canopy with the increase in the degree of polymerization of the PMA chains (Figure 5.3.6), the scaling relationship (eq. 5.3.1) showed that in every solvent system used, the chains maintained a conformation corresponding to stretched chains in a concentrated polymer brush regime.[27] Even though the addition of cyclohexane resulted in moderately less stretched chains (Table 5.3.6).

$$T \propto N^{v} \qquad (5.3.1)$$

where T is the thickness of grafted chains (T=($D_{PS\text{-}PMA}$-D_{PS})/2), N is the degree of polymerization of the PMA chains, and v is the stretching parameter. When v is equal to 1, the chains are in a completely stretched conformation. As v decreases, the chains are adopting a more and more collapsed conformation.

Table 5.3.5. Grafting density of PS-PMA NPs in different solvent mixtures.

Solvent composition	Grafting density (chains·nm^{-2})	Radius of the PS core (nm)
$x_{\text{water 1.00}}$	0.81±0.06	45
$x_{\text{DCM 1.00}}$	0.20±0.02	90
$x_{\text{Acetone 0.09}}$+$x_{\text{DCM 0.91}}$	0.21±0.02	88
$x_{\text{Acetone 0.18}}$+$x_{\text{DCM 0.82}}$	0.22±0.02	87
$x_{\text{Acetone 0.27}}$+$x_{\text{DCM 0.73}}$	0.23±0.02	85
$x_{\text{Acetone 0.36}}$+$x_{\text{DCM 0.64}}$	0.24±0.02	83
$x_{\text{Cyclohexane 0.06}}$+$x_{\text{DCM 0.94}}$	0.20±0.01	91
$x_{\text{Cyclohexane 0.13}}$+$x_{\text{DCM 0.87}}$	0.19±0.01	93
$x_{\text{Cyclohexane 0.20}}$+$x_{\text{DCM 0.80}}$	0.19±0.01	93
$x_{\text{Cyclohexane 0.28}}$+$x_{\text{DCM 0.72}}$	0.19±0.01	93

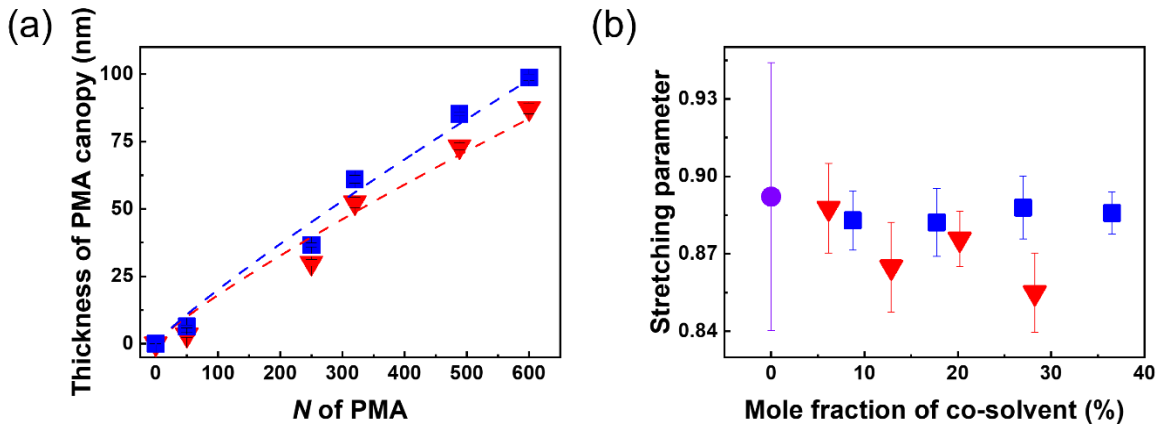

Figure 5.3.6. (a) Thickness of PMA canopy measured with DLS and scaling fitting with Eq. 5.3.1 in $DCM_{0.6}$+$cyclohexane_{0.4}$ (red triangle), and in $DCM_{0.6}$+$acetone_{0.4}$ (blue square). (b) Stretching parameter of grafted PMA chains in PS-PMA in solvent mixtures. For solvent mixtures of DCM (violet circle) with cyclohexane (red triangle), and with acetone (blue square).

Table 5.3.6. Stretching parameter of the PMA canopy of PS-PMA NPs in solvent mixtures.

Solvent composition	Stretching parameter
$x_{\text{DCM 1.00}}$	0.89±0.05
$x_{\text{Acetone 0.09}}+x_{\text{DCM 0.91}}$	0.88±0.01
$x_{\text{Acetone 0.18}}+x_{\text{DCM 0.82}}$	0.88±0.01
$x_{\text{Acetone 0.27}}+x_{\text{DCM 0.73}}$	0.89±0.01
$x_{\text{Acetone 0.36}}+x_{\text{DCM 0.64}}$	0.89±0.01
$x_{\text{Cyclohexane 0.06}}+x_{\text{DCM 0.94}}$	0.89±0.02
$x_{\text{Cyclohexane 0.13}}+x_{\text{DCM 0.87}}$	0.86±0.02
$x_{\text{Cyclohexane 0.20}}+x_{\text{DCM 0.80}}$	0.88±0.01
$x_{\text{Cyclohexane 0.28}}+x_{\text{DCM 0.72}}$	0.85±0.02

Grafting PMA chains to the PS NPs influenced the T_2 of both PS and PMA in comparison to the free components. The relaxation of the NPs in pure DCM (Figure 5.3.7) revealed that the grafting of the PMA chains on the PS core led to an increase in the T_2 of the PS core. This phenomenon is the consequence of the grafting of mobile PMA chains. At the same time, anchoring the PMA chains to the PS core resulted in a moderate decrease in the T_2 of the PMA chains due to the substrate effect decreasing the segmental dynamics of the grafted chains in comparison to free PMA chains.[213] The interplay caused by the tethering of two polymer systems with different intrinsic dynamics is reminiscent of the block copolymer, where the dynamics of a slow block can be enhanced by tethering a more rapidly relaxing block and inversely the dynamics of a fast block can be slowed down by the tethering to a slower block.[271, 272] In such situations, the fluctuation of the more rapid segment was responsible for the acceleration of the segmental mobility of the slower component.

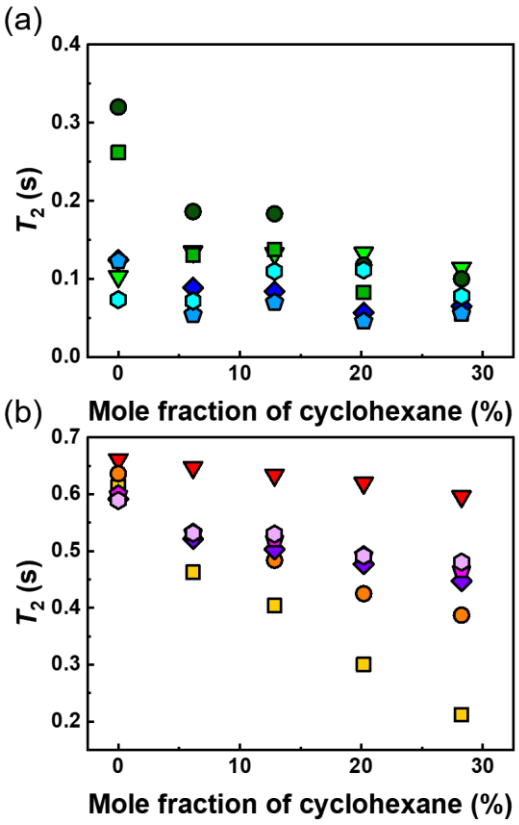

Figure 5.3.7. Effect of the addition of selective non-solvent for the PMA canopy on the local mobility of PS-PMA NPs. T_2 relaxation of ^{1}H of the (a) aromatic ring of PS of PS NPs (light green triangle), PS-PMA$_{4k}$ (green square), PS-PMA$_{22k}$ (dark green circle), PS-PMA$_{28k}$ (blue diamond), PS-PMA$_{42k}$ (light blue pentagon) and PS-PMA$_{52k}$ (cyan hexagon) and (b) methoxy group of free PMA$_{22k}$ (red triangle), PS-PMA$_{4k}$ (yellow square), PS-PMA$_{22k}$ (orange circle), PS-PMA$_{28k}$ (violet diamond), PS-PMA$_{42k}$ (magenta pentagon) and PS-PMA$_{52k}$ (light violet hexagon) in DCM/cyclohexane mixtures.

Changing the quality of the solvent by the addition of cyclohexane, a marginal solvent for PS and a non-solvent for PMA, changed the local dynamics of both the PS core and the PMA canopy of the PS-PMA NPs (Figure 5.3.7). In the case of PS NPs, the T_2 of the protons of the aromatic ring remained almost constant during the addition of cyclohexane in DCM as the quality of the solvent ($\chi_{PS\text{-}solvent}$) changed from 0.22 to 0.09 (Table 5.3.3). This observation was consistent with the swelling behavior of PS in DCM/cyclohexane mixture displaying a moderate increase in swelling with the addition of cyclohexane. Under the same conditions, the relaxation of the free PMA chains decreased linearly in keeping with the deswelling of the chains associated with the increase in $\chi_{PMA,\ solvent}$ from 0.13 to 0.43. More surprisingly,

when the PMA chains were immobilized on the PS core, the T_2 of both the aromatic protons and the protons of the methoxy group decreased with the addition of cyclohexane. The T_2 of the methoxy group decreased even more steeply for PS-PMA NPs than for free PMA chains, and this decrease was more pronounced for the PS-PMA NPs functionalized with short PMA chains. The variation of T_2 observed with the degree of polymerization of the PMA chains can be ascribed to the different conformational changes occurring in the PMA chains when they are immobilized on the surface of the PS NP, while short chains are forced to adopt an almost fully extended conformation, longer chains, because the radial decrease in the steric crowding in the canopy, can adopt, on average, a more relaxed conformation. More counterintuitively, T_2 of PS in PS-PMA decreased just like the free PMA since, even, if the solvent condition becomes better for the PS. This phenomenon can be related to the increased local mobility observed for PS in DCM when PMA chains were grafted to the PS core due to the rapid relaxation of the PMA chains. As the local mobility of surrounding PMA canopy was reduced, so was the enhancement of the PS local mobility caused by the grafting of the PMA chains. The increase in local mobility observed in pure DCM was no longer present in DCM/cyclohexane solvent mixtures. At high cyclohexane content, the local dynamics of the PS core in PS-PMA NPs became similar to the local dynamics of pure PS NPs since the PMA no longer increased the local mobility of the substrate.

The relaxation behavior of pure PS NPs, PS-PMA, and free PMA chain in DCM/acetone solvent mixture was also studied (Figure 5.3.8). Acetone is a good solvent for PMA and a poor solvent for PS. Upon the addition of acetone to DCM the T_2 of free PMA chains remained constant as the solvent quality $\chi_{\text{PMA-solvent}}$ changed from 0.13 to 0.16. Simultaneously, the T_2 of pure PS NPs moderately decreased when the mole fraction of acetone increased in the solvent mixture due to the nonsolvency of PS in acetone with $\chi_{\text{PS, solvent}}$ increasing from 0.22 to 0.35. The decrease in $\chi_{\text{PS, solvent}}$ was also associated with the deswelling of the PS NPs (Figure 5.3.3). After the addition of acetone, the T_2 of the tethered PMA chains significantly decreased, in keeping with the decrease of the local mobility of the PS core, this phenomenon was more pronounced for short PMA chains and systematically reduced as the length of the end-tethered PMA chains increased. Therefore, the local mobility of short chains was more susceptible to be influenced by the dynamics of the substrate, especially when the substrate was soft and deformable.

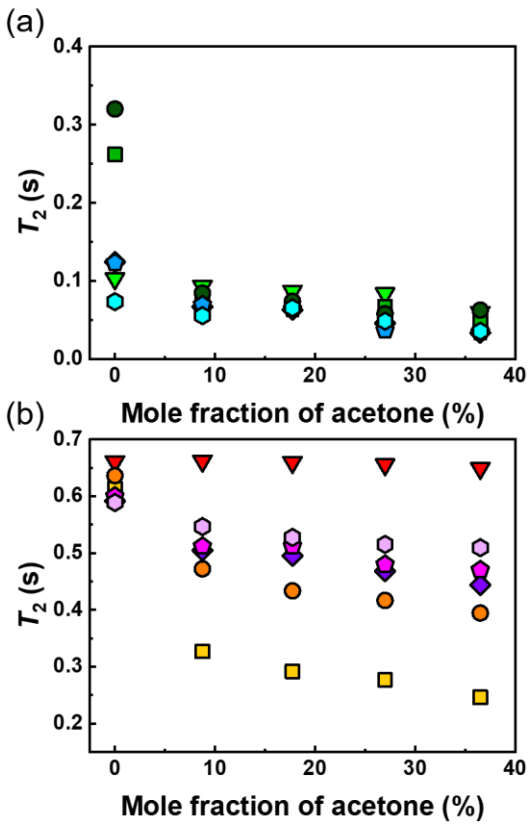

Figure 5.3.8. Effect of the addition of selective non-solvent for the PMA canopy on the local mobility of PS-PMA NPs. T_2 relaxation of ^{1}H of the (a) aromatic ring of PS of PS NPs (light green triangle), PS-PMA$_{4k}$ (green square), PS-PMA$_{22k}$ (dark green circle), PS-PMA$_{28k}$ (blue diamond), PS-PMA$_{42k}$ (light blue pentagon) and PS-PMA$_{52k}$ (cyan hexagon) and (b) methoxy group of free PMA$_{22k}$ (red triangle), PS-PMA$_{4k}$ (yellow square), PS-PMA$_{22k}$ (orange circle), PS-PMA$_{28k}$ (violet diamond), PS-PMA$_{42k}$ (magenta pentagon) and PS-PMA$_{52k}$ (light violet hexagon) in DCM/acetone mixtures.

The variation of the T_2 of PS and PMA as a function of $\chi_{\text{polymer-solvent}}$ of the polymers in the different solvent mixtures (Figure 5.3.9) emphasized the existence of an interplay between the dynamics of the PMA canopy and the dynamics of the PS core. Pure PS NPs and free PMA chains both showed the expected overall linear decrease in T_2 when the $\chi_{\text{PS-solvent}}$ varies from a good solvent to a marginal solvent (Figure 5.3.10). However, the local mobility of the grafted core-canopy system was more complex because of the synergetic effect of the co-solvent addition. The normalized T_2 of PS in PS-PMA NPs increased as the solvent quality decreased ($\chi_{\text{PS-solvent}}$ increasing from 0.09 to 0.22) and then followed the trend of pure PS NPs and decreased with a further increase of $\chi_{\text{PS-solvent}}$. This change in behavior occurred when the co-

solvent used to tune the solvent quality changed from cyclohexane to acetone and was ascribed to the interplay between the local mobility of the core and the local mobility of the PMA canopy. Initially, the addition of acetone decreased the solvent quality for the polystyrene core but had a limited influence of the solvent quality for the PMA canopy (Figure 5.3.11).

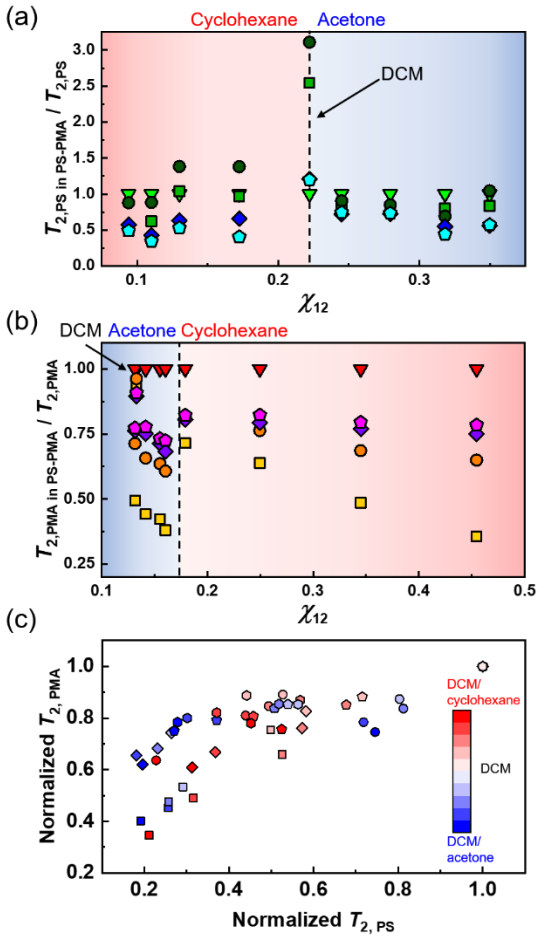

Figure 5.3.9. Normalized T_2 relaxation time of ^{1}H of the (a) aromatic ring of PS of PS NPs (light green triangle), PS-PMA$_{4k}$ (green square), PS-PMA$_{22k}$ (dark green circle), PS-PMA$_{28k}$ (blue diamond), and PS-PMA$_{42k}$ (light blue pentagon) and (b) methoxy group of free PMA$_{22k}$ (red triangle), PS-PMA$_{4k}$ (yellow square), PS-PMA$_{22k}$ (orange circle), PS-PMA$_{28k}$ (violet diamond), and PS-PMA$_{42k}$ (magenta pentagon) as a function of χ_{12} of PS and PMA. T_2 normalized to the T_2 of the pure PS NPs or free PMA chains in the same solvent composition. (c) Relation between the variation of the T_2 relaxation time of PS and PMA in solvent mixtures normalized to the T_2 observed in pure DCM for PS-PMA$_{4k}$ (●), PS-PMA$_{22k}$ (■), PS-PMA$_{28k}$ (◆), and PS-PMA$_{42k}$.

Consequently, the local mobility of the PS core followed the same trend as the local mobility of the unfunctionalized PS NPs since there were no other effects. However, the addition of cyclohexane to the DCM suspension was accompanied by an increase in the solvent quality for the PS core and a decrease in the solvent quality for the PMA canopy, and the behavior of the PS core deviated from the behavior of the unfunctionalized PS NPs, because the local mobility of the PS core was not only influenced by $\chi_{\text{PS-solvent}}$ but also by the behavior of the PMA canopy. The grafting of the PMA canopy increased the local mobility of the PS core, but this effect was observable only when the PMA canopy was in a good solvent and sufficiently mobile.

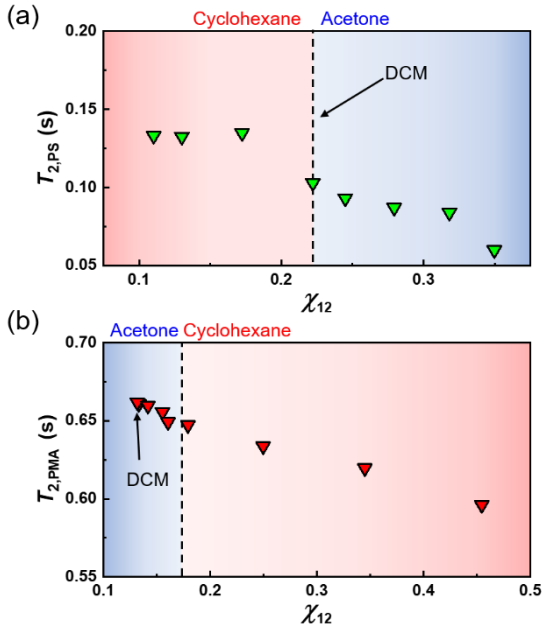

Figure 5.3.10. Variation of the T_2 relaxation time of (a) PS NPs and (b) free PMA chains in different binary solvent mixture.

The T_2 of the PMA canopy on the PS-PMA NPs was characterized by a discontinuity when the solvent mixture was changed from DCM/acetone to DCM/cyclohexane mixture. First, T_2 decreased as $\chi_{\text{PMA-solvent}}$ increased from 0.13 to 0.16 with the addition of acetone, then increased drastically when 6 mol% of cyclohexane was used as a co-solvent and $\chi_{\text{PMA-solvent}}$ changed from 0.16 and 0.18. Then, the T_2 of the PMA canopy decreased again with the increases of $\chi_{\text{PMA-solvent}}$ induced by the addition of more cyclohexane. Although the change in solvent quality experienced by the PMA chains was limited when switching the cosolvent from acetone to cyclohexane, the T_2 of the PMA canopy was simultaneously

influenced by the large variation in solvent quality sustained by the PS (Figure 5.3.12) resulting in a decrease in the local mobility of the PS core.

Consequently, the effect of $\chi_{\text{polymer-solvent}}$ for one single component of the PS-PMA system cannot solely be used to explain the variations observed in the relaxation dynamics. The simultaneous impact of the change of the solvent quality on both PS and PMA should be considered as well as the interplay between the local dynamics of the core and of the canopy. When the solvent mixture was changed from 36 mol% acetone in DCM to 6 mol% cyclohexane in DCM, the $\chi_{\text{PMA-solvent}}$ changed from 0.16 to 0.18, but the $\chi_{\text{PS-solvent}}$ changed from 0.35 to 0.17. Between those conditions, the local mobility of the naked PS NPs increases 3-folds. Thus the substrate of the PMA brushes was significantly different going from 36 mol% of acetone to 6 mol% of cyclohexane and resulted in the discontinuous behavior observed for the T_2 of the PMA canopy. As the local mobility of the PS increased, the substrate effect limiting the local mobility of the grafted chain was less prominent, and the T_2 of the PMA chains increased. The addition of more cyclohexane led to a steady decrease in the T_2 of the PMA corona in keeping with the behavior of free PMA chains. Additional evidence of the interplay between the dynamics of the core and the canopy, was the effect of the degree of polymerization of the PMA chains on local mobility of the system. The impact of the solvent quality on the local mobility of PMA chains was more pronounced for the shorter PMA chains, for which the local mobility of the canopy was more strongly dependent on the local mobility of the PS substrate.

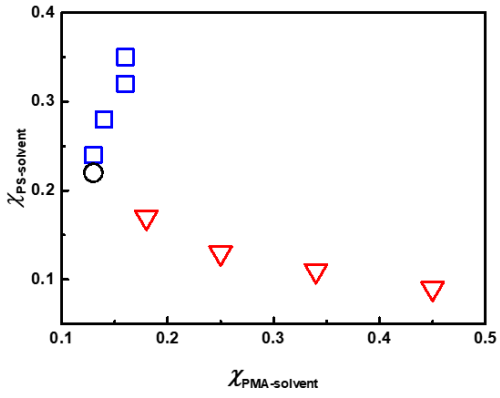

Figure 5.3.11. Flory-Huggins interaction parameter of PS as a function of that of PMA with DCM/cyclohexane (red triangle), DCM/acetone (blue square), and DCM (black circle).

The interplay between the PS core and the PMA canopy could only be understood by concurrently considering the effect of $\chi_{PS\text{-}solvent}$ and $\chi_{PMA\text{-}solvent}$ on the T_2 of both PS and PMA, (Figure 5.3.13). The solvent quality had a definite impact on the T_2 of both the PS and PMA segments. However, the T_2 of the PS was also influenced by the relaxation of the PMA segments, and inversely the relaxation of the PMA segments was affected by the local mobility of the PS core (Figure 5.3.9c). In the PS-PMA core-canopy system, the reduction of the relaxation time of the core was systematically accompanied by a decrease of the relaxation time of the canopy irrespectively of the chain length. Inversely, a reduction of the T_2 of the canopy led to a reduction of the T_2 of the core. Consequently, only when using a common good solvent resulted in fast local mobility for either PS or PMA in the coupled system. The addition of a selective non-solvent resulted in the decrease in the relaxation of both the core and the canopy irrespectively if the non-solvent was selective for the core or the canopy.

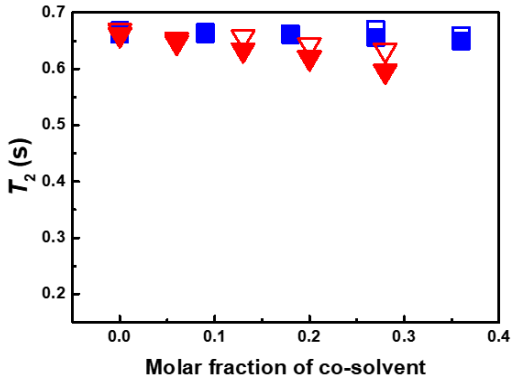

Figure 5.3.12. Influence of the molecular weight on the mobility of free PMA chain. T_2 relaxation of ^{1}H of methoxy group of free PMA4k (empty symbol) and PMA22k (filled symbol) in DCM/cyclohexane (red triangle) and DCM/acetone (blue square) mixtures measured at a Larmor frequency of 300.13 MHz at 298K.

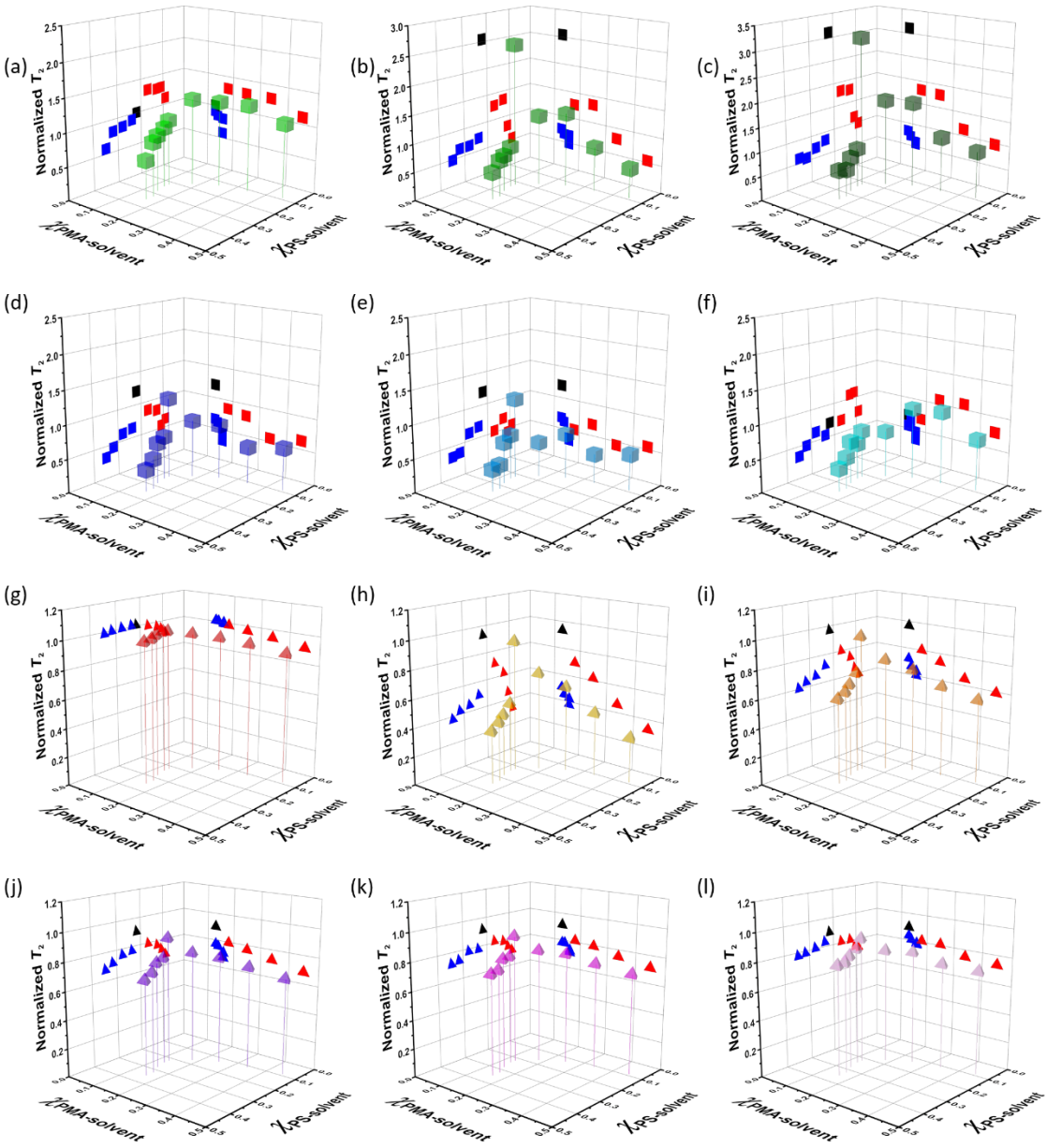

Figure 5.3.13. Normalized T_2 relaxation of ^{1}H of the aromatic ring of (a)PS NPs (light green cube), (b)PS-PMA$_{4k}$ (green cube), (c)PS-PMA$_{22k}$ (dark green cube), (d)PS-PMA$_{28k}$ (blue cube), (e)PS-PMA$_{48k}$ (light blue cube) (f)PS-PMA$_{52k}$ (cyan cube) and methoxy group of (g)free PMA$_{22k}$ (red tetrahedron) (h)PS-PMA$_{4k}$ (yellow tetrahedron), (i)PS-PMA$_{22k}$ (orange tetrahedron), (j)PS-PMA$_{28k}$ (violet tetrahedron), (k)PS-PMA$_{48k}$ (magenta tetrahedron) (l)PS-PMA$_{52k}$ (light purple tetrahedron) as a function of χ_{12} of PS and PMA. T_2 normalized to the T_2 of the pure PS NPs or free PMA chains in pure DCM. Black, blue, and red in x-z and y-z planes indicate the solvents with DCM, DCM/acetone, and DCM/cyclohexane, respectively.

5.3.3 Conclusion

In conclusion, the study of the relaxation dynamics of soft swollen gel nanoparticles functionalized with polymer chains was investigated by NMR relaxometry. The effect of the solvent quality on the swelling behavior and the relaxation dynamics of PS core and PMA canopy of PS-PMA hairy soft NPs were investigated using solvent mixtures with tunable and selective solvent quality favoring either the PS core or the PMA canopy. The results suggest a strong interplay between the dynamics of the core and the dynamics of the canopy of end-tethered chains.

In a single polymer system, either pure PS NPs of free PMA chains, the T_2 of the polymer decreased with decreasing $\chi_{\text{polymer-solvent}}$. However, in the case of PS NPs functionalized with a canopy of end-tethered PMA chains, the effect of the solvent quality on the T_2 of the polymer was more complex due to the interplay between the mobility of the PS core and of the PMA canopy. Generally, the functionalization of the PS core with a canopy of swollen and mobile PMA chains increased the T_2 of the PS in comparison to unfunctionalized PS NPs. As expected, the addition of a selective non-solvent for the PMA canopy reduced the solvent quality for the PMA canopy, and a reduction in the local mobility of the PMA chains was observed. However, this reduction in the local mobility of the PMA canopy triggered a reduction in the local mobility of the PS core, although the solvent quality for the PS core increased in that solvent mixture. Similarly, as the local mobility of the PS decreased with the addition of a selective non-solvent, the T_2 of the PMA canopy also reduced due to a stronger immobilization by the PS core.

Selectively decreasing the solvent quality for one of the polymer components, either the PS core or the PMA canopy, resulted in a decrease in the mobility of both polymer components. When a polymer system with a complex architecture, such as the core-canopy PS-PMA NPs under study, are used, the synergetic effect between composition, architecture, and environment need to be considered during their processing.

5.4 Influence of the Architecture of Soft Polymer-Functionalized Polymer Nanoparticles on their Dynamics in Suspension[4]

The macroscopic behavior of PS-PMA core-canopy NPs in suspensions studied in section 5.1 shows that the length of the grafted chains, the grafting densities, the swelling and softness of the core, all had significant effects on the rheological behavior of the suspensions. NMR relaxation was used (section 5.2 and 5.3) to investigate the impacts of the core softness, length of the grafted chains, and solvent quality on the behavior of the suspension at the sub-colloid scale, by measuring the local segmental motion in the core and in the canopy of grafted polymer chains. Finally, to correlate the global behavior observed by rheology with the local behavior measured by NMR, the combined effect of the variation of the chain length and grafting density on the local subsegmental dynamics of the core and the canopy was measured by NMR relaxation.

The grafting density is a crucial parameter in defining the conformation of the grafted chains and influences the dynamics of the grafted chains. Thus, an understanding of chain dynamics at various grafting density is essential to tune the properties of nanoparticles with polymer brushes. While the effect of the chain grafting density on the local dynamics of the tethered chains has been studied when the core particle is hard and rigid, like silica, the dynamics of the grafted system where the core particle is itself soft and mobile has not been investigated. In such systems, the dynamics of the core can influence the dynamics of the tethered chains and reversely, the dynamics of the tethered chains can influence the dynamics of the core, poly(styrene) (PS) particles functionalized with poly(methyl acrylate) (PMA) chains were prepared with various chain lengths at different grafting densities. NMR spin relaxation revealed

[4] This section is based on the article:

[redacted] Influence of the Architecture of Soft Polymer-Functionalized Polymer Nanoparticles on their Dynamics in Suspension. *Polymers,* **2020**, *12,* 1844

Author contribution: [redacted] designed the experiments. and [redacted] performed the experiments. [redacted] synthesized polymer samples [redacted] analyzed the data and discussed the results. [redacted] wrote the manuscript.

that the confinement effect on the mobility of the grafted chain was more prominent for densely grafted short chain likely due to the steric hindrance created by the close proximity to the rigid core and of the neighboring chains. More interestingly, a thick layer of a densely grafted PMA canopy efficiently increased the local mobility of the PS cores. The results obtained by NMR relaxation of the nanoparticle suspensions and thermal analysis of the dried nanoparticles suggest an interplay between the dynamics of the core and the dynamics of the canopy.

5.4.1 Motivation

Nanoparticles (NP) possess a large surface area to volume ratio, and the control of the interface has a critical influence on the properties of the NP systems by tuning their interaction with their surrounding environment. Controlling the surface properties is critical since the incompatibility of the NPs with their surrounding media can result in the agglomeration of the NPs. The surface properties of the NPs can be controlled by tethering polymer chains on the surface to improve the NPs compatibility with a solvent or a polymer matrix.[17, 273-276] The layer of tethered polymers, whether the chains are in a brush conformation or not, forms a canopy around the core particle, and this layer of grafted chains defines the interaction between the NPs and between the NPs and their environment.[277] In such cases, the final behavior of the NPs is influenced by the chemical composition of the grafted chains, but also by their degree of polymerization (N) and their grafting density, the number of grafted chains per unit of area (σ). Variations in N and σ in systems where the polymer chains are tethered to hard and rigid nanoparticle core, such as silica or gold, influence the dynamics of the grafted polymer chains. And the architecture of the canopy of grafted polymer chains defines the interfacial properties of the NPs, such as particle/particles interaction or NPs/solvent interaction.[196, 277-281] However, the behavior of systems where the core is itself soft and deformable like a nanogel has not been addressed, and the dynamics of polymer chains grafted on the surface of soft NPs need to be thoroughly understood to improve the design of such systems.[263]

The architecture of the grafted polymer system, defined by the σ and N of the canopy, affects the conformation [96-98] and the dynamics of the grafted chains.[31] Both of which, in turns, largely affect the macroscopic behavior of systems based on polymer-functionalized NPs, such as the mechanical properties of nanocomposites [31 , 195] or the rheology of colloidal suspensions.[31, 237, 281] In a polymer-grafted NPs system, usually, the polymer chains experience a deceleration of the relaxation in

comparison to free chains as a consequence of the stretched chain conformation near the surface of nanoparticles and increased confinement generated by the proximity of adjacent chains [32] at least at the scale of the local segmental motion. On a larger scale, the increased confinement experienced by densely grafting chains usually resulted in an increase of glass transition temperature of tethered chains in comparison to the free chains ascribed to the presence of a reduced number of chain ends and smaller free volume in the grafted system. [213, 282, 283]

The investigations of the behavior of polymer grafted nanoparticular systems have mostly dealt with rigid core NPs like silica or gold. However, when soft and swollen polymer NPs are used as the substrate, the intrinsic dynamics of the polymer chains in the core also needs to be taken into account. In such swollen polymer nanoparticles, the dynamics of the chains is typically constrained and sparsely crosslinked nanogel displayed a soft interface with polymer chains having a rapid relaxation, while densely crosslinked nanogels exhibited glassy surface with constrained local mobility.[284-286] In nanocolloids resulting from the self-assembly of block copolymers, this arrested core is surrounded by a canopy of swollen and mobile polymer chains. In such a case, the polymer chains within the core experienced soft confinement, where the dynamics is influenced by the fluctuation of the interface where the two polymer components are connected.[33] Such phenomena affect the design of soft particles for different applications, for example, theranostic systems.[284, 286, 287] While the block copolymer micelles are an interesting point of comparison to the polymer-functionalized nanoparticles, in such systems the effect of the density of the surface functionalization on the local dynamics cannot be addressed, since it is difficult to control the packing density.

Here, the combined effects of the N and the σ of the grafted canopy on the dynamics of both the core and the canopy of polymer-functionalized polymer nanoparticles were investigated using NMR relaxometry. Polystyrene (PS) NPs functionalized with a canopy of end-grafted poly(methyl acrylate) (PMA) were prepared by a combination of miniemulsion polymerization and surface-initiated polymerization, and dispersed in a common good solvent for both the core and the canopy. The σ was controlled and resulted in different canopies composed of either stretched polymer chains or collapsed chains (Figure 5.4.1a). The N of the grafted chains was also modified, so the contour length of the grafted PMA chains was increased from ca. 7 to 150 nm, while the radius of the swollen PS core was kept constant at ca. 100 nm. NMR relaxometry gave access to the correlation time (τ_c) associated with the subsegmental dynamics of

the polymers.[244, 288] The activation energy associated with the subsegmental dynamics of the polymer NPs in suspensions was analyzed and compared to the thermal behavior of the dried NPs.

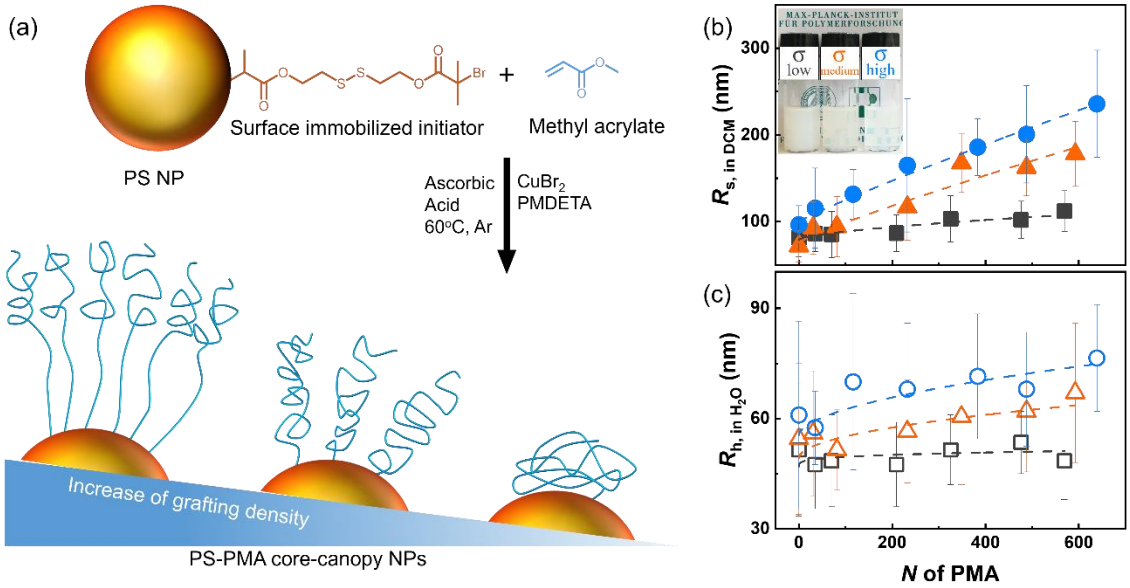

Figure 5.4.1. (a) Synthesis of poly(styrene) (PS)-poly(methyl acrylate) (PMA) core-canopy nanoparticles (NPs); (b) Solvodynamic radii (R_s) and (c) hydrodynamic radii (R_h) of PS-PMA NPs in DCM and H_2O, respectively. For NPs functionalized with PMA chains with a degree of polymerization (N) ranging from 0 to 639 units with low (0.17 chains nm^{-2}, black square), medium (0.8 chains nm^{-2}, orange triangle) and high (2.5 chains nm^{-2}, blue circle) grafting density, measured by dynamic light scattering at 25 °C. The inset photo in (b) displays the suspensions of PS-PMA_{49k}-σ_{low}, PS-PMA_{51k}-σ_{medium}, and PS-PMA_{55k}-σ_{high} in DCM at a concentration of 16.67 mg mL^{-1}.

5.4.2 Results and discussion

Using SI-ATRP, the PMA chains were successfully grafted from the surface of initiator immobilized PS NPs prepared by miniemulsion, and resulted in the formation of PS NPs having PMA canopies with different σ and varying N (Table 5.4.1). The increase in size created by the grafting of the PMA canopy resulted in a larger solvodynamic radius (R_s) for the samples with longer PMA chains or higher σ (Figure 5.4.1b); similar results were also observed in the dry state by TEM measurements (Figure 5.4.2).

Table 5.4.1 Library of PS and PS-PMA NPs

Sample	Initiator/MA/Cu(II)/PMDETA/Ascorbic acid	Time (h)	N	$M_{n,\,NMR}$ (kDa)	$M_{n,\,SEC}$ (kDa)	$Đ$	R_s in DCM (nm)
PS NPs low grafting density (0.17±0.02 chains · nm^{-2})							81±20
PS_L- PMA_{3k}	1/266/0.1/1.0/0.5	0.5	35	3	4	1.8	86±20
PS_L- PMA_{6k}	1/533/0.1/1.0/0.5	1	70	6	8	2.1	85±30
PS_L- PMA_{18k}	1/533/0.1/1.0/0.5	2	209	18	19	2.3	90±20
PS_L- PMA_{28k}	1/1066/0.1/1.0/0.5	1.5	325	28	15	2.2	100±30
PS_L- PMA_{41k}	1/1066/0.1/1.0/0.5	2	476	41	18	2.7	100±20
PS_L- PMA_{49k}	1/1066/0.1/1.0/0.5	2.5	569	49	34	2.2	110±20
PS NPs medium grafting density (0.80±0.03 chains · nm^{-2})							70±20
PS_I- PMA_{3k}	1/133/0.1/1.0/0.5	0.5	30	3	4	1.9	90±30
PS_I- PMA_{7k}	1/266/0.1/1.0/0.5	0.5	81	7	9	2.6	90±30
PS_I- PMA_{20k}	1/533/0.1/1.0/0.5	3	232	20	20	2.2	120±40
PS_I- PMA_{30k}	1/1066/0.1/1.0/0.5	2	348	30	27	2.1	170±30
PS_I- PMA_{42k}	1/1066/0.1/1.0/0.5	3	488	42	29	2.1	160±30
PS_I- PMA_{51k}	1/1066/0.1/1.0/0.5	4.5	592	51	35	2.4	180±40
PS NPs high grafting density (2.5±0.3 chains · nm^{-2})							90±20
PS_H- PMA_{3k}	1/266/0.1/1.0/0.5	0.5	35	3	4	1.7	110±50
PS_H- PMA_{10k}	1/533/0.1/1.0/0.5	2	116	10	12	2.1	130±30
PS_H- PMA_{20k}	1/533/0.1/1.0/0.5	3	232	20	21	2.1	160±70
PS_H- PMA_{33k}	1/1066/0.1/1.0/0.5	1	383	33	27	2.4	190±30
PS_H- PMA_{42k}	1/1066/0.1/1.0/0.5	3	488	42	40	2.5	200±60
PS_H- PMA_{55k}	1/1066/0.1/1.0/0.5	6	639	55	44	2.0	240±60

The comparison of the size of the NPs in DCM and in H_2O by DLS (Figure 5.4.1b,c), made it possible to study the swelling of the NPs and the evolution of thickness of the layer of end-grafted polymer chains. The size of the NPs in both DCM and water increased with increasing N and σ. In addition, DCM is a good solvent for both the PS core and the PMA canopy and both components were swollen in suspension, while water is a poor solvent for both the PS and PMA, and the NPs were in a collapsed state. This variable swelling of the core had a consequence on the apparent σ of the system. In water, because the NP cores were collapsed, the number of chains per unit of surface area was larger than for the same NP in DCM (Table 5.4.2).

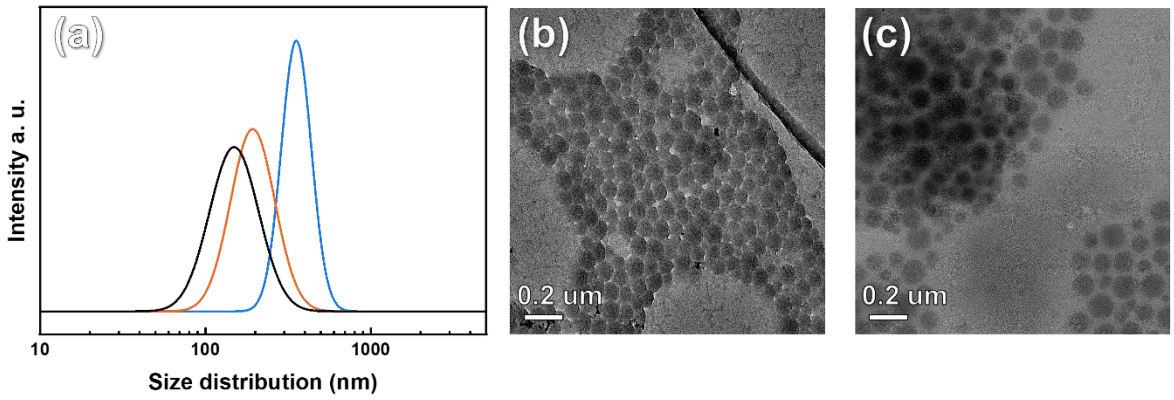

Figure 5.4.2 (a) Solvodynamic size distribution of PS NPs (**black line**), PS-PMA$_{3k}$ NPs (**orange line**) and PS-PMA$_{51k}$ NPs (**blue line**) with medium grafting density in DCM measured by DLS and transmission electron microscopy image (TEM) of (b) PS-PMA$_{3k}$ and (c) PS-PMA$_{51k}$ NPs with medium grafting density. TEM was analyzed by using an FEI Tecnai F20 operated with an accelerating voltage of 200 kV.

Table 5.4.2. Grafting density and scaling exponent of PS-PMA core-canopy NPs in DCM and H_2O.

Grafting density (σ)	**Grafting density in H_2O (chains nm^{-2})**	**Grafting density in DCM (chains nm^{-2})**	**Scaling exponent in H_2O**	**Scaling exponent in DCM**
Low	0.17	0.07	0.27	0.63
Medium	0.80	0.46	0.50	0.88
High	2.50	1.00	0.55	0.91

In DCM, R_s of bare PS NPs with σ_{low} was 81 nm and the size increased up to 110 nm for NPs functionalized with PMA chains with N=569 units. For NPs with σ_{high} , R_s of bare PS NPs was 90 nm and increased up to 240 nm when PMA chains with N=639 units were grafted. The variation of the size of the swollen NPs with the increase of N (Figure 5.4.1b,c) follows the scaling relation:

$$R_s - R_{s,0} \propto N^{v} \qquad (5.4.1)$$

where R_s is the thickness of grafted chains, N is the degree of polymerization, v is scaling exponent, and $R_{s,0}$ is the size of the PS core. The scaling factor was shown to change for different grafting regime. [27,

97, 98, 225] Here, at σ_{low} in DCM the scaling factor (v=0.63) was typical of grafted chains in the semi-collapsed chain regime in a good solvent. For the NPs with σ_{medium} and σ_{high} the scaling exponent of 0.88 and 0.91 were observed, respectively (Table 5.4.2), typical of grafted chains in the stretched regime.[97, 98] In water, a poor solvent for the PMA canopy, the stretching factor of the canopy with a σ_{low} was 0.27 typical of collapsed chains. The particles prepared at higher σ_{medium} and σ_{high} dispersed in water showed a stretching parameter corresponding to the semi-collapsed regime. The result obtained for the stretching parameter of the grafted chains the PS-PMA NPs was in keeping with the decrease in solvent quality going from DCM to water. In a good solvent, as a consequence of the polymer-solvent enthalpic attraction and the polymer-polymer entropic repulsion, the grafted polymer chains adopt a stretched and extended conformation [161, 165] resulting in a large v. Conversely, in a poor solvent, the favorable polymer-polymer attraction results in the adoption of a collapsed conformation. If the NPs were dispersed in a good solvent at a high enough concentration, the formation of colloidal gels was observed.[237] However, the NMR experiments were performed below the solution-to-gel transition to study the dynamics of single particles rather than the dynamics of the NPs network.

The NMR relaxation of the NPs suspension was measured at different magnetic fields and different temperatures to understand the local subsegmental chain dynamics in both the PS core and the PMA canopy. Both the spin-lattice relaxation (T_1) and spin-spin relaxation (T_2) were measured. The relaxation times obtained by NMR spectroscopy are influence by τ_c of the relaxation process and the interactions between the spin under study and their environment. Typically, T_2 is not largely influenced by the magnetic field used and the values of T_2 can be directly correlated to the subsegmental relaxation.[144] As the local mobility of the molecules under investigation decreases, the value of the T_2 time decreases, and for very slow systems, it can be difficult to quantify the T_2 relaxation precisely without using alternative pulse sequences. Consequently, the measurement of the T_2 of the crosslinked PS core was challenging. Thus, T_1 relaxation time, although providing less precise measurement of the local subsegmental chain relaxation, was also use to probe the PS-PMA NPs.

The T_2 of PMA was used to probe the relaxation dynamics of the tethered chains (Figure 5.4.3a). The T_2 of free PMA chains depicted ca. 0.77 s at N = 46 and slightly decreased with an increase of N. The short tethered PMA chains (N = 35) at σ_{low} showed of T_2 of 0.42 s and as chain length increased, the T_2 value also moderately increased. The increase in the T_2 value indicates an enhanced subsegmental mobility of the chains. Thus, it can be concluded that the local mobility of the tethered PMA chains with σ_{low} increased

when the N of the chain increased. Even though the PMA chains on the PS-PMA NPs at σ_{low} displayed a collapsed brush conformation, given their chain stretching factor (Table 5.4.2), their local subsegmental mobility was reduced in comparison to untethered PMA chains of the same length, likely because the presence of the PS substrate restricted the subsegmental motion of the chains. As σ increased from low to high, the T_2 of the short tethered PMA decreased due to the transition from a collapsed conformation to a stretched brush regime (Table 5.4.2) generated by the crowding produced by the adjacent chains. The relaxation of the free and untethered PMA chains was not influenced by the N in the range of molecular weights studied. However, for the grafted chains, as the chain length increased, the T_2 of the grafted PMA chains systematically increased for all σ. The increase in the local mobility of the grafted PMA chains as N increased was attributed to the reduction in the spatial crowding observed as the distance from the core increased with increasing N.[96] These observations are in keeping with what has been observed for the local subsegmental dynamics of polymer chains grafted to the rigid nanoparticles.[32, 241]

In the PS-PMA NPs system, both the PMA and the PS were undergoing relaxation. Addressing the effect of the grafting of polymer chains on the dynamics of the soft core can be the key to explain the divergences observed when comparing the macroscopic properties of soft and hard polymer-functionalized particles.[237] However, the local dynamics of the crosslinked PS core was too slow to be probed efficiently by the measurement of the T_2 (Figure 5.4.4). In the slow regime, the T_1 of a proton will increase as the local chain τ_c decreases. Furthermore, the T_1 values are significantly influenced by the local magnetic field. Consequently, to get a clear picture of the chain relaxation in the PS cores T_1 relaxation times were measured at different magnetic fields (Figure 5.4.5).

The relaxation of all the unfunctionalized PS cores exhibited similar T_1 relaxation times. The grafting of PMA chains of different N at σ_{low} resulted in no significant changes in the T_1 value observed. However, when PS cores were functionalized with PMA chains at σ_{medium} and σ_{high}, the T_1 of the PS core decreased with the increase of N_{PMA} (Figure 5.4.3b). Consequently, at σ_{medium} and σ_{high} the grafting of the PMA chains increased the mobility of the PS core, and this effect was more pronounced with longer chains.

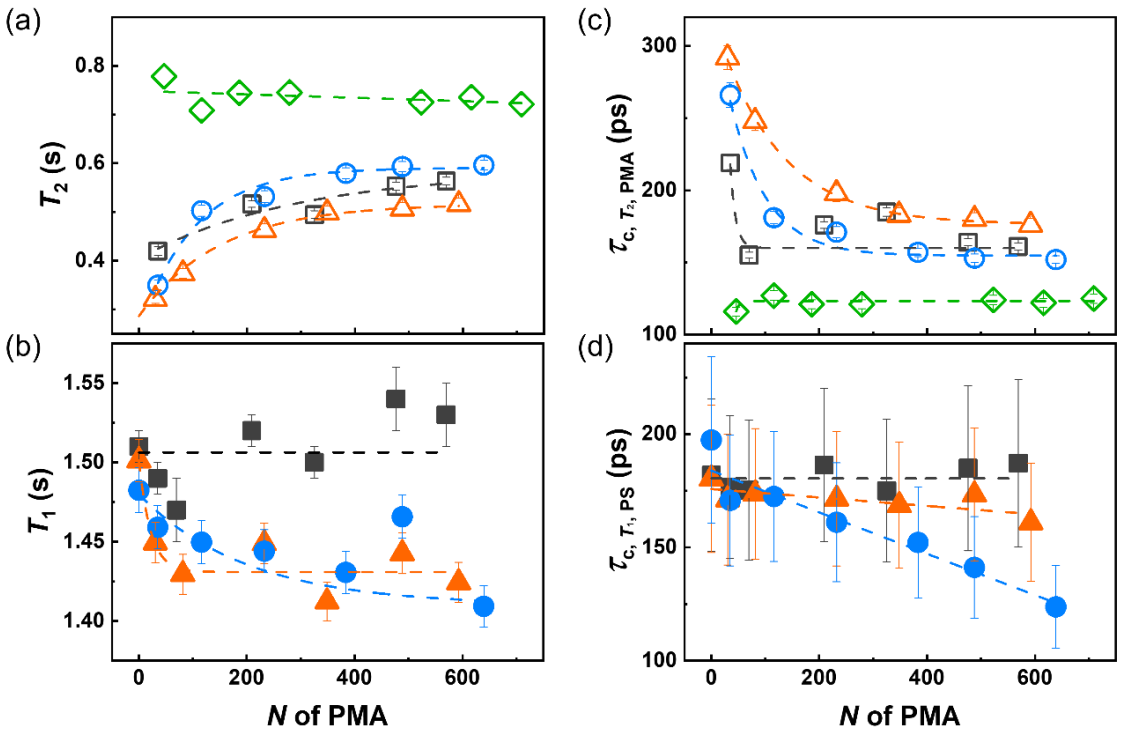

Figure 5.4.3. a) ^{1}H spin–spin relaxation time of methoxy group of the PMA canopy and b) ^{1}H spin-lattice relaxation time of aromatic ring of the PS core in the PS–PMA NPs with different degrees of polymerization of the PMA chains (*N*) grafted on PS cores with different grafting density, measured at 298K by using an NMR spectrometer at a Larmor frequency of 700.02MHz; c) Correlation time of ^{1}H of methoxy group of PMA canopy obtained from T_2 relaxation and d) correlation time of ^{1}H of the aromatic ring of PS core obtained from T_1 relaxation, calculated from BPP theory. For PS-PMA NPs with low- (0.17 chains nm^{-2}, black square), medium- (0.8 chains nm^{-2}, orange triangle), high-grafting density (2.5 chains nm^{-2}, blue circle) and free PMA chain (green diamond).

The relaxation time T_1 and T_2 obtained by NMR spectroscopy are measures of the relaxation of the spins system, an indirect measurement of the local dynamics, those values can be used to calculate the τ_c of subsegmental motions of the chains.[144] The average τ_c of the PMA chains and of the PS core were independently measured from the T_2 for the PMA and T_1 for the PS. The τ_c of free PMA chains was not significantly affected by *N* (Figure 5.4.3c) in the range of molecular weight studied. The grafting of the PMA chains to the PS core resulted in a decrease of in the local subsegmental mobility of the PMA chains resulting in larger τ_c values for the grafted PMA chains in comparison to the free PMA chains. As the σ increased, the constrain on each chain created by the neighboring chains increased and led to the increase

in τ_c observed especially at low N. At every σ as N increased, the difference in τ_c of the free and grafted PMA chains decreased. The τ_c measured by NMR relaxation is the average τ_c for the chains, and the decrease in the average τ_c of the PMA chain with increasing N suggested that the reduced dynamics experienced by the PMA segments was more important close to the interface with the PS core, in keeping with the decrease of monomer concentration as the distance from the surface increases, which reduced the crowding generated by neighboring chains.[96] Furthermore, as the length of the chains increased the difference observed for the nanoparticles with different σ decreased, because the segments of the grafted chains farther away from the core are less constrained at every σ, in keeping with observation of polymer chains grafted to hard nanoparticle cores.[31]

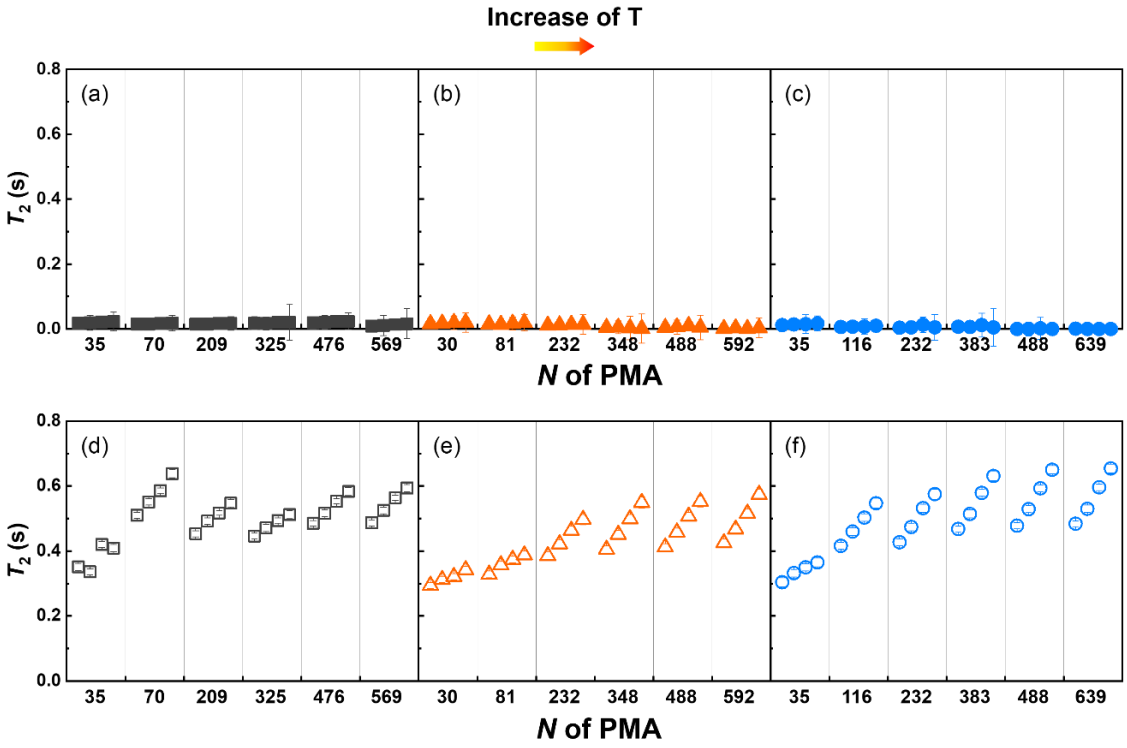

Figure 5.4.4. Temperature dependence of ^{1}H spin–spin relaxation time of (a), (b), (c) aromatic ring of the PS core and (d), (e), (f) methoxy group of PMA canopy in the PS–PMA NPs with different degrees of polymerization of the PMA chains (N) grafted on PS cores with different grafting density, measured at 278K, 288K, 298K and 308K by using NMR spectrometer at a Larmor frequency of 700.02MHz. For PS-PMA NPs with low- (0.17 chains nm^{-2}, black square), medium- (0.8 chains nm^{-2}, orange triangle) and high-grafting density (2.5 chains nm^{-2}, blue circle).

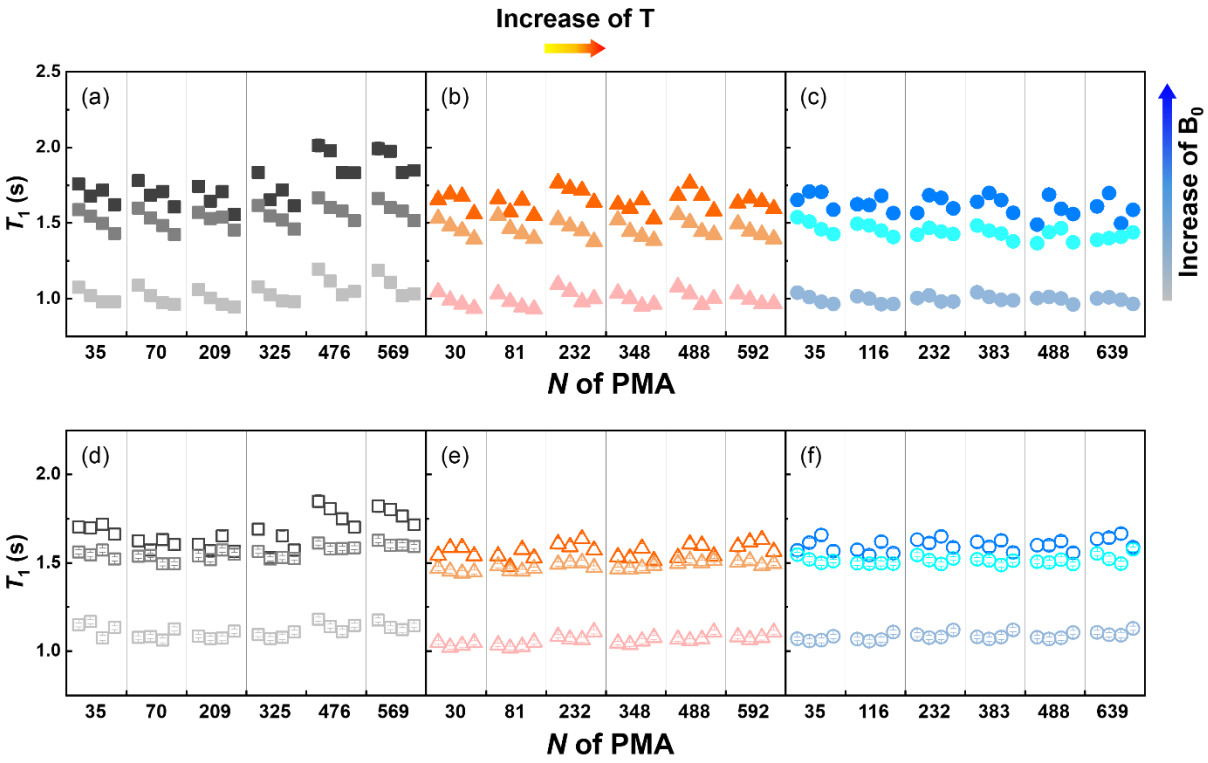

Figure 5.4.5. Temperature and magnetic field strength dependence of ^{1}H spin-lattice relaxation time of (a), (b), (c) PS core and (d), (e), (f) of PMA canopies in the PS-PMA NPs with low- (0.17 chains nm^{-2}, black square), medium- (0.8 chains nm^{-2}, orange triangle) and high-grafting density (2.5 chains nm^{-2}, blue circle) at Larmor frequencies of 500.13 MHz, 700.02 MHz and 850.27 MHz NMR at 278 K, 288 K, 298 K and 308 K. The magnetic field strength increases from the bottom set of T_1 to the above set. The temperature rises from the left (278 K) to the right (308 K) within one column.

Furthermore, the grafting of the PMA chains to the PS core influenced the local dynamics of the PS cores. After the grafting of the PMA chain at the interface of the PS NPs, a limited decrease in the τ_c of the PS core was observed, and this effect was stronger when the surface of the PS NPs was functionalized with long PMA chains (Figure 5.4.3d). Furthermore, as σ increased, the impact of the PMA chains on the dynamics of the PS core increased. This result can be attributed to an interplay between the slow dynamics of PS core and faster dynamics of PMA canopy. A similar behavior can be observed for block copolymer when a component with a high relaxation rate, increases the local dynamics of a slower block, because of the increased local fluctuations of the junction between the two segments initiated by the faster component.[271, 272] Additionally, the effect of σ suggests that the number of grafted chains, rather than

the dynamics of the grafted chains themselves, was the driving force for the faster dynamics observed with the PS core functionalized with a high number of long PMA chains.

The variation of the τ_c of a solvated polymer at different temperatures (Figure 5.4.6) can be described as an Arrhenius relation, where the activation energy associated with the subsegmental relaxation of the chains (Figure 5.4.7a,b) is a measure of the cooperativity of the segmental movement.[289-291] As the temperature increased, the τ_c of the PMA chains decreased as expected (Figure 5.4.6a,b), since higher temperatures increase the local subsegmental mobility of the polymer. However, in the case of the PS core, the τ_c increased with an increase in the temperature (Figure 5.4.6c,d). This unexpected result is related to the deswelling of crosslinked PS observed at high temperatures in specific solvent systems (Figure 5.4.8).[227, 263]

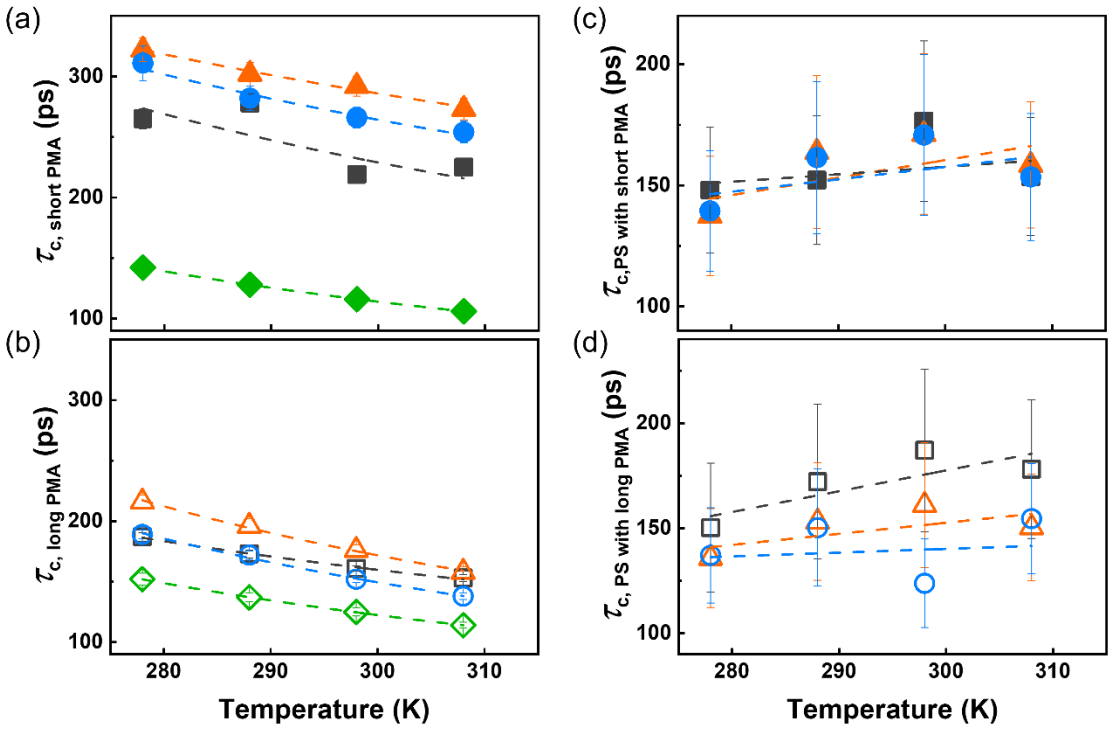

Figure 5.4.6. Temperature dependence of correlation time of PMA canopy with a) short chains (N<50), b) long chains (N>500), PS core with c) short PMA chains and d) long PMA chains. For PS-PMA NPs with low- (0.17 chains nm^{-2}, black square), medium- (0.8 chains nm^{-2}, orange triangle), high-grafting density (2.5 chains nm^{-2}, blue circle) and free PMA chain (green diamond).

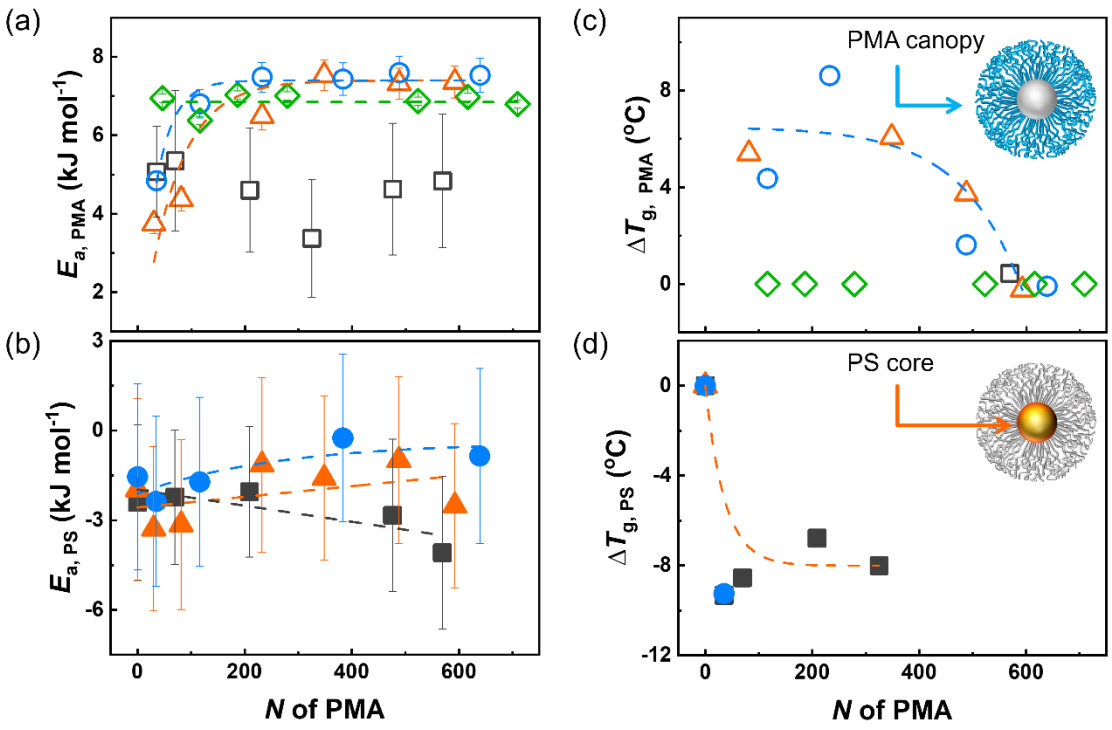

Figure 5.4.7. Energy of activation of local segmental motion of a) PMA canopy and b) PS core in PS-PMA NPs; Glass transition temperature (T_g) difference between c) free PMA and tethered PMA in PS-PMA with different degrees of polymerization of the PMA chains ($\Delta T_{g,PMA} = T_{g,PMA\ in\ PS-PMA} - T_{g,free\ PMA}$) and d) bare PS NPs and PS core of PS-PMA NPs ($\Delta T_{g,PS} = T_{g,PS\ in\ PS-PMA} - T_{g,bare\ PS}$). For PS-PMA NPs with low (0.17 chains nm^{-2}, black square), medium (0.8 chains nm^{-2}, orange triangle), high (2.5 chains nm^{-2}, blue circle) grafting density and free PMA chain (green diamond).

The energy of activation of the PMA chains of PS-PMA core-canopy NPs was calculated using the τ_c measured at different temperatures (Figure 5.4.7a). As expected, the activation energy associated with the subsegmental dynamics of the untethered PMA chains did not change significantly with *N*. However, short grafted chains displayed lower activation energy than the free chains, indicative of a decrease in the degree of cooperativity associated with the relaxation process, in keeping with the conformational changes of the PMA chains upon grafting when the chains adopted a partially stretched conformation. As the *N* increases, the difference in the extent of cooperativity of the relaxation process between the grafted chain and the free chains decreased. As a result of the limited weight fraction of PMA in the PS-PMA samples prepared at a low σ, the measurements were not as precise, and no clear conclusion

to the effect of the σ can be drawn. In the case of the PS core, the results are more complex; the deswelling of the PS core led to the reduction in the local subsegmental mobility of the PS core and resulted in apparent negative activation energy for the relaxation process (Figure 5.4.4). Nonetheless, the results clearly show that the grafting of the PMA chains facilitated the relaxation of the PS core, and this effect was more pronounced for long chains grafted with σ_{high} and σ_{medium} than with σ_{low}.

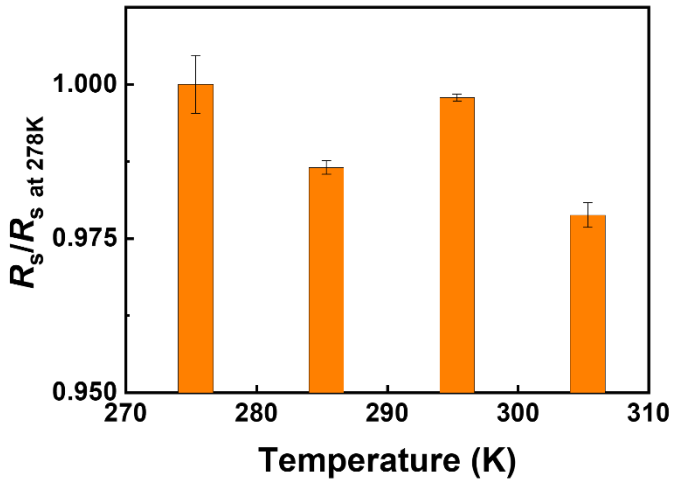

Figure 5.4.8. Normalized solvodynamic radius of pure PS NPs in DCM at given temperatures normalized by solvodynamic radius of NPs at 278K.

The activation energy measured for the DCM suspensions of the PS-PMA NPs clearly demonstrated an interaction between the dynamics of the PS core and the dynamics of the PMA canopy. Similar trends are also observed in the solid-state. The thermal behavior of dried PS-PMA (Figure 5.4.7c,d) showed that both the glass transition temperature of the PS core and of the PMA canopy was affected by the architecture of the PMA canopy. The untethered PMA chains displayed a moderate increase (ca. 2 °C) of glass transition temperature with the *N* as expected from the Flory-Fox equation.[292, 293] Short PMA chains grafted to the PS core displayed a glass transition temperature systematically higher than free PMA chains of the same molecular weight. The difference in the glass transition temperature of free and tethered chains decreased with increasing *N*. The results observed for the grafted PMA chains were consistent with what has been observed when polymer chains tethered to rigid NP cores transitioned between a highly stretched to a more relaxed brush regime.[282, 294] In addition, it was found that the glass transition temperature of PS core (Figure 5.4.7b and Table 5.4.3) significantly decreased by grafting PMA chains to the PS core. The grafting of the PMA chains on the surface of the PS core softened the core, in keeping

with the increased local subsegmental mobility observed by NMR relaxation in the swollen nanoparticles suspensions.

Table 5.4.3 Glass transition temperature of PS and PMA, measured by DSC.

Type of samples	*N* of PMA	T_g of PMA (°C)	T_g of PS (°C)
PS-PMA with Low σ	0		107.7
	35		98.4
	70		99.2
	209		100.9
	325		99.7
	569	14.4	
PS-PMA with Intermediate σ	0		107.9
	81	17.2	
	232	13.4	
	348	17.0	
	488	16.0	
	592	13.7	
PS-PMA with High σ	0		108.3
	35		99.0
	116	16.2	
	232	18.9	
	383	13.0	
	488	13.8	
	639	13.8	
Free PMA chain	46	11.8	
	116	10.3	
	186	10.9	
	279	12.2	
	523	13.9	
	616	13.8	

5.4.3 Conclusion

In conclusion, using NMR relaxation, we showed that the local segmental dynamics of PS-PMA NPs in suspension depends on the architecture of the system. The degree of polymerization and the grafting density influenced the dynamics of the interfacial layer of end-tethered PMA chain, as observed in other systems where mobile chains were grafted to rigid substrates, but also influenced the dynamics of the PS core. The results presented here also show a unique phenomenon: the grafting of a polymer canopy to a swollen and deformable PS core also influenced the dynamics of the core. The grafting of PMA chain to the PS core facilitated the subsegmental relaxation of the PS network. The fastest local PS dynamics were observed when long chains were densely grafted to the PS core. The cooperative nature of the relaxation decreased for the grafted PMA chains in comparison to the free PMA chains. However, this effect was amplified for short chains, and this can be related to the conformational change in the polymer chains upon grafting. The local subsegmental motion of the PS-PMA NPs in suspensions correlates with the global thermal movement of the system in dry state measured by differential calorimetry.

6. Summary and perspective

6.1 Summary

The focus of this doctoral dissertation was to explore the effect of the architecture of polymer-functionalized polymer nanoparticles on their behavior for colloidal systems composed of soft and deformable core particles functionalized with a canopy of end-tethered, but mobile, polymer chains. A series of core-canopy architectures of cross-linked poly(styrene) core with surface-immobilized poly(methyl acrylate) chains were successfully prepared by a combination of miniemulsion polymerization and surface-initiated atom transfer radical polymerization. The resulting nanoparticles yielded, when using a common good solvent, nanoparticles with a nanogel core functionalized with a canopy of swollen end-tethered polymer chains. Using a combination of rheology, NMR spin relaxometry and dynamic light scattering, four essential parameters governing the dynamics and the properties of polymer canopy-*grafted*-soft nanoparticles have been addressed, i.e., grafting density, degree of polymerization of end-tethered chains, stiffness of core nanoparticles, solvent quality. The results obtained showed how the macroscopic viscoelastic properties of the colloidal suspension and the local mobility of the polymer chains were influenced by the nanoparticle architecture and the surrounding medium.

In **Section 5.1**, the effect of the architecture of poly(methyl acrylate) canopy and resulting mechanical properties and viscoelastic behavior of colloidal suspension with selective solvent have been investigated. Different architectures of poly(methyl acrylate) chain-*grafted*-soft poly(styrene) core-canopy nanoparticles were prepared by varying the chain length and the grafting density of the canopy. The suspension of soft nanoparticles surface-functionalized with end-tethered polymer chain displayed a transition from liquid to gel. This transition occurred at a volume fraction occupied by the nanoparticle larger than what would be expected for hard spheres indicating that deformation, compression, or interdigitation of the nanoparticles occurred, and the liquid to gel transition was influenced by the architecture of the nanoparticles. The formation of colloidal gels was promoted for NPs with moderate

grafting density, and with sufficiently long end tethered chains. Moreover, the mechanical properties of the resulting colloidal gels were measured, and the results showed that, similarly to hard nanoparticles, the stiffness and yield strength of the colloidal was maximized for nanoparticles with long grafted chains at a grafting density high enough to induce some stretching of the chains, but not too high to produce an impenetrable layer of grafted chains. Two solvent systems were used, DMSO, a good solvent only for the PMA canopy and anisole, a good solvent for both PS and PMA, the properties of the colloidal gels highlighted a new phenomenon, even at a similar volume fraction of nanoparticles, the gels obtained in anisole were both stiffer and more deformable, this is the result of the softness of the core which likely influences the interaction between adjacent nanoparticles and their canopies. The most crucial new information from this study is that the rheological behavior and mechanical properties of suspensions of polymer nanoparticles can be tuned by controlling the architecture of polymer canopy but also by controlling the softness of the core.

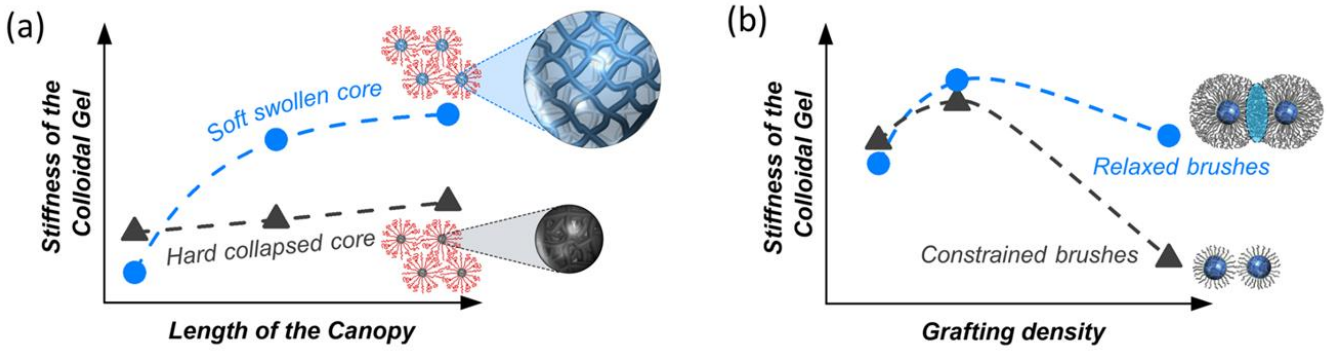

Figure 6.1.1 Influence of the nanoparticle architecture and swelling on the rheological properties of colloidal gels (**Section 5.1**.) The architecture of nanoparticle is controlled as functions of (a) length of the PMA canopy and (b) grafting density.

In **Section 5.2**, the effect of the rigidity of the core nanoparticles and thickness of the canopy on the local dynamics of polymer nanoparticles functionalized with end-tethered polymer chains was highlighted using NMR relaxation. Poly(styrene) nanoparticles cross-linked with different amounts of divinylbenzene were functionalized by grafting different lengths of poly(methyl acrylate) chains from the surface. Highly cross-linked poly(styrene) cores only marginally swelled in a good solvent and yield rigid substrate for the PMA canopy. As the rigidity of the substrate increased, the subsegmental dynamics of the polystyrene

obviously decreased, but more interestingly, the dynamics of the poly(methyl acrylate) canopy slowed down due to the interplay between the rigid core and the soft canopy. Additionally, grafting polymer chains on the polystyrene core resulted in a faster subsegmental relaxation dynamics for the polystyrene core. The increased mobility of the PS core was more important when the length of the grafted chains increased, and, remarkably, more important for highly cross-linked nanoparticles core. The substrate effect on the local mobility of the grafted chains can be observed only in close proximity to rigid cores, with soft core and long polymer chains, the local dynamics of the grafted chains was only marginally different than free polymer chains. Consequently, the softness of the nanoparticles core influence the mobility of the polymer canopy, and the mobility of the polymer canopy influence the behavior of the core; there is a clear interplay between the local mobility of the core and the mobility of the canopy.

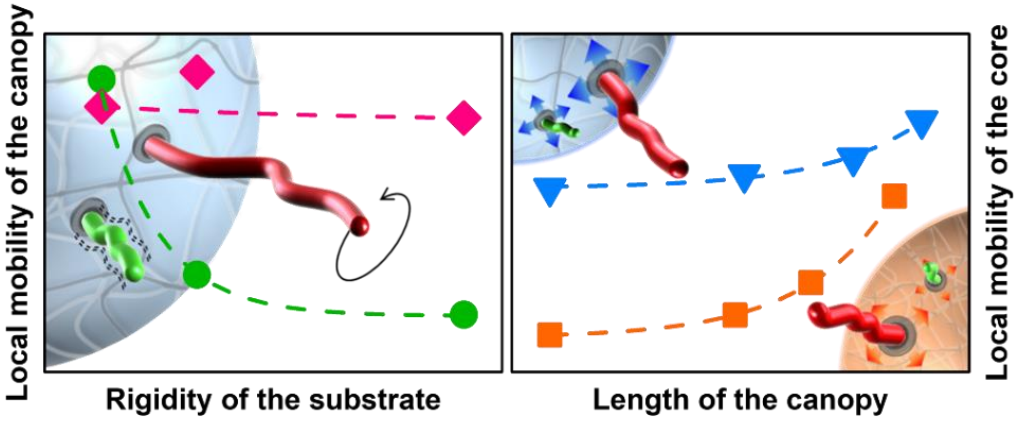

Figure 6.1.2 Interplay between the local dynamics of the polystyrene core and the poly(methyl acrylate) canopy (**Section 5.2**).

In **Section 5.3**, the interplay between the local dynamics of the canopy and of the core for deformable soft poly(styrene) nanoparticles functionalized with surface-grafted poly(methyl acrylate) chains was studied by NMR and investigated using different solvent quality. Based on the Flory-Huggins solvent-polymer interaction parameter, the solvent quality was tuned to selectively favored either the swelling of the poly(styrene) core or the swelling of the poly(methyl acrylate) canopy. While local mobility of unfunctionalized poly(styrene) nanoparticles and untethered poly(methyl acrylate) chains were independently influenced by the set of solvent quality used, there was a strong correlation between the local mobility of the PS core and the local mobility of the PMA canopy when different selective solvents were used with the PS-PMA NPs. The local subsegmental dynamics of each component of the NP was

highly influenced by the dynamics of the other component. When the solvent quality changed either in favor of the core or the canopy, the local subsegmental dynamics of both the core and the canopy significantly decreased compared to the dynamics observed in a common good solvent. This is attributed to the interplay between core and canopy under controlled solvent quality due to the interconnected architecture.

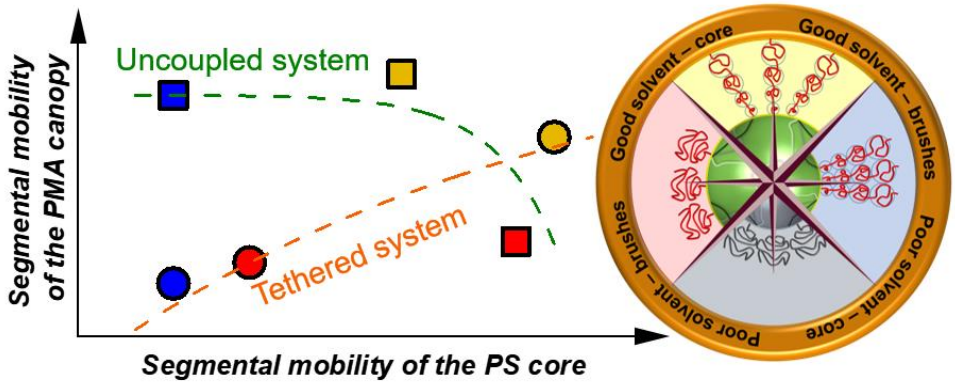

Figure 6.1.3 The effect of solvent quality on the local mobility of core and canopy and their interplay. (**Section 5.3**)

In **Section 5.4**, the architecture of the PS-PMA core-canopy NPs was controlled by tuning the grafting density and the degree of polymerization of the PMA chain to understand the effect of structural factors on the local dynamics of polymer chains in confinement. The swelling behavior in good solvent showed that when the grafting density increases from sparsely grafted to the densely grafted, the chain conformation changed from random coil to stretched polymer brushes. The NMR spin relaxometry revealed that the local mobility of densely grafted chains is highly constrained near the core. However, the confinement of the stretched brush created by the presence of a stiff substrate was negligible when the chain length was long enough. The constrained local dynamics of the stretched brush was reflected in the increased glass transition of PMA canopy.

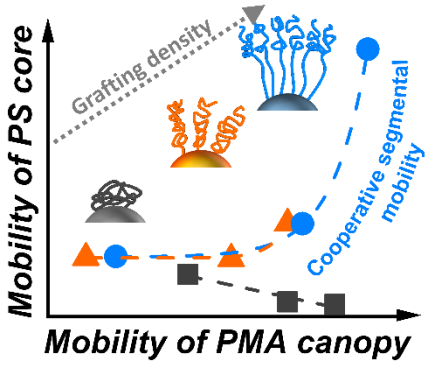

Figure 6.1.4 The effect of grafting density of PMA canopy on the dynamics of PMA canopy and the dynamics of PS core. (**Section 5.4**.)

The colloidal behavior of suspensions of deformable soft polymer nanoparticles functionalized with a surface-immobilized canopy of end-tethered polymer chains was studied. By controlling the grafting density (**Section 5.1 and 5.4**), length of grafted chain (**Section 5.1, 4.2 and 5.4**), the stiffness and swelling of the soft core (**Section 5.2 and 5.3**) and solvent quality (**Section 5.3**), the impact of the architecture of the surface-functionalized nanoparticles on the rheological properties and local dynamics of suspensions of those soft polymer nanoparticles functionalized with polymer chains was successfully investigated. The suspensions of polymer chain grafted nanoparticles showed liquid-gel transition with intermediate and high grafting density due to the potential interdigitation of the tethered chains, or the deformation of the canopy, occurring between adjacent nanoparticles. The strongest nanoparticle-nanoparticle interaction was found for canopies having a high degree of polymerization with intermediate grafting density and caused high modulus of the suspensions. (**Section 5.1**) The change in viscoelastic behavior can be linked to the local subsegmental dynamics of the tethered chains; the fastest local mobility was obtained when the length of the grafted chain was sufficiently long (**Section 5.2 and 5.4**) and the concentrated suspensions of those particles yielded the strongest and less brittle gels. This would suggest that the improved stiffness and deformability of the colloidal gels were obtained when the grafted chains were sufficiently mobile. These results would be in keeping with a nanoparticle-nanoparticle interaction occurring through interdigitation of the canopy. Furthermore, when the core of the nanoparticle became more rigid due to a decrease of the solvent quality for only the polystyrene core, softer and more brittle gels were obtained. This could be the result of the interplay between the mobility of the core and of the canopy, the deswelling of the core influenced the dynamics of the canopy as observed in local dynamics

in NMR relaxation and could be responsible for a less efficient canopy-canopy interaction. (**Section 5.2 and 5.3**)

6.2 Perspective

The Deborah number is defined as the relaxation time divided by the time of observation. At unlimited time of observation, even a mountain flows. With one phenomenon, different time scales may be observed and yield different behaviors. In fact, this is frequently a challenge in the study of the dynamics of materials. From long-range movement by mechanical analysis to the subsegmental dynamics by relaxation measurement, all results look at the same phenomenon, but at different time scale. One single fragment of the relaxation spectrum in a narrow time scale can only explain the dynamics occurring within that time scale and cannot directly be translated to another time-scale. In order to fully understand the properties of core-canopy system from the atomic level to the bulk behavior, the dynamics of the system at different time scales should be conducted to get a better insight into the NPs interactions. Furthermore, such studies performed in colloidal gels rather than in dilute colloidal suspensions would also be helpful to get a better understanding between the dynamics and macroscopic properties like viscosity. The measure of the relaxation of core-canopy nanoparticles in suspension by neutron spin echo would provide information on relaxation phenomenon at different time scales and elucidate the change in conformation and definitely answer the question whether the interdigitation of the canopies is influenced by the architecture of the nanoparticles. Additionally, field-cycling NMR relaxometry could be used to probe relaxation mechanisms occurring in a time range of milliseconds to picoseconds and would be useful to explore the slower dynamics of core-canopy nanoparticles in suspension and transition of polymer chains from rouse motion to constrained reptation.

Moreover, even if NMR relaxation offers information on subsegmental dynamics of the grafted chains and of the chains in the core, it is an average over the entire polymer chains. To fully understand the effect of the nanoparticle architecture on the dynamics, specific segments of the polymer chain could be labeled with isotopes such as ^{13}C or ^{2}H. Since SI-ATRP was used successfully to grow the PMA chains from the

surface, it could be relatively simple to prepare chains that are multi-block copolymers containing specific and precisely localized polymer blocks labeled with the same monomer containing an isotope. The controlled labeling of the polymer chains and subsequent NMR relaxometry will provide a more precise picture of the effect of the architecture of the core-canopy NPs on the local subsegmental dynamics.

In this dissertation, the model system of soft polymer core- grafted polymer canopy used was designed to minimize the interactions between the core and the canopy by using two immiscible polymers. However, this model system is far removed from polymer nanoparticles functionalized with a polymer canopy that is finding applications. The study of dynamics and viscoelastic properties should be expanded to systems closer to those used for drug delivery or coating applications. For example, nanocarriers made of biopolymers, have been used as drug delivery system. And to avoid the unfavorable interaction with protein and white blood cells, the particles can be functionalized with hydrophilic polymer chains, such as poly(ethylene glycol) chains (PEG). Changing the length and the surface density of the PEG chains have shown to influence the fate of the nanoparticles in biological media. Based on the results from this dissertation and on the stealth ability of the PEG-functionalized nanoparticles, it would be interesting to understand what is happening in such systems. Currently, the are indications that the canopy of PEG chains need to be sufficiently mobile to efficiently prevent protein absorption and extend the circulation time of the nanoparticles in vivo. But the role of chain mobility and conformation in such phenomena remains unclear.

More generally, the techniques used in this dissertation can be used to address specific challenges faced by the applications involving polymer-functionalized nanoparticles. Based on the versatility of the synthetic method developed and the universality of the characterization method, there are no limits on how and where the results of such studies could potentially be applied.

7. Acknowledgment

8. Curriculum vitae

[redacted]

[redacted]

[redacted]

[redacted]

[redacted]

9. Scientific contributions

9.1 Publications

9.2 Conferences

10. References

1. Heiligtag, F. J.; Niederberger, M. The fascinating world of nanoparticle research. *Mater. Today* **2013,** *16*, 262-271.

2. Qiu Zhao, Q.; Boxman, A.; Chowdhry, U. Nanotechnology in the Chemical Industry – Opportunities and Challenges. *J. Nanopart. Res.* **2003,** *5*, 567-572.

3. Rao, C. N. R.; Cheetham, A. K. Science and technology of nanomaterials: current status and future prospects. *J. Mater. Chem.* **2001,** *11*, 2887-2894.

4. Slomkowski, S.; Aleman, J. V.; Gilbert, R. G.; Hess, M.; Horie, K.; Jones, R. G.; Kubisa, P.; Meisel, I.; Mormann, W.; Penczek, S.; Stepto, R. F. T. Terminology of polymers and polymerization processes in dispersed systems. *Pure Appl. Chem.* **2011,** *83*, 2229-2259.

5. Bantz, C.; Koshkina, O.; Lang, T.; Galla, H.-J.; Kirkpatrick, C. J.; Stauber, R. H.; Maskos, M. The surface properties of nanoparticles determine the agglomeration state and the size of the particles under physiological conditions. *Beilstein J. Nanotechnol.* **2014,** *5*, 1774-1786.

6. Lazzari, M.; López-Quintela, M. A. Block Copolymers as a Tool for Nanomaterial Fabrication. *Adv. Mater.* **2003,** *15*, 1583-1594.

7. Guerrero-Ramírez, L. G.; Nuño-Donlucas, S. M.; Cesteros, L. C.; Katime, I. Smart copolymeric nanohydrogels: Synthesis, characterization and properties. *Mater. Chem. Phys.* **2008,** *112*, 1088-1092.

8. Cuggino, J. C.; Molina, M.; Wedepohl, S.; Igarzabal, C. I. A.; Calderón, M.; Gugliotta, L. M. Responsive nanogels for application as smart carriers in endocytic pH-triggered drug delivery systems. *Eur. Polym. J.* **2016,** *78*, 14-24.

9. Oh, J. K.; Siegwart, D. J.; Lee, H.-i.; Sherwood, G.; Peteanu, L.; Hollinger, J. O.; Kataoka, K.; Matyjaszewski, K. Biodegradable Nanogels Prepared by Atom Transfer Radical Polymerization as Potential Drug Delivery Carriers: Synthesis, Biodegradation, in Vitro Release, and Bioconjugation. *J. Am. Chem. Soc.* **2007,** *129*, 5939-5945.

10. Li, J.; Fan, J.; Cao, R.; Zhang, Z.; Du, J.; Peng, X. Encapsulated Dye/Polymer Nanoparticles Prepared via Miniemulsion Polymerization for Inkjet Printing. *ACS Omega* **2018,** *3*, 7380-7387.

11. Mokude, D.; Takasu, A.; Higuchi, M. Electrophoretic non-ionic nano-spheres (latexes) for structural coloring. *Polymer* **2017,** *117*, 243-248.

12. Lee, H. J.; Koo, A. N.; Lee, S. W.; Lee, M. H.; Lee, S. C. Catechol-functionalized adhesive polymer nanoparticles for controlled local release of bone morphogenetic protein-2 from titanium surface. *J. Controlled Release* **2013,** *170*, 198-208.

13. Cho, Y.-H.; Jones, O. G., Chapter Two - Assembled protein nanoparticles in food or nutrition applications. In Adv. Food Nutr. Res., Lim, L.-T., Rogers, M., Eds. Academic Press: **2019**; *88*, 47-84.

14. Bahamonde-Norambuena, D.; Molina-Pereira, A.; Muñoz, M.; Zepeda, K.; Vilos, C. Polymeric Nanoparticles in Dermocosmetic. *Int. J. Morphol.* **2015,** *33*, 1563-1568.

15. El-Say, K. M.; El-Sawy, H. S. Polymeric nanoparticles: Promising platform for drug delivery. *Int. J. Pharm.* **2017,** *528*, 675-691.

16. Jabbareh, M. A. Size, shape and temperature dependent surface energy of binary alloy nanoparticles. *Appl. Surf. Sci.* **2017,** *426*, 1094-1099.

17. Zoppe, J. O.; Ataman, N. C.; Mocny, P.; Wang, J.; Moraes, J.; Klok, H.-A. Surface-Initiated Controlled Radical Polymerization: State-of-the-Art, Opportunities, and Challenges in Surface and Interface Engineering with Polymer Brushes. *Chem. Rev.* **2017,** *117*, 1105-1318.

18. Ma, S.; Zhang, X.; Yu, B.; Zhou, F. Brushing up functional materials. *NPG Asia Mater.* **2019,** *11*, 24.

19. de Gennes, P. G. Conformations of Polymers Attached to an Interface. *Macromolecules* **1980,** *13*, 1069-1075.

20. Advincula, R. C. Surface initiated polymerization from nanoparticle surfaces. *J. Dispersion Sci. Technol.* **2003,** *24*, 343-361.

21. Genzer, J. Surface-Bound Gradients for Studies of Soft Materials Behavior. *Annu. Rev. Mater. Res.* **2012,** *42*, 435-468.

22. Hood, M. A.; Mari, M.; Munoz-Espi, R. Synthetic Strategies in the Preparation of Polymer/Inorganic Hybrid Nanoparticles. *Materials* **2014,** *7*, 4057-4087.

23. Hui, C. M.; Pietrasik, J.; Schmitt, M.; Mahoney, C.; Choi, J.; Bockstaller, M. R.; Matyjaszewski, K. Surface-Initiated Polymerization as an Enabling Tool for Multifunctional (Nano-)Engineered Hybrid Materials. *Chem. Mater.* **2014,** *26*, 745-762.

24. Kumar, S. K.; Krishnamoorti, R. Nanocomposites: Structure, Phase Behavior, and Properties. *Annu. Rev. Chem. Biomol. Eng.* **2010,** *1*, 37-58.

25. Huang, X.; Wirth, M. J. Surface-Initiated Radical Polymerization on Porous Silica. *Anal. Chem.* **1997,** *69*, 4577-4580.

26. Matyjaszewski, K. Advanced Materials by Atom Transfer Radical Polymerization. *Adv. Mater.* **2018,** *30*, 1706441.

27. Hore, M. J. A. Polymers on nanoparticles: structure & dynamics. *Soft Matter* **2019,** *15*, 1120-1134.

28. Kim, S. A.; Archer, L. A. Hierarchical Structure in Semicrystalline Polymers Tethered to Nanospheres. *Macromolecules* **2014,** *47*, 687-694.

29. Agarwal, P.; Kim, S. A.; Archer, L. A. Crowded, Confined, and Frustrated: Dynamics of Molecules Tethered to Nanoparticles. *Phys. Rev. Lett.* **2012,** *109*, 258301.

30. Kim, D.; Srivastava, S.; Narayanan, S.; Archer, L. A. Polymer nanocomposites: polymer and particle dynamics. *Soft Matter* **2012,** *8*, 10813-10818.

31. Kim, S. A.; Mangal, R.; Archer, L. A. Relaxation Dynamics of Nanoparticle-Tethered Polymer Chains. *Macromolecules* **2015,** *48*, 6280.

32. Wei, Y.; Xu, Y.; Faraone, A.; Hore, M. J. A. Local Structure and Relaxation Dynamics in the Brush of Polymer-Grafted Silica Nanoparticles. *ACS Macro Lett.* **2018,** *7*, 699-704.

33. Richter, D.; Kruteva, M. Polymer dynamics under confinement. *Soft Matter* **2019,** *15*, 7316-7349.

34. Vlassopoulos, D.; Fytas, G., From Polymers to Colloids: Engineering the Dynamic Properties of Hairy Particles. In High Solid Dispersions, Cloitre, M., Ed. Springer-Verlag Berlin: Berlin, **2010**; *236*, 1-54.

35. Thickett, S. C.; Gilbert, R. G. Emulsion polymerization: State of the art in kinetics and mechanisms. *Polymer* **2007,** *48*, 6965-6991.

36. Tauer, K.; Hernandez, H.; Kozempel, S.; Lazareva, O.; Nazaran, P. Towards a consistent mechanism of emulsion polymerization—new experimental details. *Colloid Polym. Sci.* **2008,** *286*, 499-515.

37. Herk, A. M. v.; Gilbert, R. G., Emulsion Polymerisation. In Chem. Technol. Emulsion Polym., **2013**; 43-73.

38. Morgan, J. D.; Lusvardi, K. M.; Kaler, E. W. Kinetics and Mechanism of Microemulsion Polymerization of Hexyl Methacrylate. *Macromolecules* **1997,** *30*, 1897-1905.

39. Co, C. C.; de Vries, R.; Kaler, E. W. Microemulsion Polymerization. 1. Small-Angle Neutron Scattering Study of Monomer Partitioning. *Macromolecules* **2001,** *34*, 3224-3232.

40. O'Donnell, J.; Kaler, E. W. Microstructure, Kinetics, and Transport in Oil-in-Water Microemulsion Polymerizations. *Macromol. Rapid Commun.* **2007,** *28*, 1445-1454.

41. Landfester, K. Miniemulsion Polymerization and the Structure of Polymer and Hybrid Nanoparticles. *Angew. Chem., Int. Ed.* **2009,** *48*, 4488-4507.

42. Landfester, K. The Generation of Nanoparticles in Miniemulsions. *Adv. Mater.* **2001,** *13*, 765-768.

43. Ugelstad, J.; Hansen, F. K.; Lange, S. Emulsion polymerization of styrene with sodium hexadecyl sulphate/hexadecanol mixtures as emulsifiers. Initiation in monomer droplets. *Makromol. Chem.* **1974,** *175*, 507-521.

44. McNaught, A. D.; Wilkinson, A., IUPAC. Compendium of Chemical Terminology (Gold Book). 2nd ed. Blackwell Scientific Publications: Oxford: **2014**.

45. Pashley, R. M.; Karaman, M. E., Applied Colloid and Surface Chemistry. John Wiley & Sons Ltd: West Sussex, England, **2004**.

46. Cosgrove, T., Colloid Science: Principles, Methods and Applications. John Wiley & Sons: **2010**.

47. Tanford, C., The Hydrophobic Effect: Formation of Micelles and Biological Membranes. 2nd ed ed.; Wiley: **1980**.

48. Mollet, H.; Grubenmann, A.; Payne, H., Formulation Technology: Emulsions, Suspensions, Solid Forms. Wiley-VCH: Weinheim: **2008**.

49. Griffin, W. C. Classification of Surface-Active Agents by "HLB". *J. Cosmet. Sci.* **1949,** *1*, 311-326.

50. Davies, J. T. In *A quantitative kinetic theory of emulsion type, I. Physical chemistry of the emulsifying agent*, Proc. Int. Congr. Surf. Act. , Butterworths, London, 1957; Butterworths, London, 1957; pp 426-438.

51. El-Aasser, M. S.; Sudol, E. D. Miniemulsions: Overview of research and applications. *JCT Res.* **2004,** *1*, 21-31.

52. Munoz-Espi, R.; Weiss, C. K.; Landfester, K. Inorganic nanoparticles prepared in miniemulsion. *Curr. Opin. Colloid Interface Sci.* **2012,** *17*, 212-224.

53. Higuchi, W. I.; Misra, J. Physical Degradation of Emulsions Via the Molecular Diffusion Route and the Possible Prevention Thereof. *J. Pharm. Sci.* **1962,** *51*, 459-466.

54. Webster, A. J.; Cates, M. E. Stabilization of emulsions by trapped species. *Langmuir* **1998,** *14*, 2068-2079.

55. Webster, A. J.; Cates, M. E. Osmotic stabilization of concentrated emulsions and foams. *Langmuir* **2001,** *17*, 595-608.

56. Landfester, K. Recent developments in miniemulsions - Formation and stability mechanisms. *Macromol. Symp.* **2000,** *150*, 171-178.

57. Landfester, K.; Bechthold, N.; Tiarks, F.; Antonietti, M. Formulation and stability mechanisms of polymerizable miniemulsions. *Macromolecules* **1999,** *32*, 5222-5228.

58. Ha, J.-W.; Park, I. J.; Lee, S.-B.; Kim, D.-K. Preparation and Characterization of Core−Shell Particles Containing Perfluoroalkyl Acrylate in the Shell. *Macromolecules* **2002,** *35*, 6811-6818.

59. Li, N.; Panagiotopoulos, A. Z.; Nikoubashman, A. Structured Nanoparticles from the Self-Assembly of Polymer Blends through Rapid Solvent Exchange. *Langmuir* **2017,** *33*, 6021-6028.

60. Lee, V. E.; Sosa, C.; Liu, R.; Prud'homme, R. K.; Priestley, R. D. Scalable Platform for Structured and Hybrid Soft Nanocolloids by Continuous Precipitation in a Confined Environment. *Langmuir* **2017,** *33*, 3444-3449.

61. Böker, A.; He, J.; Emrick, T.; Russell, T. P. Self-assembly of nanoparticles at interfaces. *Soft Matter* **2007,** *3*, 1231-1248.

62. Pawar, A. B.; Kretzschmar, I. Fabrication, Assembly, and Application of Patchy Particles. *Macromol. Rapid Commun.* **2010,** *31*, 150-168.

63. Gröschel, A. H.; Walther, A.; Löbling, T. I.; Schmelz, J.; Hanisch, A.; Schmalz, H.; Müller, A. H. E. Facile, Solution-Based Synthesis of Soft, Nanoscale Janus Particles with Tunable Janus Balance. *J. Am. Chem. Soc.* **2012,** *134*, 13850-13860.

64. Nie, Z.; Li, W.; Seo, M.; Xu, S.; Kumacheva, E. Janus and Ternary Particles Generated by Microfluidic Synthesis: Design, Synthesis, and Self-Assembly. *J. Am. Chem. Soc.* **2006,** *128*, 9408-9412.

65. Corten, C. C.; Urban, M. W. Shape evolution control of phase-separated colloidal nanoparticles. *Polym. Chem.* **2011,** *2*, 244-250.

66. Tanaka, T.; Okayama, M.; Minami, H.; Okubo, M. Dual Stimuli-Responsive "Mushroom-like" Janus Polymer Particles as Particulate Surfactants. *Langmuir* **2010,** *26*, 11732-11736.

67. Gröschel, A. H.; Schacher, F. H.; Schmalz, H.; Borisov, O. V.; Zhulina, E. B.; Walther, A.; Müller, A. H. E. Precise hierarchical self-assembly of multicompartment micelles. *Nat. Commun.* **2012,** *3*, 710.

68. Lunn, D. J.; Finnegan, J. R.; Manners, I. Self-assembly of "patchy" nanoparticles: a versatile approach to functional hierarchical materials. *Chem. Sci.* **2015,** *6*, 3663-3673.

69. Isojima, T.; Lattuada, M.; Vander Sande, J. B.; Hatton, T. A. Reversible Clustering of pH- and Temperature-Responsive Janus Magnetic Nanoparticles. *Acs Nano* **2008,** *2*, 1799-1806.

70. Yoshida, M.; Lahann, J. Smart Nanomaterials. *Acs Nano* **2008,** *2*, 1101-1107.

71. Fernandes, N. J.; Koerner, H.; Giannelis, E. P.; Vaia, R. A. Hairy nanoparticle assemblies as one-component functional polymer nanocomposites: opportunities and challenges. *MRS Commun.* **2013,** *3*, 13-29.

72. Yi, C.; Zhang, S.; Webb, K. T.; Nie, Z. Anisotropic Self-Assembly of Hairy Inorganic Nanoparticles. *Acc. Chem. Res.* **2017,** *50*, 12-21.

73. Butt, H.-J.; Graf, K.; Kappl, M., Physics and Chemistry of Interfaces. Wiley-VCH: **2006**.

74. Nonappa; Ikkala, O. Hydrogen Bonding Directed Colloidal Self-Assembly of Nanoparticles into 2D Crystals, Capsids, and Supracolloidal Assemblies. *Adv. Funct. Mater.* **2018,** *28*, 1704328.

75. Mathur, S.; Moudgil, B. M. Adsorption Mechanism(s) of Poly(Ethylene Oxide) on Oxide Surfaces. *J. Colloid Interface Sci.* **1997,** *196*, 92-98.

76. Barnes, T. J.; Prestidge, C. A. PEO−PPO−PEO Block Copolymers at the Emulsion Droplet−Water Interface. *Langmuir* **2000,** *16*, 4116-4121.

77. Tadros, T. F., Colloid Stability: The Role of Surface Forces - Part I, Vol. 1. Wiley-VCH Verlag GmbH & Co. KGaA: **2007**.

78. Schramm, L. L., Emulsions, Foams, and Suspensions: Fundamentals and Applications. Wiley-VCH Verlag GmbH & Co. KGaA: **2005**.

79. Napper, D. H. Colloid Stability. *Ind. Eng. Chem. Prod. Res. Dev.* **1970,** *9*, 467-477.

80. Boersma, W. H.; Laven, J.; Stein, H. N. Shear thickening (dilatancy) in concentrated dispersions. *AIChE J.* **1990,** *36*, 321-332.

81. Barnes, H. A. Shear-Thickening ("Dilatancy") in Suspensions of Nonaggregating Solid Particles Dispersed in Newtonian Liquids. *J. Rheol.* **1989,** *33*, 329-366.

82. Pinto, F.; Meo, M. Design and Manufacturing of a Novel Shear Thickening Fluid Composite (STFC) with Enhanced out-of-Plane Properties and Damage Suppression. *Appl. Compos. Mater.* **2017,** *24*, 643-660.

83. Hojjat, M.; Etemad, S. G.; Bagheri, R.; Thibault, J. Rheological characteristics of non-Newtonian nanofluids: Experimental investigation. *Int. Commun. Heat Mass Transfer* **2011,** *38*, 144-148.

84. Guvendiren, M.; Lu, H. D.; Burdick, J. A. Shear-thinning hydrogels for biomedical applications. *Soft Matter* **2012,** *8*, 260-272.

85. Raghavan, S. R.; Hou, J.; Baker, G. L.; Khan, S. A. Colloidal interactions between particles with tethered nonpolar chains dispersed in polar media: direct correlation between dynamic rheology and interaction parameters. *Langmuir* **2000,** *16,* 1066-1077.

86. Egres, R. G.; Wagner, N. J. The rheology and microstructure of acicular precipitated calcium carbonate colloidal suspensions through the shear thickening transition. *J. Rheol.* **2005,** *49*, 719-746.

87. Wagner, N. J.; Brady, J. F. Shear thickening in colloidal dispersions. *Phys. Today* **2009,** *62*, 27-32.

88. Cheng, X.; McCoy, J. H.; Israelachvili, J. N.; Cohen, I. Imaging the Microscopic Structure of Shear Thinning and Thickening Colloidal Suspensions. *Science* **2011,** *333,* 1276-1279.

89. Bünsow, J.; Kelby, T. S.; Huck, W. T. S. Polymer Brushes: Routes toward Mechanosensitive Surfaces. *Acc. Chem. Res.* **2010,** *43*, 466-474.

90. Ma, H.; Hyun, J.; Stiller, P.; Chilkoti, A. "Non-Fouling" Oligo(ethylene glycol)- Functionalized Polymer Brushes Synthesized by Surface-Initiated Atom Transfer Radical Polymerization. *Adv. Mater.* **2004,** *16,* 338-341.

91. El Harrak, A.; Carrot, G.; Oberdisse, J.; Eychenne-Baron, C.; Boué, F. Surface−Atom Transfer Radical Polymerization from Silica Nanoparticles with Controlled Colloidal Stability. *Macromolecules* **2004,** *37,* 6376-6384.

92. Azzaroni, O.; Brown, A. A.; Huck, W. T. S. Tunable Wettability by Clicking Counterions Into Polyelectrolyte Brushes. *Adv. Mater.* **2007,** *19,* 151-154.

93. Thérien-Aubin, H.; Chen, L.; Ober, C. K. Fouling-resistant polymer brush coatings. *Polymer* **2011,** *52,* 5419-5425.

94. Wei, Q.; Pei, X.; Hao, J.; Cai, M.; Zhou, F.; Liu, W. Surface Modification of Diamond-Like Carbon Film with Polymer Brushes Using a Bio-Inspired Catechol Anchor for Excellent Biological Lubrication. *Adv. Mater. Interfaces* **2014,** *1*, 1400035.

95. Milner, S. T. Polymer Brushes. *Science* **1991,** *251*, 905-914.

96. Daoud, M.; Cotton, J. P. Star Shaped Polymers: A Model for the Conformation and Its Concentration Dependence. *J. Phys.* **1982,** *43*, 531-538.

97. Dukes, D.; Li, Y.; Lewis, S.; Benicewicz, B.; Schadler, L.; Kumar, S. K. Conformational Transitions of Spherical Polymer Brushes: Synthesis, Characterization, and Theory. *Macromolecules* **2010,** *43*, 1564-1570.

98. Ohno, K.; Morinaga, T.; Takeno, S.; Tsujii, Y.; Fukuda, T. Suspensions of Silica Particles Grafted with Concentrated Polymer Brush: Effects of Graft Chain Length on Brush Layer Thickness and Colloidal Crystallization. *Macromolecules* **2007,** *40*, 9143.

99. H H Kausch, a.; Tirrell, M. Polymer Interdiffusion. *Annu. Rev. Mater. Sci.* **1989,** *19*, 341-377.

100. Brochard, F.; Jouffroy, J.; Levinson, P. Polymer-polymer diffusion in melts. *Macromolecules* **1983,** *16*, 1638-1641.

101. de Gennes, P. G. Reptation of a Polymer Chain in the Presence of Fixed Obstacles. *J. Chem. Phys.* **1971,** *55*, 572-579.

102. Scher, H.; Shlesinger, M. F. On reptation in polymer melts. *J. Chem. Phys.* **1986,** *84*, 5922-5924.

103. Doi, M.; Edwards, S. F., The theory of polymer dynamics. oxford university press: **1988**.

104. Saalwachter, K.; Spiess, H. W., Solution NMR. In Polymer Science: A Comprehensive Reference. Elsevier: **2012**.

105. Rubinstein, M.; Colby, R. H., Polymer physics. Oxford university press New York: **2003**.

106. Lang, M.; Werner, M.; Dockhorn, R.; Kreer, T. Arm Retraction Dynamics in Dense Polymer Brushes. *Macromolecules* **2016,** *49*, 5190-5201.

107. Klushin, L. I.; Skvortsov, A. M. Critical dynamics of a polymer chain in a grafted monolayer. *Macromolecules* **1991,** *24*, 1549-1553.

108. Wang, J.-S.; Matyjaszewski, K. Controlled/"living" radical polymerization. atom transfer radical polymerization in the presence of transition-metal complexes. *J. Am. Chem. Soc.* **1995,** *117*, 5614-5615.

109. Barbey, R.; Lavanant, L.; Paripovic, D.; Schüwer, N.; Sugnaux, C.; Tugulu, S.; Klok, H.-A. Polymer Brushes via Surface-Initiated Controlled Radical Polymerization: Synthesis, Characterization, Properties, and Applications. *Chem. Rev.* **2009,** *109*, 5437-5527.

110. Kim, J.-B.; Huang, W.; Miller, M. D.; Baker, G. L.; Bruening, M. L. Kinetics of surface-initiated atom transfer radical polymerization. *J. Polym. Sci., Part A: Polym. Chem.* **2003,** *41*, 386-394.

111. Choudalakis, G.; Gotsis, A. D. Permeability of polymer/clay nanocomposites: A review. *Eur. Polym. J.* **2009,** *45*, 967-984.

112. Kruk, M.; Jaroniec, M. Gas adsorption characterization of ordered organic-inorganic nanocomposite materials. *Chem. Mater.* **2001,** *13*, 3169-3183.

113. Adhikari, R.; Michler, G. H. Polymer Nanocomposites Characterization by Microscopy. *Polym. Rev.* **2009,** *49*, 141-180.

114. Kopecek, J. Hydrogel biomaterials: A smart future? *Biomaterials* **2007,** *28*, 5185-5192.

115. Lee, J. E.; Lee, N.; Kim, T.; Kim, J.; Hyeon, T. Multifunctional Mesoporous Silica Nanocomposite Nanoparticles for Theranostic Applications. *Acc. Chem. Res.* **2011,** *44*, 893-902.

116. Yeh, J. M.; Liou, S. J.; Lai, C. Y.; Wu, P. C. Enhancement of corrosion protection effect in polyaniline via the formation of polyaniline-clay nanocomposite materials. *Chem. Mater.* **2001,** *13*, 1131-1136.

117. Seentrakoon, B.; Junhasavasdikul, B.; Chavasiri, W. Enhanced UV-protection and antibacterial properties of natural rubber/rutile-TiO2 nanocomposites. *Polym. Degrad. Stab.* **2013,** *98*, 566-578.

118. Shahnazar, S.; Bagheri, S.; Abd Hamid, S. B. Enhancing lubricant properties by nanoparticle additives. *Int. J. Hydrogen Energy* **2016,** *41*, 3153-3170.

119. Mizutani, T.; Arai, K.; Miyamoto, M.; Kimura, Y. Application of silica-containing nano-composite emulsion to wall paint: A new environmentally safe paint of high performance. *Prog. Org. Coat.* **2006,** *55*, 276-283.

120. Kashiwagi, T.; Du, F. M.; Douglas, J. F.; Winey, K. I.; Harris, R. H.; Shields, J. R. Nanoparticle networks reduce the flammability of polymer nanocomposites. *Nat. Mater.* **2005,** *4*, 928-933.

121. Stuber, M.; Leiste, H.; Ulrich, S.; Holleck, H.; Schild, D. Microstructure and properties of low friction TiC-C nanocomposite coatings deposited by magnetron sputtering. *Surf. Coat. Technol.* **2002,** *150*, 218-226.

122. Akhavan, O. Lasting antibacterial activities of Ag-TiO2/Ag/a-TiO2 nanocomposite thin film photocatalysts under solar light irradiation. *J. Colloid Interface Sci.* **2009,** *336*, 117-124.

123. Beecroft, L. L.; Ober, C. K. Nanocomposite materials for optical applications. *Chem. Mater.* **1997,** *9*, 1302-1317.

124. Kumar, S. K.; Ganesan, V.; Riggleman, R. A. Perspective: Outstanding theoretical questions in polymer-nanoparticle hybrids. *J. Chem. Phys.* **2017,** *147*, 020901.

125. Kumar, S. K.; Benicewicz, B. C.; Vaia, R. A.; Winey, K. I. 50th Anniversary Perspective: Are Polymer Nanocomposites Practical for Applications? *Macromolecules* **2017,** *50*, 714-731.

126. Marson, R. L.; Nguyen, T. D.; Glotzer, S. C. Rational design of nanomaterials from assembly and reconfigurability of polymer-tethered nanoparticles. *MRS Commun.* **2015,** *5*, 397-406.

127. Krystosiak, P.; Tomaszewski, W.; Megiel, E. High-density polystyrene-grafted silver nanoparticles and their use in the preparation of nanocomposites with antibacterial properties. *J. Colloid Interface Sci.* **2017,** *498*, 9-21.

128. Bockstaller, M. R. Progress in polymer hybrid materials. *Prog. Polym. Sci.* **2015,** *40*, 1-2.

129. Wei, Y.; Xu, Y.; Faraone, A.; Hore, M. J. A. Local Structure and Relaxation Dynamics in the Brush of Polymer-Grafted Silica Nanoparticles. *Acs Macro Lett.* **2018,** *7*, 699-704.

130. Mark, C.; Holderer, O.; Allgaier, J.; Hübner, E.; Pyckhout-Hintzen, W.; Zamponi, M.; Radulescu, A.; Feoktystov, A.; Monkenbusch, M.; Jalarvo, N.; Richter, D. Polymer Chain Conformation and Dynamical Confinement in a Model One-Component Nanocomposite. *Phys. Rev. Lett.* **2017,** *119*, 047801.

131. Midya, J.; Cang, Y.; Egorov, S. A.; Matyjaszewski, K.; Bockstaller, M. R.; Nikoubashman, A.; Fytas, G. Disentangling the Role of Chain Conformation on the Mechanics of Polymer Tethered Particle Materials. *Nano Lett.* **2019,** *19*, 2715-2722.

132. Duncan, R. The dawning era of polymer therapeutics. *Nat. Rev. Drug Discovery* **2003,** *2*, 347-360.

133. Meng, F.; Engbers, G. H. M.; Feijen, J. Polyethylene glycol–grafted polystyrene particles. *J. Biomed. Mater. Res., Part A* **2004,** *70A*, 49-58.

134. Lai, S. K.; Hanlon, D. E.; Harrold, S.; Man, S. T.; Wang, Y.-Y.; Cone, R.; Hanes, J. Rapid transport of large polymeric nanoparticles in fresh undiluted human mucus. *Proc. Natl. Acad. Sci. U. S. A.* **2007,** *104*, 1482.

135. Tobío, M.; Gref, R.; Sánchez, A.; Langer, R.; Alonso, M. J. Stealth PLA-PEG Nanoparticles as Protein Carriers for Nasal Administration. *Pharm. Res.* **1998,** *15*, 270-275.

136. Vila, A.; Gill, H.; McCallion, O.; Alonso, M. a. J. Transport of PLA-PEG particles across the nasal mucosa: effect of particle size and PEG coating density. *J. Controlled Release* **2004,** *98*, 231-244.

137. Gref, R.; Lück, M.; Quellec, P.; Marchand, M.; Dellacherie, E.; Harnisch, S.; Blunk, T.; Müller, R. H. 'Stealth' corona-core nanoparticles surface modified by polyethylene glycol (PEG): influences of the corona (PEG chain length and surface density) and of the core composition on phagocytic uptake and plasma protein adsorption. *Colloids Surf., B* **2000,** *18*, 301-313.

138. Bielecki, R. M.; Benetti, E. M.; Kumar, D.; Spencer, N. D. Lubrication with Oil-Compatible Polymer Brushes. *Tribol. Lett.* **2012,** *45*, 477-487.

139. Yan, J.; Bockstaller, M. R.; Matyjaszewski, K. Brush-modified materials: Control of molecular architecture, assembly behavior, properties and applications. *Prog. Polym. Sci.* **2020,** *100*, 101180.

140. Liu, G.; Liu, Z.; Li, N.; Wang, X.; Zhou, F.; Liu, W. Hairy Polyelectrolyte Brushes-Grafted Thermosensitive Microgels as Artificial Synovial Fluid for Simultaneous Biomimetic Lubrication and Arthritis Treatment. *ACS Appl. Mater. Interfaces* **2014,** *6*, 20452-20463.

141. Wright, R. A. E.; Wang, K.; Qu, J.; Zhao, B. Oil-Soluble Polymer Brush Grafted Nanoparticles as Effective Lubricant Additives for Friction and Wear Reduction. *Angew. Chem., Int. Ed.* **2016,** *55*, 8656-8660.

142. Levitt, M. H., Spin Dynamics: Basics of Nuclear Magnetic Resonance. Wiley: New York, **2008**.

143. Hore, P., Nuclear Magnetic Resonance. Oxford University Press: Oxford, **1995**.

144. Bloembergen, N.; Purcell, E. M.; Pound, R. V. Relaxation Effects in Nuclear Magnetic Resonance Absorption. *Phys. Rev.* **1948,** *73*, 679-712.

145. Thomas C. Farrar, E. D. B., Pulse and Fourier Transform NMR: Introduction to Theory and Methods. Academic Press: New York and London, **1971**.

146. Jerrold T. Bushberg , J. A. S., Edwin M. Leidholdt Jr. , John M. Boone The Essential Physics of Medical Imaging. Lippincott Williams & Wilkins: Philadelphia, **2002**.

147. Leblanc, J. L. Rubber-filler interactions and rheological properties in filled compounds. *Prog. Polym. Sci.* **2002,** *27*, 627-687.

148. Lim, L. T.; Auras, R.; Rubino, M. Processing technologies for poly(lactic acid). *Prog. Polym. Sci.* **2008,** *33*, 820-852.

149. Winnik, M. A.; Yekta, A. Associative polymers in aqueous solution. *Curr. Opin. Colloid Interface Sci.* **1997,** *2*, 424-436.

150. Deshpande, A. P.; Krishnan, J. M.; Sunil, P. B.; (Eds.), K., Rheology of Complex Fluids. Springer: New York, **2010**.

151. Ferry, J. D., Viscoelastic properties of polymers. Wiley: New York, **1980**.

152. Berne, B. J.; Pecora, R., Dynamic Light Scattering: With Applications to Chemistry, Biology, and Physics. Dover Publications Inc.: **2000**.

153. Graff, R. W.; Wang, X.; Gao, H. Exploring Self-Condensing Vinyl Polymerization of Inimers in Microemulsion To Regulate the Structures of Hyperbranched Polymers. *Macromolecules* **2015,** *48*, 2118-2126.

154. Krieger, I. M.; Dougherty, T. J. A Mechanism for Non-Newtonian Flow in Suspensions of Rigid Spheres. *Trans. Soc. Rheol.* **1959,** *3*, 137-152.

155. Shapiro, Y. E. Structure and dynamics of hydrogels and organogels: An NMR spectroscopy approach. *Prog. Polym. Sci.* **2011,** *36*, 1184-1253.

156. Lindvig, T.; Michelsen, M. L.; Kontogeorgis, G. M. A Flory–Huggins model based on the Hansen solubility parameters. *Fluid Phase Equilib.* **2002,** *203*, 247-260.

157. Devaux, C.; Cousin, F.; Beyou, E.; Chapel, J. P. Low Swelling Capacity of Highly Stretched Polystyrene Brushes. *Macromolecules* **2005,** *38*, 4296-4300.

158. Wu, T.; Efimenko, K.; Genzer, J. Combinatorial Study of the Mushroom-to-Brush Crossover in Surface Anchored Polyacrylamide. *J. Am. Chem. Soc.* **2002,** *124*, 9394-9395.

159. Brittain, W. J.; Minko, S. A Structural Definition of Polymer Brushes. *J. Polym. Sci., Part A: Polym. Chem.* **2007,** *45*, 3505-3512.

160. Moh, L. C. H.; Losego, M. D.; Braun, P. V. Solvent Quality Effects on Scaling Behavior of Poly(methyl methacrylate) Brushes in the Moderate- and High-Density Regimes. *Langmuir* **2011,** *27*, 3698-3702.

161. Dimitrov, D. I.; Milchev, A.; Binder, K. Polymer brushes in solvents of variable quality: Molecular dynamics simulations using explicit solvent. *J. Chem. Phys.* **2007,** *127*, 084905.

162. Yang, S.; Akcora, P. Deformation of Chemically Heterogeneous Interfacial Layers of Polymer Nanocomposites. *ACS Macro Lett.* **2019,** *8*, 1635-1641.

163. Borisov, O. V.; Birshtein, T. M.; Zhulina, E. B. Collapse of Grafted Polyelectrolyte Layer. *J. Phys. II* **1991,** *1*, 521-526.

164. Nomura, A.; Okayasu, K.; Ohno, K.; Fukuda, T.; Tsujii, Y. Lubrication Mechanism of Concentrated Polymer Brushes in Solvents: Effect of Solvent Quality and Thereby Swelling State. *Macromolecules* **2011,** *44*, 5013-5019.

165. Grest, G. S.; Murat, M. Structure of Grafted Polymeric Brushes in Solvents of Varying Quality - A Molecular-Dynamic Study. *Macromolecules* **1993,** *26*, 3108-3117.

166. LoVerso, F.; Egorov, S. A.; Binder, K. Interaction Between Polymer Brush-Coated Spherical Nanoparticles: Effect of Solvent Quality. *Macromolecules* **2012,** *45*, 8892-8902.

167. Choueiri, R. M.; Galati, E.; Thérien-Aubin, H.; Klinkova, A.; Larin, E. M.; Querejeta-Fernández, A.; Han, L.; Xin, H. L.; Gang, O.; Zhulina, E. B.; Rubinstein, M.; Kumacheva, E. Surface patterning of nanoparticles with polymer patches. *Nature* **2016,** *538*, 79-83.

168. Zhang, Q.; Liao, Y.; He, L. P.; Bu, W. F. Spherical Polymer Brushes in Solvents of Variable Quality: An Experimental Insight by TEM Imaging. *Langmuir* **2013,** *29*, 4181-4186.

169. Klinkova, A.; Therien-Aubin, H.; Choueiri, R. M.; Rubinstein, M.; Kumacheva, E. Colloidal analogs of molecular chain stoppers. *Proc. Natl. Acad. Sci. U. S. A.* **2013,** *110*, 18775-18779.

170. Arietaleaniz, S.; Malgaretti, P.; Pagonabarraga, I.; Hidalgo, R. C. Rheological behavior of colloidal suspension with long-range interactions. *Phys. Rev. E* **2018,** *98*, 042603.

171. Cohen, I.; Mason, T. G.; Weitz, D. A. Shear-Induced Configurations of Confined Colloidal Suspensions. *Phys. Rev. Lett.* **2004,** *93*, 046001.

172. Zaccarelli, E. Colloidal gels: equilibrium and non-equilibrium routes. *J. Phys.: Condens. Matter* **2007,** *19*, 323101.

173. Morris, J. F. A review of microstructure in concentrated suspensions and its implications for rheology and bulk flow. *Rheol. Acta* **2009,** *48*, 909-923.

174. Mattsson, J.; Wyss, H. M.; Fernandez-Nieves, A.; Miyazaki, K.; Hu, Z.; Reichman, D. R.; Weitz, D. A. Soft colloids make strong glasses. *Nature* **2009,** *462*, 83-86.

175. Khabaz, F.; Liu, T.; Cloitre, M.; Bonnecaze, R. T. Shear-induced ordering and crystallization of jammed suspensions of soft particles glasses. *Phys. Rev. Fluids* **2017,** *2*, 093301.

176. Zakhari, M. E. A.; Hütter, M.; Anderson, P. D. Effect of particle-size dynamics on flow properties of dense spongy-particle systems. *J. Rheol.* **2018,** *62*, 543-557.

177. Scotti, A.; Denton, A. R.; Brugnoni, M.; Houston, J. E.; Schweins, R.; Potemkin, I. I.; Richtering, W. Deswelling of Microgels in Crowded Suspensions Depends on Cross-Link Density and Architecture. *Macromolecules* **2019,** *52*, 3995-4007.

178. Koumakis, N.; Pamvouxoglou, A.; Poulos, A. S.; Petekidis, G. Direct comparison of the rheology of model hard and soft particle glasses. *Soft Matter* **2012,** *8*, 4271-4284.

179. van der Scheer, P.; van de Laar, T.; van der Gucht, J.; Vlassopoulos, D.; Sprakel, J. Fragility and Strength in Nanoparticle Glasses. *Acs Nano* **2017,** *11*, 6755-6763.

180. Cang, Y.; Reuss, A. N.; Lee, J.; Yan, J. J.; Zhang, J. N.; Alonso-Redondo, E.; Sainidou, R.; Rembert, P.; Matyjaszewski, K.; Bockstaller, M. R.; Fytas, G. Thermomechanical Properties and Glass Dynamics of Polymer-Tethered Colloidal Particles and Films. *Macromolecules* **2017,** *50*, 8658-8669.

181. Ndoro, T. V. M.; Bohm, M. C.; Muller-Plathe, F. Interface and Interphase Dynamics of Polystyrene Chains near Grafted and Ungrafted Silica Nanoparticles. *Macromolecules* **2012,** *45*, 171-179.

182. Lo Verso, F.; Yelash, L.; Binder, K. Dynamics of Macromolecules Grafted in Spherical Brushes under Good Solvent Conditions. *Macromolecules* **2013,** *46*, 4716-4722.

183. Ghanbari, A.; Rahimi, M.; Dehghany, J. Influence of Surface Grafted Polymers on the Polymer Dynamics in a Silica-Polystyrene Nanocomposite: A Coarse-Grained Molecular Dynamics Investigation. *J. Phys. Chem. C* **2013,** *117*, 25069-25076.

184. Srivastava, S.; Schaefer, J. L.; Yang, Z.; Tu, Z.; Archer, L. A. 25th Anniversary Article: Polymer–Particle Composites: Phase Stability and Applications in Electrochemical Energy Storage. *Adv. Mater.* **2014,** *26*, 201-234.

185. Choudhury, S.; Mangal, R.; Agrawal, A.; Archer, L. A. A highly reversible room-temperature lithium metal battery based on crosslinked hairy nanoparticles. *Nat. Commun.* **2015,** *6*, 10101.

186. Ying, Q.; Chu, B. Overlap concentration of macromolecules in solution. *Macromolecules* **1987,** *20*, 362-366.

187. Dalsin, S. J.; Hillmyer, M. A.; Bates, F. S. Linear Rheology of Polyolefin-Based Bottlebrush Polymers. *Macromolecules* **2015,** *48*, 4680-4691.

188. Dorgan, J. R.; Williams, J. S.; Lewis, D. N. Melt rheology of poly(lactic acid): Entanglement and chain architecture effects. *J. Rheol.* **1999,** *43*, 1141-1155.

189. Khabaz, F.; Khare, R. Effect of chain architecture on the size, shape, and intrinsic viscosity of chains in polymer solutions: A molecular simulation study. *J. Chem. Phys.* **2014,** *141*, 214904.

190. Jabbarzadeh, A.; Atkinson, J. D.; Tanner, R. I. Effect of Molecular Shape on Rheological Properties in Molecular Dynamics Simulation of Star, H, Comb, and Linear Polymer Melts. *Macromolecules* **2003,** *36*, 5020-5031.

191. Erwin, B. M.; Cloitre, M.; Gauthier, M.; Vlassopoulos, D. Dynamics and rheology of colloidal star polymers. *Soft Matter* **2010,** *6*, 2825-2833.

192. Takahashi, Y.; Suzuki, F.; Miyachi, M.; Noda, I.; Nagasawa, M. Zero-Shear Viscosity of Branched Polymer Solutions. *Polym. J.* **1986,** *18*, 89.

193. Currie, E. P. K.; Norde, W.; Cohen Stuart, M. A. Tethered polymer chains: surface chemistry and their impact on colloidal and surface properties. *Adv. Colloid Interface Sci.* **2003,** *100-102*, 205-265.

194. Liu, S.; Senses, E.; Jiao, Y.; Narayanan, S.; Akcora, P. Structure and Entanglement Factors on Dynamics of Polymer-Grafted Nanoparticles. *ACS Macro Lett.* **2016,** *5*, 569-573.

195. Akcora, P.; Liu, H.; Kumar, S. K.; Moll, J.; Li, Y.; Benicewicz, B. C.; Schadler, L. S.; Acehan, D.; Panagiotopoulos, A. Z.; Pryamitsyn, V.; Ganesan, V.; Ilavsky, J.; Thiyagarajan, P.; Colby, R. H.; Douglas, J. F. Anisotropic Self-Assembly of Spherical Polymer-Grafted Nanoparticles. *Nat. Mater.* **2009,** *8*, 354-U121.

196. Ethier, J. G.; Hall, L. M. Structure and Entanglement Network of Model Polymer-Grafted Nanoparticle Monolayers. *Macromolecules* **2018,** *51*, 9878-9889.

197. Krishnamurthy, L.-N.; Wagner, N. J.; Mewis, J. Shear thickening in polymer stabilized colloidal dispersions. *J. Rheol.* **2005,** *49*, 1347-1360.

198. Voudouris, P.; Choi, J.; Dong, H.; Bockstaller, M. R.; Matyjaszewski, K.; Fytas, G. Effect of Shell Architecture on the Static and Dynamic Properties of Polymer-Coated Particles in Solution. *Macromolecules* **2009,** *42*, 2721-2728.

199. Asai, M.; Cacciuto, A.; Kumar, S. K. Surface Fluctuations Dominate the Slow Glassy Dynamics of Polymer-Grafted Colloid Assemblies. *ACS Cent. Sci.* **2018,** *4*, 1179-1184.

200. Zhang, C.; Yang, S.; Padmanabhan, V.; Akcora, P. Solution Rheology of Poly(acrylic acid)-Grafted Silica Nanoparticles. *Macromolecules* **2019,** *52*, 9594-9603.

201. Antonietti, M.; Landfester, K. Polyreactions in miniemulsions. *Prog. Polym. Sci.* **2002,** *27*, 689-757.

202. Ramli, R. A.; Laftah, W. A.; Hashim, S. Core–shell polymers: a review. *RSC Adv.* **2013,** *3*, 15543-15565.

203. Min, K.; Gao, H.; Matyjaszewski, K. Use of Ascorbic Acid as Reducing Agent for Synthesis of Well-defined Polymers by ARGET ATRP. *Macromolecules* **2007,** *40*, 1789-1791.

204. Zhao, B.; Brittain, W. J.; Zhou, W.; Cheng, S. Z. D. AFM Study of Tethered Polystyrene-b-poly(methyl methacrylate) and Polystyrene-b-poly(methyl acrylate) Brushes on Flat Silicate Substrates. *Macromolecules* **2000,** *33*, 8821-8827.

205. Men'shikov, E. A.; Bol'shakova, A. V.; Yaminskii, I. V. Determination of the Flory-Huggins parameter for a pair of polymer units from AFM data for thin films of block copolymers. *Prot. Met. Phys. Chem. Surf.* **2009,** *45*, 295-299.

206. Zhao, B.; Brittain, W. J. Synthesis, Characterization, and Properties of Tethered Polystyrene-b-polyacrylate Brushes on Flat Silicate Substrates. *Macromolecules* **2000,** *33*, 8813-8820.

207. Wijmans, C. M.; Zhulina, E. B. Polymer brushes at curved surfaces. *Macromolecules* **1993,** *26*, 7214-7224.

208. Brandrup, J.; Immergut, E. H.; Grulke, E. A., Polymer Handbook. 4th ed.; Wiley: **2003**.

209. Alexander, S. Adsorption of chain molecules with a polar head a scaling description. *J. Phys. France* **1977,** *38*, 983-987.

210. De Gennes, P. G. Scaling theory of polymer adsorption. *J. Phys. France* **1976,** *37*, 1445-1452.

211. Steeneken, P. A. M. Rheological properties of aqueous suspensions of swollen starch granules. *Carbohydr. Polym.* **1989,** *11*, 23-42.

212. Fetters, L. J.; Lohse, D. J.; Graessley, W. W. Chain dimensions and entanglement spacings in dense macromolecular systems. *J. Polym. Sci., Part B: Polym. Phys.* **1999,** *37*, 1023-1033.

213. Savin, D. A.; Pyun, J.; Patterson, G. D.; Kowalewski, T.; Matyjaszewski, K. Synthesis and Characterization of Silica-graft-Polystyrene Hybrid Nanoparticles: Effect of Constraint on the Glass-Transition Temperature of Spherical Polymer Brushes. *J. Polym. Sci., Part B: Polym. Phys.* **2002,** *40*, 2667-2676.

214. Jhalaria, M.; Buenning, E.; Huang, Y. C.; Tyagi, M.; Zorn, R.; Zamponi, M.; Garcia-Sakai, V.; Jestin, J.; Benicewicz, B. C.; Kumar, S. K. Accelerated Local Dynamics in Matrix-Free Polymer Grafted Nanoparticles. *Phys. Rev. Lett.* **2019,** *123*, 6.

215. Ghugare, S. V.; Chiessi, E.; Telling, M. T. F.; Deriu, A.; Gerelli, Y.; Wuttke, J.; Paradossi, G. Structure and Dynamics of a Thermoresponsive Microgel around Its Volume Phase Transition Temperature. *J. Phys. Chem. B* **2010,** *114*, 10285-10293.

216. Cendoya, I.; Alegria, A.; Alberdi, J. M.; Colmenero, J.; Grimm, H.; Richter, D.; Frick, B. Effect of Blending on the PVME Dynamics. A Dielectric, NMR, and QENS Investigation. *Macromolecules* **1999,** *32*, 4065-4078.

217. Malveau, C.; Baille, W. E.; Zhu, X. X.; Ford, W. T. Molecular Dynamics of Hydrophilic Poly(propylene imine) Dendrimers in Aqueous Solutions by H-1 NMR Relaxation. *J. Polym. Sci., Part B: Polym. Phys.* **2003,** *41*, 2969-2975.

218. Pinto, L. F.; Correa, J.; Martin-Pastor, M.; Riguera, R.; Fernandez-Megia, E. The Dynamics of Dendrimers by NMR Relaxation: Interpretation Pitfalls. *J. Am. Chem. Soc.* **2013,** *135*, 1972-1977.

219. de Graaf, A. J.; Boere, K. W. M.; Kemmink, J.; Fokkink, R. G.; van Nostrum, C. F.; Rijkers, D. T. S.; van der Gucht, J.; Wienk, H.; Baldus, M.; Mastrobattista, E.; Vermonden, T.; Hennink, W. E. Looped Structure of Flowerlike Micelles Revealed by H-1 NMR Relaxometry and Light Scattering. *Langmuir* **2011,** *27*, 9843-9848.

220. Sayed, J. E.; Lorthioir, C.; Perrin, P.; Sanson, N. PEGylated NiPAM Microgels: Synthesis, Characterization and Colloidal Stability. *Soft Matter* **2019,** *15*, 963-972.

221. Pietrasik, J.; Sumerlin, B. S.; Lee, H. I.; Gil, R. R.; Matyjaszewski, K. Structural Mobility of Molecular Bottle-Brushes Investigated by NMR Relaxation Dynamics. *Polymer* **2007,** *48*, 496-501.

222. Martin, H. J.; White, B. T.; Scanlon, C. J.; Saito, T.; Dadmun, M. D. Tunable Synthetic Control of Soft Polymeric Nanoparticle Morphology. *Soft Matter* **2017,** *13*, 8849-8857.

223. Wei, W. C.; Feng, S.; Zheng, C. X.; Liang, G. D.; Gao, H. Y.; Wu, Q.; Zhu, F. M. Glass Transition and Quantum Yield for Fluorescent Labelled Polystyrene Core-forming Block in Self-assembled Nanomicelles of Amphiphilic Diblock Copolymers. *J. Polym. Res.* **2015,** *22*, 8.

224. Kang, E.; Graczykowski, B.; Jonas, U.; Christie, D.; Gray, L. A. G.; Cangialosi, D.; Priestley, R. D.; Fytas, G. Shell Architecture Strongly Influences the Glass Transition, Surface Mobility, and Elasticity of Polymer Core-Shell Nanoparticles. *Macromolecules* **2019,** *52*, 5399-5406.

225. Birshtein, T. M.; Zhulina, E. B. Conformations of Star-Branched Macromolecules. *Polymer* **1984,** *25*, 1453-1461.

226. Oconnor, P. J.; Cutie, S. S.; Smith, P. B.; Martin, S. J.; Sammler, R. L.; Harris, W. I.; Marks, M. J.; Wilson, L. H-1 NMR Characterization of Swelling in Cross-linked Polymer Systems. *Macromolecules* **1996,** *29*, 7872-7884.

227. Erman, B.; Baysal, B. M. Temperature Dependence of Swelling of Polystyrene Networks. *Macromolecules* **1985,** *18*, 1696-1700.

228. Pincus, P. Colloid Stablization with Grafted Polyelectrolytes. *Macromolecules* **1991,** *24*, 2912-2919.

229. Synytska, A.; Svetushkina, E.; Puretskiy, N.; Stoychev, G.; Berger, S.; Ionov, L.; Bellmann, C.; Eichhorn, K. J.; Stamm, M. Biocompatible Polymeric Materials with Switchable Adhesion Properties. *Soft Matter* **2010,** *6*, 5907-5914.

230. Song, J. B.; Zhou, J. J.; Duan, H. W. Self-Assembled Plasmonic Vesicles of SERS-Encoded Amphiphilic Gold Nanoparticles for Cancer Cell Targeting and Traceable Intracellular Drug Delivery. *J. Am. Chem. Soc.* **2012,** *134*, 13458-13469.

231. Zhan, X. L.; Yan, Y. D.; Zhang, Q. H.; Chen, F. Q. A Novel Superhydrophobic Hybrid Nanocomposite Material Prepared by Surface-Initiated AGET ATRP and its Anti-Icing Properties. *J. Mater. Chem. A* **2014,** *2*, 9390-9399.

232. Sunday, D.; Ilavsky, J.; Green, D. L. A Phase Diagram for Polymer-Grafted Nanoparticles in Homopolymer Matrices. *Macromolecules* **2012,** *45*, 4007-4011.

233. Srivastava, S.; Kandar, A. K.; Basu, J. K.; Mukhopadhyay, M. K.; Lurio, L. B.; Narayanan, S.; Sinha, S. K. Complex dynamics in polymer nanocomposites. *Phys. Rev. E* **2009,** *79*, 021408.

234. Jiang, N.; Endoh, M. K.; Koga, T.; Masui, T.; Kishimoto, H.; Nagao, M.; Satija, S. K.; Taniguchi, T. Nanostructures and Dynamics of Macromolecules Bound to Attractive Filler Surfaces. *ACS Macro Lett.* **2015,** *4*, 838-842.

235. Weaver, J. V. M.; Tang, Y.; Liu, S.; Iddon, P. D.; Grigg, R.; Billingham, N. C.; Armes, S. P.; Hunter, R.; Rannard, S. P. Preparation of Shell Cross-Linked Micelles by Polyelectrolyte Complexation. *Angew. Chem., Int. Ed.* **2004,** *43*, 1389-1392.

236. Posel, Z.; Posocco, P. Tuning the Properties of Nanogel Surfaces by Grafting Charged Alkylamine Brushes. *Nanomaterials* **2019,** *9*, 14.

237. Wichaita, W.; Kim, Y.-G.; Tangboriboonrat, P.; Thérien-Aubin, H. Polymer-functionalized polymer nanoparticles and their behaviour in suspensions. *Polym. Chem.* **2020,** *11*, 2119-2128.

238. Bachhar, N.; Kumaraswamy, G.; Kumar, S. K. Core-Size Dispersity Dominates the Self-Assembly of Polymer-Grafted Nanoparticles in Solution. *Macromolecules* **2019,** *52*, 4888-4894.

239. Kim, S. Y.; Meyer, H. W.; Saalwächter, K.; Zukoski, C. F. Polymer Dynamics in PEG-Silica Nanocomposites: Effects of Polymer Molecular Weight, Temperature and Solvent Dilution. *Macromolecules* **2012,** *45*, 4225-4237.

240. Martin, T. B.; Mongcopa, K. I. S.; Ashkar, R.; Butler, P.; Krishnamoorti, R.; Jayaraman, A. Wetting–Dewetting and Dispersion–Aggregation Transitions Are Distinct for Polymer Grafted Nanoparticles in Chemically Dissimilar Polymer Matrix. *J. Am. Chem. Soc.* **2015,** *137*, 10624-10631.

241. Holt, A. P.; Bocharova, V.; Cheng, S.; Kisliuk, A. M.; White, B. T.; Saito, T.; Uhrig, D.; Mahalik, J. P.; Kumar, R.; Imel, A. E.; Etampawala, T.; Martin, H.; Sikes, N.; Sumpter, B. G.; Dadmun, M. D.; Sokolov, A. P. Controlling Interfacial Dynamics: Covalent Bonding versus Physical Adsorption in Polymer Nanocomposites. *Acs Nano* **2016,** *10*, 6843-6852.

242. Poling-Skutvik, R.; Olafson, K. N.; Narayanan, S.; Stingaciu, L.; Faraone, A.; Conrad, J. C.; Krishnamoorti, R. Confined Dynamics of Grafted Polymer Chains in Solutions of Linear Polymer. *Macromolecules* **2017,** *50*, 7372-7379.

243. McLeish, T. C. B. Tube theory of entangled polymer dynamics. *Adv. Phys.* **2002,** *51*, 1379-1527.

244. Heatley, F. Nuclear Magnetic-Relaxation of Synthetic-Polymers in Dilute-Solution. *Prog. Nucl. Magn. Reson. Spectrosc.* **1979,** *13*, 47-85.

245. Dais, P.; Spyros, A. 13C Nuclear magnetic relaxation and local dynamics of synthetic polymers in dilute solution and in the bulk state. *Prog. Nucl. Magn. Reson. Spectrosc.* **1995,** *27*, 555-633.

246. Klein, P. G.; Ries, M. E. The dynamics and physical structure of polymers above the glass transition—transverse relaxation studies of linear chains, star polymers and networks. *Prog. Nucl. Magn. Reson. Spectrosc.* **2003,** *42*, 31-52.

247. Palmer, A. G. NMR characterization of the dynamics of biomacromolecules. *Chem. Rev.* **2004,** *104*, 3623-3640.

248. Charlier, C.; Khan, S. N.; Marquardsen, T.; Pelupessy, P.; Reiss, V.; Sakellariou, D.; Bodenhausen, G.; Engelke, F.; Ferrage, F. Nanosecond Time Scale Motions in Proteins Revealed by High-Resolution NMR Relaxometry. *J. Am. Chem. Soc.* **2013,** *135*, 18665-18672.

249. Ashkar, R. Selective dynamics in polymeric materials: Insights from quasi-elastic neutron scattering spectroscopy. *J. Appl. Phys.* **2020,** *127*, 151101.

250. Derakhshan, M.; Ansarian, H. R.; Rahman, M. M.; Sakurai, T.; Takafuji, M.; Ihara, H. A new method for evaluation of the mobility of silica-grafted alkyl chains by suspension-state 1H NMR. *Can. J. Chem.* **2005,** *83*, 1792-1798.

251. Friedrichs, C.; Emmerling, S.; Kircher, G.; Graf, R.; Wolfgang Spiess, H. Glass transition of poly(ethylmethacrylate) admixed and bound to nanoparticles. *J. Chem. Phys.* **2013,** *138*, 12A503.

252. Spiess, H. W. 50th Anniversary Perspective: The Importance of NMR Spectroscopy to Macromolecular Science. *Macromolecules* **2017,** *50*, 1761-1777.

253. Schweizerhof, S.; Demco, D. E.; Mourran, A.; Keul, H.; Fechete, R.; Möller, M. Temperature-Induced Phase Transition Characterization of Responsive Polymer Brushes Grafted onto Nanoparticles. *Macromol. Chem. Phys.* **2017,** *218*.

254. Zhang, J.; Pelton, R. Poly(N-isopropylacrylamide) Microgels at the Air-Water Interface. *Langmuir* **1999,** *15*, 8032-8036.

255. Senff, H.; Richtering, W. Temperature Sensitive Microgel Suspensions: Colloidal Phase Behavior and Rheology of Soft Spheres. *J. Chem. Phys.* **1999,** *111*, 1705-1711.

256. Gao, J.; Hu, Z. B. Optical Properties of N-isopropylacrylamide Microgel Spheres in Water. *Langmuir* **2002,** *18*, 1360-1367.

257. Cai, T.; Marquez, M.; Hu, Z. Monodisperse Thermoresponsive Microgels of Poly(ethylene glycol) Analogue-Based Biopolymers. *Langmuir* **2007,** *23*, 8663-8666.

258. Xun, W. W.; Richtering, W. Dilution Leading to Viscosity Increase based on the Cononsolvency Effect of Temperature-Sensitive Microgel Suspensions. *Colloids Surf., A* **2015,** *484*, 377-385.

259. Scherzinger, C.; Lindner, P.; Keerl, M.; Richtering, W. Cononsolvency of Poly(N,N-diethylacrylamide) (PDEAAM) and Poly(N-isopropylacrylamide) (PNIPAM) Based Microgels in Water/Methanol Mixtures: Copolymer vs Core−Shell Microgel. *Macromolecules* **2010,** *43*, 6829-6833.

260. Scherzinger, C.; Holderer, O.; Richter, D.; Richtering, W. Polymer Dynamics in Responsive Microgels: Influence of Cononsolvency and Microgel Architecture. *Phys. Chem. Chem. Phys.* **2012,** *14*, 2762-2768.

261. Chen, L.; Peng, Z. P.; Zeng, Z. P.; She, Y. Q.; Wei, J. C.; Chen, Y. W. Hairy Polymeric Nanocapsules with pH-Responsive Shell and Thermoresponsive Brushes: Tunable Permeability for Controlled Release of Water-Soluble Drugs. *J. Polym. Sci., Part A: Polym. Chem.* **2014,** *52*, 2202-2216.

262. Berndt, I.; Pedersen, J. S.; Richtering, W. Temperature-Sensitive Core–Shell Microgel Particles with Dense Shell. *Angew. Chem., Int. Ed.* **2006,** *45*, 1737-1741.

263. Kim, Y.-G.; Wagner, M.; Thérien-Aubin, H. Dynamics of Soft and Hairy Polymer Nanoparticles in a Suspension by NMR Relaxation. *Macromolecules* **2020,** *53*, 844-851.

264. Hansen, C. M., Hansen Solubility Parameters: A User's Handbook, Second Edition. CRC Press: **2007**.

265. Schreiber, E.; Ziener, U.; Manzke, A.; Plettl, A.; Ziemann, P.; Landfester, K. Preparation of Narrowly Size Distributed Metal-Containing Polymer Latexes by Miniemulsion and Other Emulsion Techniques: Applications for Nanolithography. *Chem. Mater.* **2009,** *21*, 1750-1760.

266. Tanaka, N.; Matsukawa, S.; Kurosu, H.; Ando, I. A Study on Dynamics of Water in Crosslinked Poly(N-isopropylacrylamide) Gel by NMR Spectroscopy. *Polymer* **1998,** *39*, 4703-4706.

267. Besghini, D.; Mauri, M.; Simonutti, R. Time Domain NMR in Polymer Science: From the Laboratory to the Industry. *Appl. Sci.* **2019,** *9*, 33.

268. Lipari, G.; Szabo, A. Model-free approach to the interpretation of nuclear magnetic resonance relaxation in macromolecules. 1. Theory and range of validity. *J. Am. Chem. Soc.* **1982,** *104*, 4546-4559.

269. Carr, H. Y.; Purcell, E. M. Effects of Diffusion on Free Precesion in Nuclear Magnetic Resonance Experiments *Phys. Rev.* **1954,** *94*, 630-638.

270. Meiboom, S.; Gill, D. Modified Spin-Echo Method for Measuring Nuclear Relaxation Times. *Rev. Sci. Instrum.* **1958,** *29*, 688-691.

271. Lund, R.; Willner, L.; Alegría, A.; Colmenero, J.; Richter, D. Self-Concentration and Interfacial Fluctuation Effects on the Local Segmental Dynamics of Nanostructured Diblock Copolymer Melts. *Macromolecules* **2008,** *41*, 511-514.

272. Alegria, A.; Lund, R.; Barroso-Bujans, F.; Arbe, A.; Colmenero, J. Component dynamics in nanostructured PI-PDMS diblock copolymers with PI segregated in lamellas, cylinders, and spheres. *Colloid Polym. Sci.* **2014,** *292*, 1863-1876.

273. Srivastava, S.; Agarwal, P.; Archer, L. A. Tethered Nanoparticle-Polymer Composites: Phase Stability and Curvature. *Langmuir* **2012,** *28*, 6276-6281.

274. Hu, H.; Xiu, K. M.; Xu, S. L.; Yang, W. T.; Xu, F. J. Functionalized Layered Double Hydroxide Nanoparticles Conjugated with Disulfide-Linked Polycation Brushes for Advanced Gene Delivery. *Bioconjugate Chem.* **2013,** *24*, 968-978.

275. Vogiatzis, G. G.; Theodorou, D. N. Structure of Polymer Layers Grafted to Nanoparticles in Silica-Polystyrene Nanocomposites. *Macromolecules* **2013,** *46*, 4670-4683.

276. Sato, T.; Ohishi, T.; Higaki, Y.; Takahara, A.; Otsuka, H. Radical crossover reactions of alkoxyamine-based dynamic covalent polymer brushes on nanoparticles and the effect on their dispersibility. *Polym. J.* **2016,** *48*, 147-155.

277. Schöttler, S.; Becker, G.; Winzen, S.; Steinbach, T.; Mohr, K.; Landfester, K.; Mailänder, V.; Wurm, F. R. Protein adsorption is required for stealth effect of poly(ethylene glycol)- and poly(phosphoester)-coated nanocarriers. *Nat. Nanotechnol.* **2016,** *11*, 372-377.

278. Prencipe, G.; Tabakman, S. M.; Welsher, K.; Liu, Z.; Goodwin, A. P.; Zhang, L.; Henry, J.; Dai, H. PEG Branched Polymer for Functionalization of Nanomaterials with Ultralong Blood Circulation. *J. Am. Chem. Soc.* **2009,** *131*, 4783-4787.

279. Koerner, H.; Drummy, L. F.; Benicewicz, B.; Li, Y.; Vaia, R. A. Nonisotropic Self-Organization of Single-Component Hairy Nanoparticle Assemblies. *ACS Macro Lett.* **2013,** *2*, 670-676.

280. Dahal, U.; Wang, Z.; Dormidontova, E. E. Hydration of Spherical PEO-Grafted Gold Nanoparticles: Curvature and Grafting Density Effect. *Macromolecules* **2018,** *51*, 5950-5961.

281. Sakib, N.; Koh, Y. P.; Huang, Y.; Mongcopa, K. I. S.; Le, A. N.; Benicewicz, B. C.; Krishnamoorti, R.; Simon, S. L. Thermal and Rheological Analysis of Polystyrene-Grafted Silica Nanocomposites. *Macromolecules* **2020**.

282. Dang, A.; Hui, C. M.; Ferebee, R.; Kubiak, J.; Li, T.; Matyjaszewski, K.; Bockstaller, M. R. Thermal Properties of Particle Brush Materials: Effect of Polymer Graft Architecture on the Glass Transition Temperature in Polymer-Grafted Colloidal Systems. *Macromol. Symp.* **2013,** *331-332*, 9-16.

283. Askar, S.; Li, L.; Torkelson, J. M. Polystyrene-Grafted Silica Nanoparticles: Investigating the Molecular Weight Dependence of Glass Transition and Fragility Behavior. *Macromolecules* **2017,** *50*, 1589-1598.

284. Holley, D. W.; Ruppel, M.; Mays, J. W.; Urban, V. S.; Baskaran, D. Polystyrene nanoparticles with tunable interfaces and softness. *Polymer* **2014,** *55*, 58-65.

285. Arbe, A.; Pomposo, J. A.; Moreno, A. J.; LoVerso, F.; González-Burgos, M.; Asenjo-Sanz, I.; Iturrospe, A.; Radulescu, A.; Ivanova, O.; Colmenero, J. Structure and dynamics of single-chain nanoparticles in solution. *Polymer* **2016,** *105*, 532-544.

286. Klonos, P. A.; Patelis, N.; Glynos, E.; Sakellariou, G.; Kyritsis, A. Molecular Dynamics in Polystyrene Single-Chain Nanoparticles. *Macromolecules* **2019,** *52*, 9334-9340.

287. Munkhbat, O.; Canakci, M.; Zheng, S.; Hu, W.; Osborne, B.; Bogdanov, A. A.; Thayumanavan, S. 19F MRI of Polymer Nanogels Aided by Improved Segmental Mobility of Embedded Fluorine Moieties. *Biomacromolecules* **2019,** *20*, 790-800.

288. McCall, D. W. Nuclear Magnetic Resonance Studies of Molecular Relaxation Mechanisms in Polymers. *Acc. Chem. Res.* **1971,** *4*, 223-&.

289. Helfand, E. Dynamics of Conformational Transitions in Polymers. *Science* **1984,** *226*, 647-650.

290. Ngai, K. L.; Roland, C. M. Chemical structure and intermolecular cooperativity: dielectric relaxation results. *Macromolecules* **1993,** *26*, 6824-6830.

291. Pethrick, R. A. Molecular-Motion of Polymers in Solution. *Sci. Prog.* **1975,** *62*, 599-631.

292. Fox, T. G.; Flory, P. J. Second-Order Transition Temperatures and Related Properties of Polystyrene. I. Influence of Molecular Weight. *J. Appl. Phys.* **1950,** *21*, 581-591.

293. Fox, T. G.; Flory, P. J. The glass temperature and related properties of polystyrene. Influence of molecular weight. *J. Polym. Sci.* **1954,** *14*, 315-319.

294. Zuo, B. A.; Zhang, S. S.; Niu, C.; Zhou, H.; Sun, S. Z.; Wang, X. P. Grafting density dominant glass transition of dry polystyrene brushes. *Soft Matter* **2017,** *13*, 2426-2436.